VOLUME 27 (1961) No. 2

NUCLEAR PHYSICS

JOURNAL DEVOTED TO THE EXPERIMENTAL AND THEORETICAL STUDY OF THE FUNDAMENTAL CONSTITUENTS OF MATTER AND THEIR INTERACTIONS

EDITOR: L. ROSENFELD - COPENHAGEN

YU. F. SMIRNOV, Talmi transformations for particles with different masses 177
W. H. KELLY and G. B. BEARD, Nuclear resonance fluorescence measurements on the 845 keV level in Fe^{56} 188
A. BUDZANOWSKI, R. W. CLIFFT and B. HIRD, Inelastic proton scattering asymmetries at 8.9 MeV. 193
G. R. ALLCOCK, A space-time model of isospace 204
GRACE P. HO and EDWIN L. ILOFF, The relative deuteron/proton yield from 45 MeV bremsstrahlung irradiation of copper 234
M. UMEZAWA, Pairings in the shell model (III) 248
W. T. PINKSTON and G. R. SATCHLER, Collective effects in inelastic scattering from nuclei. 270
V. MEYER, H. MÜLLER, H. H. STAUB and R. ZURMÜHLE, The γ-radiation of the $Li^7(p, \gamma)$ resonance at 441.3 keV 284
ROGER BALIAN, CLAUDE BLOCH et CYRANO DE DOMINICIS, Formulation de la mécanique statistique en termes de nombres d'occupation (II) 294
V. V. BALASHOV, V. G. SHEVCHENKO and N. P. YUDIN, Two-body forces and the giant resonance in photonuclear reactions 323
V. V. BALASHOV and V. N. FETISOV, Rôle of nucleon clusters in deep photo-disintegration of light nuclei 337
J. M. FERGUSON, Isomeric level in Y^{90} 344
V. M. STRUTINSKI, Dependence of the angular distribution of fission fragments on the target nuclear spin 348
Erratum 352

October 1961

NORTH-HOLLAND PUBLISHING COMPANY-AMSTERDAM

EDITORIAL BOARD

AUSTRALIA & NEW ZEALAND:	H. Messel (Sydney), M. L. Oliphant (Canberra)
AUSTRIA:	B. Karlik (Vienna), H. Thirring (Vienna)
BELGIUM:	M. de Hemptinne (Louvain), J. Verhaeghe (Ghent)
CANADA:	G. Volkoff (Vancouver)
DENMARK:	C. Møller (Copenhagen), S. Rozental (Copenhagen), G. E. Brown (Copenhagen)
FINLAND:	L. Simons (Helsinki)
FRANCE:	A. Berthelot (Saclay), S. Gorodetzky (Strasbourg)
GERMANY (DEM. REP.):	G. Hertz (Leipzig)
GERMANY (FED. REP.):	W. Gentner (Freiburg i. B.), J. H. D. Jensen (Heidelberg)
GREAT BRITAIN:	W. E. Burcham (Birmingham)
HUNGARY:	L. Janossy (Budapest)
INDIA:	H. Bhabha (Bombay), R. Ramanna (Trombay)
IRISH REPUBLIC:	J. McConnell (Maynooth)
ISRAEL:	G. Racah (Jerusalem)
ITALY:	E. Amaldi (Rome)
JAPAN:	S. Kikuchi (Tokay), S. Tomonaga (Tokyo)
MEXICO:	M. Moshinsky (Mexico)
NETHERLANDS:	H. Brinkman (Groningen), S. R. de Groot (Leiden)
NORWAY:	E. Hylleraas (Oslo), A. Lundby (Oslo), H. Wergeland (Trondheim)
POLAND:	L. Infeld (Warsaw), J. Werle (Warsaw)
PORTUGAL:	J. M. Araújo (Porto), J. R. de Almeida Santos (Coimbra)
SOUTH AMERICA:	G. Beck (Rio de Janeiro), J. Leite Lopes (Rio de Janeiro)
SPAIN:	J. M. Otero (Madrid), C. Sanchez del Rio (Madrid)
SWEDEN:	O. Klein (Stockholm), K. Siegbahn (Uppsala), I. Waller (Uppsala)
SWITZERLAND:	P. Huber (Basel), P. Scherrer (Zürich)
U.A.R. & ARAB COUNTRIES:	F. El Bedewi (Cairo), M. G. Nooh (Cairo)
U.S.A.:	H. H. Barschall (Madison, Wisconsin), S. Devons (New York)
U.S.S.R.:	M. A. Markov (Moscow), I. S. Shapiro (Moscow), D. V. Skobeltzyn (Moscow)
YUGOSLAVIA:	I. Supek (Zagreb)

CONTRIBUTIONS may be sent to the Editor, Professor L. Rosenfeld, NORDITA, Blegdamsvej 17, Copenhagen Ø, either directly, or preferably through the intermediary of one of the members of the Editorial Board of the country or region in which the author is working. They may be written in English, French or German.

NUCLEAR PHYSICS is published in fortnightly issues. The subscription price per volume of 700 pages is fl 57.00; 114s; $ 15.00. Post-free.

SUBSCRIPTIONS should be sent to the publishers, NORTH-HOLLAND PUBLISHING COMPANY P.O. Box 103, Amsterdam or to any subscription-agent.

BOOKS FOR REVIEW should be sent to Professor Rosenfeld.

No part of this issue may be reproduced in any form, by print, photoprint, microfilm or any other means without permission from the publisher.

Printed in the Netherlands

NUCLEAR PHYSICS 1962

Personal subscription scheme

Only to be used for new personal subscriptions, not for renewals

When Nuclear Physics was started at the end of 1955, the intention was to publish one or two volumes a year of 700 pages each. Neither the publisher nor the editor could envisage that the influx of papers would make it necessary to publish eight such volumes a year, as were in 1961.

Although since 1955 the guilder has been revaluated with 4 %, the production costs of mathematical composition have risen by approximately 25% and the number of words per page has been increased by 20% since the first volume, the subscription price per volume has been maintained at $ 15.00 (108s.).

Moreover Nuclear Physics does not impose any page charge, in order to make it easier for scientists from countries with a weak currency to contribute to the journal.

It is difficult to compare subscription prices, but per page Nuclear Physics is undoubtedly one of the less expensive journals in the field of physics.

However, we realize that a total subscription price per year of $ 120.00 for eight volumes is prohibitive for a private subscriber and the suggestion has been made that Nuclear Physics could fix a special price for personal subscriptions.

Indeed, there are a number of scientific journals which give a certain discount to private subscribers. In the case of Nuclear Physics a discount of 30% or even 50% would not be sufficient to attract private subscriptions.

Now it is known that for technical publications the composition of the type is the most expensive part of the production and that as soon as the break-even point is reached, the run-on costs are comparatively low.

Accordingly, we decided early 1961 to make Nuclear Physics available to personal subscribers at the run-on costs. This meant that starting with 1961 individual physicists could subscribe for their own use to the eight volumes (approx. 5600 pages) of Nuclear Physics scheduled for 1961 at a total price of $ 20.00 or the equivalent in other currency (postage included).

Should you want to join this personal subscription scheme for 1962, please return the order-form.

It has to be understood that the publisher has the right to refuse a personal subscription or its renewal. In case of refusal, the publisher will return the cheque.

We were glad to see that this new arrangement appealed to many nuclear physicists and that it did not lead to any misunderstanding about the extremely complicated way of fixing subscription prices for learned journals.

THE EDITOR
L. Rosenfeld

THE PUBLISHER
M. D. Frank

How to act:

Write a letter to the Subscription Department of North-Holland Publishing Company, P.O. Box 103, Amsterdam, Netherlands, asking for a personal subscription.

This letter should contain:

- **a cheque or banknotes for $ 20.00**
  (£ 7.4.0-; DM 80; N.Frs. 100)
- **a statement running as follows:**

"This subscription is for personal use only and will not replace an existing library subscription, nor will it be put at the disposal of any library now or in the future.

My position is: ..... "

(Mention should be made of the institution to which you are attached.)

Any enquiry or communication concerning the personal subscription scheme should be addressed to the publisher, North-Holland Publishing Company, P.O. Box 103, Amsterdam, Netherlands.

Only to be used for NEW personal subscriptions, not for renewals

SUBSCRIPTION FORM

NORTH-HOLLAND PUBLISHING COMPANY
P.O. BOX 103
AMSTERDAM - NETHERLANDS

Date _____

Please enter my personal subscription to

NUCLEAR PHYSICS 1962

(VOLUMES 29–36)

(tear off here)

at the **total** subscription price of $ 20.00

(£ 7.4.0.; DM. 80; N. Frs. 100)

I declare that this subscription is for my personal use only and that it will not replace an existing library subscription, nor will it be put at the disposal of any library now or in the future.

I enclose ☐ banknotes

☐ cheque

My position is _____

(mention should be made of the institution to which you are attached)

Name (please print) _____

_____

Address _____

_____

City, Zone, State _____

Signature

_____

1.D.1.

Nuclear Physics **27** (1961) 177—187; © *North-Holland Publishing Co., Amsterdam*

Not to be reproduced by photoprint or microfilm without written permission from the publisher

TALMI TRANSFORMATIONS FOR PARTICLES WITH DIFFERENT MASSES

YU. F. SMIRNOV

Nuclear Physics Research Institute, Moscow State University, USSR

Received 8 December 1960

Abstract: A general formula for Talmi coefficients is obtained, making it possible to pass from the wave functions of two particles having different masses μ_1 and μ_2 moving in the oscillator potential $V(r_1, r_2) = \frac{1}{2}\mu_1\omega r_1^2 + \frac{1}{2}\mu_2\omega r_2^2$ to the wave functions describing the relative motion of these particles and the motion of their centre of mass. These coefficients are necessary for isolating the motion of the centre-of mass of several nucleons in the shell model. They are also applied in calculating the energy matrix, etc.

1. Introduction

The transition to the centre-of-mass system of two particles with identical masses in the oscillator potential is performed via the Talmi coefficients [1]) designated in the following manner:

$$\left\langle \begin{matrix} n_1 l_1 m_1 \\ n_2 l_2 m_2 \end{matrix} \middle| \begin{matrix} NLM \\ n\, l\, m \end{matrix} \right\rangle. \tag{1}$$

The Talmi coefficients are determined by the equation

$$\psi_{n_1 l_1 m_1}(\mathbf{r}_1/r_0)\psi_{n_2 l_2 m_2}(\mathbf{r}_2/r_0) = \sum_{\substack{NLM \\ nlm}} \left\langle \begin{matrix} n_1 l_1 m_1 \\ n_2 l_2 m_2 \end{matrix} \middle| \begin{matrix} NLM \\ n\, l\, m \end{matrix} \right\rangle \psi_{NLM}(\mathbf{R}/\tfrac{1}{2}\sqrt{2}r_0)\psi_{nlm}(\mathbf{r}/\tfrac{1}{2}\sqrt{2}r_0). \tag{2}$$

Here $\psi_{n_1 l_1 m_1}(\mathbf{r}_1/r_0)$ and $\psi_{n_2 l_2 m_2}(\mathbf{r}_2/r_0)$ are the oscillator wave functions of the first and second nucleons, n being the main quantum number. The eigenvalue of the energy is $E_{nl} = (2n+l+\frac{3}{2})\hbar\omega$. The quantity l is the orbital momentum of the nucleon and m is its projection, $r_0 = (\hbar/\mu\omega)^{\frac{1}{2}}$ is the "radius" of the oscillator well (μ is the mass of the nucleon), $\mathbf{R}$ is the radius vector of the centre-of-mass of two nucleons and $\mathbf{r}$ their relative radius vector. The summation indices in eq. (2) run through a series of values limited by three conservation laws:

1) law of energy conservation:

$$2n_1+l_1+2n_2+l_2 = 2N+L+2n+l. \tag{2a}$$

2) *Law of conservation of angular momentum and its projection*:

$$\mathbf{l}_1+\mathbf{l}_2 = \mathbf{L}+\mathbf{l}, \qquad m_1+m_2 = M+m. \tag{2b}$$

3) *Law of parity conservation*:

$$(-1)^{l_1+l_2} = (-1)^{L+l}. \tag{2c}$$

From these equations it follows that the sum in eq. (2) contains a limited number of terms.

The Talmi coefficients for particles with identical masses were given in ref. [5]). There as well as in ref. [4]) a number of these coefficients were calculated. Later general formulas for these coefficients were obtained [2]) for $n_1 = 0$ and $n_2 = 0$. For determining the coefficients in the other cases recurrent relations were proposed. Mang [3]) gives the general formula for the Talmi coefficients in the case $l = 0$ and $m = 0$. Useful recurrent formulas were obtained by Arima [4]).

If a third nucleon is added to the two nucleons already considered and an attempt is made to pass to the system of the general centre-of-mass, the product of the wave function of the centre-of-mass of the first two particles by the wave function of the third nucleon has to be considered:

$$\psi_{NLM}\left(\frac{\mathbf{R}_{12}}{r_0/\sqrt{2}}\right)\psi_{n_3l_3m_3}\left(\frac{\mathbf{r}_3}{r_0}\right), \tag{3}$$

and one should pass to the new variables $\mathbf{R} = \frac{1}{3}(\mathbf{r}_1+\mathbf{r}_2+\mathbf{r}_3) = \frac{1}{3}(2\mathbf{R}_{12}+\mathbf{r}_3)$. It can easily be seen that the product (3) is the eigenfunction of the following Hamiltonian:

$$H = -\frac{\hbar^2}{4\mu}\Delta_{R_{12}} - \frac{\hbar^2}{2\mu}\Delta_{r_3} + \frac{2\mu\omega^2 R_{12}^2}{2} + \frac{\mu\omega^2 r_3^2}{2}. \tag{4a}$$

This Hamiltonian describes the motion of a particle with mass 2μ and a particle with mass μ in the oscillator potential with the frequency ω. For passing to the centre-of-mass system of two such particles it is necessary to introduce the Talmi coefficients for particles with different masses. A problem of this type arises, for example, in isolating the motion of the centre-of-mass of three nucleons when calculating the reduced width for the emission of a triton [8]). Since the case of particles with different masses has not been considered it is of interest to obtain the general formula of Talmi coefficients for this case (which of course is suitable for calculating the conventional coefficients (1)) and determine their dependence on the projections m_1, m_2, M, m.

We shall consider a Hamiltonian of a more general type than (4a).

$$H = -\frac{\hbar^2}{2\mu_1}\Delta_{r_1} - \frac{\hbar^2}{2\mu_2}\Delta_{r_2} + \tfrac{1}{2}\mu_1\omega^2 r_1^2 + \tfrac{1}{2}\mu_2\omega^2 r_2^2. \tag{4b}$$

The eigenfunctions of this Hamiltonian are of the form

$$\psi_{n_1 l_1 m_1}\left(\frac{\mathbf{r}_1}{r_{01}}\right)\psi_{n_2 l_2 m_2}\left(\frac{\mathbf{r}_2}{r_{02}}\right),$$

where (5a)

$$r_{01}=\left(\frac{\hbar}{\mu_1\omega}\right)^{\frac{1}{2}}, \qquad r_{02}=\left(\frac{\hbar}{\mu_2\omega}\right)^{\frac{1}{2}}.$$

In passing to the centre-of-mass system

$$\mathbf{R}=\frac{\mu_1\mathbf{r}_1+\mu_2\mathbf{r}_2}{\mu_1+\mu_2}, \qquad \mathbf{r}=\mathbf{r}_1-\mathbf{r}_2,$$

the Hamiltonian (4b) assumes the form

$$H=-\frac{\hbar^2}{2(\mu_1+\mu_2)}\Delta_R-\frac{\hbar^2(\mu_1+\mu_2)}{2\mu_1\mu_2}\Delta_r+\tfrac{1}{2}(\mu_1+\mu_2)\omega^2R^2+\frac{\mu_1\mu_2\omega^2r^2}{2(\mu_1+\mu_2)}. \quad (4c)$$

Now its eigenfunctions are the products

$$\psi_{NLM}\left(\frac{\mathbf{R}}{R_0}\right)\psi_{nlm}\left(\frac{\mathbf{r}}{r_0}\right),$$

where (5b)

$$R_0=\left[\frac{\hbar}{(\mu_1+\mu_2)\omega}\right]^{\frac{1}{2}}, \qquad r_0=\left[\frac{\hbar(\mu_1+\mu_2)}{\mu_1\mu_2\omega}\right]^{\frac{1}{2}}.$$

The functions (5a) can be expressed in the form of linear combinations of the functions (5b) (and vice-versa) relating to the same eigenvalue of energy. The coefficients of these linear combinations will be called Talmi coefficients for particles with different masses and will be designated by the symbol

$$\left\langle \begin{matrix} n_1 l_1 m_1 \\ n_2 l_2 m_2 \end{matrix} \middle| \mu_1\mu_2 \middle| \begin{matrix} NLM \\ n\, l\, m \end{matrix} \right\rangle.$$

Thus these coefficients are determined by the equality

$$\psi_{n_1 l_1 m_1}\left(\frac{\mathbf{r}_1}{r_{01}}\right)\psi_{n_2 l_2 m_2}\left(\frac{\mathbf{r}_2}{r_{02}}\right)=\sum_{\substack{NLM\\ n\,l\,m}}\left\langle \begin{matrix} n_1 l_1 m_1 \\ n_2 l_2 m_2 \end{matrix} \middle| \mu_1\mu_2 \middle| \begin{matrix} NLM \\ n\, l\, m \end{matrix} \right\rangle \psi_{NLM}\left(\frac{\mathbf{R}}{R_0}\right)\psi_{nlm}\left(\frac{\mathbf{r}}{r_0}\right). \quad (6)$$

The conservation laws (2) also hold for this expansion. The Talmi coefficients form a unitary matrix for which the following orthogonality relations are valid:

$$\sum_{\substack{NLM\\ n\,l\,m}}\left\langle \begin{matrix} n_1 l_1 m_1 \\ n_2 l_2 m_2 \end{matrix} \middle| \mu_1\mu_2 \middle| \begin{matrix} NLM \\ n\, l\, m \end{matrix} \right\rangle\left\langle \begin{matrix} n'_1 l'_1 m'_1 \\ n'_2 l'_2 m'_2 \end{matrix} \middle| \mu_1\mu_2 \middle| \begin{matrix} NLM \\ n\, l\, m \end{matrix} \right\rangle=\delta^{n'_1 l'_1 m'_1}_{n_1 l_1 m_1}\,\delta^{n'_2 l'_2 m'_2}_{n_2 l_2 m_2},$$

$$\sum_{\substack{n_1 l_1 m_1\\ n_2 l_2 m_2}}\left\langle \begin{matrix} n_1 l_1 m_1 \\ n_2 l_2 m_2 \end{matrix} \middle| \mu_1\mu_2 \middle| \begin{matrix} NLM \\ n\, l\, m \end{matrix} \right\rangle\left\langle \begin{matrix} n_1 l_1 m_1 \\ n_2 l_2 m_2 \end{matrix} \middle| \mu_1\mu_2 \middle| \begin{matrix} N'L'M' \\ n'\, l'\, m' \end{matrix} \right\rangle=\delta^{N'L'M'}_{NLM}\,\delta^{n'l'm'}_{nlm}. \quad (7)$$

2. Derivation of a General Formula for Talmi Coefficients

The oscillator functions are of the form [1, 3])

$$\psi_{nlm}\left(\frac{\mathbf{r}}{r_0}\right) = R_{nl}\left(\frac{r}{r_0}\right) Y_{lm}(\theta, \varphi),$$

$$R_{nl}\left(\frac{r}{r_0}\right) = N_{nl} e^{-\frac{r}{2r_0^2}} \left(\frac{r}{r_0}\right)^l \sum_{k=0}^{n} (-1)^k 2^k \binom{n}{k} \frac{(2l+1)!!}{(2l+2k+1)!!} \left(\frac{r}{r_0}\right)^{2k}, \tag{8}$$

$$N_{nl}^2 = 2^{l-n+2}(2l+2n+1)!! \frac{1}{\sqrt{\pi} n![(2l+1)!!]^2 r_0^3}.$$

For determining Talmi coefficients it is necessary to pass from the variables

$$\begin{matrix} r_1\theta_1\varphi_1 \\ r_2\theta_2\varphi_2 \end{matrix} \quad \text{to} \quad \begin{matrix} R\theta\phi \\ r\vartheta\varphi \end{matrix}$$

on the left-hand side of eq. (6) and it is sufficient to do so only in the term containing the highest power $r_1^{2n_1+l_1} r_2^{2n_2+l_2}$ and then compare it with the right-hand side. As a preliminary let us mention these simple equalities:

$$\begin{aligned} r_1 Y_{1m}(\theta_1 \varphi_1) &= R\mathscr{Y}_{1m}(\theta, \phi) + \frac{\mu_2}{\mu_1+\mu_2} r y_{1m}(\vartheta, \varphi), \\ r_2 Y_{1m}(\theta_2 \varphi_2) &= R\mathscr{Y}_{1m}(\theta, \phi) - \frac{\mu_1}{\mu_1+\mu_2} r y_{1m}(\vartheta, \varphi), \end{aligned} \tag{9}$$

$$Y_{lm}(\theta\varphi) = \sqrt{\frac{4\pi(2l+1)}{(2l_1+1)(2l_2+1)}} (C^{l0}_{l_1 0 l_2 0})^{-1} \sum_{m_1 m_2} C^{lm}_{l_1 m_1 l_2 m_2} Y_{l_1 m_1}(\theta, \varphi) Y_{l_2 m_2}(\theta, \varphi), \tag{10}$$

where $C^{lm}_{l_1 m_1 l_2 m_2}$ is the Clebsch-Gordan coefficient.

Further on, for the sake of brevity, we shall designate the vector sum of two spherical functions in the following manner:

$$\sum_{m_1 m_2} C^{lm}_{l_1 m_1 l_2 m_2} Y_{l_1 m_1} Y_{l_2 m_2} \equiv |l_1, l_2 : l_m\rangle \equiv |Y_{l_1}, Y_{l_2} : lm\rangle. \tag{11}$$

Let us first transform the expression $r_1^{l_1} Y_{l_1 m_1}$. According to eq. (10) we can write, using the notation (11),

$$\begin{aligned} Y_{LM} &= \sqrt{\frac{4\pi(2L+1)}{(2L-1)3}} (C^{L0}_{L-10L0})^{-1} |L-1, 1 : LM\rangle \\ &= \sqrt{\frac{4\pi(2L+1)}{3L}} |L-1, 1 : LM\rangle. \end{aligned} \tag{12}$$

The latter equation is obtained on account of the relation $C^{L0}_{L-1010} = \sqrt{\{L/(2L-1)\}}$. Applying the relation (12) $L-1$ times we obtain

$$Y_{LM} = \left(\frac{4\pi}{3}\right)^{\frac{1}{2}(L-1)} \sqrt{\frac{(2L+1)!!}{L!3}} |1, 1(2); 1(3); \ldots 1(L-1); 1 : LM\rangle$$

$$= \left(\frac{4\pi}{3}\right)^{\frac{1}{2}(L-1)} \sqrt{\frac{(2L+1)!!}{L!3}} \sum_{m_1 m_2 \ldots m_L} C^{1M_1}_{001m_1} C^{2M_2}_{1M_1 1m_2} C^{3M_3}_{2M_2 1m_3} \ldots C^{LM}_{L-1M_{L-1}1M_L} Y_{1m_1} Y_{1m_2} \ldots Y_{1m_L}$$

$$= (\tfrac{4}{3}\pi)^{\frac{1}{2}(L-1)} \sqrt{\frac{(2L+1)!!}{L!3}} \sum_{m_1 m_2 \ldots m_L} \prod_{i=1}^{L} C^{iM_i}_{i-1M_{i-1}1m_i} Y_{1m_i}. \tag{13}$$

The coefficient $C^{1M_1}_{001m_1} = \delta_{m_1 M_1}$ is introduced for the symmetry of the expression. With the aid of (13) it is easy to change over in the expression $r_1^{l_1} Y_{l_1 m_1}(\theta_1 \varphi_1)$ to the variables **R** and **r** by using eq. (9):

$$r_1^{L} Y_{LM}(\theta_1 \varphi_1) = (\tfrac{4}{3}\pi)^{\frac{L-1}{2}} \sqrt{\frac{(2L+1)!!}{L!3}} \sum_{m_1 m_2 \ldots m_L} \prod_{i=1}^{L} C^{iM_i}_{i-1M_{i-1}1m_i} (RY_{1m_i} + ary_{m_i}). \tag{14}$$

Here $a = \mu_2/(\mu_1+\mu_2)$. Eq. (14) is the sum of terms of the form

$$R^F a^f r^f \sum_{\mathrm{P}} \mathrm{P} |\mathscr{Y}_1 \mathscr{Y}_1(2); \mathscr{Y}_1(3); \ldots \mathscr{Y}_1(F) \ldots y_1(F+1) \ldots y_1(L-1); y_1 : LM\rangle, \tag{15}$$

where $F+f = L$, and P denotes the permutations corresponding to all kinds of combinations F of the factors $\mathscr{Y}_1$ in the general product L of the factors. Their number is obviously equal to the number of combinations $\binom{L}{F}$.

In the function $|\mathscr{Y}_1 \mathscr{Y}_1(2), \mathscr{Y}_1(3) \ldots \mathscr{Y}_1(F);\ y_1(F+1) \ldots y_1 : LM\rangle$ let us change the coupling scheme of momenta by adding separately all $\mathscr{Y}_1$ to the momentum F and all y_1 to the momentum f, and then adding these partial momenta into the total momenta L; i.e. we pass to the function

$$|\mathscr{Y}_1 \mathscr{Y}_1(2); \mathscr{Y}_1(3); \ldots \mathscr{Y}_1(F); y_1 y_1(2); y_1(3) \ldots y_1(f) : LM\rangle.$$

Since the matrix of the transition from one coupling scheme of momenta to another does not depend on M, it is easy to conclude, by taking the particular case $M = L$, that the transition matrix equals 1.

We shall therefore write by using (13)

$$|\mathscr{Y}_1 \mathscr{Y}_1(2); \mathscr{Y}_1(3); \ldots \mathscr{Y}_1(F); y_1(F+1) \ldots y_1 : LM\rangle$$

$$= |\mathscr{Y}_1 \mathscr{Y}_1(2); \mathscr{Y}_1(3) \ldots \mathscr{Y}_1(F); y_1 y_1(2); y_1(3) \ldots y_1(f) : LM\rangle \tag{16}$$

$$= \left(\frac{3}{4\pi}\right)^{\frac{1}{2}(F+f)-1} \sqrt{\frac{F!\,f!\,9}{(2F+1)!!(2f+1)!!}} \sum_{m_F m_f} C^{LM}_{Fm_F fm_f} \mathscr{Y}_{Fm_F} y_{fm_f}.$$

It can easily be seen that all terms in the sum over permutations P in (15) are identical, and consequently we have

$$r_1^L Y_{LM}(\theta_1\varphi_1) = \sum_{F=0}^{L} \sqrt{4\pi \frac{(2L+1)!!\,F!\,f!}{(2F+1)!!(2f+1)!!\,L!}}\, R^F a^f r^f \binom{L}{F} |\mathscr{Y}_F, y_f : LM\rangle$$
$$= \sum_{F=0}^{L} \sqrt{4\pi \frac{(2L+1)!}{(2F+1)!\,(2f+1)!}}\, R^F a^f r^f |\mathscr{Y}_F, y_f : LM\rangle. \tag{17}$$

This result coincides with an analogous formula obtained in ref. [2]) in a different manner.

Now let us transform the therm $r_1^{2n_1}$. With the aid of (9) and (10) we readily obtain

$$r_1^2 = r_1^2\sqrt{4\pi}Y_{00}(\theta_1, \varphi_1) = r_1^2\sqrt{4\pi}\sqrt{\frac{4\pi}{9}}\,(C^{00}_{1010})^{-1}|Y_1, Y_1 : 00\rangle$$
$$= -r_1^2\frac{4\pi}{\sqrt{3}}|Y_1, Y_1 : 00\rangle = R^2+a^2r^2-2arR\frac{4\pi}{\sqrt{3}}|\mathscr{Y}_1, y_1 : 00\rangle. \tag{18}$$

Let us consider $|\mathscr{Y}_l, y_l : 00\rangle|\mathscr{Y}_1, y_1 : 00\rangle$. Let us connect with the aid of $9j$-symbols [5]) $\mathscr{Y}_l$ and $\mathscr{Y}_1$ to the momentum L (and likewise y_l and y_1) and pass, with the aid of eq. (10), to the functions $\mathscr{Y}_L$ and y_L

$$|\mathscr{Y}_l y_l(0); \mathscr{Y}_1 y_1(0) : 00\rangle = \sum_L (2L+1)\begin{Bmatrix} l & l & 0 \\ 1 & 1 & 0 \\ L & L & 0 \end{Bmatrix} |\mathscr{Y}_l\mathscr{Y}_1(L); y_l y_1(L) : 00\rangle$$
$$= \sum_L \frac{3(2l+1)}{4\pi}\begin{Bmatrix} l & l & 0 \\ 1 & 1 & 0 \\ L & L & 0 \end{Bmatrix} |\mathscr{Y}_L, y_L : 00)\rangle(C^{L0}_{l010})^2 = \tag{19}$$
$$= \sum_L \frac{\sqrt{3}}{4\pi}\sqrt{\frac{2l+1}{2L+1}}\,(C^{L0}_{l010})^2|\mathscr{Y}_L, y_L : 00\rangle.$$

In passing to eq. (19) the property of the $9j$ symbols

$$\begin{Bmatrix} l & l & 0 \\ 1 & 1 & 0 \\ L & L & 0 \end{Bmatrix} = \frac{1}{\sqrt{3(2l+1)(2L+1)}}$$

is used. Let us now consider $|\mathscr{Y}_1 y_1 : 00\rangle^k$. Let us collect all functions $\mathscr{Y}_1$ to the momentum L and likewise the functions y_1. Let us determine the coefficient in this linear combination for each value L. Using eq. (19) several times we obtain

$$|\mathscr{Y}_1 y_1(0)\rangle^k$$

$$= \left(\frac{\sqrt{3}}{4\pi}\right)^{k-1} \sum_{L_2 L_3 \ldots L_{k-1} L} \sqrt{\frac{3(2L_2+1)\ldots(2L_{k-1}+1)}{(2L_2+1)(2L_3+1)\ldots(2L+1)}}\, (C^{L_2 0}_{1010} C^{L_3 0}_{L_2 010} \ldots C^{L0}_{L_{k-1}010})^2 |\mathscr{Y}_L, y_L : 00\rangle$$

$$= \left(\frac{\sqrt{3}}{4\pi}\right)^{k-1} \sum_L G(k, L) \sqrt{\frac{3}{2L+1}}\, |\mathscr{Y}_L, y_L : 00\rangle, \tag{20}$$

where the notation

$$G(k, L) = \sum_{L_2 L_3 \ldots L_{k-1}} (C^{L_2 0}_{1010} C^{L_3 0}_{L_2 010} \ldots C^{L0}_{L_{k-1}010})^2$$

is introduced. According to Elliott [7]) we have

$$G(k, L) = \frac{(2L+1)2^L k!(\frac{1}{2}(k+L))!}{(k+L+1)!(\frac{1}{2}(k-L))!} \tag{21}$$

Now that the preliminary calculations have been completed it is possible, with the aid of eqs. (17), (18), (20) and (21), to transform $r_1^{2n_1+l_1} Y_{l_1 m_1}(\theta_1, \varphi_1)$ $r_2^{2n_2+l_2} Y_{l_2 m_2}(\theta_2, \varphi_2)$ to the centre-of-mass system and, by isolating the factor before $R^{2N+L}\mathscr{Y}_{LM}(\theta, \phi) r^{2n+l} y_{lm}(\vartheta, \varphi)$, to obtain the corresponding Talmi coefficient:

$$r_1^{2n_1+l_1} Y_{l_1 m_1}(\theta_1, \varphi_1) = \left\{R^2 + a^2 r^2 - 2arR\,|\mathscr{Y}_1 y_1 : 00\rangle \frac{4\pi}{\sqrt{3}}\right\}^{n_1}$$

$$\times \sqrt{4\pi} \sum_{F_1=0}^{l_1} \sqrt{\frac{(2l_1+1)!}{(2F_1+1)!(2f_1+1)!}}\, R^{F_1} a^{f_1} r^{f_1} |\mathscr{Y}_{F_1}, y_{f_1} : l_1 m_1\rangle$$

$$= \sum_{s_1 s_2 s_3 F_1} \frac{n_1!}{s_1! s_2! s_3!} (-2)^{s_3} \sqrt{4\pi} \left(\frac{4\pi}{\sqrt{3}}\right)^{s_3} a^{f_1+2s_3+s_3} \sqrt{\frac{(2l_1+1)!}{(2F_1+1)!(2f_1+1)!}}$$

$$\times R^{F_1+2s_1+s_3} r^{f_1+2s_2+s_3} |\mathscr{Y}_1, y_1(0)\rangle^{s_3} |\mathscr{Y}_{F_1}, y_{f_1} : l_1 m_1\rangle.$$

Writing out $r_2^{2n_2+l_2} Y_{l_2 m_2}(\theta_2, \varphi_2)$ in the same manner we can find

$$r_1^{2n_1+l_1} Y_{l_1 m_1} r_2^{2n_2+l_2} Y_{l_2 m_2}$$

$$= \sum_{\substack{s_1 s_2 s_3 F_1 \\ q_1 q_2 q_3 F_2}} (-1)^{s_2+f_2} \frac{n_1! n_2!}{s_1! s_2! s_3! q_1! q_2! q_3!}\, 2^{s_3+q_3} \frac{(4\pi)^{s_3+q_3+1}}{(\sqrt{3})^{s_3+q_3}} \tag{22}$$

$$\times \sqrt{\frac{(2l_1+1)!(2l_2+1)!}{(2F_1+1)!(2f_1+1)!(2F_2+1)!(2f_2+1)!}}\, a^{f_1+2s_3+s_3} b^{f_2+2q_3+q_3} R^{F_1+F_2+2s_1+2q_1+s_3+q_3}$$

$$\times r^{f_1+f_2+2s_2+2q_2+s_3+q_3} |\mathscr{Y}_1 y_1(0)\rangle^{s_3+q_3} |\mathscr{Y}_{F_1 y_{f_1}} : l_1 m_1\rangle |\mathscr{Y}_{F_2 y_{f_2}} : l_2 m_2\rangle.$$

Let us transform the last three factors in eq. (22) similarly to what was done

in deriving eq. (19); we get

$$|\mathscr{Y}_{F_1 f_1}: l_1 m_1\rangle|\mathscr{Y}_{F_2 f_2}: l_2 m_2\rangle$$
$$= \sum_{\lambda} C^{\lambda M_0}_{l_1 m_1 l_2 m_2}|\mathscr{Y}_{F_1 f_1}(l_1); \mathscr{Y}_{F_2 f_2}(l_2): \lambda M_0\rangle$$
$$= \sum_{\lambda L_1 L_2} C^{\lambda M_0}_{l_1 m_1 l_2 m_2}\sqrt{(2l_1+1)(2l_2+1)(2L_1+1)(2L_2+1)}\begin{Bmatrix} F_1 & f_1 & l_1 \\ F_2 & f_2 & l_2 \\ L_1 & L_2 & \lambda \end{Bmatrix}\frac{1}{4\pi} \tag{23}$$
$$\times \sqrt{\frac{(2F_1+1)(2F_2+1)(2f_1+1)(2f_2+1)}{(2l_1+1)(2l_2+1)}}\, C^{L_1 0}_{F_1 0 F_2 0} C^{L_2 0}_{f_1 0 f_2 0}|\mathscr{Y}_{L_1}, y_{L_2}: \lambda M_0\rangle.$$

Finally, using (19) we obtain

$$|\mathscr{Y}_1 y_1(0)\rangle^{s_3+q_3}|\mathscr{Y}_{L_1}, y_{L_2}: \lambda M_0\rangle$$
$$= \left(\frac{\sqrt{3}}{4\pi}\right)^{s_3+q_3+1}\sum_J G(s_3+q_3, J)\sqrt{\frac{3}{2J+1}}\,|\mathscr{Y}_J, y_J(0); \mathscr{Y}_{L_1}, y_{L_2}(\lambda): \lambda M_0\rangle \tag{24}$$
$$= \left(\frac{\sqrt{3}}{4\pi}\right)^{s_3+q_3}\sum_{JLlMm}\begin{Bmatrix} J & J & 0 \\ L_1 & L_2 & \lambda \\ L & l & \lambda \end{Bmatrix} G(s_3+q_3, J)\sqrt{(2\lambda+1)(2J+1)(2L_2+1)(2L_1+1)}$$
$$\times C^{L0}_{J0 L_1 0} C^{l0}_{J0 L_2 0} C^{\lambda M_0}_{LM lM}\mathscr{Y}_{LM}(\theta, \phi)\, y_{lm}(\vartheta, \varphi).$$

Comparing eqs. (22), (23) and (24) it can be shown that

$$\left\langle \begin{matrix} n_1 l_1 m_1 \\ n_2 l_2 m_2 \end{matrix}\middle|\, \mu_1\mu_2 \,\middle| \begin{matrix} NLM \\ n\, l\, m \end{matrix}\right\rangle = \sum_{\lambda} B_\lambda C^{\lambda M_0}_{l_1 m_1 l_2 m_2} C^{\lambda M_0}_{LM lm}, \tag{25}$$

where B_λ does not depend on the projection $m_1 m_2 M m$. The total number of the coefficients B_λ for given $n_1 l_1 n_2 l_2$ is less than that of the usual Talmi coefficients and therefore it is more convenient to use the former, as was done in refs.[2,3,5]). Introducing a more elaborate notation for the coefficients B_λ from (25) we have

$$B_\lambda \equiv \langle n_1 l_1 n_2 l_2: \lambda|\mu_1\mu_2|NLnl: \lambda\rangle$$
$$= \sum_{m_1 m_2 M m} C^{\lambda M_0}_{l_1 m_1 l_2 m_2} C^{\lambda M_0}_{LM lm}\langle \begin{matrix} n_1 l_1 m_1 \\ n_2 l_2 m_2 \end{matrix}|\mu_1\mu_2|^{NLM}_{nlm}\rangle, \tag{26}$$

and finally combining (22), (23), (24), (26) and (28) we obtain

$$\langle n_1 l_1 n_2 l_2: \lambda|\mu_1\mu_2|NLnl: \lambda\rangle = (-1)^{n_1+n_2+N+n}\, 2^{\frac{1}{2}(n_1+n_2+l_1+l_2-N-n-L-l)}$$
$$\times \left[\frac{N!n!(2L+2N+1)!!(2l+2n+1)!!}{n_1!n_2!(2l_1+2n_1+1)!!(2l_2+2n_2+1)!!}\right]^{\frac{1}{2}} \frac{R_0^{2N+L} r_0^{2n+l}}{r_{01}^{2n_1+l_1} r_{02}^{2n_2+l_2}}$$
$$\times \sum (-1)^{s_3+f_2}\frac{n_1!n_2!}{s_1!s_2!s_3!q_1!q_2!q_3!}\, 2^{s_3+q_3}\left[\binom{2l_1}{2F_1}\binom{2l_2}{2F_2}(2L_1+1)(2L_2+1)\right. \tag{27}$$

$$\times(2J+1)(2\lambda+1)\Big]^{\frac{1}{2}} C^{L_1 0}_{F_1 0 F_2 0} C^{L_2 0}_{f_1 0 f_2 0} C^{L 0}_{J 0 L_1 0} C^{l 0}_{J 0 L_2 0} (2l_1+1)(2l_2+1)$$

$$\times G(s_3+q_3, J) a^{f_1+2s_2+s_3} b^{f_2+2s_1+q_3} \begin{Bmatrix} F_1 & f_1 & l_1 \\ F_2 & f_2 & l_2 \\ L_1 & L_2 & \lambda \end{Bmatrix} \begin{Bmatrix} J & J & O \\ L_1 & L_2 & \lambda \\ L & l & \lambda \end{Bmatrix}. \tag{27}$$

Summation in eq. (27) is performed over all values of the subscripts $F_1 F_2 f_1 f_2 s_1 s_2 s_3 q_1 q_2 q_3 L_1 L_2 J$ with the following restrictions:

$$F_1+f_1 = l_1, \qquad F_1 = 0, 1, 2 \ldots l_1,$$
$$F_2+f_2 = l_2, \qquad F_2 = 0, 1, 2 \ldots l_2,$$
$$s_1+s_2+s_3 = n_1, \qquad s_i \geqq 0, \qquad \text{(all } s_i \text{ are integers)},$$
$$q_1+q_2+q_3 = n_2, \qquad q_i \geqq 0, \qquad \text{(all } q_i \text{ are integers)},$$
$$F_1+F_2+2s_1+2q_1+s_3+q_3 = 2N+L,$$
$$f_1+f_2+2s_2+2q_2+s_3+q_3 = 2n+l,$$
$$J = s_3+q_3, s_3+q_3-2, \ldots, 1 \text{ or } 0.$$

The momenta L_1, L_2 assume any values permitted by the triangular rules in vectorial addition

$$\mathbf{F}_1+\mathbf{F}_2 = \mathbf{L}_1, \quad \mathbf{f}_1+\mathbf{f}_2 = \mathbf{L}_2, \quad \mathbf{J}+\mathbf{L}_1 = \mathbf{L}, \quad \mathbf{J}+\mathbf{L}_2 = \mathbf{l}, \quad \mathbf{L}_1+\mathbf{L}_2 = \boldsymbol{\lambda} \tag{28}$$

Besides, the Clebsch-Gordan coefficients with zero projections ensure that the first four equations (28) contain only such L_1, L_2, J that the parities of both sides of these equations are equal.

It will be noted that in eq. (27) we have $a = (r_{01}/r_0)^2$, $b = (r_{02}/r_0)^2$. The $9j$ symbols in this formula offer no special difficulties for calculations since one of them contains a zero momentum and in the other $F_1+f_1 = l_1$ and $F_2+f_2 = l_2$. We have

$$\begin{Bmatrix} J & J & 0 \\ L_1 & L_2 & \lambda \\ L & l & \lambda \end{Bmatrix} = (-1)^{-l-L_1+\lambda+J} W(lLL_2L_1 : \lambda J) \frac{1}{\sqrt{(2\lambda+1)(2J+1)}}.$$

The formula for the second $9j$ symbol can be obtained if the latter is expressed through the Racah coefficients W (see for example ref. [6])) and the formulas of ref. [9]) are used. As a result we have

$$\begin{Bmatrix} F_1 & f_1 & l_1 \\ F_2 & f_2 & l_2 \\ L_1 & L_2 & \lambda \end{Bmatrix} = (-1)^{L_1+L_2+\lambda} \Big[\frac{(2F_1)!(2F_2)!(2f_1)!(2f_2)!}{(2l_1+1)!(2l_2+1)!(F_1+l_1-F_2)!(F_1+F_2-L_1)!}$$

$$\times \frac{(L_1+F_2-F_1)!(L_2+f_1-f_2)!}{(F_1+F_2+L_1+1)!(f_1+L_2-f_1)!(f_1+f_2-L_2)!(f_1+f_2+L_2+1)!} \Big]^{\frac{1}{2}}$$

$$\times \sum_x \frac{(2x+1)W(L_1L_2l_1l_2:\lambda x)}{(f_1+f_2-x)!\,(f_1+F_2+x+1)!}\left[\frac{(l_1+L_1+x+1)!(l_2+L_2+x+1)!}{(L_1+x-l_1)!(L_2+x-l_2)!}\right.$$
$$\left.\times (l_1+x-L_1)!(l_2+x-L_2)!(L_1+l_1-x)!(L_2+l_2-x)\right]^{\frac{1}{2}}.$$

The formula for an important particular case $n=0$ and $l=0$ is especially simple:

$$\langle n_1l_1n_2l_2:\lambda|\mu_1\mu_2|N\lambda 00:\lambda\rangle$$
$$=(-1)^{n_1+n_2+N}\,2^{\frac{1}{2}(n_1+n_2+l_1+l_2-N-\lambda)}\left[\frac{N!(2\lambda+2N+1)!!}{n_1!\,n_2!(2l_1+2n_1+1)!!(2l_2+2n_2+1)!!}\right]^{\frac{1}{2}} \tag{29}$$
$$\times\frac{R_0^{2N+\lambda}}{r_{01}^{2n_1+l_1}r_{02}^{2n_2+l_2}}C^{\lambda 0}_{l_1 0 l_2 0}\sqrt{\frac{(2l_1+1)(2l_2+1)}{(2\lambda+1)}}.$$

This formula as well as the relation

$$\langle 00nl:l|\mu_1\mu_2|00nl:l\rangle=\left(\frac{\mu_1}{\mu_1+\mu_2}\right)^{\frac{2n+l}{2}} \tag{30}$$

is applied to the calculation of the reduced widths for the emission of d, t and α particles by the method of ref. [8]).

TABLE 1

Coefficients $\langle 0l_101:\lambda|\mu_1\mu_2|NLnl:\lambda\rangle$

$NLnl:\lambda$	$l_1=0$	$l_1=1$
0001 : 1	$-\left(\frac{\mu_1}{\mu_1+\mu_2}\right)^{\frac{1}{2}}$	
0100 : 1	$\left(\frac{\mu_2}{\mu_1+\mu_2}\right)^{\frac{1}{2}}$	
0200 : 2		$\frac{(2\mu_1\mu_2)^{\frac{1}{2}}}{\mu_1+\mu_2}$
1000 : 0		$\frac{(2\mu_1\mu_2)^{\frac{1}{2}}}{\mu_1+\mu_2}$
0002 : 2		$-\frac{(2\mu_1\mu_2)^{\frac{1}{2}}}{\mu_1+\mu_2}$
0010 : 0		$-\frac{(2\mu_1\mu_2)^{\frac{1}{2}}}{\mu_1+\mu_2}$
0101 : 0		$\frac{\mu_2-\mu_1}{\mu_1+\mu_2}$
0101 : 1		1
0101 : 2		$\frac{\mu_2-\mu_1}{\mu_1+\mu_2}$

With our selection of variables it is impossible to obtain simple relations of symmetry of the Talmi coefficients with respect to the permutation of the quantum numbers $n_1 l_1$ and $n_2 l_2$ or NL and nl. The calculation of certain coefficients can be simplified by using the unitarity of the Talmi transformation and by passing, not from $n_1 l_1 n_2 l_2$ to $NLnl$, but the other way round. The corresponding formula can easily be obtained in a similar manner.

The dependence of the usual Talmi coefficients [1]) on the projection of momenta is established by eqs. (25) and (26). The dependence of these coefficients on the relation of the masses μ_1 and μ_2 in the general formula (27) is not sufficiently transparent, since the relations of masses enters the sum through a and b.

To illustrate this dependence table 1 gives values for some of the Talmi coefficients.

In conclusion I express gratitude to V. V. Balashov and V. G. Neudachin for discussion of the present paper.

References

1) I. Talmi, Helv. Phys. Acta **25** (1952) 185
2) M. Moshinsky, Nuclear Physics **13** (1959) 104
3) H. S. Mang, Z.f. Phys. **148** (1957) 582
4) A. Arima and T. Teresawa, Progr. Theor. Phys. **23** (1960) 115
5) V. V. Balashov and V. A. Eltekov, Nuclear Physics **16** (1960) 423
6) A. Edmonds, Angular Momentum in Quantum Mechanics (Princeton, 1957)
7) J. P. Elliott, Proc. Roy. Soc. A. **245** (1958) 562
8) V. V. Balashov *et al.*, JETP **37** (1959) 1385
9) L. G. Bidenharn *et al.*, Rev. Mod. Phys. **24** (1952) 249

1.E.4:
3.A

Nuclear Physics **27** (1961) 188—192; © *North-Holland Publishing Co., Amsterdam*
Not to be reproduced by photoprint or microfilm without written permission from the publisher

NUCLEAR RESONANCE FLUORESCENCE MEASUREMENTS ON THE 845 keV LEVEL IN Fe^{56}

W. H. KELLY

Department of Physics and Astronomy, Michigan State University, E. Lansing, Michigan, U.S.A †

and

G. B. BEARD

Department of Physics, Wayne State University, Detroit, Michigan, U.S.A. †

Received 17 April 1961

Abstract: Nuclear resonance fluorescence has been observed for the 845 keV level of Fe^{56}. A gaseous source of Mn^{56} as $MnCl_2$ was used in order to utilize the recoil due to previous radiations to compensate for the recoil Doppler broadening of the emission and absorption lines. Resonant self-absorption measurements gave a half-life of 6 ± 2 p sec for the state.

1. Introduction

The life time of the 845 keV 2^+ state of Fe^{56} has been measured previously using the methods of nuclear resonance fluorescence [1]) and Coulomb excita-

TABLE 1

Experimental half-life of the 845 keV state of Fe^{56}

Half-life (p sec)	Method	Ref.
6.0 ± 0.9	Coulomb excitation (4.0, 6.5 MeV alphas)	Temmer and Heydenberg [3])
8.7	Coulomb excitation (15.9, 35 MeV N^{14})	Alkazov *et al.* [4])
10	Coulomb excitation (16.3, 36.0 MeV N^{14})	Andreyev *et al.* [2])
6.5 ± 1.6	Coulomb excitation (30.5 MeV O^{16})	Adams *et al.* [5])
6.5	Coulomb excitation (27 MeV O^{16})	H. E. Gove and C. Broude [6])
>5.5	Nuclear resonance fluorescence, liquid source, (Mn^{56} decay)	Ilakovac [1])
$6\ \pm2$	Nuclear resonance fluorescence, gaseous source, (Mn^{56} decay)	this work

† Work supported in part by the United States Air Force under contract no. AF 49(638)-10 monitored by the Air Force Office of Scientific Research of the Air Research and Development Command.

tion [2–6]). Ilakovac [1]) in nuclear resonance scattering experiments using a liquid source, was not able to detect any resonant scattering. Since the mean collision time expected [1]) is of the order 7×10^{-14} sec, the absence of a positive effect was taken to indicate the half-life of the state is longer than 5.5 p sec. This result and those of the Coulomb excitation experiments are summarized in table 1. Since there is some discrepancy in the values quoted [2–6]), it was felt that a new investigation using nuclear resonance fluorescence measurements would be worthwhile.

2. The Experiment and Results

According to the presently accepted decay scheme [7]) of 2.56 Mn^{56}, the 845 keV state of Fe^{56} is fed by a 2.86 MeV beta in 60 % of the decays, by a 1.05 MeV beta and 1.81 MeV gamma in cascade in 24 % of the decays, by a 0.750 MeV beta, 2.12 MeV gamma in 15 % of the decays, and by a 0.33 MeV beta and 2.52 MeV gamma in less than 1 % of the decays. Sufficient energy is available to enable one to make use of the recoil due to the transitions populating the 845 keV state to compensate for the recoil Doppler shift occurring in the emission and absorption of the 845 keV gamma. Since the lifetime of the state is of the order of 10^{-11} sec, it is desirable to use a gaseous source so that only a small fraction of the recoiling Fe^{56} nuclei will undergo collisions with a resultant loss of momentum memory before being deexcited to the ground state.

Several samples of $MnCl_2 \cdot 4H_2O$ weighing 4—7 mg were heated to a few hundred degrees in a vacuum to drive off the waters of crystallization and then vacuum distilled into quartz ampoules ($\approx$ 3 ml volume). The encapsulated samples were irradiated for periods of 5—8 h in a thermal neutron flux of $\approx 5 \times 10^{12}$ n $cm^{-2} \cdot sec^{-1}$ in the University of Michigan Ford Reactor.

Fig. 1 shows the experimental arrangements used for the scattering and absorption measurements. An iron ring 30.5 cm in diameter, 10.2 cm high and 1.27 cm thick, was used as the resonant scatterer and a similar one made of copper was used for comparison measurements. No resonant scattering was noted at room temperature. Fig. 2 shows the scattering obtained in a typical 10 min run with the source heated to approximately 970° C. Shown also, for comparison, is the scattered counting rate obtained with the non-resonant scatterer corrected for decay of the source. The relatively high non-resonant counting rate is mainly due to the inelastic scattering of the higher energy gammas that are present.

The resonant scattering is of sufficient magnitude to make possible the determination of the life-time of the 845 keV state by self-absorption measurements [8, 9]). The position and shape of the absorbers used are shown in fig. 1 by broken lines. Table 2 gives a summary of the results obtained with resonant (Fe) and non-resonant (Cu) absorbers. The two absorbers were matched to

within 1.5 % for electronic absorption with the source at room temperature. Runs to determine the resonant absorption were of 10 min. duration each, and were made in the following repeating order: no absorber, Cu absorber, Fe absorber, no, Fe, Cu. These runs were approximately evenly spaced in time.

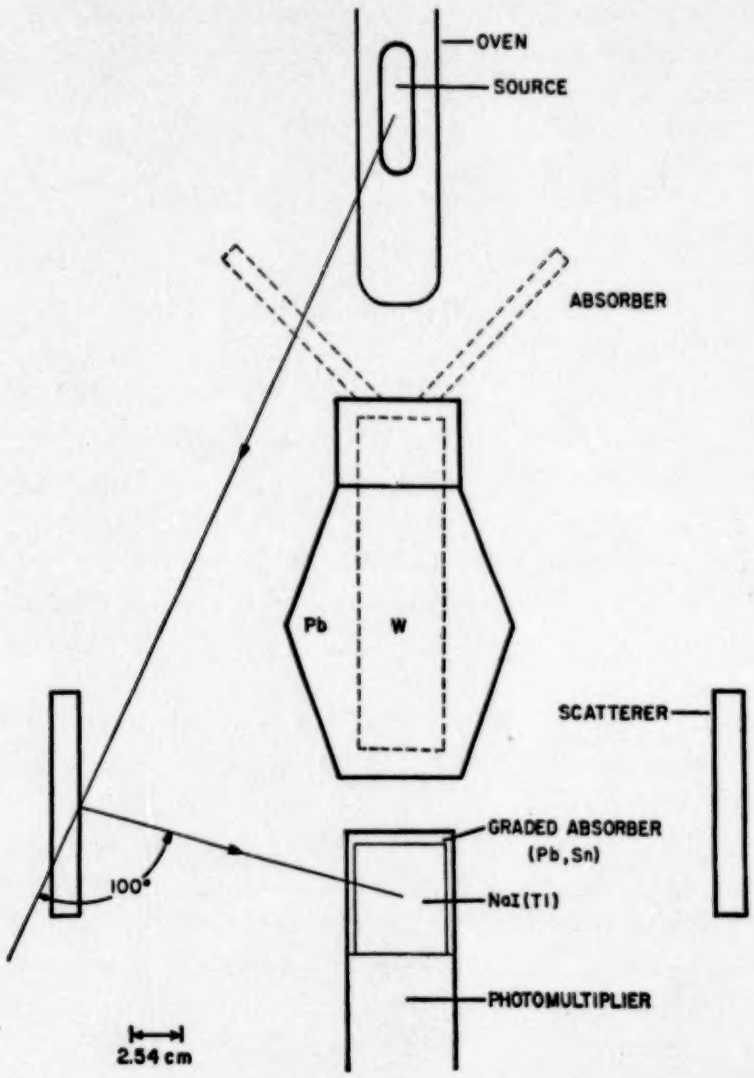

Fig. 1. The experimental arrangement for the resonant scattering and self-absorption measurements.

This facilitated the corrections for source decay and for pulse-height analyzer dead time. The absorbers were lined with thin sheets of aluminium foil which acted as a heat reflector thereby maintaining the temperatures of the absorbers to within 10° C of room temperature.

The thin absorber approximation was used to determine the resonant absorption cross section [8, 9]). Using it, a level width of $(7.3 \pm 2.5) \times 10^{-3}$ keV for the 0.845 MeV state is found. From the uncertainty relation one obtains

a half-life of 6 ± 2 p sec for this state. This value is also given in table 1 for comparison with the Coulomb excitation measurements.

The life time of the state can also be determined from the measured counting

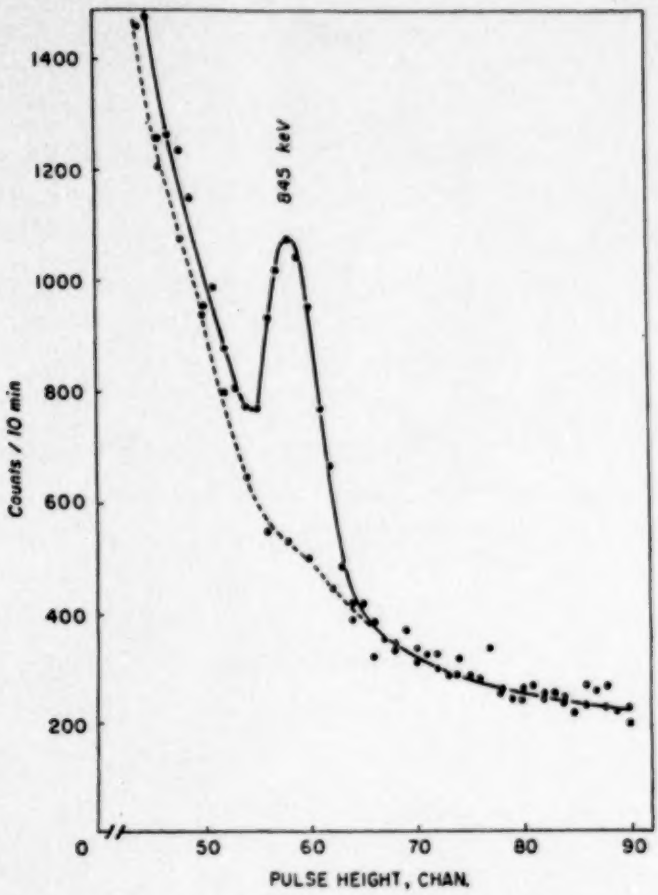

Fig. 2. Resonantly scattered 845 keV quanta. The top curve was taken with the source at approximately 970°C and the lower curve was taken with a non-resonant scatterer. These data are from a typical set of 10 min runs. They have been corrected for room background and source decay.

TABLE 2

Results of resonant absorption measurements

Absorber	Direct	Resonance effect
Copper absorber	1.00	1.00
Iron absorber	1.015 ± 0.002	0.957 ± 0.009

The counting rates are quoted relative to those with the copper absorber.

rate of the resonantly scattered quanta. In order to make such a calculation it is necessary that the emission line shape be known. Since the 845 keV excited state of Fe^{56} is reached by several different ways in the decay of Mn^{56} and the details of the breakup of the $MnCl_2$ molecule would be involved, the emission

line shape in this case would be difficult to determine. No attempt was made to analyze the data in this way.

The transition probability obtained here is approximately 16 times that predicted for single particle transitions. Other E2 transition probabilities in even A nuclei in this mass region are found with approximately the same degree of enhancement [1, 10]).

We would like to acknowledge the assistance of Mrs. Mary Spaeth in the recording of the data, and the assistance of Mr. W. B. Chaffee and Dr. M. Garber in the preparation of the encapsulated sources. We wish to thank Dr. C. Kikuchi, Mr. Wm. Dunbar and the staff of the University of Michigan Ford Reactor for their kind assistance and hospitality during these measurements.

Note added in proof: Recently, F. Metzger (Nuclear Physics, to be published) has made a similar measurement using Co^{56} as a source and obtained a half-life of 7.3 ± 1.2 p sec for the 845 keV state. This result is in agreement with our value of 6 ± 2 p sec.

References

1) K. Ilakovac, Proc. Phys. Soc. **67** (1954) 601
2) D. S. Andreyev, A. P. Grinberg, K. I. Erokhina and I. Kh. Lemberg, Nuclear Physics **19** (1960) 400
3) G. M. Temmer and N. P. Heydenburg, Phys. Rev. **104** (1956) 967
4) D. G. Alkazov, A. P. Grinberg, L. I. Yeorkhina and I. Kh. Lemberg, Izvest. Akad. Nauk. SSSR, Ser. Fiz. **23** (1959) 233
5) B. M. Adams, D. Eccleshall and M. J. L. Yates, In Proc. Second Conf. reactions between complex nuclei ed. by A. Zucker, E. D. Halbert and F. T. Howard (John Wiley and Sons, Inc., New York, 1960) p. 95
6) H. E. Gove and C. Broude, in Proc. Second Conf. reactions between complex nuclei, ed. by A. Zucker, E. D. Halbert and F. T. Howard (John Wiley and Sons, Inc., New York, 1960) p. 65
7) Nuclear Data Sheets, NRC 59-4-51
8) F. R. Metzger, Phys. Rev. **103** (1956) 983
9) F. R. Metzger, Progress in nuclear physics, vol. 7, ed. by O. R. Frisch (Pergamon Press, New York, 1959)
10) D. E. Alberger in Handbuch der Physik, vol. XLII, ed. by S. Flugge (Springer-Verlag, Berlin, 1957 p. 1

2.E: 2.L

Nuclear Physics **27** (1961) 193—203; © *North-Holland Publishing Co., Amsterdam*

Not to be reproduced by photoprint or microfilm without written permission from the publisher

INELASTIC PROTON SCATTERING ASYMMETRIES AT 8.9 MeV

A. BUDZANOWSKI †, R. W. CLIFFT and B. HIRD ††

University of Liverpool

Received 11 March 1961

Abstract: The asymmetry in the inelastic scattering of a polarized proton beam from a magnesium target has been measured at a number of angles and at three different energies. A comparison between the inelastic asymmetries and the corresponding elastic asymmetries shows that in all cases they have opposite sign.

1. Introduction

Following the great success of the optical model to describe eleastic proton scattering angular distributions, there have been several theoretical attempts to account for inelastic proton scattering differential cross sections by a direct process [1–3]).

In these calculations the transfer of energy from the bombarding nucleon is assumed to occur, not with the nucleus as a whole, but only in a restricted region. Sometimes it is a region of the nuclear configuration, as when the energy interchange is confined to a few extra-core nucleons, or to a mode of collective excitation, and sometimes the restriction is spatial, the reaction being confined to the nuclear surface. In some calculations both restrictions are applied simultaneously.

Before and after this energy interchange occurs, the nucleon is assumed to move in a distorting potential of the type assumed for elastic scattering. At medium energies the experimental angular distributions are very far from the $J_L(QR)$ dependence predicted by a plane wave theory, so that it is evident that at these energies the distorting potentials before and after the energy exchange play an important part. It has been suggested both by detailed comparison with experiment [4]) and analytically [5]) that the potential well depth required for these distortions in inelastic scattering is less than that required for the corresponding elastic scattering process.

In optical model analysis it has been found advantageous in fitting experimental differential cross sections to include a spin dependent part to the potential. This has been confirmed directly, with a more accurate determination of the spin orbit potential, by experimental measurements of the angular

† Now at the Institute for Nuclear Research Cracow, Poland

†† Now at Queen Mary College, London

distribution of the polarization produced in the scattering. It seems probable that in a similar way the distorting potentials encountered in inelastic scattering will be found to be spin dependent, and, since these potentials have such a profound effect on the differential cross sections, it seems likely that the spin dependent part will also be the cause of significant polarization.

There is another source of polarization which has no counterpart in elastic scattering. This is due to the transfer of spin as well as angular momentum in the energy interchange part of the reaction. For this type of polarization the situation is somewhat similar to that in the distorted theory of stripping where the orbital angular momentum and spin transfer is accompanied also by the transfer of a nucleon. There has been extensive theoretical investigation of this source of stripping polarization [6, 7]) and many of the rules can immediately be transferred to the case of inelastic scattering. These are as follows: without distortion of the ingoing or outgoing waves, the spin transfer is unable to produce any polarization in the emitted particle, but a combination of central distortion and spin transfer can produce a sizeable polarization whose sign depends on whether the distortion is considered to be in the ingoing or the outgoing wave. When the central distortions occur in both, they have substantially opposite effects and it can be shown [8, 19]) that under certain conditions they will cancel each other out. For inelastic scattering these conditions are that a) the proportion of energy transferred in the reaction must be small and b) the ingoing and outgoing potentials are equal. In so far as these are good approximations this part of the reaction process is unlikely to contribute significantly to the polarization. A consequence of this is that one should not expect the experimental polarization to show, for example, the difference in shell model configurations between the ground state and the final excited state of the target nucleus. In the case of inelastic scattering to the first excited state of Mg^{24} where the difference between the two levels seems to be mainly collective, involving no change in the intrinsic spin configuration, there should be a further reduction in the effects produced by this source of polarization.

The reciprocal nature of the polarization and the asymmetry is not strictly valid for inelastic scattering, but under the approximation that the proportion of energy transferred to the target is small the two will probably be very similar [7])

Recently Yamamuro *et al.* [9]) have shown that in the energy range of our measurements, both the elastic and inelastic scattering differential cross sections of the reaction we have investigated, Mg^{24} (p, p) Mg^{24}, show considerable resonance structure (fig. 1). The assumptions necessary to describe the reaction as purely direct are not therefore valid. However, it is known that in such situations the polarization in elastic scattering is at least similar to that predicted by the optical model [10–12]. We can expect the same thing to apply in general to the inelastic process. In order to obtain some idea of the importance

of resonances in confusing the simple picture proposed for inelastic scattering asymmetries, we have used an energy resolution comparable to what appears to be the resonance spacing, and made measurements on, and between two of them. The elastic group asymmetry was also measured at the same angles and energies as that of the inelastic group in order to make a comparison between the two processes.

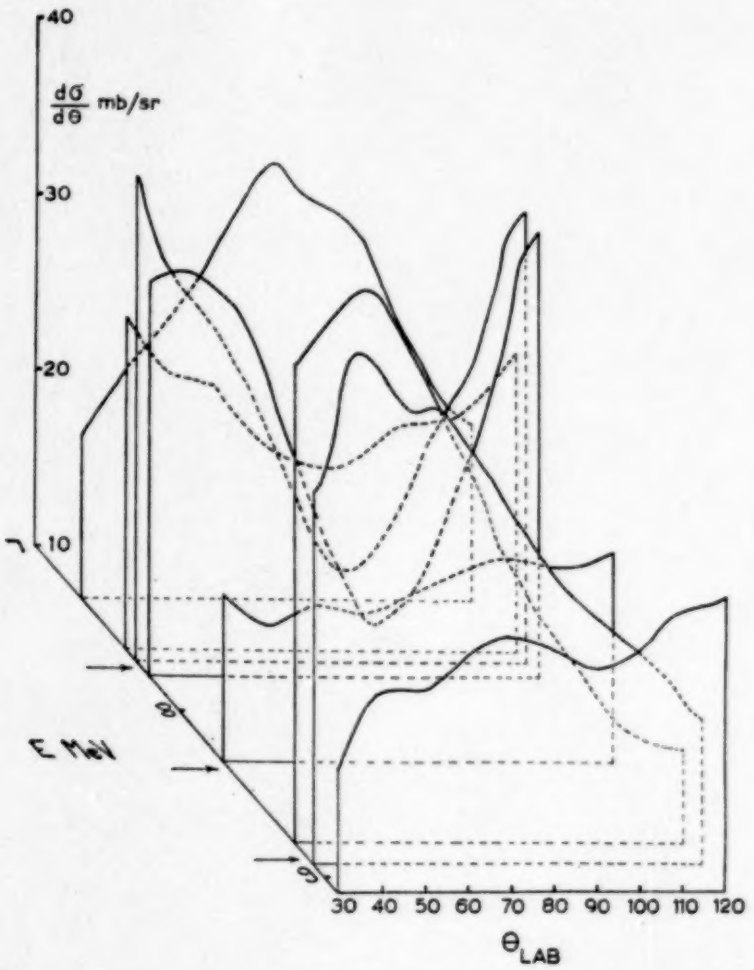

Fig. 1. The energy variation of the differential cross section of the reaction Mg^{24} (p,p) Mg^{24}, $Q = -1.37$ MeV. Taken from Yamamura *et al.* [9])

2. Experimental arrangement

The polarized proton beam was produced by the C^{12} (d, p) C^{13} stripping reaction, a graphite target being placed in the internal deuteron beam of the 37 inch cyclotron [13]). The stripped protons, emitted at 45° from the target, passed through a hole in one of the dees and emerged from the cyclotron. The proton focussing system differed from that used in previous measurements. A large 12 cm aperture quadrupole lens was placed close to the cyclotron and this, together with the cyclotron fringe field, produced an image about 1 cm^2

at a distance of 6 m from the cyclotron. In order to remove any deuterons having the same momentum as the protons, which would otherwise reach the second target, an electrostatic separation system was used, consisting of a roughly uniform electric field region 80 cm long and placed 2 m from the focus. This deflected the protons through an angle of 1.3° which was sufficient entirely to free the proton focus from deuterons.

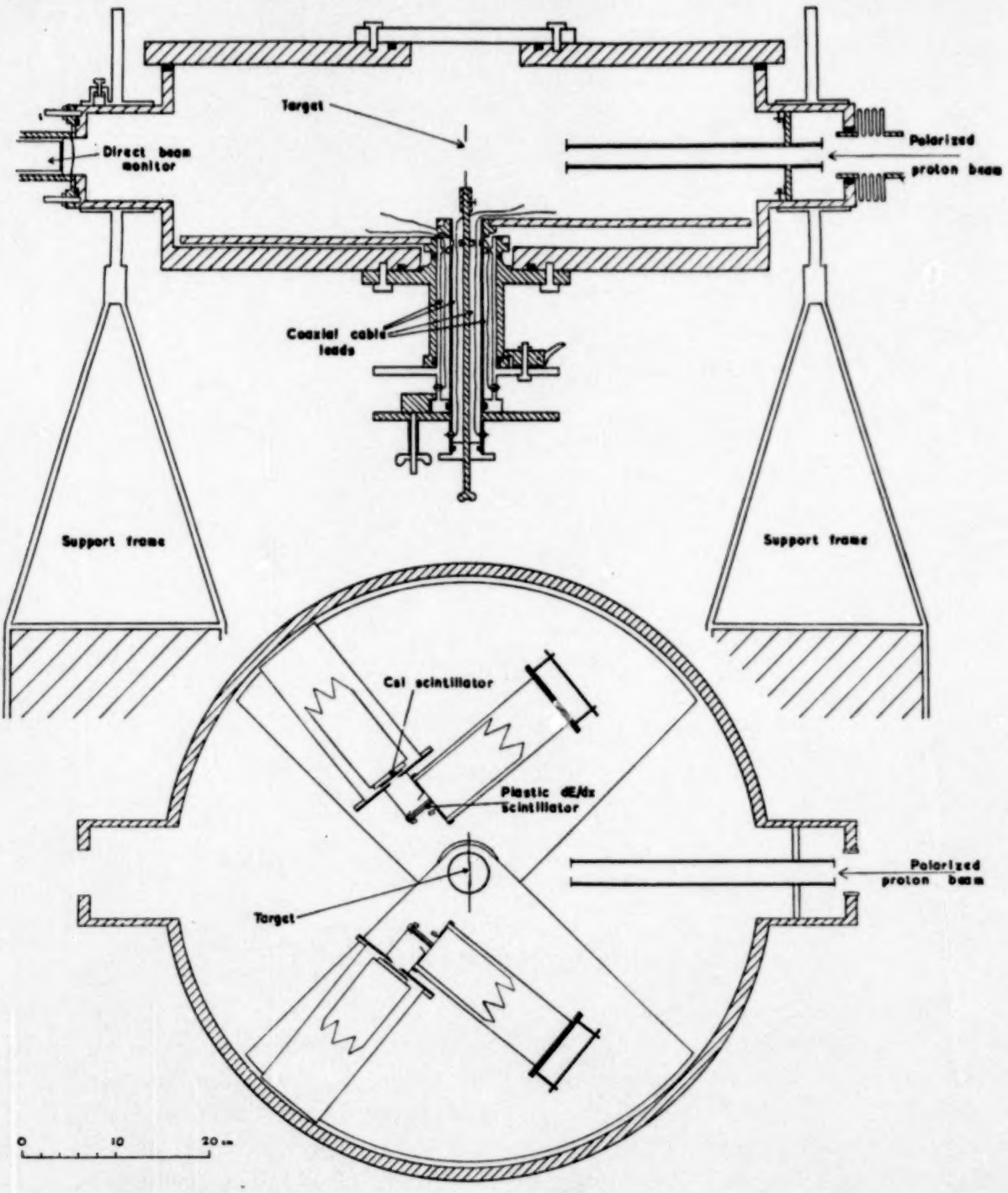

Fig. 2. The scattering chamber.

The scattering chamber is shown in fig. 2. It contained two identical counter telescopes, each made up of a thin plastic dE/dx scintillator and a thick CsI scintillator, and these were used to detect the scattered protons at identical angles, left and right. During measurements the pulse height spectrum of each CsI counter, which was coincident with the dE/dx pulses, was continuously recorded and the asymmetry was calculated from the areas under the appropriate proton group peaks in these spectra. The design of the chamber was such that the angle of the counters could be changed and reset to $\frac{1}{2}°$ from outside the chamber. An external screw system also enabled the angle of the target to be changed, or the target itself to be entirely screwed out of the beam for background measurements. With 9 mm beam slits and 9 mm slits covering the CsI crystals the angular resolution was $\pm 2°$ at all the angles of measurement.

The scattering chamber was supported so that it could be rotated about an axis which was lined up accurately parallel to the beam direction. Measurements were made with the chamber right way up and with it upside down, so effectively interchanging the counters. Many of the geometrical errors and the effects of differing counter efficiencies do not appear when the asymmetry is calculated from the product of the two left-right counting ratios as measured in the two positions. Errors due to proton beam misalignments were also minimised by fixing the slit system to the scattering chamber so that it rotated in one unit with the counters. During measurements the chamber was turned over once an hour to reduce the effects of long term drifts.

To determine the polarization of the proton beam a helium gas cell replaced the magnesium target at the centre of the scattering chamber, and the left-right asymmetry was measured at a nominal scattering angle of 75°. The phase shift analyses [14]) of the helium scattering have been made at energies of 9.485 MeV and 7.5 MeV and the polarizations which they predict are large and differ only slightly over the range of angles used in the helium calibration. In view of the difficulty in estimating the error in these phase shift calculations of the polarization, the 9.485 MeV data were used without any attempt at interpolation to the actual beam energy of 8.9 MeV. To define accurately the geometry of the helium gas which acted as the target, extra slits were placed in front of each dE/dx counter so that a numerical integration of the product of the polarization cross section and solid angle could be made over the range of angles corresponding to the helium scattering geometry. As a result of this calibration measurement the proton beam was found to have a polarization -44.2 ± 3.4 %, in good agreement with other data on the polarization in the reaction $C^{12}(dp)C^{13}$ at 45°.

The magnesium target consisted of natural isotopic content, 99.9 % purity metal rolled to 20 μm thickness. This represented 0.14 MeV energy loss to normally incident protons. Several strips of the metal were fastened horizontally across the support frame in order to cover as much as possible of the

beam cross section and at the same time minimise the left-right thickness variations.

3. Errors

The scattering chamber was constructed so that the axis of rotation of the counters in the chamber and the centre line of the slits defining the beam could both be made to intersect the axis of rotation of the chamber to within 0.1 mm. With the method adopted for measuring the asymmetry this error would have a negligible effect. On the other hand any relative movement of the counters inside the chamber would have a serious effect on the results and this part of the apparatus was rigidly made to withstand any flexing on inversion.

There are two errors which are not reduced by the rotation of the chamber, one due to the difference in direction between the beam and the axis of rotation and the other to the non-uniform illumination of the slit system by the beam. It proved possible to detect both these errors simultaneously by traversing one of the counter telescopes, with a much reduced slit width, in small angular steps through the proton beam, and then comparing the resulting beam profiles obtained with the chamber in the two positions. Any difference in the angular position of the beam edges was due to the angular error, the rotation axes not being parallel to the beam, whereas differences in the shape of the beam profile gave an indication of any uneven slit illumination. Fine adjustments to the latter were made by altering the electrostatic deflector voltage and it proved possible to set the mean position of the beam to 0.1 mm. However, the internal graphite target of the cyclotron was gradually eroded during the measurements, causing a shift of the source of protons, and therefore of the image, so a figure of 0.5 mm was adopted in calculating this error. The angular error between the beam and the rotation axis measured from the beam profile method was found to be $0.2° \pm 0.1°$.

As a check on these geometrical errors, measurements were made of the asymmetry in proton elastic scattering from gold at 25°, and a value of $2 \pm 3\%$ was obtained. This would be particularly sensitive to these errors because that part of the asymmetry which depends on geometrical misalignments is also proportional to the rate of variation of the differential cross section with angle, and this latter quantity was at least 10 times larger for 25° Coulomb scattering than for the inelastic scattering measurements. In the elastic scattering from magnesium it decreases from the value at 25° as the angle is increased.

4. Results

Fig. 3 shows a typical pulse height spectrum obtained from one of the counter telescopes. The resolution was not sufficient to prevent overlap of the two groups and this region had to be divided up between the two groups.

Two symmetrical distributions were therefore constructed which, when added together, produced the experimental shape. The rather arbitrary nature of this construction was allowed for in the error calculation by treating the smaller count in each channel where there was overlap as if it where a background correction, slightly increasing the final statistical error. The actual background from slit scattering, neutrons and γ rays, as determined with the magnesium target screwed out of the beam, was confined to smaller channels than were used in the asymmetry calculations, and no correction was necessary for it in any of the measurements.

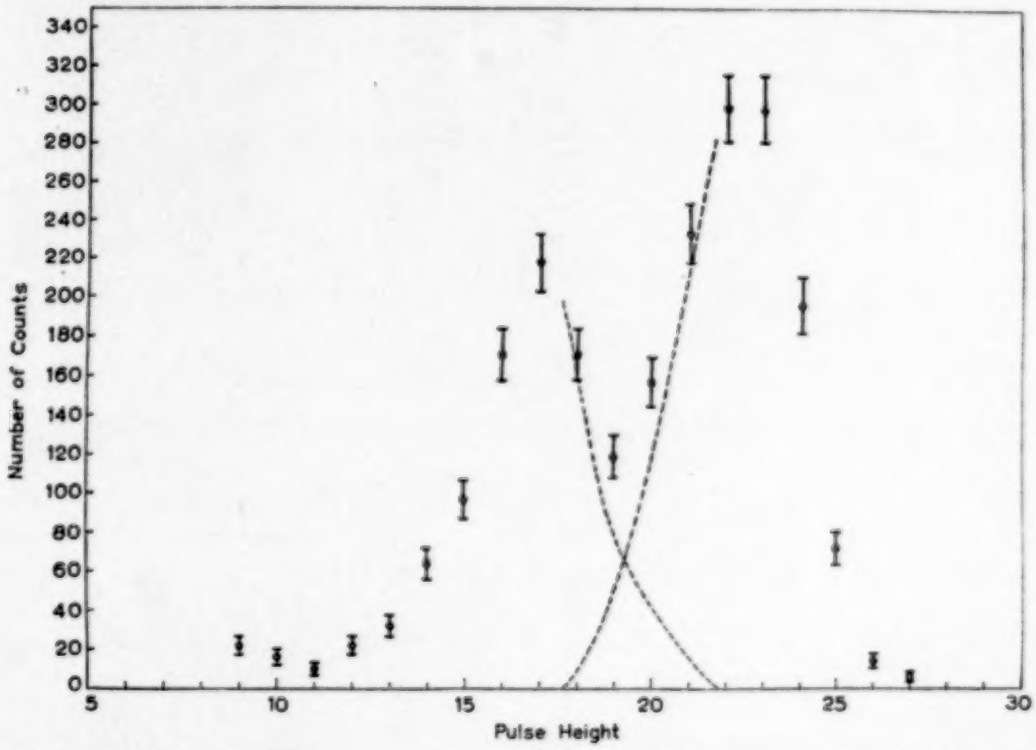

Fig. 3. A typical pulse-height spectrum of one of the counter telescopes. Scattering left at 75°, showing the incomplete resolution of the elastic and the inelastic proton groups. The lines show the method of dividing up the overlapping region between the two peak areas.

Because of the overlap of the two groups it was impossible to measure the inelastic asymmetry at angles less than 50° where the large Coulomb cross section for elastic scattering predominated.

For scattering angles up to 75° the target was set perpendicular to the incident beam, but for greater angles it was found that the target thickness reduced the resolution too much, and it was therefore set at the optimum angle for one counter only. The other counter then had a poorer energy resolution and was used effectively only as a monitor, the combined area of the ground state and first excited state groups being compared with the same quantity in the good resolution spectrum to provide the geometrical and beam intensity cancellation parts of the asymmetry calculation.

In order to obtain an indication of the energy dependence of the asymmetries, the energy was reduced in two successive steps by placing appropriate thicknesses of aluminium foil over the last slits in the proton beam. These foils had a negligible effect on the energy and directional spreads of the beam. The results of the measurements are shown in table 1 and graphically in fig. 4.

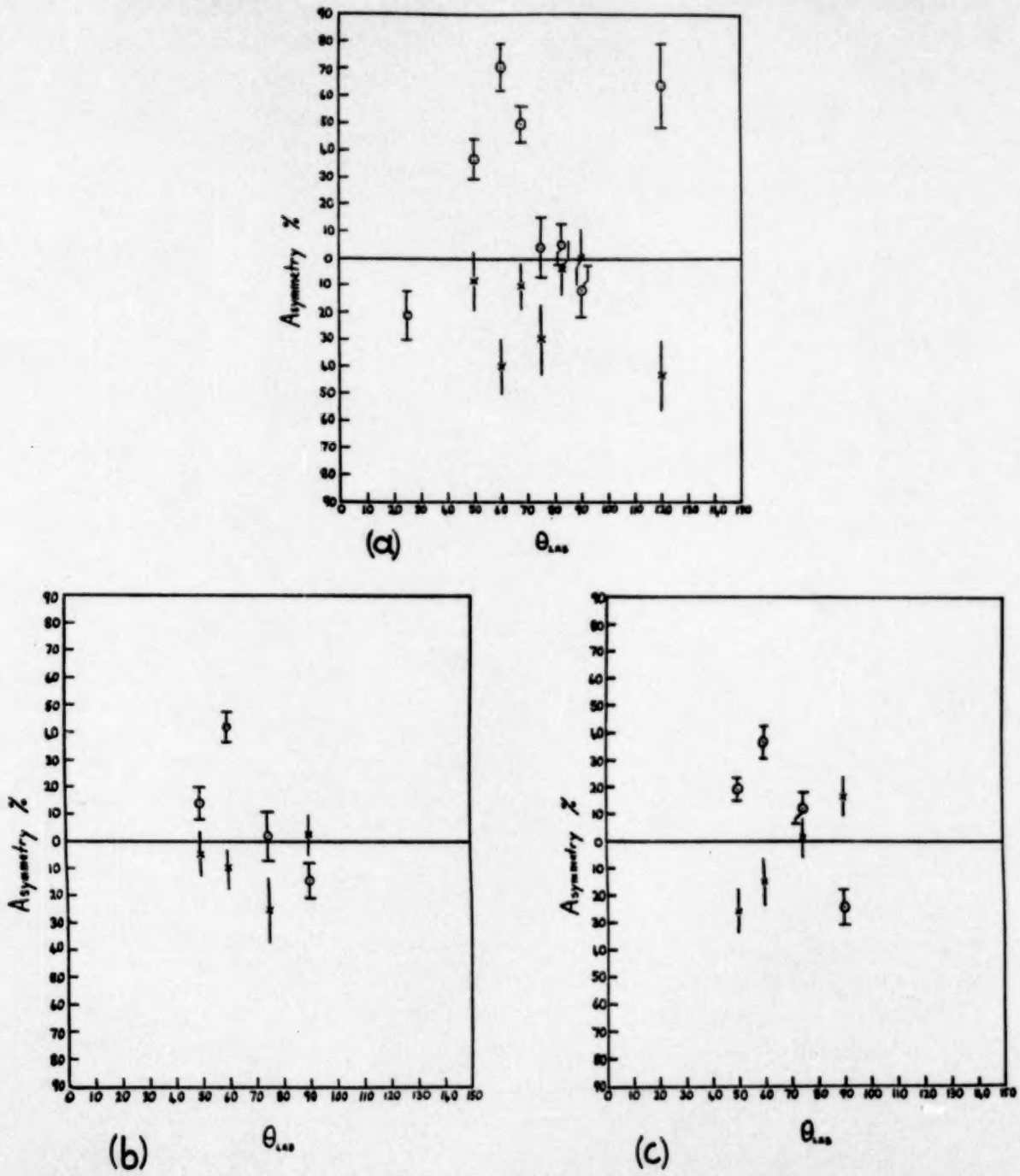

Fig. 4. The left-right asymmetry in elastic scattering and in the inelastic scattering of protons which leave Mg^{24} in the first excited state. Normalised to 100 % incoming proton polarization. (a) at 8.9 MeV, (b) at 8.35 MeV and (c) at 7.75 MeV. The inelastic scattering asymmetry is shown by crosses and the elastic scattering asymmetry by circles.

TABLE 1

Measurements of elastic and inelastic asymmetry

Proton energy (MeV)	Scattering angle (Lab)	Elastic asymmetry %	Inelastic asymmetry %
8.9	25°	−21±9	
	50°	+37±7	− 8±11
	60°	+71±8	−40±11
	67.5°	+50±7	−10±9
	75°	+ 4±11	−30±13
	82.5°	+ 5±8	−3 ±10
	90°	−12±10	+1 ±10
	120°	+64±15	−43+13
8.35	50°	+14±6	− 4±8
	60°	+42±5	−10±8
	75°	+ 2±9	−25±12
	90°	−14±6	+ 3±7
7.75	50°	+19±4	−26±8
	60°	+37±6	−15±9
	75°	+13±6	+ 1±7
	90°	−24±6	+17±7

5. Discussion

The outstanding feature of these results, apart from the large difference between the elastic and inelastic asymmetries is that they have everywhere the opposite sign. This seems to apply at all energies. When one asymmetry changes sign at some angle the other does also, but in the opposite direction.

A direct interaction theory which would satisfactorily account for this opposite sign is an extension of that given by Blair [15]) for α particle scattering. Blair calculated the classical Fraunhofer diffraction scattering of a totally absorbing nucleus whose changes in shape correspond to rotational excitations. He found that for the excitation of states with the same parity as the ground state, the case for the 1.37 MeV level of Mg^{24}, the scattering amplitude angular variation was made up of $J_L(QR)$ terms of even order. The corresponding Fraunhofer elastic scattering amplitude has an angular dependence $J_1(QR)/QR$. When QR is fairly large the even ordered $J_L(QR)$ oscillate out of phase with the $J_1(QR)$. If this theory were extended to spin half particles, the strong angular relationship between the gradient of the differential cross section and the polarization [16]) in distorted wave calculations would produce the opposite sign required in the experiment.

A direct surface interaction theory of this type is clearly inconsistent with the experimental differential cross section data. The angular variations show little indication of a diffraction pattern, so that the optical model distorting potentials are evidently not strong enough to confine the reaction to the surface. Also it is very doubtful if a direct interaction of any sort could account for the observed rapid changes of the differential cross section with energy, which are more likely to be the effect of resonance structure in some of the partial waves.

However there is some possibility that the asymmetry emphasizes surface effects in the scattering more strongly than does the differential cross section. This is because the nuclear potential is approximately independent of the spin direction in the central regions of the nucleus and becomes more and more spin dependent towards the surface, partly because the spin orbit potential may peak there, and partly because higher order partial waves are then involved. In this way the central region may contribute little to the asymmetry, though it does to the scattering. The surface enhancement effect ought also to some extent to apply to the resonance structure if this enters the asymmetry mainly through interference terms.

There is some justification therefore for attempting to use a surface diffraction theory to account for the general features of the asymmetry even though this approach clearly cannot be justified for the differential cross section.

If a reduced potential well depth is required in inelastic scattering calculations, compared to that required for the elastic scattering, it will have some effect on the relative angular positions of their respective asymmetry oscillations; reducing the potential has the effect of spreading out the diffraction pattern to larger angles. It is possible to make a rough calculation of the magnitude of such an angular change. Assuming the constancy of the optical model predictions [17]) with the product VR^n, where $n = 2(1+E/V)$, the effect of different potentials may be compared by comparing the effects of different nuclear radii. The suggested reduction of about $\frac{1}{6}$ in the potential then corresponds to an 8 % reduction of the nuclear radius or a reduction to about that of fluorine. It seems from the optical model calculations of Bjørklund and Fernbach [18]) that the elastic polarization oscillations of fluorine and magnesium are displaced relative to one another by about 10° in the angular range of interest, so that we may expect this order of change to be produced by the reduction of the potential. Of course if the asymmetry is to be considered more of a surface effect than the differential cross section, this way of estimating the difference provides an upper limit. In any case such a difference is too difficult to detect with the accuracy of the present measurements.

References

1) C. A. Levinson and M. K. Banerjee, Ann. Phys. **2** (1957) 471
2) S. T. Butler, N. Austern and C. Pearson, Phys. Rev. **112** (1958) 1227
3) N. K. Glendenning, Phys. Rev. **114** (1959) 1297
4) C. A. Levinson and M. K. Banerjee, Ann. Phys. **3** (1958) 67
5) L. S. Rodberg, Ann. Phys. **9** (1960) 373
6) R. Huby, N. Y. Refai, and G. R. Satchler, Nuclear Physics **9** (1958) 94
7) L. J. B. Goldfarb and R. C. Johnson, Nuclear Physics **18** (1960) 353
8) G. R. Satchler, Nuclear Physics **18** (1960) 110
9) N. Yamamuro, S. Kobayashi, K. Matsuda, K. Oda and Y. Nagahara, University of Tokyo report, INSJ-29 (1960)
10) A. Strzalkowski, M. S. Bokhari, M. A. Al-Jeboori and B. Hird, Proc. Phys. Soc. **75** (1960) 502
11) L. Rosen, Proc. Int. Conf. on the Nuclear Optical Model, Florida, (1959)
12) A. B. Robbins and G. W. Greenlees, Phys. Rev. **118** (1960) 803
13) M. A. Al-Jeboori, M. S. Bokhari, B. Hird and A. Strzalkowski, Proc. Phys. Soc. **74** (1959) 705
14) T. M. Putnam, J. E. Brolley and L. Rosen, Phys. Rev. **104** (1956) 1303
15) J. S. Blair, Phys. Rev. **115** (1959) 928
16) L. S. Rodberg, Nuclear Physics **15** (1960) 72
17) J. S. Nadvik, Proc. Int. Conf. on the Nuclear Optical Model, Florida (1959)
18) F. Bjørklund and S. Fernbach, private communication
19) S. Okai, Prog. Theor. Phys. **22** (1959) 89

8.B

Nuclear Physics **27** (1961) 204—233; © *North-Holland Publishing Co., Amsterdam*

Not to be reproduced by photoprint or microfilm without written permission from the publisher

A SPACE-TIME MODEL OF ISOSPACE

G. R. ALLCOCK

Department of Theoretical Physics, University of Liverpool

Received 17 February 1961

Abstract: The principle of combined inversion indicates a close relationship between isospace and ordinary space. The possible nature of this relationship is demonstrated with the help of a model, in which the isospin, baryon number, hypercharge and charge conjugation operators appear as displacement operators, producing rotations within space-time itself. In the model the asymmetry of isospace appears as a consequence of relativistic covariance, and charge conjugation and parity appear as continuous transformations.

1. Introduction

The present paper explores the possibility that the various internal attributes of the elementary particles, such as baryon charge, isospin, hypercharge and parity, may all be manifestations of angular degrees of freedom, and that the angles are not located in an abstract space, but within space-time itself. Apart from one important circumstance which will be mentioned below, there is no present experimental indication as to whether or not this is the case. But if it is, it may be expected to come into evidence when a way is found to take account of the structure of the elementary particles, the neglect of which is no doubt the root cause of the troubles of quantum field theory.

The paper finds its motivation in the current quantal treatment of invariance groups and their generating operators. Some of the generating operators, namely the energy operator, the momentum operators and the orbital angular momentum operators, are directly related to the way in which waves oscillate through space-time. The other operators, those for spin and the internal attributes, appear only in the formal language of matrix algebra, and do not seem to permit direct interpretation in terms of space-time waves. They are related to groups of linear transformations among several quantized fields, or equivalently among sets of many-particle wave functions. These linear transformations among quantized fields are to some extent satisfactory, in that they do represent the various groups. But some basic structural element seems to be missing. Some idea of what it may be can be obtained by way of an allegory.

Let us take a hydrogen atom in, say, a 2p-state. Its remaining degrees of freedom can be completely represented by three functions of position (we

neglect the spins). The rotation group induces linear transformations among these three functions. The internal angular momentum of the atom is thus represented by 3×3 matrices. The kinematics of several such atoms can now be correctly described by subjecting the three functions of position to a process of second quantization. The linear orthogonal transformations among these three quantized fields of 2p-hydrogen furnish a representation of the group of rotations of the atoms, but of course they do not give a full account of the mode of operation of the group. For the physical effect of rotations here is to displace the internal wave function of each atom, turning it around in space. One can only obtain a proper physical picture with the help of the internal wave function and the angular variables on which it depends. In this much more basic picture the 3×3 angular momentum matrices are replaced by differential operators which act on the internal angular variables. With these variables brought into consideration the way opens towards a unified description encompassing all the other states of the atom. But it is appropriate here to emphasize that the unified description entails also a radial variable, which enters the problem in a way which cannot be settled or decided by the theory of rotations alone.

With this parable in mind one may well ask, as indeed people often do, whether the 2×2 Pauli spin matrices cannot also be replaced by differential operators, acting on a suitable set of angular variables. The answer to this question is in the affirmative. The angular space is not however, that of a particle moving on the surface of a three-dimensional sphere. It is that of a rigid body free to rotate around a point. We can see at once why this kind of angular space is required. The rotation group is concerned with angular relationships between sets of coordinate axes, and most needs therefore be capable of realising all its potentialities when the object being rotated can serve as the carrier of a set of axes.

The theory of the angular momentum eigenstates of a rigid body was treated in some detail by Bopp and Haag [1]), who used Euler's angles (ϕ, θ, ψ) to parametrize the spatial orientation of the body. They found that the differential operators of angular momentum admit half-integer eigenvalues. The eigenfunctions are nothing but the $D^j_{mm'}(\phi, \theta, \psi)$ familiar in the theory of the representations of the rotation group [2]).

The reader will notice that besides the usual quantum numbers j and m we have here a third quantum number m', which evidently arises because three angles are needed to specify the orientation of the body. It corresponds to the manner in which the wave function oscillates with respect to the variable ψ. This variable describes rotation of the body around its own third axis, and m' is the eigenvalue of the angular momentum about this axis. This angular momentum component commutes with all three spatial components, and hence provides us with an 'internal' quantum number. In a recent paper, Hillion

and Vigier [3]) suggest that it might be interpreted as baryon charge, for it can assume both positive and negative eigenvalues, and is half-integral only when j is half-integral. They also point out an instructive analogy with isospin, earlier discovered and emphasized by Schremp [23]). All three projections of the angular momentum on the body axes commute with the spatial components of angular momentum, and among themselves they obey (apart from a sign) the commutation relations of angular momentum. Here then there is an example of something very like isospin, yet seated in physical space. It seems plausible that isospin should find its origin in some such way as this, for then the dimensionality of isospace becomes immediately explicable.

The rotational properties and rules of commutation of the body-axis projections of angular momentum have been known since the early days of wave mechanics [4]). But until recently, perhaps because these things are so inaccessible to experiment, the possibility of an explanation of isospin or even of ordinary spin along these lines has not been taken very seriously, and has generally been dismissed as metaphysical speculation. During the past two years, however, quite a number of papers have appeared on the subject [3, 5]). For, with the discovery of parity violation, and the apparent validity of the principle of combined inversion CP, we have now a piece of experimental evidence bearing directly on the matter. The CP principle asserts that the basic quantal laws take exactly the same form in left-handed and right-handed coordinate systems, and that the signs of the electric charges, baryon charges, hypercharges and the third (and first) components of isospin change on passing from one type of coordinate system to the other [6]). This principle cannot be said to be 'understood' unless we suppose that all these internal attributes are due to relationships *within* the geometry of space-time itself. The first problem is then to develop some internal variables, set in space-time and deriving their relevant properties from the geometry of space-time, and such that the intrinsic spin and the internal attributes can be realized on them as geometrical displacement operators. Here again, Hillion and Vigier [3]) have shown that the wave function of a rotating body admits a transformation quite analogous to the CP transformation. In fact the projection of angular momentum on any axis rigidly fixed in a body, being the product of a pseudovector and a vector, necessarily changes sign when the axes of the space frame are inverted.

In the following a relativistic model is built up, in which the internal group operations are realized as rotations around various axes set in space-time. The model is apparently the simplest that can be constructed, in that it employs the minimum number of internal variables compatible with achieving the desired realization. The isospin appears as a non-linear transformation of a set of four variables irreducible under the Lorentz group. This is in marked contrast to the situation prevailing in quantum field theories, for there isospin

generates transformations between the elements of at least two such irreducible sets. The model thus establishes a very close linkage between ordinary space and isospace, and although this is concealed under ordinary Lorentz transformations it shows up directly under space inversion. It is found that inversion of the space axes necessarily entails rotations of magnitude π around two internal axes, affecting the internal attributes in such a way as to indicate the CP transformation.

Another feature of the model which may be significant for future developments concerns the well known asymmetry of isospace with respect to its first and second axes. In the model the third axis assumes a naturally privileged position by virtue of the Lorentz transformation properties of its space-time constituents. One usually asks why isospace is not symmetric, but when we look at the model now proposed it seems equally natural to ask why it is as nearly symmetric as it is.

The paper is divided into nine main sections. In sects. 2 and 3 the 'trigonometry' of the rotation group is developed. The customary Euler angles are not used, for they transform in a complicated and unsymmetrical manner, and are singular at the poles. The less familiar Euler parameters are employed instead. These four parameters, found by Euler [7]) in 1776, are everywhere regular. Their transformation rule, which was discovered independently by Gauss, Rodrigues, Hamilton, and Cayley [7]), is that of the four components of a Majorana spinor, with the spin matrices written in a particular and especially pertinent representation! The theory of the Euler parameters is expounded in the following with the help of Hamilton's powerful quaternion calculus. The Pauli spin matrices multiplied by i are taken as quaternion units, in order to make evident the relationship with the more familiar parametrization by 2×2 unimodular unitary matrices. The latter parametrization is not used, for it amounts essentially to combining the four real Euler parameters, in a rather arbitrary way, to make two complex parameters transforming as a Pauli spinor. Many of the equations which are needed in the development of the theory make particular reference to the four individual Euler parameters, and cannot be written nicely in terms of the two complex parameters. Indeed Pauli spinors find their proper function in the discussion of the representations of the rotation group, and are inappropriate to a discussion of the 'trigonometry' of rotations as such. No more would the familiar orbital angular momentum variables $-x-iy$, z, $x-iy$ be suited to a discussion of the trigonometry of three-dimensional Euclidean space. Since only the rudiments of the very beautiful Euler parametrization are presented in physical texts, these sections may prove of interest apart from the subsequent developments.

With the above preliminaries established, a non-relativistic model of isospace is set up in sect. 4. The relativistic properties of the Euler parameters are developed in sect. 5. The parameters are assumed to transform as a Majorana

spinor, as under space rotations. It then proves expedient to set out a special Majorana representation of the Dirac matrices, and various properties of these matrices are investigated. The transformation properties of the body axes of the rotator are next studied. It is found that they transform like the velocity and electric and magnetic vectors of an electromagnetic wave. Thus relativity links together two of the body axes, and treats the third by itself.

In sect. 6 the model of isospace is made relativistic. It is found necessary at this point to introduce a further variable, namely a velocity four-vector. The physical interpretation of this four-vector is not evident at present. Mathematically, it serves to define a frame of rest in which isospace can be constructed. It might be perhaps that its introduction could be avoided by assuming a different relativistic transformation rule for the Euler parameters. This possibility has not been explored, however, in view of the very suggestive asymmetry of the transformation rules actually assumed. It turns out that the asymmetry of isospace can be regarded as a manifestation of this asymmetry. The relationship between charge, isospin and hypercharge can be interpreted in the same spirit.

In sect. 7 the operations of charge conjugation, parity, space inversion and time inversion are defined. It is shown that the group structure of these transformations is compatible with that pertaining in quantum field theories. Nevertheless, the operations are such that they can be achieved in a continuous manner, in accord with Fröhlich's recently enunciated continuity principle [8]). These matters are further discussed in sect. 9. In sect. 8 a few mathematical results are obtained, to facilitate comparison with other work. Such comparisons are made in sect. 9, and some possibilities for further research are briefly mentioned.

2. Euler's Parametrization of the Rotation Group

Let us define the sense of rotations of the reference frame $Oxyz$ by reckoning a small rotation around Ox as positive if it moves Oy toward Oz. Then, if the frame be rotated in a positive sense through an infinitesimal angle $\delta\omega$ around an axis with direction cosines α^j, the coordinates x^j of any point fixed in space undergo the transformation

$$x^j \to x'^j = x^j + \delta\omega\alpha^l \varepsilon^{jkl} x^k. \tag{1}$$

Here, and throughout, ε^{jkl} is the alternating symbol, such that $\varepsilon^{123} = 1$, and the indices j, k, l, m, n run over the values 1, 2 and 3.

A column of two complex numbers (u_1, u_2) is said to constitute a Pauli spinor if it transforms under (1) by the infinitesimal unitary transformation

$$u \to u' = u + \delta\omega\alpha^l \tfrac{1}{2} i\sigma^l u, \tag{2}$$

with

$$\sigma^1 = \begin{pmatrix} 0 & 1 \\ 1 & 0 \end{pmatrix}, \qquad \sigma^2 = \begin{pmatrix} 0 & -i \\ i & 0 \end{pmatrix}, \qquad \sigma^3 = \begin{pmatrix} 1 & 0 \\ 0 & -1 \end{pmatrix}. \tag{3}$$

Rotations through finite angles ω can now be obtained by compounding the infinitesimal rotations (1) and (2), to which end the following multiplication rules are appropriate:

$$\varepsilon^{jkl}\varepsilon^{mnl} = \delta^{jm}\delta^{kn} - \delta^{jn}\delta^{km}, \tag{4}$$

$$\sigma^j\sigma^k = \delta^{jk} + i\varepsilon^{jkl}\sigma^l. \tag{5}$$

The finite transformations are found to be

$$x'^j = R^{jk}x^k, \qquad u' = Su, \tag{6}$$

with

$$R^{jk} = \delta^{jk}\cos\omega + \alpha^j\alpha^k(1-\cos\omega) + \alpha^l\varepsilon^{jkl}\sin\omega, \tag{7}$$

$$S = \cos\tfrac{1}{2}\omega + \alpha^k i\sigma^k \sin\tfrac{1}{2}\omega. \tag{8}$$

As well known, the spinor transformation (8) is such that

$$S^\dagger\sigma^j S = R^{jk}\sigma^k. \tag{9}$$

Here $S^\dagger$ denotes the hermitian conjugate of S.

It will be seen that S can always be written in the form

$$S = \xi^4 - i\sigma^j\xi^j, \tag{10}$$

where ξ^4 and the ξ^j are defined by

$$\xi^4 = \cos\tfrac{1}{2}\omega, \qquad \xi^j = -\alpha^j\sin\tfrac{1}{2}\omega. \tag{11}$$

We now introduce indices a, b, c, d which throughout will run over the values 1, 2, 3 and 4. The real parameters ξ^a are called the Euler parameters [7]) of the rotation R. It is evident that they characterize R completely. Although four in number, they embody just the three degrees of freedom of the rotation group since, by (11), any one can be expressed in terms of the other three through the relation

$$\xi^a\xi^a = 1. \tag{12}$$

This relation implies that the 2×2 matrix S is both unitary and unimodular.

2.1. THE QUATERNION METHOD

The rotation group in the large is completely defined by its infinitesimal structure, and many of its properties can be obtained without integrating the latter. But it is better to use integrated equations, such as (7) and (8), and for the following investigations this will be essential. By far the most simple and effective calculus devised for this purpose is based on the method of quaternions.

It has been particularly exploited in recent times by Gursey [9,10]), Skyrme [22]), and Schremp [23]). The procedure may be stated as follows: Each rotation is in the first place parametrized by four parameters ξ^a satisfying (12). The corresponding rotation matrix R^{jk} is not introduced by eq. (7), but is instead defined as the solution of eq. (9), the matrix S which appears in that equation being expressed as a function of the ξ by (10). Eq. (9) is readily solved with the help of (5), and yields

$$R^{jk} = \delta^{jk}(\xi^4\xi^4 - \xi^l\xi^l) + 2\xi^j\xi^k - 2\varepsilon^{jkl}\xi^4\xi^l. \tag{13}$$

This equation evidently checks with (7) if the rotation angles are identified through (11). Orthogonality of R^{jk} can be demonstrated either from (13) directly, or by evaluating

$$S^\dagger(\sigma^j\sigma^k + \sigma^k\sigma^j)S.$$

The Euler parameters obey a particularly simple composition rule [7]). Let the rotation $\xi(x \to x' = Rx)$ of the axes $Oxyz$ be followed by the rotation $\xi'(x' \to x'' = R'x')$ of the axes $Ox'y'z'$. The resultant rotation may then be denoted by $\xi''(x \to x'' = R''x = R'Rx)$. Applying (9) repeatedly, one finds that the unitary unimodular matrices S must obey the group property

$$S'' = S'S. \tag{14}$$

This equation is readily solved with the help of (5), and gives

$$\begin{aligned} \xi''^4 &= \xi'^4\xi^4 - \xi'^k\xi^k, \\ \xi''^j &= \xi'^4\xi^j + \xi'^j\xi^4 + \varepsilon^{jkl}\xi'^k\xi^l. \end{aligned} \tag{15}$$

These beautiful composition rules are already sufficient to recommend Euler's parameters, but we shall find still more compelling reasons for using them in sect. 2.4.

In the above the three $-i\sigma^j$ correspond to Hamilton's quaternion units, and the unitary unimodular matrix S to a quaternion as such. In the remainder of this paper however, we shall refer to any set of four ξ (not necessarily normalized by (12)) as a quaternion.

2.2. EULER'S PARAMETERS FOR A ROTATED RIGID BODY

Let $Oxyz$ be the space axes, and $O\bar{x}\bar{y}\bar{z}$ a set of axes fixed in the body. The body axes are understood to be drawn with the same handedness (chirality) as the space axes. Then the orientation of the body relative to the space frame can be specified by the quaternion $\bar{\xi}$ of the rotation $\bar{R}$ which, applied to the body axes, would carry them into the space axes †. Thus, if x^j refer any fixed space

† It is more usual to rotate the space axes into the body axes, in which case $\bar{\omega}$ will have the opposite sign. However, the $\bar{\xi}$ defined above are just the same as those usually attributed to a rigid body [7]). For we have put a minus sign into our definition of the $\bar{\xi}^j$ (eq. 11) to compensate the sign which we attribute to $\bar{\omega}$.

point to the space axes, and $\bar{x}^j$ refer the same point to the body axes, we have

$$x^j = \bar{R}^{jk}\bar{x}^k, \tag{16}$$

with $\bar{R}^{jk}$ specified in terms of the $\bar{\xi}$ by an equation like (9). The vectors $\bar{R}^{j1}$, $\bar{R}^{j2}$, $\bar{R}^{j3}$ represent the three body axes with respect to the space frame.

We shall now investigate the transformation properties of the $\bar{\xi}$ under rotation of the space axes. Let the frame of reference be subjected to the rotation (6), whose quaternion is ξ. Then to carry the body axes into the new space axes will require a rotation

$$\bar{R}'^{jk} = R^{j1}\bar{R}^{1k}. \tag{17}$$

Correspondingly, the new body parameters $\bar{\xi}'$ will be given by

$$\bar{S}' = S\bar{S} \qquad \text{(rotation of space axes)}. \tag{18}$$

Eq. (18) asserts that the columns of $\bar{S}$, which are

$$\begin{pmatrix} \bar{\xi}^4 - i\bar{\xi}^3 \\ \bar{\xi}^2 - i\bar{\xi}^1 \end{pmatrix} \quad \text{and} \quad \begin{pmatrix} -\bar{\xi}^2 - i\bar{\xi}^1 \\ \bar{\xi}^4 + i\bar{\xi}^3 \end{pmatrix}, \tag{19}$$

transform as Pauli spinors (eq. (6)) under rotation of the space axes. Thus the Euler parameters of a rigid body combine to make a unit-normalized Pauli spinor [4, 9, 11]. But, as mentioned in the introduction, the two-dimensional spinor calculus is not very well suited to the problem presently under investigation. We shall take up the construction of an appropriate four-dimensional matrix calculus in subsect. 2.5.

2.3. ROTATIONS AROUND THE BODY AXES

In view of the fully reciprocal nature of the relationship between the body axes and the space axes, we have the possibility of rotating the body axes around themselves, keeping the space axes fixed. We parametrize the body frame as in subsect. 2.2, and subject it to a rotation R with quaternion ξ. Under such a rotation the coordinates $\bar{x}$ referring a fixed space point to the body axes undergo the transformation

$$\bar{x}^j \to \bar{x}'^j = R^{jk}\bar{x}^k. \tag{20}$$

Then the body orientation $\bar{R}$, defined by eq. (16), changes to

$$\bar{R}'^{jk} = \bar{R}^{j1}R^{-1k}, \tag{21}$$

and the new quaternion $\bar{\xi}'$ is therefore given by

$$\bar{S}' = \bar{S}S^{-1} \qquad \text{(rotation of body axes)}. \tag{22}$$

The group of body axis rotations (21) obviously commutes with the group of space axis rotations (17). In this respect they are like rotations in isobaric

space. Thus, by the very introduction of rotation coordinates capable of carrying half-integral spin we are presented *gratis*, so to speak, with three further components of angular momentum, scalars with respect to rotations of the space frame †.

An inspection of (22) with (8) and (3) shows that a rotation around the third body axis induces only phase changes of the Pauli spinors (19). But rotations around the other two body axes induce rather messy transformations of the Pauli spinors, in which linear and antilinear terms are mixed together.

2.4. TOPOLOGY, CONTINUITY AND QUANTIZATION

The topology of the rotation group, that is, the overall structure of the group, arises entirely from the structure of its infinitesimal elements. Nevertheless, it is not easily seen in the latter. Indeed the converse is the case. The properties of the infinitesimal elements, and particularly the eigenvalue spectra of their generators, can most easily be understood by reference to the overall topology of the group [11, 12]). And it is here that the Euler parameters perform their most vital service. For they are entirely free of singularities, such as those encountered when one uses ω and the α^j, or the three Euler angles, for the parametrization. Moreover, as we shall presently see, they move over a simply connected manifold, a property not enjoyed by the nine regular parameters R^{jk}.

Let us now consider some finite body rotation, represented by a point ξ on the surface of the four-dimensional sphere (12). According to (18), any infinitesimal rotation of the body around the space frame produces a unique infinitesimal shift of the ξ over the surface of the four-sphere. The converse is also true, every infinitesimal shift of the ξ over the four-sphere corresponds to a unique infinitesimal rotation of the body around the space frame. This one-to-one correspondence of infinitesimal transformations is maintained at all points of the four-sphere. Suppose now that we deal with a wave function defined over the surface of the four-sphere. According to general physical principles, we must demand that the wave function be continuous with respect to small changes in the spatial orientation of the body. Since such small changes are always mapped one-to-one into small changes of the ξ, we see that our wave function must be continuous in every small region of the four-sphere. This in turn implies that it must also be single valued on the four-sphere. For a four-sphere, like a three-sphere, is simply connected; all paths running over the sphere between two fixed points on it can be continuously deformed into each other.

Thus we infer the appropriate conditions of continuity in ξ-space. These conditions are easily taken into account in practice. For, as Lochak [13]) has shown, all functions which are continuous (and therefore single valued) over

† The isomorphism between body-axis rotations and isobaric rotations was used by Gürsey [10]) to write the nucleon field equations in a new form. But eq. (36) shows that one cannot describe isospin in general except with the help of a second body.

the four-sphere can be expanded in integral powers of the $\bar{\xi}$. This is then the 'quantization condition' appropriate to the rotation group, and to our model of isospace †.

It will be seen that every body orientation $\bar{R}$ occurs twice in the Euler parametrization, at the point $\bar{\xi}$ and at the point $-\bar{\xi}$. The points $\bar{\xi}$ and $-\bar{\xi}$ are topologically inequivalent. That is to say, a continuous sequence of rotations carrying the body from some orientation $\bar{R}_0, \bar{\xi}_0$ to $\bar{R}, \bar{\xi}$ cannot be deformed continuously to a sequence carrying it from $\bar{R}_0, \bar{\xi}_0$ to $\bar{R}, -\bar{\xi}$, keeping $\bar{R}_0$ and $\bar{R}$ fixed the while. For to do so would necessitate changing the $\bar{\xi}$ of one of the end-points, and this cannot be done continuously while holding the corresponding $\bar{R}$ fixed.

Thus the Euler parametrization both demonstrates, and takes very neatly into account, the fact that every rotation can be realized in two topologically inequivalent ways. And thus, when we deal with wave functions in $\bar{\xi}$-space, we need impose no relation between the value of the wave function at $\bar{\xi}$ and the value at $-\bar{\xi}$. Accordingly, arbitrary polynomials in the $\bar{\xi}$ may be admitted, the even terms describing integral spin and the odd terms half-integral spin.

It may at first sight seem peculiar that a wave function should refer not only to the orientation $\bar{R}$, but also to the way in which it was realized. But Bohm and Schiller [11]) have given an explanation of why this should be so, and the reader may be referred to their article.

The above discussion is essential to the development of our model of spin and isospace. It may also be applied advantageously to the theory of the representations of the rotation group. A rotation through 4π around, say, the z-axis, takes the representative point in $\bar{\xi}$-space around a great circle, and is therefore topologically equivalent to the zero rotation. The commutation relations of the angular momentum are nothing but the assertion that topologically equivalent rotations are represented by one and the same matrix. Thus consideration of topology both suggests and supplies a straightforward algebraic derivation of the relation $\exp(i4\pi J^3) = 1$, whence the possible quantized values of J^3 follow at once.

2.5. THE ANGULAR MOMENTUM OPERATORS

The infinitesimal space rotation (1) produces a change $\delta\bar{\xi}$ in the quaternion $\bar{\xi}$ which describes the orientation of a body. The $\delta\bar{\xi}$ may be calculated easily with the help of (18), the quaternion of the matrix S in that equation being given by $\xi^j = -\frac{1}{2}\alpha^j\,\delta\omega$, $\xi^4 = 1$. We find

$$\delta\xi^4 = \tfrac{1}{2}\alpha^j\,\delta\omega\xi^j, \qquad \delta\xi^j = -\tfrac{1}{2}\alpha^j\,\delta\omega\xi^4 - \tfrac{1}{2}\varepsilon^{jkl}\,\delta\omega\alpha^k\,\xi^l. \tag{23}$$

† The corresponding continuity conditions on the Euler angles of the body follow through the relations [7])

$$\xi^1 = \sin\tfrac{1}{2}\theta\sin\tfrac{1}{2}(\psi-\phi), \qquad \xi^2 = \sin\tfrac{1}{2}\theta\cos\tfrac{1}{2}(\psi-\phi),$$
$$\xi^3 = \cos\tfrac{1}{2}\theta\sin\tfrac{1}{2}(\psi+\phi), \qquad \xi^4 = \cos\tfrac{1}{2}\theta\cos\tfrac{1}{2}(\psi+\phi).$$

The angular momentum components with respect to the space axes can now be introduced as displacement operators. These operators, denoted by J^k, are defined by the equation

$$\delta\bar{\xi}^a = i[\bar{\xi}^a, \alpha^k \delta\omega J^k]. \tag{24}$$

Substituting (23), one obtains the explicit expression

$$J^k = \tfrac{1}{2}i\left\{\bar{\xi}^k \frac{\partial}{\partial \bar{\xi}^4} - \bar{\xi}^4 \frac{\partial}{\partial \bar{\xi}^k} - \varepsilon^{klm}\bar{\xi}^l \frac{\partial}{\partial \bar{\xi}^m}\right\}. \tag{25}$$

In a similar way one can introduce angular momentum components I^k with respect to the body axes. Eq. (24) serves to define them if we replace J^k by I^k, and calculate the $\delta\bar{\xi}$ from (22). The result is

$$I^k = \tfrac{1}{2}i\left\{-\bar{\xi}^k \frac{\partial}{\partial \bar{\xi}^4} + \bar{\xi}^4 \frac{\partial}{\partial \bar{\xi}^k} - \varepsilon^{klm}\bar{\xi}^l \frac{\partial}{\partial \bar{\xi}^m}\right\}. \tag{26}$$

The I^k and J^l commute with each other. Each separately obey the commutation relations of angular momentum. Their eigenvalues are half-integral with respect to odd polynomials in the $\bar{\xi}$.

2.6. THE ANGULAR MOMENTUM MATRICES

In the remainder of the paper we shall not have occasion to use simultaneously the quaternions of body orientation ($\bar{\xi}$) and the quaternions of rotation of the reference frame (ξ). We shall therefore write ξ instead of $\bar{\xi}$ from now on.

It will be seen that the angular momentum operators (25) and (26) can be written

$$I^k = \tfrac{1}{2}iP^{kab}\xi^a \frac{\partial}{\partial \xi^b}, \tag{27}$$

$$J^k = \tfrac{1}{2}i\Sigma^{kab}\xi^a \frac{\partial}{\partial \xi^b}, \tag{28}$$

with

$$P^{kab} = -\delta^{ak}\delta^{b4} + \delta^{bk}\delta^{a4} - \varepsilon^{kab4}, \tag{29}$$

$$\Sigma^{kab} = \delta^{ak}\delta^{b4} - \delta^{bk}\delta^{a4} - \varepsilon^{kab4}. \tag{30}$$

Here and in the following ε^{abcd} is the alternating symbol such that $\varepsilon^{1234} = 1$.

The skew matrices P^k and Σ^k obey the relations

$$\begin{aligned} &[P^k, \Sigma^l] = 0, \qquad P^k P^l = -\delta^{kl} + \varepsilon^{klm} P^m, \\ &\Sigma^k \Sigma^l = -\delta^{kl} + \varepsilon^{klm}\Sigma^m. \end{aligned} \tag{31}$$

Evidently the iP and the $i\Sigma$ are Dirac's 4×4 matrices ρ and σ written in a special Majorana representation.

The rotation matrix R^{jk} (eq. (13)) can be conveniently expressed in terms of the products ΣP. One finds

$$(\Sigma^j P^k)^{ab} = -\delta^{a4}\varepsilon^{bjk4} - \delta^{b4}\varepsilon^{ajk4} - \delta^{jk}\delta^{ab} + 2\delta^{jk}\delta^{a4}\delta^{b4} + \delta^{aj}\delta^{bk} + \delta^{bj}\delta^{ak}, \quad (32)$$

whence

$$R^{jk} = (\Sigma^j P^k)^{ab}\xi^a\xi^b \equiv \xi\Sigma^j P^k \xi. \quad (33)$$

In (29), (30) and (32) we have six real skew traceless matrices P^k and Σ^k, and nine real symmetric traceless matrices $\Sigma^j P^k$. Together with the unit matrix these constitute a complete set of sixteen linearly independent 4×4 matrices. The matrices Σ^k and P^3 by themselves are reducible (cf. the remarks at the end of subsect. 2.3).

The orthogonality of the rotation matrix R^{jk} is most advantageously expressed through the following identities:

$$\begin{aligned} P^{jab}P^{jcd} &= \delta^{ac}\delta^{bd} - \delta^{ad}\delta^{bc} + \varepsilon^{abcd}, \\ \Sigma^{jab}\Sigma^{jcd} &= \delta^{ac}\delta^{bd} - \delta^{ad}\delta^{bc} - \varepsilon^{abcd}. \end{aligned} \quad (34)$$

These identities are easily verified by direct evaluation. They can be used to show that I is the projection of $-J$ onto the body axes, that J is the projection of $-I$ onto the space axes, and that the squares of I and J are equal,

$$I^k = -R^{lk}J^l, \qquad J^k = -R^{kl}I^l, \quad (35)$$

$$I^kI^k = J^kJ^k. \quad (36)$$

It will be seen that eqs. (31) and (34) are invariant under unimodular orthogonal 4×4 transformations of the P and Σ. But such transformations correspond only to a rotation of the standard position of the body axes, and do not serve any useful purpose.

2.7. A REAL QUATERNION CALCULUS

The quaternion calculus of subsect. 2.1 could equally be developed with the Σ^k (or the P^k) as quaternion units. We would then have equations of the form

$$\mathcal{S} \equiv \xi^4 + \xi^k\Sigma^k, \qquad \mathcal{S}^{\mathrm{T}}\mathcal{S} = 1, \qquad \mathcal{S}^{\mathrm{T}}\Sigma^j\mathcal{S} = R^{jk}\Sigma^k, \quad (37)$$

the index T denoting the transposed matrix.

3. The Mutual Orientation of Two Rigid Bodies

Let us now take two bodies, the orientation of the first relative to the space frame being described by a quaternion ξ, and that of the second by a quaternion η. According to the convention established in subsect. 2.2, the orientation of the second body relative to the first will be described by a rotation matrix $R(\xi)^{-1}R(\eta)$, and therefore by a unitary unimodular matrix $S(\xi)^{-1}S(\eta)$. The

Euler parameters of this matrix will be denoted by χ. The χ can be calculated from eqs. (15),

$$\chi^4 = \xi^4\eta^4+\xi^k\eta^k, \qquad \chi^j = \xi^4\eta^j-\xi^j\eta^4-\varepsilon^{jkl}\xi^k\eta^l. \tag{38}$$

It is evident that $S(\xi)^{-1}S(\eta)$ is invariant under the rotations (18) of the space frame. Therefore the χ constitute a rotationally invariant quaternion. The invariance of χ is rendered evident if we rewrite (38) in the form

$$\chi^4 = \xi^a\eta^a \equiv \xi\eta, \qquad \chi^j = \xi^a P^{jab}\eta^b \equiv \xi P^j\eta. \tag{39}$$

Using (15) again, we can invert these equations to express η in terms of χ and ξ. The result can be written

$$\eta^a = \xi^a\chi^4-P^{jab}\xi^b\chi^j,$$

or

$$\eta = \xi\chi^4-P^j\xi\chi^j. \tag{40}$$

4. A Non-Relativistic Model of Isospace

We shall denote the spin by S^k, the baryon number by N, the isospin by T^k, the hypercharge by Y, and the electric charge by $Q = T^3+Y$. To each of these attributes we associate a differential operation on the parameters ξ and χ of sect. 3, according to the following scheme:

S^k	$\frac{1}{2}i\xi\Sigma^k\dfrac{\partial}{\partial\xi}\Big\vert_x$
$\frac{1}{2}N$	$\frac{1}{2}i\xi P^3\dfrac{\partial}{\partial\xi}\Big\vert_x$
T^k	$\frac{1}{2}i\chi\Sigma^k\dfrac{\partial}{\partial\chi}\Big\vert_\xi$
Y	$-\frac{1}{2}i\chi P^3\dfrac{\partial}{\partial\chi}\Big\vert_\xi$
Q	$\frac{1}{2}i\chi(\Sigma^3-P^3)\dfrac{\partial}{\partial\chi}\Big\vert_\xi = i\left(\chi^3\dfrac{\partial}{\partial\chi^4}-\chi^4\dfrac{\partial}{\partial\chi^3}\right)\Big\vert_\xi$

(41)

It will be seen that $\frac{1}{2}N$ is related to the spin and that Y is related in a similar way to the isospin. So far as $\frac{1}{2}N$ is concerned, the relation is one which arises from our experience of the Dirac equation. That a similar relation holds between isospin and hypercharge was first noticed by d'Espagnat and Prentki [14]). These relationships have a very deep significance, in terms of the topology of the corresponding group operations. For, as we saw in subsect 2.4, the quantum conditions holding in representations of a continuous group are a direct consequence of the way the group closes back upon itself. The known

quantum conditions on $\frac{1}{2}N$ and Y must therefore be understood as manifestations of the fact that these operations form part of larger groups of transformations, with the closed topology of the rotation group in three dimensions†.

In the present model we demand, in accord with the discussion of subsect. 2.4, that all wave functions must be polynomials in the ξ and χ. The structure of (41) then ensures that the eigenvalues of Q are integral, and that $\frac{1}{2}N$ is half-integral only when S is. The eigenfunctions appropriate to the various elementary particles may be found in the book by Roman [15]).

In (41) the spin angular momentum S^k corresponds to rotations of the two bodies together, in a negative sense, around the space axes, while $\frac{1}{2}N$ corresponds to rotation of the two bodies together around the third axis of the first body. The three isospin components describe rotation of the second body alone, in a negative sense, around the three axes of the first, and the hypercharge Y produces a rotation of the second body alone, in a negative sense, around its own third axis. Taking into account these geometrical features, and paying due regard to the sense of the various rotations, the operators (41) can be written directly as operators on the spatial quaternions ξ and η. Writing $R^{lk}(\xi)$ for $\xi\Sigma^l P^k \xi$, we have the following scheme:

S^k	$\frac{1}{2}i\xi\Sigma^k \dfrac{\partial}{\partial\xi}\Big\vert_\eta + \frac{1}{2}i\eta\Sigma^k \dfrac{\partial}{\partial\eta}\Big\vert_\xi$
$\frac{1}{2}N$	$\frac{1}{2}i\xi P^3 \dfrac{\partial}{\partial\xi}\Big\vert_\eta - \frac{1}{2}iR^{l3}(\xi)\eta\Sigma^l \dfrac{\partial}{\partial\eta}\Big\vert_\xi$
T^k	$\frac{1}{2}iR^{lk}(\xi)\eta\Sigma^l \dfrac{\partial}{\partial\eta}\Big\vert_\xi$
Y	$-\frac{1}{2}i\eta P^3 \dfrac{\partial}{\partial\eta}\Big\vert_\xi$
Q	$\frac{1}{2}i\left\{R^{l3}(\xi)\eta\Sigma^l \dfrac{\partial}{\partial\eta}\Big\vert_\xi - \eta P^3 \dfrac{\partial}{\partial\eta}\Big\vert_\xi\right\}$

(42)

These relations can be proved analytically with the help of the matrix identities (34). They express the various attributes as differential operators of displacement, acting on the coordinates ξ and η which describe orientations relative to the space axes.

† The operator Y *by itself* can be regarded as the infinitesimal generator of rotations around the circumference of a circle. There are infinitely many ways of realizing a given displacement around the circle, corresponding to the number of revolutions made. The corresponding paths are topologically different; they cannot be deformed continuously into each other keeping the end points fixed. The eigenvalues of Y in this problem are therefore m/n, with m and n arbitrary integers. Physics demands only the values $\frac{1}{2}m$, and so indicates that Y is just part of a larger group. Similar remarks apply to $\frac{1}{2}N$.

5. Relativistic Transformation of a Quaternion

The relativistic extension of the space rotation (1) is the Lorentz transformation

$$x^\mu \to x'^\mu = x^\mu + \delta\omega^{\mu\nu} x_\nu, \tag{43}$$

with $\delta\omega^{\mu\nu}$ an infinitesimal skew matrix, and $x_\nu \equiv x^\mu g_{\mu\nu}$. We shall use the metric signature $+ - - -$, and all Greek indices will run over the values 0, 1, 2, 3. According to subsect. 2.2 the column

$$u \equiv \begin{pmatrix} \xi^4 - i\xi^3 \\ \xi^2 - i\xi^1 \end{pmatrix} \tag{44}$$

transforms as a Pauli spinor under spatial rotations of the reference frame. It seems natural therefore to transform it as a Pauli spinor under Lorentz transformations too. The consequences of this assumption appear to be physically reasonable, as we shall see presently.

The spinor transformations associated with (43) is thus taken to be

$$u \to u' = \{1 - \tfrac{1}{4} i\varepsilon^{jkl}\delta\omega^{jk}\sigma^l \pm \tfrac{1}{2}\delta\omega^{0j}\sigma^j\} u. \tag{45}$$

In the notation set out by Umezawa [16]) the upper (positive) sign corresponds to a contravariant spinor, and the lower sign to a complex conjugated covariant spinor. Eq. (45) may be transcribed to the real quaternion notation with the help of eqs. (3), (44), (30) and (32), to give

$$\xi \to \xi' = \{1 + \tfrac{1}{4}\varepsilon^{jkl}\delta\omega^{jk}\Sigma^l \pm \tfrac{1}{2}\delta\omega^{0j}\Sigma^j P^3\}\xi. \tag{46}$$

This transformation rule evidently distinguishes between the third body axis and the other two. In the succeeding sections we shall see that this leads very naturally to a corresponding anisotropy in the properties of the isospace of our model.

5.1. A MAJORANA REPRESENTATION OF THE DIRAC MATRICES

The relativistic development of the theory is considerably simplified by the introduction of a special set of real Dirac matrices Γ^μ and Γ^5. We shall define them by the equations

$$\Gamma^{0a}{}_b = P^{2ab}, \qquad \Gamma^{ja}{}_b = -(P^1\Sigma^j)^{ab}, \qquad \Gamma^{5a}{}_b = P^{3ab}. \tag{47}$$

They obey the anticommutation relations

$$\{\Gamma^\mu, \Gamma^\nu\} = -2g^{\mu\nu}, \qquad \{\Gamma^\mu, \Gamma^5\} = 0, \tag{48}$$

and Γ^5 is related to the Γ^μ through the equation

$$\Gamma^5 = \Gamma^0\Gamma^1\Gamma^2\Gamma^3.$$

The positions of the quaternion indices in (47) correspond to the fact that two types of quaternion, contravariant and covariant, appear when one discusses Lorentz transformations.

The symmetry properties of the Γ are as follows:

$$\Gamma^{0a}{}_{b} = -\Gamma^{0b}{}_{a}, \qquad \Gamma^{ja}{}_{b} = \Gamma_{a}{}^{jb}, \qquad \Gamma^{5a}{}_{b} = -\Gamma_{a}{}^{5b}, \tag{49}$$

i.e.

$$\Gamma^{0T} = -\Gamma^{0}, \qquad \Gamma^{jT} = \Gamma^{j}, \qquad \Gamma^{5T} = -\Gamma^{5}.$$

Thus $\Gamma^{4} \equiv i\Gamma^{0}$ and the Γ^{j} constitute a hermitian Pauli set of Dirac matrices [15, 16, 17]) while the $i\Gamma^{\mu}$ constitute a Feynman set [18]). The reality of the Γ^{μ} labels them as a Majorana representation [15]).

5.2. CONTRAVARIANT AND COVARIANT QUATERNIONS

The transformation of a contravariant Pauli spinor (upper sign in eqs. (45) and (46)) now appears as the real unimodular transformation

$$\xi^{a} \to \xi'^{a} = \{\delta^{a}{}_{b} - \tfrac{1}{4}\delta\omega_{\mu\nu}(\Gamma^{\mu}\Gamma^{\nu})^{a}{}_{b}\}\xi^{b}. \tag{50}$$

Eq. (50) will be taken as the transformation rule defining a *contravariant quaternion*. A *covariant quaternion* will then be one which transforms by the transposed reciprocal matrix, that is,

$$\eta_{a} \to \eta'_{a} = \{\delta^{b}{}_{a} + \tfrac{1}{4}\delta\omega_{\mu\nu}(\Gamma^{\mu}\Gamma^{\nu})^{b}{}_{a}\}\eta_{b}. \tag{51}$$

Then the product $\eta_{a}\,\xi^{a}$ is invariant.

Quaternion indices may be lowered and raised by a covariant real skew metric C_{ab} and a contravariant real skew metric $\hat{C}^{ab}$, respectively. The appropriate metric turns out to be $-P^{2}$;

$$C_{ab} \equiv -P^{2ab} = -C_{ba}, \qquad \hat{C}^{ab} \equiv P^{2ab} = -\hat{C}^{ba}. \tag{52}$$

The sign of C has been chosen to make $C\Gamma^{0}$ positive and $\hat{C}$ is the inverse of C,

$$\hat{C}^{ab}C_{bd} = \delta^{a}{}_{d}. \tag{53}$$

The procedure for raising and lowering quaternion indices has to be stated with some care, since the metrics are skew. A suitable convention is

$$\xi_{a} \equiv \xi^{b}C_{ba}, \tag{54}$$

then

$$\xi^{a} = \xi_{b}\hat{C}^{ba}. \tag{55}$$

It is important to notice that

$$\xi_{a}\eta^{a} = -\xi^{a}\eta_{a}. \tag{56}$$

This is a consequence of the skew nature of C, and cannot be avoided if we wish to keep all matrices real. The usual hermitian metric β of Dirac matrix theory is evidently equal to iC.

The indices of any Dirac matrix $\Gamma^a{}_b$ can be raised and lowered by the rules (53). We have, as a matter of definition,

$$\Gamma_a{}^b \equiv \Gamma^{a'}{}_{b'} C_{a'a} \hat{C}^{b'b}. \tag{57}$$

Using the explicit forms of the matrices (eqs. 47), one finds the important symmetry properties

$$\Gamma^\mu{}_{ab} = \Gamma^\mu{}_{ba}, \qquad \Gamma^5{}_{ab} = -\Gamma^5{}_{ba}. \tag{58}$$

Taking note of these properties and remembering that the C are skew, one can check that $\xi^b C_{ba}$ transforms covariantly if ξ^a transforms contravariantly. Thus our definition of C is confirmed.

5.3. MATRIX NOTATION

A superabundance of quaternion indices and suffices may be avoided by introducing a matrix notation similar to that usually used with Dirac spinors. But, since the metric C is skew, and therefore antihermitian, our notation must differ in some minor respects from that usually employed.

We first agree that the symbol Γ shall always imply the corresponding Dirac matrix $\Gamma^a{}_b$, and not Γ_{ab}, $\Gamma_a{}^b$ etc. On the other hand we agree that C and $\hat{C}$ shall always denote C_{ab} and $\hat{C}^{ab}$ respectively. We regard each contravariant quaternion ξ as a column vector. The corresponding covariant quaternion is then denoted by $\hat{\xi}$, and is regarded as a row vector. Then eqs. (54) and (55) become

$$\hat{\xi} \equiv \xi^{\mathrm{T}} C, \qquad \xi^{\mathrm{T}} = \hat{\xi}\hat{C}. \tag{59}$$

We also have

$$\xi_a \Gamma^a{}_b \eta^b \equiv \hat{\xi}\Gamma\eta. \tag{60}$$

The transposition properties of scalar products like (60) must next be considered. Defining first the transposed matrix Γ^{T} (cf. eqs. 49) by

$$(\Gamma^{\mathrm{T}})^a{}_b \equiv \Gamma^b{}_a, \tag{61}$$

we find that the symmetry relations (58) can be written in the form $\Gamma^{\mu\mathrm{T}} = -C\Gamma^\mu\hat{C}$, $\Gamma^{5\mathrm{T}} = C\Gamma^5\hat{C}$, so that C is a charge conjugation matrix of the type defined in refs. [15, 16]). That the metric and the charge conjugation matrix coincide is a special and advantageous feature of the real representation we are using. They do not coincide in all real representations.

It is evident from the position of the indices in (61) that what is really needed for transposition of scalar products is not the transposed matrix Γ^{T}, but a matrix $\hat{\Gamma}$ defined by the rule

$$\hat{\Gamma}^a{}_b \equiv -\Gamma_b{}^a, \qquad \text{or} \qquad \hat{\Gamma} \equiv \hat{C}\Gamma^{\mathrm{T}}C. \tag{62}$$

The sign here is introduced so that

$$\widehat{\Gamma^{(1)}\Gamma^{(2)}} = \hat{\Gamma}^{(2)}\hat{\Gamma}^{(1)}. \tag{63}$$

All transpositions can be accomplished with the help of the following rules:

$$\hat{\hat{\Gamma}} = \Gamma, \quad \hat{\Gamma}^{\mu} = -\Gamma^{\mu}, \quad \hat{\Gamma}^{5} = \Gamma^{5}, \quad \widehat{\Gamma\xi} = \hat{\xi}\hat{\Gamma}, \quad \xi\eta = -\hat{\eta}\xi, \quad \xi\Gamma\eta = -\hat{\eta}\hat{\Gamma}\xi. \tag{64}$$

Tensors of various types can be constructed from two contravariant quaternions ξ and η in a manner familiar in connection with Dirac wave functions. Thus $\hat{\xi}\eta$ and $\hat{\xi}\Gamma^{5}\eta$ are scalars, $\hat{\xi}\Gamma^{\mu}\eta$ and $\hat{\xi}\Gamma^{5}\Gamma^{\mu}\eta$ are four-vectors, and so forth.

The Dirac matrices obey a number of Lorentz covariant indentities similar in structure to the identities (34), and one which will turn out to be useful in the following is

$$\Gamma^{\mu a}{}_{b}\Gamma_{\mu}{}^{c}{}_{d} = -\delta^{a}{}_{d}\delta^{c}{}_{b} - \Gamma^{5a}{}_{d}\Gamma^{5c}{}_{b} - \hat{C}^{ac}C_{bd} - (\Gamma^{5}\hat{C})^{ac}(C\Gamma^{5})_{bd}, \tag{65}$$

or

$$\Gamma^{\mu}{}_{ab}\Gamma_{\mu cd} = C_{ad}C_{bc} + \Gamma^{5}{}_{ad}\Gamma^{5}{}_{bc} + C_{ac}C_{bd} + \Gamma^{5}{}_{ac}\Gamma^{5}{}_{bd}. \tag{65a}$$

This identity may be verified by Pauli's method of spurs [15, 16, 17]). A direct evaluation proves to be exceedingly tedious.

5.4. TRANSFORMATION PROPERTIES OF THE BODY AXES

The transformation properties of the three body axes of the contravariant quaternion ξ will now be investigated, with the help of the transformation rule (50). The normalization condition $\xi^{a}\xi^{a} = 1$ can no longer be maintained, but non-normalized body axes R^{jk} can still be defined by eqs. (33). Transcribing into relativistic notation with the help of eqs. (47), (52) and (59) they become

$$R^{j1} = \hat{\xi}\Gamma^{j}\Gamma^{0}\xi, \qquad R^{j2} = \tfrac{1}{2}\varepsilon^{jkl}\hat{\xi}\Gamma^{k}\Gamma^{l}\xi, \qquad R^{j3} = -\hat{\xi}\Gamma^{j}\xi. \tag{66}$$

The asymmetry in the treatment of the body axes in the transformation rule (46) may now be understood as a manifestation of their different transformation properties. The third axis R^{j3} is the space part of a four-vector $-\hat{\xi}\Gamma^{\mu}\xi$. This four-vector has a negative time part, and eq. (65) shows that it is light-like. The axes R^{j1} and R^{j2} are linked together in the skew tensor $\hat{\xi}[\Gamma^{\mu}, \Gamma^{\nu}]\xi$.

One can also use eqs. (33) to associate a set of body axes with a covariant quaternion ξ_{a}. In this case the third axis is the space part of a light-like four-vector with positive time part. But this possibility need not be given independent consideration, since the equation $\hat{\xi} = \xi C$ establishes an invariant correspondence with the case already discussed.

5.5. SPACE INVERSION

We shall now study the behaviour of a quaternion ξ under inversion ($x^j \to x'^j = -x^j$) of the spatial coordinate system, the body described by ξ being left undisturbed. In order that the matrix R^{jk} (eq. 33) shall continue to express the relationship (16) between body axes and space axes, it will be necessary to accompany the space inversion by a reversal of one of the body axes. For R^{jk} is continuous with the identity, and cannot relate sets of axes of opposite handedness. This is, however, a purely formal matter, and does not need to imply any change in the body. Indeed the orientation of a body is completely specified by two axes fixed rigidly in it. We can agree to draw in the remaining axis in such a direction as to give a set with the same handedness as the space frame. We may call the last mentioned body axis the dummy axis. Under space inversion then, the components R^j of the dummy axis relative to the space frame do not change, while the components R^j of the other two axes relative to the space frame change sign. These geometrical considerations lead us to suppose that the most likely transformation rule for ξ comprises a rotation through π around a dummy axis.

Thus, the transformation rule should be of the form $\xi \to \xi' = I\xi$, with I descriptive of a body rotation π. Relativity confirms this argument, and tells us that the dummy axis is orthogonal to the third one. For the integrability conditions for the Lorentz group are

$$[I, \Sigma^j] = \{I, \Sigma^j P^3\} = 0, \tag{67}$$

the general solution of which is, apart from a factor,

$$I = P^1 \sin\theta + P^2 \cos\theta, \tag{68}$$

with θ some angle. The matrix (68) is descriptive of a rotation π, around an axis orthogonal to the 3-axis. We are still at liberty to locate the first axis in the body in such a way that θ becomes zero, and doing this we obtain $I = P^2 = \Gamma^0$. The rule appropriate for space inversion can therefore be put into the form

$$x^j \to -x^j, \qquad \xi \to \Gamma^0 \xi, \tag{69}$$

and the second body axis is then the dummy axis.

Under (69) Γ^μ behaves as a vector, and Γ^5 as a pseudoscalar. For we have

$$\hat{\Gamma}^0 \Gamma^0 = 1, \quad \hat{\Gamma}^0 \Gamma^0 \Gamma^0 = \Gamma^0, \quad \hat{\Gamma}^0 \Gamma^j \Gamma^0 = -\Gamma^j, \quad \hat{\Gamma}^0 \Gamma^5 \Gamma^0 = -\Gamma^5. \tag{70}$$

The transformation (69) looks like the customary parity transformation of a Dirac spinor. But it is more properly conceived here as an operation of combined inversion CP, for only one quaternion or Pauli spinor is involved in it. The various transformations of Dirac spinors are written out in eqs. (89), and the situation may be clarified by reference to them and to eq. (103).

5.6. TIME INVERSION

Under time inversion ξ will undergo a transformation

$$\xi \to \tau\xi, \qquad x^0 \to -x^0. \tag{71}$$

The integrability condition for τ is the same as (67), and the solutions are therefore (68). We shall take the solution (68) with $\theta = 0$. This choice is dictated by the requirement that the time reversal operation shall commute with the charge conjugation operation of subsect 7.3. The matrix τ is different from the matrix T appropriate to a spinor appearing in the Dirac equation. We have in fact

$$\tau = P^2 = \Gamma^0, \qquad T = P^1 = \Gamma^0\Gamma^5. \tag{72}$$

The properties of τ are listed in eqs. (70). For completeness we list also the corresponding properties of T,

$$\hat{T}T = -1, \qquad \hat{T}\Gamma^0 T = \Gamma^0, \qquad \hat{T}\Gamma^j T = -\Gamma^j, \qquad \hat{T}\Gamma^5 T = \Gamma^5. \tag{73}$$

Under the transformation (71) the third body axis behaves as a three-velocity (its components change sign), and the first body axis likewise.

6. A Relativistic Model of Isospace

The work of sect. 5 tells us the transformation properties of the components of the mutual orientation χ of two contravariant quaternions ξ and η. The component χ^1 is a Lorentz pseudoscalar and the component χ^2 a Lorentz scalar. But the component χ^3 is the time part of a Lorentz pseudovector and the component χ^4 is the time part of a Lorentz vector.

$$\chi^1 = \xi P^1 \eta = -\hat{\xi}\Gamma^5\eta, \qquad \chi^2 = \xi P^2 \eta = -\hat{\xi}\eta, \tag{74}$$

$$\chi^3 = \xi P^3 \eta = -\hat{\xi}\Gamma^5\Gamma^0\eta, \qquad \chi^4 = \xi\eta = \hat{\xi}\Gamma^0\eta. \tag{75}$$

The Lorentz invariance of isospace can be maintained by introducing a velocity four-vector V^μ with positive time part,

$$V^\mu V_\mu = 1, \qquad V^0 \geqq 1. \tag{76}$$

This permits us to redefine χ^3 and χ^4 as follows:

$$\chi^3 = -V_\mu \hat{\xi}\Gamma^5\Gamma^\mu\eta, \qquad \chi^4 = V_\mu \hat{\xi}\Gamma^\mu\eta. \tag{77}$$

These new definitions reduce to the former ones in any Lorentz frame whose time axis is directed along V^μ. Such frames will be called rest frames.

Referring to eqs. (41), it will be seen that the operations for spin, baryon number, isospin, hypercharge and charge may be modified as in the following scheme:

S^k	$\frac{1}{2}i\xi\Sigma^k\dfrac{\partial}{\partial\xi}\Big\vert_{\chi,V} - ie^{klm}V^l\dfrac{\partial}{\partial V^m}\Big\vert_{\chi,\xi}$
$\frac{1}{2}N$	$\frac{1}{2}i\xi P^3\dfrac{\partial}{\partial\xi}\Big\vert_{\chi,V}$
T^k	$\frac{1}{2}i\chi\Sigma^k\dfrac{\partial}{\partial\chi}\Big\vert_{\xi,V}$
Y	$-\frac{1}{2}i\chi P^3\dfrac{\partial}{\partial\chi}\Big\vert_{\xi,V}$
Q	$\frac{1}{2}i\chi(\Sigma^3-P^3)\dfrac{\partial}{\partial\chi}\Big\vert_{\xi,V} = i\left(\chi^3\dfrac{\partial}{\partial\chi^4}-\chi^4\dfrac{\partial}{\partial\chi^3}\right)\Big\vert_{\xi,V}$

(78)

6.1. ASYMMETRY OF THE ISOSPACE OF THE MODEL

The appearance of P^3 in $\frac{1}{2}N$ and Y is readily understood, for the body rotations around the other two axes are not Lorentz invariant. More interesting, however, is the space-time asymmetry implied between T^3 and the other two components of isospin. For T^3 describes rotation of η around the privileged third axis of ξ (in the rest frame). As such it commutes with the operator generating rotations of ξ around its own third axis (namely with the operator $\frac{1}{2}N+T^3$). The components T^1 and T^2 do not commute with these rotations of ξ.

The very peculiar sum of angular momenta around two different axes, which goes to make up the electric charge Q, may also be related to space-time asymmetries of the model. For χ^1 and χ^2 are constructed without V^μ (eqs. 74), while χ^3 and χ^4 depend on V^μ (eqs. 77). There are three possible Σ-rotations of χ and three possible P-rotations, and the only combination from these six leaving invariant the scalars χ^1 and χ^2 is Q.

7. The Discontinuous Groups

7.1. THE MODEL AND SPACE INVERSION (I)

Suppose that under space inversion the equaternions ξ and η undergo the transformation (69), while V^μ transforms as a four-vector, so that

$$\xi \to \Gamma^0\xi, \qquad \eta \to \Gamma^0\eta, \qquad V^0 \to V^0, \qquad V^j \to -V^j. \tag{79}$$

Then the isospace quaternion χ, defined by (74) and (77), undergoes the transformation

$$\chi^1 \to -\chi^1, \qquad \chi^2 \to \chi^2, \qquad \chi^3 \to -\chi^3, \qquad \chi^4 \to \chi^4. \tag{80}$$

Hence the operators (78) transform as follows:

$$\begin{aligned} &S^k \to S^k, \quad \tfrac{1}{2}N \to -\tfrac{1}{2}N, \quad T^3 \to -T^3, \\ &T^2 \to T^2, \quad T^1 \to -T^1, \quad Y \to -Y, \quad Q \to -Q. \end{aligned} \tag{81}$$

These are just the rules usually associated with combined inversion CP. It is noteworthy that they are obtained in spite of the complete absence of anti-commuting variables. In quantum field theories of spin-$\frac{1}{2}$ particles, on the other hand, the correct CP transformation cannot be obtained without anti-commutation. It also seems significant that there is no way of constructing a set of four scalar χ from the ingredients available in our model. Some of the χ have to be pseudoscalar, and thus the model makes it inevitable that isospace undergoes a transformation when the space axes are inverted.

7.2. THE MODEL AND TIME INVERSION (T)

Under time inversion ξ and η will be taken to transform by (71), and V^μ to transform as a pseudovector, so that

$$\xi \to \Gamma^0 \xi, \quad \eta \to \Gamma^0 \eta, \quad V^0 \to V^0, \quad V^j \to -V^j. \tag{82}$$

Then eqs. (76) remain valid. For χ we obtain

$$\chi^1 \to -\chi^1, \quad \chi^2 \to \chi^2, \quad \chi^3 \to -\chi^3, \quad \chi^4 \to \chi^4, \tag{83}$$

and so, as with space inversion,

$$\begin{aligned} &S^k \to S^k, \quad \tfrac{1}{2}N \to -\tfrac{1}{2}N, \quad T^3 \to -T^3, \\ &T^2 \to T^2, \quad T^1 \to -T^1, \quad Y \to -Y, \quad Q \to -Q. \end{aligned} \tag{84}$$

The usual transformation rules for expectation values under time reversal are however,

$$\begin{aligned} &S^k \to -S^k, \quad \tfrac{1}{2}N \to \tfrac{1}{2}N, \quad T^3 \to T^3, \\ &T^2 \to -T^2, \quad T^1 \to T^1, \quad Y \to Y, \quad Q \to Q. \end{aligned} \tag{85}$$

Evidently the transformations (84) for our model differ throughout by a sign from the customary transformations (85). And therefore, since each of the operators (84) is pure imaginary, the usual transformation rule can be obtained by changing the sign of i.

The reader will notice that i appears in two different capacities in the preceding work. In the first place it is introduced in a rather accidental and unnecessary capacity, in connection with Pauli spinors. All i of this type can be avoided by using the real quaternion calculus of subsect. 2.7 from the very beginning. The second capacity, in which its appearance is no mere accident, is in the Poisson bracket operation (24), and in the displacement operators which arise from it. Our assertion is then that the i of the second type may be

conjugated when time is reversed. Such a change in sign of the i which arise from Poisson bracket operations always appears in the time reversal of quantal systems. The i of this type are usually distinguished from the accidental i by transposing all linear operators, and interchanging bras and kets. But in our model this more elaborate procedure is not necessary, since no accidental i appear.

7.3. THE MODEL AND CHARGE CONJUGATION (C)

The operation of charge conjugation is one which achieves the transformations (81) while commuting with the full Lorentz group. An appropriate transformation may be obtained by rotating ξ and η through angles π around their respective second axes (dummy axes), this being done in a rest frame. In a rest frame this transformation is $\xi \to P^2\xi$, $\eta \to P^2\eta$, and hence, in a general coordinate system,

$$\xi \to \Gamma^\mu V_\mu \xi, \qquad \eta \to \Gamma^\mu V_\mu \eta, \qquad V^\mu \to V^\mu. \tag{86}$$

These rotations commute with the full Lorentz group as required, and induce the transformation (80) of the isospace quaternion χ and the transformation (81) of the various attributes.

It is important to notice that charge conjugation is hereby achieved by a continuous sequence of infinitesimal displacements, in accordance with ref. [8]).

7.4. THE MODEL AND PARITY (P)

The parity operation can be defined by the requirement that charge conjugation preceded by or followed by parity yields space inversion. The parity operation may thus be calculated from (79) and (86). It is

$$\begin{aligned} &x^j \to -x^j, \qquad \xi \to -\Gamma^0\Gamma^\mu V_\mu \xi, \qquad \eta \to -\Gamma^0\Gamma^\mu V_\mu \eta, \\ &V^0 \to V^0, \qquad V^j \to -V^j, \qquad \chi^a \to \chi^a. \end{aligned} \tag{87}$$

It leaves S^k, $\frac{1}{2}N$, T^k, Y and Q invariant, and reduces to the identity transformation in any rest frame.

7.5. STRUCTURE OF THE DISCONTINUOUS GROUPS

Let us introduce an operation $\tilde{\omega}$ which changes the sign of all quaternions. Then the multiplication rules for the discrete operations I, T, C and P obtained in subsects. 7.1—7.4 can be written

$$\begin{array}{lllll} \tilde{\omega}^2 = 1, & \tilde{\omega}\mathrm{I} = \mathrm{I}\tilde{\omega}, & \tilde{\omega}\mathrm{T} = \mathrm{T}\tilde{\omega}, & \tilde{\omega}\mathrm{C} = \mathrm{C}\tilde{\omega}, & \tilde{\omega}\mathrm{P} = \mathrm{P}\tilde{\omega}, \\ \mathrm{I} = \mathrm{CP}, & \mathrm{I}^2 = \tilde{\omega}, & \mathrm{IT} = \mathrm{TI}, & \mathrm{IC} = \mathrm{CI}, & \mathrm{IP} = \mathrm{PI}, \\ & & \mathrm{T}^2 = \tilde{\omega}, & \mathrm{TC} = \mathrm{CT}, & \mathrm{TP} = \mathrm{PT}, \\ & & & \mathrm{C}^2 = \tilde{\omega}, & \mathrm{CP} = \mathrm{PC}, \\ & & & & \mathrm{P}^2 = 1. \end{array} \tag{88}$$

In a conventional quantum field theory the multiplication table does not turn out quite this way. In our special representation of the Dirac matrices the transformation rules [15, 16]) are given by the following scheme:

I	$\psi \to \Gamma^0 \psi^\dagger$
T	$\psi \to \Gamma^0 \Gamma^5 \psi^{\dagger\sim}$
C	$\psi \to \psi^\dagger$
P	$\psi \to \Gamma^0 \psi$

(89)

Here ψ denotes a quantized Dirac field, each component of which is a linear operator or matrix. The symbol $\psi^\dagger$ denotes the field obtained by hermitian conjugation of each of the four components of ψ, and $\psi^\sim$ denotes the field obtained by transposition of each component. These rules give a multiplication table which differs from (88) in the following respects:

$$\mathrm{IT} = \tilde{\omega}\mathrm{TI}, \qquad \mathrm{C}^2 = 1, \qquad \mathrm{P}^2 = \tilde{\omega}, \qquad \mathrm{PI} = \tilde{\omega}\mathrm{IP}. \tag{90}$$

This difference will appear in any theory which may be based on the model, or on any similar model in which C and P are represented by continuous operations in space-time. It is important therefore that the difference between (88) and (90) can be eliminated by a suitable change in the quantal rules (89). In all known quantum field theories the parity of the fermion number, namely $(-)^N$, is conserved irrespective of whether N itself is conserved or not, and this means that the operations in any discontinuous group can not be uniquely characterized [19]). We are in fact free to adopt the rules

I	$\psi \to \Gamma^0 \psi^\dagger$
T	$\psi \to \Gamma^0 \Gamma^5 (-)^{N\sim} \psi^{\dagger\sim}$
C	$\psi \to -i(-)^N \psi^\dagger$
P	$\psi \to i\Gamma^0 (-)^N \psi$

(91)

The new rules (91) give just the multiplication table (88) of our model.

8. Quaternions and Lorentz Transformations

The isospace quaternion χ, which was introduced by eqs. (74) and (77), refers the space-time quaternion η to a space-time quaternion ξ and a velocity four-vector V^μ. One would expect therefore that V^μ and ξ determine a Lorentz frame of reference, and that χ is just η transformed into this frame. We shall now see that this is indeed the case.

First we must define an auxiliary quaternion ζ,

$$\zeta \equiv \Gamma^\mu V_\mu \xi, \quad \text{then also} \quad \xi = -\Gamma^\mu V_\mu \zeta. \tag{92}$$

A study of the symmetry of the Dirac matrices shows that the four components of ζ are related by the equation

$$\bar{\xi}\Gamma^5\zeta = 0. \tag{93}$$

Thus ζ is just an alternative carrier for the three degrees of freedom inherent in V^μ. We can now use ξ and ζ to construct a tetrad of four-vectors $\Gamma^\mu{}_0$, $\Gamma^\mu{}_1$, $L^\mu{}_2$, $\Gamma^\mu{}_3$.

$$\begin{aligned} L^\mu{}_0 &\equiv \tfrac{1}{2}(\bar{\xi}\Gamma^\mu\xi + \hat{\bar{\zeta}}\Gamma^\mu\zeta)/\bar{\xi}\zeta, \\ L^\mu{}_1 &\equiv \bar{\xi}\Gamma^\mu\zeta/\bar{\xi}\zeta, \\ L^\mu{}_2 &\equiv \bar{\xi}\Gamma^\mu\Gamma^5\zeta/\bar{\xi}\zeta, \\ L^\mu{}_3 &\equiv \tfrac{1}{2}(\hat{\bar{\zeta}}\Gamma^\mu\zeta - \bar{\xi}\Gamma^\mu\xi)/\bar{\xi}\zeta. \end{aligned} \tag{94}$$

With the help of eq. (65) it can be shown that $L^\mu{}_\nu$ is an orthonormal tetrad, i.e.

$$L^\mu{}_\nu L_{\mu\rho} = g_{\nu\rho}. \tag{95}$$

Thus (94) parametrize a Lorentz transformation by two quaternions, in much the same way that (33) parametrizes a space rotation by one quaternion. The condition (93) is not essential here, for it is not needed to obtain (95), However this may be, it *is* necessary to use (93) in connection with our model, for in the model ζ is only an auxiliary quaternion, defined by (92) and therefore subject to (93).

If we use (92) to eliminate ζ from $L^\mu{}_0$ we obtain

$$L^\mu{}_0 = V^\mu \tag{96}$$

The transformation $L^\mu{}_\nu$ has in fact been designed to transform from a system with velocity V^μ into a system with zero velocity. Moreover, in any rest frame, i.e. any frame such that $V^\mu = \delta^\mu{}_0$, we have $L^0{}_k = L^k{}_0 = 0$, $L^j{}_k = R^{jk}/\xi^a\xi^a$, where R^{jk} is the rotation matrix (33). It is quite evident therefore that the Lorentz frame we are seeking is none other than $L^\mu{}_\nu$.

8.1. A COMPLETE SET OF QUATERNIONS

Let us now resume our discussion of the isospace quaternion χ. The relativistic definitions of χ (eqs. (74) and (77)) reduce to the non-relativistic definitions (39) in any rest frame. The non-relativistic definitions imply an inverse relation (40), which, allowing for the normalization of ξ, now reads

$$\eta = (-P^j\bar{\xi}\chi^j + \bar{\xi}\chi^4)/\xi^a\xi^a, \qquad \text{(rest frame only)}. \tag{97}$$

Making use of the Dirac matrices (47) and (52) and the auxiliary quaternion ζ (92) we can write (97) in the form

$$\eta = (\Gamma^5\zeta\chi^1 - \zeta\chi^2 - \Gamma^5\xi\chi^3 + \xi\chi^4)/\hat{\xi}\zeta. \tag{98}$$

This equation, being explicitly covariant, is valid in all Lorentz frames. It asserts that the χ^a are the expansion coefficients of η with respect to a complete quaternion tetrad. Denoting the four quaternions by $Q_{(1)} \ldots Q_{(4)}$ respectively, and using (93), we find that their normalization matrix is

$$\hat{Q}_{(a)} Q_{(b)} = C_{ab}/\hat{\xi}\zeta. \tag{99}$$

The isospin T generates rotations of η in the three spatial planes of the tetrad $L^\mu{}_\nu$. The third spatial plane occupies a privileged position because the tetrad is not conceived as a primary entity. The primary entities are V^μ and ξ, and the rotations of ξ around its own third axis induce rotations of the third spatial plane of $L^\mu{}_\nu$.

With the help of the analysis of the present section we are able to write the various displacement operators (78) as partial differential operators on ξ, η and V. We have the following scheme:

S^k	$\frac{1}{2}i\xi\Sigma^k\frac{\partial}{\partial\xi} + \frac{1}{2}i\eta\Sigma^k\frac{\partial}{\partial\eta} - i\epsilon^{klm}V^l\frac{\partial}{\partial V^m}$
$\frac{1}{2}N$	$-\frac{1}{2}i\hat{\xi}\Gamma^5 C\frac{\partial}{\partial\xi} - \frac{1}{2}i\epsilon^{klm}L^\mu{}_l L^\nu{}_m\hat{\eta}\Gamma_\nu\Gamma_\mu C\frac{\partial}{\partial\eta}$
T^k	$\frac{1}{2}i\epsilon^{klm}L^\mu{}_l L^\nu{}_m\hat{\eta}\Gamma_\nu\Gamma_\mu C\frac{\partial}{\partial\eta}$
Y	$\frac{1}{2}i\hat{\eta}\Gamma^5 C\frac{\partial}{\partial\eta}$

(100)

9. Discussion

We discuss first the group properties of the model. It associates the continuous groups (Lorentz, baryon gauge, isospin, and hypercharge) with displacement operations. The objects displaced are carried in space-time, and derive all their relevant transformation rules, kinematics, and topology from the geometry of space-time. They are parametrized by two independent space-time Majorana spinors ξ and η, and a time-like four-vector V. The expressions $\hat{\xi}\Gamma^\mu V_\mu\xi$, $\hat{\eta}\Gamma^\mu V_\mu\eta$ and $V^\mu V_\mu$ are invariant under all the group operations, both continuous and discrete. There are therefore only nine variables participating in the group operations. The continuous group itself is an eleven parameter group. Thus not all representations of the continuous group can be realized in the model. The empirical relations between spin and baryon number. and between isospin and hypercharge, are taken into account in this way.

The quantum conditions of the continuous group appear in a most fundamental way in the model. The infinitesimal operators for spin, baryon charge, isospin and hypercharge exhibit discrete spectra simply as a consequence of demanding continuity within the nine-dimensional group manifold. For they generate displacements in directions in which the group manifold closes back upon itself. There is no discrete spectrum associated with the acceleration operators of the Lorentz group. The latter operators generate displacements in directions in which the group manifold is open and infinite.

The operators of the discrete group I, T, C, P are exhibited as finite displacements of the same nine variables. The multiplication table of the discrete group is different from that usually associated with quantum field theories. But the difference can be resolved by invoking the superselection rule for the parity of the fermion number.

The behaviour of isospace under space inversion and time inversion arises automatically and, it seems, inevitably, from the space-time properties of the underlying variables. This feature gives perhaps the most direct evidence that the model contains some aspect of physical truth.

It is known that all group operations under which a dynamics is invariant can be manifested in two different senses. The primary or *passive* sense implies that the dynamical system itself is left quite unaltered, while the variables describing it are transformed so as to refer it to a new reference frame. The original variables, being supposed to be subject to a set of fundamental dynamical laws, furnish a particular set of solutions of these laws. If the new variables obtained by transformation of the old always turn out to satisfy the same set of fundamental dynamical laws the dynamics is said to be invariant under the transformation. Every invariance transformation can evidently be used in a secondary, or *active* sense, in which no change of the coordinate system is contemplated. The effect of an active transformation is to associate with each solution of the dynamical laws a further, and usually different, solution. In this context Fröhlich [8]) has recently enunciated a principle of continuity, according to which it should be possible to realize every active discrete transformation of a system by a sequence of active and kinematically possible infinitesimal transformations of the same system.

Now it will be seen that the model of isospace established herein satisfies Fröhlich's continuity principle in all respects. For example space inversion, conceived in the active sense, can be realized by rotating the bodies described by ξ and η through angles π around their respective second axes, the velocity $\mathbf{V}$ being rotated through an angle π about any axis perpendicular to itself. These are continuous transformations within the kinematical scheme of the model. A similar situation prevails with regard to the other three discrete transformations. The only apparent element of discontinuity lies in the substitution $i \to -i$ which is associated with time reversal. But this is not a kinematical

discontinuity, and would appear to be irrelevant to the present argument.

It is often said, and quite rightly, that the elementary particles contain a screw sense. But an ordinary material screw does not satisfy Fröhlich's principle. A right-handed screw does not turn into a left-handed one by being rotated. In view of this it may seem quite remarkable that the reflection properties can be obtained correctly by rotations in space-time.

We shall now make a comparison between the variables of our model and the basic fields which have been suggested in connection with various composite models of the elementary particles. Let us first consider spinor models. In this case Gürsey [20]) and Thirring [21]) have come to the conclusion that six Majorana spinors are required to give a representation of the discrete group as well as the continuous group. Yet our model can be described in terms of just three Majorana spinors, namely ξ, η and ζ. The transformation rules for these are

$$\begin{aligned} &\text{C:} \quad \xi \to \zeta, \qquad \zeta \to -\xi, \qquad \eta \to \Gamma^{\mu} V_{\mu} \eta, \\ &\text{P:} \quad \xi \to -\Gamma^{0} \zeta, \qquad \zeta \to \Gamma^{0} \xi, \qquad \eta \to -\Gamma^{0} \Gamma^{\mu} V_{\mu} \eta. \end{aligned} \tag{101}$$

Here V is a function of ξ and ζ, given by eqs. (96) and (94). Thus our model manages with half the usual number of Majorana fields, but only by introducing non-linear transformation rules.

A closer correspondence with the ideas of field theory is obtained if we compare the model with a mixed set of fields, also proposed by Gürsey [20]). These fields comprise a Λ-particle Dirac field ψ, and a K-particle scalar quaternion field χ. To achieve the comparison we state the model in terms of the quaternion ξ, the auxiliary quaternion ζ, and the isospace quaternion χ. The number of fields is then the same as in Gürsey's mixed model, and in fact all the continuous transformations match up. There is again however a difference in the treatment of C and P, as we shall now see. In Gürsey's mixed model the Dirac field ψ is supposed, and rightly so, to undergo the conventional charge conjugation and parity operations

$$\text{C:} \quad \psi \to \psi^{\dagger}, \qquad \text{P:} \quad \psi \to \Gamma^{0} \psi. \tag{102}$$

Moreover ψ undergoes just a phase change when subject to the baryon gauge transformation, so that the only possible way of relating it to our fields ξ and ζ is by the equation

$$\psi = (1+i\Gamma^{5})\xi + (1-i\Gamma^{5})\zeta. \tag{103}$$

Substituting (102) in (103), one obtains

$$\begin{aligned} &\text{C:} \quad \xi \to \zeta, \qquad \zeta \to \xi, \\ &\text{P:} \quad \xi \to \Gamma^{0} \zeta, \qquad \zeta \to \Gamma^{0} \xi. \end{aligned} \tag{104}$$

These rules are different from those of our model, namely from (101). The real

reason for this discrepancy is that Gürsey's ψ is supposed to be a quantized field, such as that associated with the Λ-particle, while our ξ and ζ are not seen as quantized fields, but rather as numerical variables which can serve as the arguments of a wave functional. Nevertheless, one may ask whether it is not possible to modify the transformation rules of our model in such a way as to achieve the rules (104). And indeed it does turn out to be possible, but only at the expense of violating Fröhlich's continuity principle. The transformation rule for ζ, in our model, is conditioned by that for the velocity four-vector V, through eq. (92). If we agree to impose an additional change of sign on all four components of V, in both the C and P operations, we obtain (104). But such a change of sign of V cannot be produced by any continuous operation of the Lorentz group, and it is therefore kinematically impossible. There is another strong reason for not proceeding in this way. The appearence of past time-like as well as future time-like V would bring in a peculiar dichotomy in our space-time description, not in any obvious correspondence to the physical world.

This discussion brings up a further matter concerning the possible utilization of the model. It is clear that one might seek to extend ξ, η and V into local space-time fields. The question then arises as to whether there would be any sense in trying to quantize these fields.

The work of subsect. 7.5 indicates that one cannot establish any complete connection with existing field theories at the 'classical' level, because the group properties of our model are different from those of any such classical theory. The difference arises of course because our C and P transformations are non-linear. One might hope that by quantizing ξ, η and V this discrepancy could be resolved. But the non-linearity of the isospin and baryon gauge transformations, as well as of C and P, make it most improbable that any conventional field quantization method would lead to results of significance. And it is quite clear that if we would nevertheless try to proceed in this way, we would lose the space-time picture which we have been trying to obtain.

These considerations lead one back to consider the sort of representation suggested by the theory of the spinning top. Thus one might look for a quantal amplitude Ψ, which would be a functional of fields $\xi(x)$, $\eta(x)$, $V(x)$, (or of some similar set of classical fields). The main problem would then be to investigate the possibility of representing anti-commuting fields as linear operators on such c-number functionals.

It is a pleasure to thank Professor Fröhlich for many discussions bearing on these and related matters.

References

1) F. Bopp and R. Haag, Zeits. f. Naturforsch. **5a** (1950) 644
2) A. R. Edmonds, Angular momentum in quantum mechanics (Princeton University Press, 1957);

M. E. Rose, Elementary theory of angular momentum (Wiley, New York, 1957)
3) P. Hillion and J.-P. Vigier, Ann. Inst. H. Poincaré **16** (1959) 161, 217
4) H. B. G. Casimir, Rotations of a rigid body in quantum mechanics (J. B. Wolters, Groningen, 1931).
5) T. Takabayasi, Prog. Theor. Phys. **23** (1960) 915;
D. Bohm, P. Hillion and J. -P. Vigier, Prog. Theor. Phys. **24** (1960) 761
6) L. Landau, Nuclear Physics **3** (1957) 127
7) E. T. Whittaker, Analytical dynamics (Cambridge University Press 1937) 8—13
8) H. Fröhlich, Proc. Roy. Soc. A **257** (1960) 147, 283; Helv. Phys. Acta **33** (1960) 803
9) F. Gürsey, Nuovo Cim. **3** (1956) 988, **5** (1957) 784
10) F. Gürsey, Nuovo Cim. **7** (1958) 411
11) D. Bohm and R. Schiller, Suppl. Nuovo Cim. **1** (1955) 67
12) F. D. Murnaghan, The theory of group representations (Johns Hopkins Press, 1938) 318;
H. Weyl, Theory of groups and quantum mechanics, transl. H. P. Robertson (Methuen, 1931) 180;
E. P. Wigner, Group theory and its applications to the theory of atomic spectra, transl. J. J. Griffin (Academic Press, 1959) 247
13) G. Lochak, Comptes Rendus **246** (1958) 2855
14) B. d'Espagnat and J. Prentki, Nuclear Physics **1** (1956) 33
15) P. Roman, Theory of elementary particles (North-Holland Publishing Co., Amsterdam, 1960)
16) H. Umezawa, Quantum field theory (North-Holland Publishing Co., Amsterdam, 1956)
17) W. Pauli, Ann. Inst. H. Poincaré **6** (1936) 109;
R. H. Good, Jr., Revs. Mod. Phys. **27** (1955) 187
18) S. S. Schweber, H. A. Bethe and F. de Hoffman, Mesons and Fields (Row, Peterson and Co., 1955) Vol. 1
19) G. C. Wick, A. S. Wightman, and E. P. Wigner, Phys. Rev. **88** (1952) 101
20) F. Gürsey, Nuclear Physics **8** (1958) 675
21) W. Thirring, Nuclear Physics **10** (1959) 97
22) T. H. R. Skyrme, Proc. Roy. Soc. A **260** (1961) 127
23) E. J. Schremp Phys. Rev. **85** (1952) 721, **99** (1959) 1603

2.1

Nuclear Physics **27** (1961) 234—247; © *North-Holland Publishing Co., Amsterdam*

Not to be reproduced by photoprint or microfilm without written permission from the publisher

THE RELATIVE DEUTERON/PROTON YIELD FROM 45 MeV BREMSSTRAHLUNG IRRADIATION OF COPPER

GRACE P. HO † and EDWIN L. ILOFF

Institute for Atomic Research and Department of Physics, Iowa State University, Ames, Iowa ††

Received 16 February 1961

Abstract: A new method has been developed and used to measure the photo-deuteron to photo-proton ratio for copper irradiated with 45 MeV maximum energy bremsstrahlung. The photo-particles leaving the 50 μm thick target were deflected by a magnetic field in an evacuated chamber and were detected with nuclear emulsion plates. The particles were identified by using their ranges in emulsion and angles of entrance to retrace their paths back to the target. Of the 1614 tracks detected, 1134 were due to particles from the target. Of these 1114 were identified as protons and only 20 were found to be deuterons, giving a deuteron to proton ratio of 0.018 ± 0.009. This result is not in agreement with the much larger values found for this ratio by other investigators using nuclear emulsion grain-counting techniques and a magnetic cloud chamber method.

1. Introduction

The relative yield of deuterons to that of protons due to X-ray bombardment of various targets has been the subject of many investigations [1–9]). For bremsstrahlung of maximum energies less than 100 MeV, measurements on various elements and at various beam energies have resulted in values for the ratio of deuterons to protons that vary greatly and in no obviously systematic fashion. Some of the results are much too large to be explained easily by a simple theory such as the evaporation model or a model based on direct interaction with a preformed deuteron in the nucleus. It has been suggested that a two stage pick-up process may be responsible for the large ratios.

Four different techniques have been used to study this problem. The method used most often [1–5]) separates deuterons from protons by comparing grain-densities and ranges of particle tracks in nuclear emulsion plates. A second method [6, 7]) makes the identification by comparing track curvatures and ranges of particles in a magnetic cloud chamber. A third method [8]) has made use of the activation curve near threshold to make a separation between γ, d and γ, pn cross sections. Each of these methods is subject either to poor resolution, or to difficulties in analyzing enough tracks to obtain good statistics, or to both.

† Now at Winona State College, Winona, Minnesota.

†† A preliminary report of this work, performed in the Ames Laboratory of the U. S. Atomic Energy Commission (Contribution No. 982), was presented at the Karlsruhe Photonuclear Conference, August 18—22, 1960.

Another method [9]) uses the energy loss rate and range in a pair of scintillation counters. This method allowed measurements only of particles with energies greater than about 16 MeV so that most of the particles produced would be excluded from the measurement. Copper has been measured three times by the grain-counting technique [1–3]) for bremsstrahlung of maximum energies in the vicinity of 24 to 30 MeV and once by the magnetic cloud chamber method for 65 MeV beam energy. In each of these measurements a large ratio (greater than 0.15) was found. Other elements have been measured only once each except in the case of cobalt [2, 4]) for which the two results are conflicting, one yielding a high ratio and the other a low one. This paper is a report on a determination of the photodeuteron to photoproton yield ratio for copper measured by a new technique for 45 MeV maximum energy bremsstrahlung. Particles from the target were bent by a magnetic field in a vacuum chamber and were detected by nuclear emulsions. Measurements of particle ranges, positions and track-angles in the emulsion plates allowed particles to be identified by tracing them back to the target.

2. Experimental Procedure

2.1. DESCRIPTION OF THE METHOD

A copper foil target placed in a vacuum chamber was irradiated with bremsstrahlung of 45 MeV maximum energy. A magnetic field was applied perpendicular to the floor of the chamber so that the charged particles leaving the target followed helical paths to the nuclear emulsion plates used for particle detection. These plates, placed to one side of and slightly below the target, were arranged in three rows and were placed horizontally with the emulsion surfaces facing upward. The residual range of a particle in the emulsion allowed us to evaluate its energy if its identity was assumed. Knowing the energy of a particle, the strength of the magnetic field, the point at which the particle entered the emulsion, the horizontal orientation angle and the dip angle of the track in the emulsion, we constructed its path from the point at which it entered the emulsion back to where it originated from the target. The reconstruction was done numerically. All measured tracks were treated first as protons and their paths were retraced back to the target plane to see how many of them appeared to be coming from the irradiated area of the target. Those falling inside this area (within the accuracy of the measurements) were taken to be photoprotons ejected from the target. Deuteron tracks, when treated as protons, would apparently have smaller radii of curvature than they actually had and their paths would appear to bend more than they actually did, and they would therefore appear to originate in a region away from the irradiated part of the target as shown in fig. 1(a). Next, all measured tracks were treated as though they were deuterons and their paths were traced back to the target. This time, all those that fell

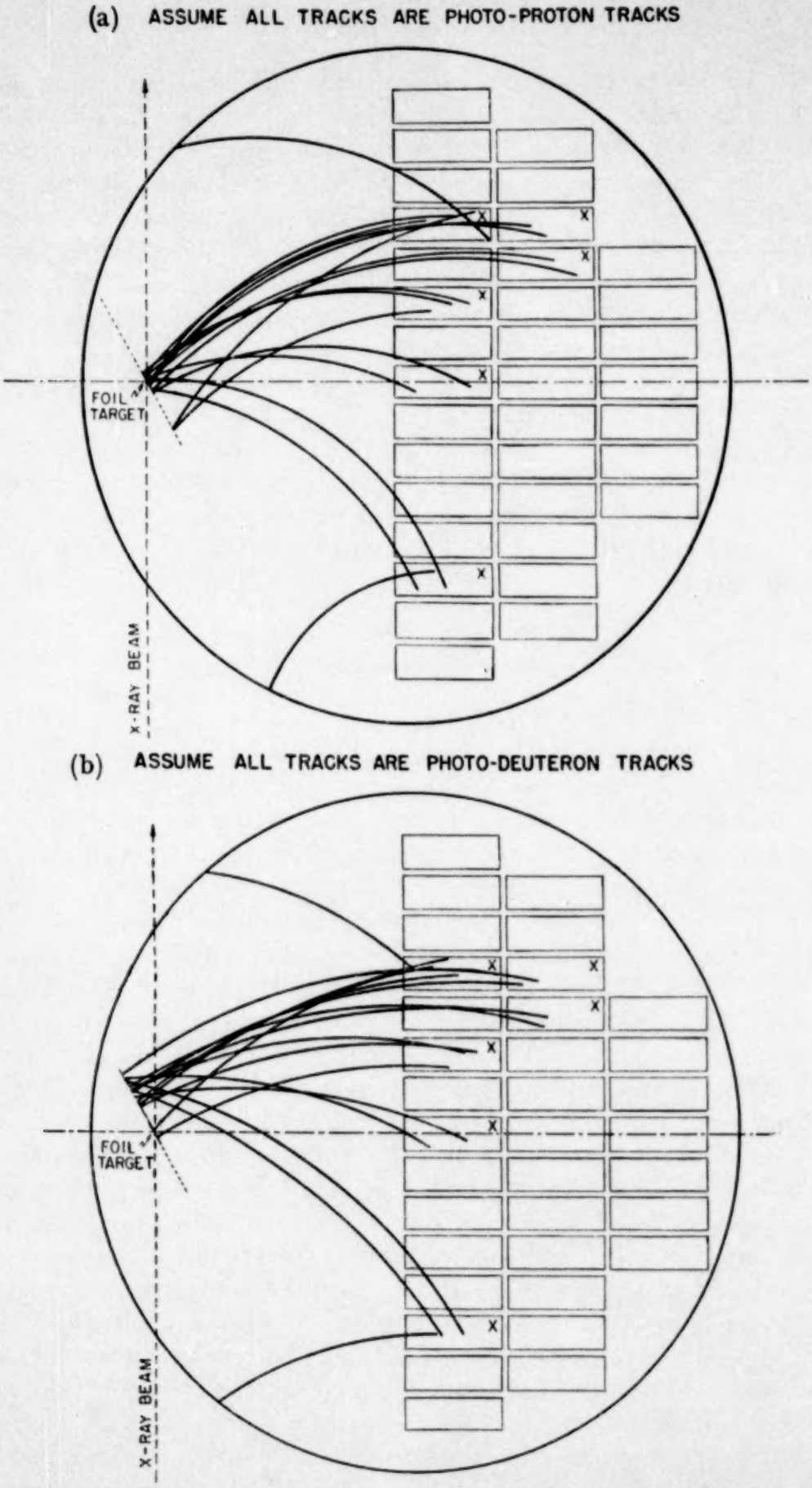

Fig. 1. Schematic view of camera showing how particles are traced back to point of origin at the target. (a) All particles are assumed to be protons. (b). All particles are assumed to be deuterons.

within the effective target area were taken to be photodeuterons from the target. Those particles that were actually protons would appear to have radii of curvature larger than the actual values; they would bend less than they should and would appear to originate in a region off to the other side of the irradiated part of the target as shown in fig. (1b).

2.2. EXPERIMENTAL ARRANGEMENT

The experimental arrangement is shown in figs. 2 and 3. The vacuum chamber consisted of a stainless steel cylinder that fitted around the magnet pole-

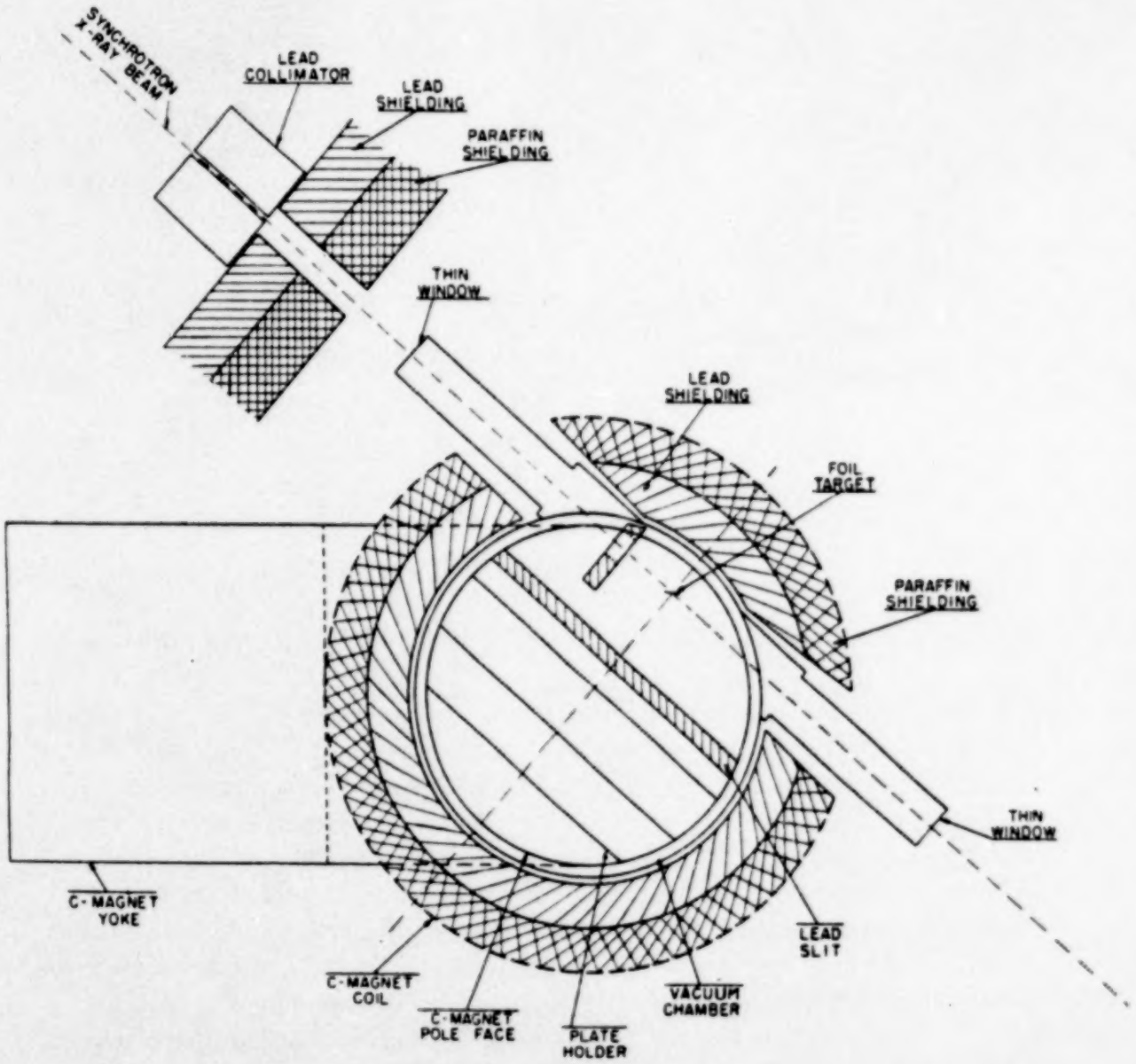

Fig. 2. Experimental arrangement.

faces so that the pole-faces formed its top and bottom walls. The X-ray beam entered and left through two long brass tube extensions of the chamber. Thin mylar windows (covered with thin black paper to keep out light) on the outer ends of the tubes allowed the beam to enter and leave the chamber in such a way that few photoparticles from the windows could get to the detecting plates. The magnet pole-faces were 15 cm apart and 50.8 cm in diameter. A mechanical vacuum pump kept the pressure in the chamber below 200 μm of mercury during the exposure.

Inside the chamber the emulsion plate-holder and the target-holder were mounted so that the beam would irradiate the centre of the target. The emul-

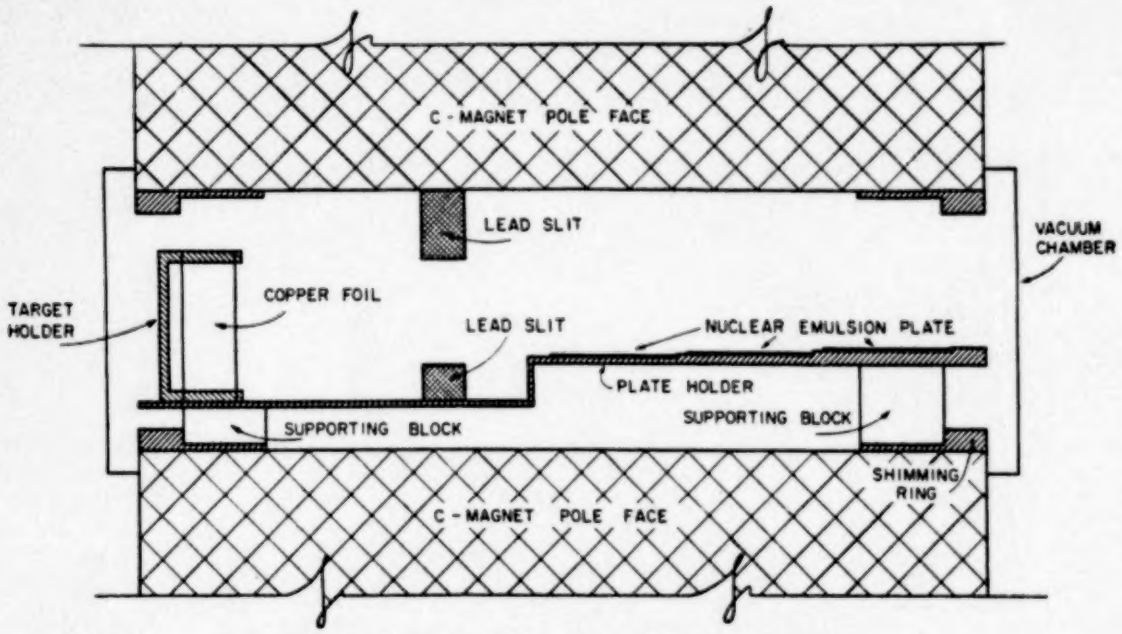

Fig. 3. Cutaway side view of emulsion camera.

sion plates were placed at such a level, with respect to the position of the beam at the target, that the tracks of particles having energies up to 25 MeV and originating from the target would end inside the emulsions.

A 50 μm thick copper foil was used as the target and was mounted on the target-holder which was about two meters away from the Iowa State Synchrotron. The target was placed at an angle of 30° with respect to the direction of the X-ray beam. Thirty-five Ilford C-2 nuclear emulsion plates, 200 μm thick, 2.54 cm by 7.62 cm, were used for the registration of the particle tracks. They were placed on the plate-holder with their surfaces facing the upper pole-face during the exposure. Short pegs fixed in the plate-holder were used to position the plates precisely with respect to the target. The plates were kept in place by springs. The vacuum chamber was shielded with lead bricks and paraffin blocks to block stray X-rays, positive and negative electrons and neutrons from hitting the chamber walls and producing undesirable background. There were also lead

slits placed inside the vacuum chamber at positions that would minimize the possibility of those secondary particles originating from the pole-faces and the chamber walls being recorded in the emulsions.

The magnet pole-faces were shimmed to give a magnetic field variation of less than 1 %, as measured by a nuclear magnetic resonance technique, over an area 40.6 cm in diameter. The magnetic field used during the exposure was 10 850 G. The X-ray beam was collimated with lead bricks. In order to check the alignment of the X-ray beam, the collimator and the vacuum chamber, several pictures of the beam were taken with X-ray films mounted at the entrance and the exit windows and at the target-holder. Adjustments were made after each exposure until the beam and the apparatus were aligned. The beam at the target was rectangular in shape, 1 cm wide and 1.1 cm high. The maximum bremsstrahlung energy was 45 MeV, and the target was irradiated for a period of 12 h continuously. The chamber was evacuated during the exposure to prevent energy loss of particles in flight, and also to reduce the number of background photoparticles that would be produced by the beam striking air nuclei.

2.3. EMULSION PROCESSING AND MEASUREMENTS

The 200 μm thick Ilford C-2 nuclear emulsion plates were developed in Kodak D-19 developer (diluted 6 to 1) at 9°C for an hour and fixed in Kodak acid fixer. The development at this low temperature for a long period reduced the number of single exposed grains due to the general electron and photon background, but still allowed protons up to energies of 30 MeV to be seen easily as they entered the surface of the emulsion.

A Leitz Ortholux microscope provided with wide field 10X oculars and a Leitz 22X oil immersion objective was used for the scanning and measuring. All the tracks within a given area that entered the emulsion from the top were recorded. In addition to the 1614 detected tracks that entered from the top and stopped in the emulsion there were only about a half-dozen that did not stop. All the tracks that did stop were measured and were included in the analysis. The projected range of each track was measured with a calibrated reticle scale, the horizontal orientation angle was read to the closest 0.2° on an angular scale mounted on an eyepiece, and the track dip-angle was obtained in the standard way with the aid of the vertical fine focusing mechanism of the microscope. For the dip-angle determination the thickness of the emulsion before development was taken to be 200 μm as specified by the manufacturer. The coordinates of the entrance point of each particle were determined from two travelling micrometers mounted on the microscope stage.

3. Analysis and Results

The quantities measured for each track were fed into an IBM 650 computer and the following quantities were found:

(i) the energy of the particle that produced the track,

(ii) the position of the point of intersection of the computed particle path with the target plane,

(iii) the initial ejection space angle of the particle with respect to the X-ray beam direction.

All these quantities were computed twice for each of the tracks. The first time all tracks were assumed to be due to protons while the second time they were all assumed to be deuteron tracks. The energies were calculated using range-energy relation data from the tables of Barkas and Young [10]). To obtain sufficient accuracy the particles were divided into two groups by range and the following expressions were used:

$$E_p = 72.26\,\lambda^{0.647} \quad \text{for } \lambda \leqq 75\times10^{-4}\text{ cm},$$

$$E_p = 56.57\,\lambda^{0.596} \quad \text{for } \lambda > 75\times10^{-4}\text{ cm},$$

$$E_d = 105.3\,\lambda^{0.673} \quad \text{for } \lambda \leqq 100\times10^{-4}\text{ cm},$$

$$E_d = 76.6\,\lambda^{0.603} \quad \text{for } \lambda > 100\times10^{-4}\text{ cm},$$

where λ is the range of the particle in emulsion (cm), E_p the proton kinetic energy (MeV) and E_d the deuteron kinetic energy (MeV).

Any effects due to drying of the emulsion during the 12 h spent in vacuum was neglected. Since the magnetic field varied by less than 1 % over the area of interest it was taken as constant at 10 850 G.

Some of the computed particle paths did not intersect the target plane. For these the distances of closest approach to the target centre were computed. In no case did such a computed path come anywhere near the target, and therefore all these particles were rejected as background at this point. For the remaining particles the following two coordinates for the point of intersection of the computed path with the target plane were found:

1) the horizontal distance t from the centre line of the effective target area to the point of intersection, where t is positive if the point of intersection falls in back of the target centre (i.e. farther from the synchrotron).

2) the vertical distance h from the emulsion surface to the point of intersection.

Fig. 4 is a histogram of the number of particles plotted against the coordinate t when all the particles were assumed to be protons. Fig. 5 shows the same distribution when all particles were assumed to be deuterons. The t-histogram for all particles assumed to be protons shows a very sharp and well defined peak centred within 1 mm of the target centre. In fig. 4 most of the particles fall within the region -2 cm $\leqq t \leqq +2$ cm. The beam itself extended from $t = -1$ cm to $t = +1$ cm. The observed distribution is, of course, broadened by errors in the track measurements. For the other diagram, where all the particles are assumed to be deuterons, the peak is shifted to larger values of t,

broadened, and assumes a skewed shape. This is just what would be expected if most of the particles were protons. Clearly the number of deuterons present is quite small since no well defined peak can be seen in the -2 cm $\leqq t \leqq +2$ cm region.

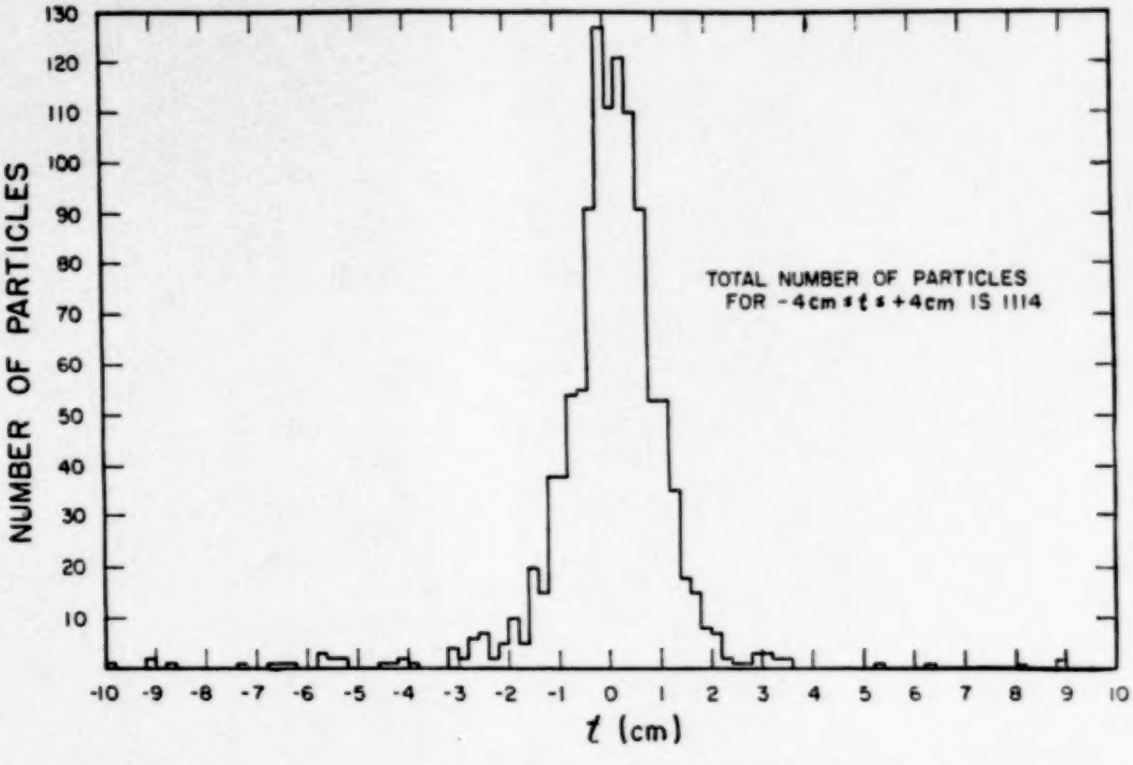

Fig. 4. Number of particles plotted as a function of t if all particles are assumed to be protons. (Only particles with $h \leqq 7$ cm are included.)

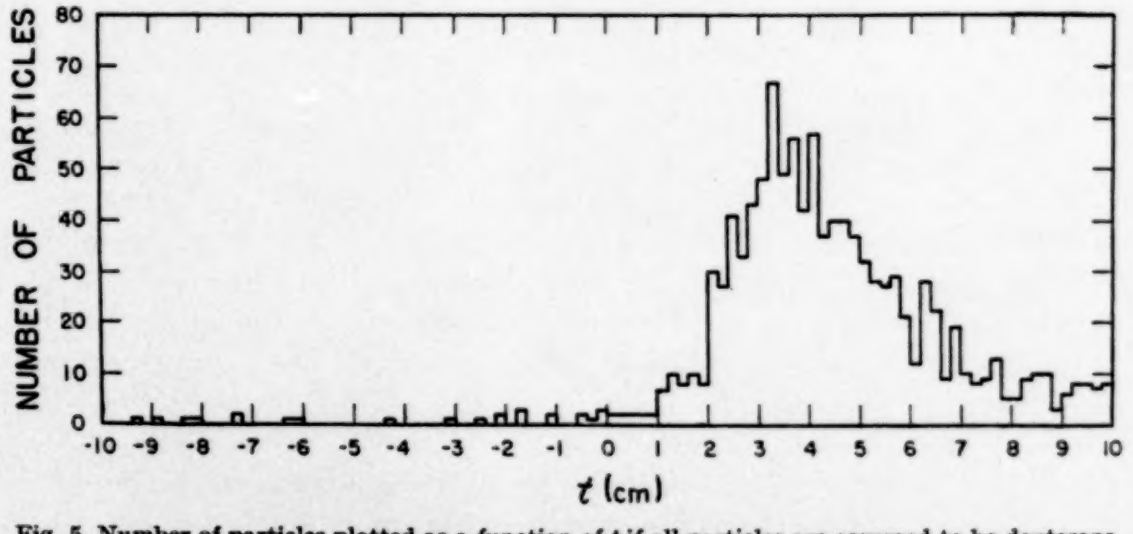

Fig. 5. Number of particles plotted as a function of t if all particles are assumed to be deuterons. (Only particles with $h \leqq 7$ cm are included.)

Fig. 6 shows the number of particles plotted as a function of h when all the particles were assumed to be protons. It is clear from this histogram that nearly all the photoparticles apparently come from the region $0 \leqq h \leqq 7$ cm. The spread in height is obviously much larger than 1.1 cm, the height of the effective area of the target. This is due to the very poor accuracy that can be attained for track dip-angle measurements.

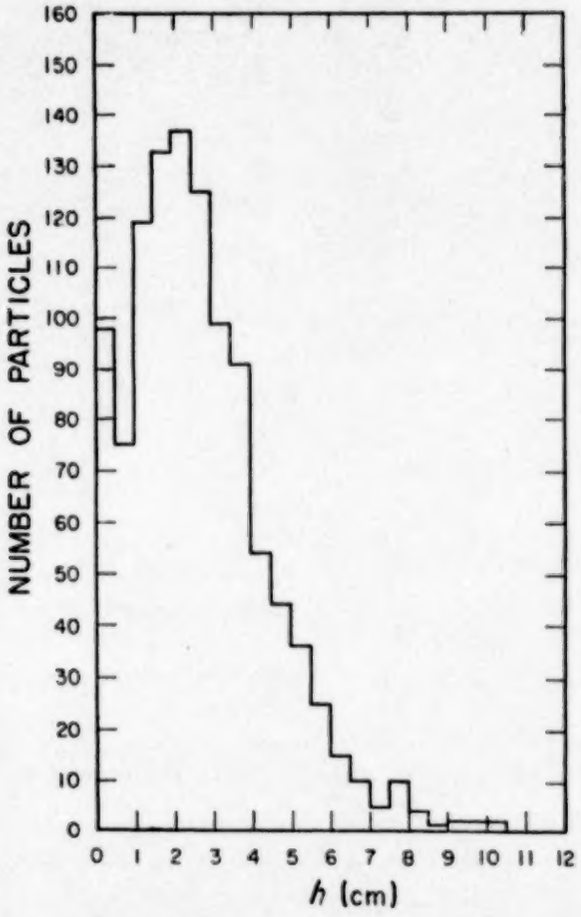

Fig. 6. Number of particles plotted as a function of h if all particles are assumed to be protons. (Only particles with -2 cm $\leqq t \leqq +2$ cm are included.)

From figs. 4 and 6 the criteria for selection of acceptable detected particles were chosen. All particles that fall within the limits of -4 cm $\leqq t \leqq 4$ cm and $h \leqq 7$ cm were taken to be particles emitted from the irradiated region of the target. The number of acceptable photoprotons may easily be determined accurately from fig. 4 and was found to be 1114. Since the number of acceptable photodeuterons is so small it is much harder to obtain. This number was estimated by two different methods.

Method 1. From fig. 5 it is clear that some of the protons overlap into the region from $t = -4$ cm to $t = +4$ cm where the deuterons are expected to be, but they do not overlap as far as $t = 0$. Thus, aside from the background, all

particles in the region from $t = -4$ cm to $t = 0$ cm should be deuterons. The number of particles in this region is 15. The background was found by taking the number of particles from $t = -10$ cm to $t = -4$ cm and dividing by the distance of 6 cm over which they were distributed to obtain a density of 1.5 background particles/cm. Thus in the interval $t = -4$ cm to $t = 0$ cm, we find there are 6 background particles, leaving 9 deuterons. We then assume that the deuteron distribution for fig. 5 should have the same shape as the proton distribution in fig. 4. Since this shape is fairly symmetric the 9 deuterons between $t = +4$ cm and $t = 0$ cm are multiplied by 2 to give 18 as an estimate for the total number of deuterons between $t = -4$ cm and $t = +4$ cm.

Method 2. In fig. 4 the part of the particle distribution due to protons only should be symmetric since its shape is due to the shape of the effective target area (rectangular) and the random errors in the track measurements. There is, however, a significant deviation from symmetry at the foot of the peak on the left side just where some of the deuterons are expected to appear. In order to determine the number of deuterons near the foot of the left side of the peak, the proton distribution was subtracted from the total particle distribution. Since the right side of the total particle distribution peak is due only to protons, the shape of this side and the assumed symmetry were used to determine the shape of the proton distribution. The particles farther from the foot were identified as deuterons if these same particles fell between $t = -4$ cm and $t = +4$ cm in fig. 5. Background was estimated as before. This method resulted in an estimate of 22 for the number of deuterons.

The two estimates appear to be about equally accurate and the number of deuterons was therefore finally taken to be 20, the average of the two. The standard deviation of the result from each of the methods was estimated to amount to 10 particles, which was taken as the error in the average. With 20 deuterons and 1114 protons we obtain for the ratio of the yield of photodeuterons to that of photoprotons for copper irradiated with 45 MeV maximum energy bremsstrahlung the result

$$Y(\gamma, \mathrm{d})/Y(\gamma, \mathrm{p}) = 0.018 \pm 0.009.$$

Since the deuterons are so small in number and located so near to a very large proton peak in both figs. 4 and 5, the presence of a very few small mistakes (as opposed to errors) in track measurements could throw a few tracks from the large peaks where they belong to the regions near the feet of the peaks. The inclusion of a very small number of such mistakes could change the estimates of the number of deuterons very considerably. To prevent this possibility all tracks that fell in regions where they might be counted as deuterons, or in a similar position on the other side of the peak, or in regions used for the background estimate, were re-measured. Two such mistakes were found and eliminated; there should thus be no significant error from this source.

It should be kept in mind that the ratio was found for particles of an arbitrary selection of momenta and directions determined by the geometry of the experi-

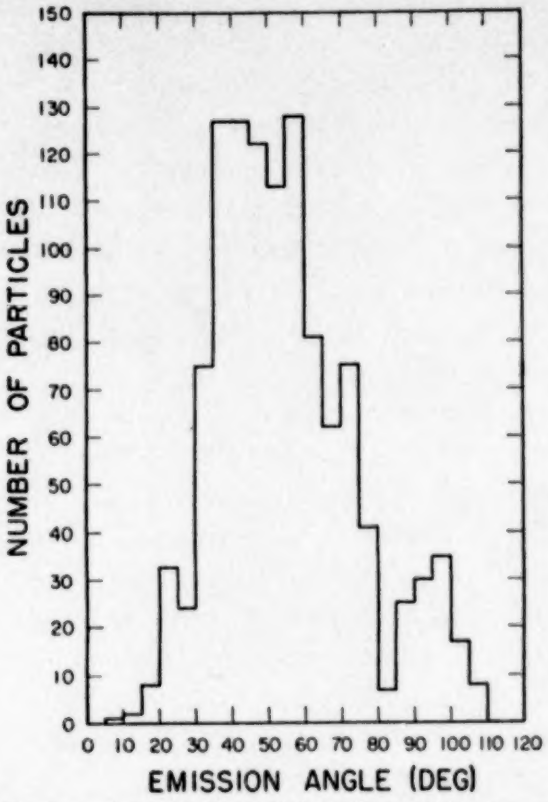

Fig. 7. Angular distribution of detected particles (all particles assumed to be protons).

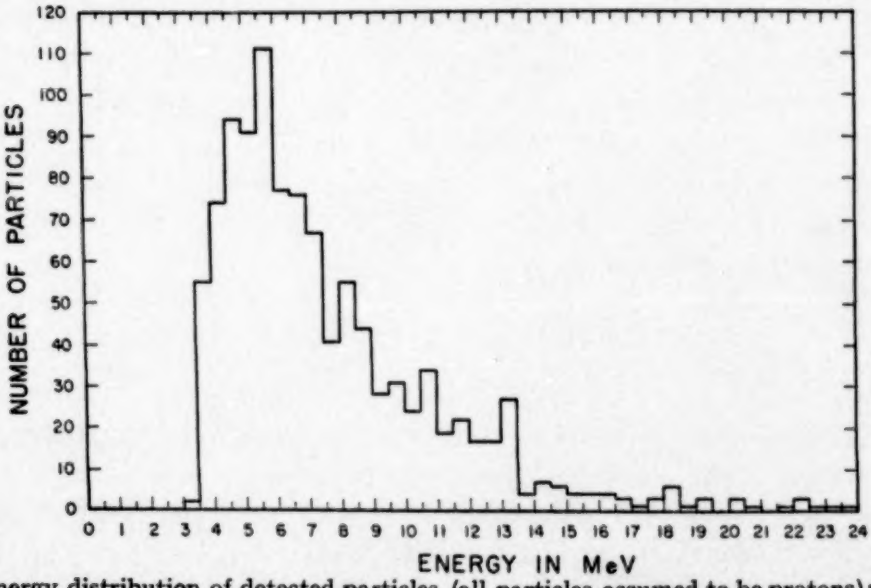

Fig. 8. Energy distribution of detected particles (all particles assumed to be protons); $h \leqq 7$ cm, $t \leqq 3$ cm.

ment and the plates that were chosen for analysis. The particular plates that were scanned are marked with crosses in fig. 1. The number of accepted photoprotons is plotted in fig. 7 as a function of the space angle between the beam

direction and the direction of each proton as it leaves the target. The number of accepted photoprotons as a function of the energy of arrival at the detecting plates is plotted in fig. 8. There is a cut-off in this distribution due to the distance of the detecting plates from the target, since low energy particles will move in spirals of small radius and thus will not reach the plates. The energies of particles arriving at the plates are, of course, not the energies at which they are ejected from the nucleus since their energies are degraded in the target. This, as well as the presence of the magnetic field, reduces the number of particles produced at low energies that will be detected. One effect of the target thickness is to discriminate more against deuterons than against protons in the lowest energy part of the distribution. This applies mainly to particles with energies below that of the peak in the energy distribution. It should be noted that the position of the peak is about the same as that found by Byerly and Stephens [1]) for the energy distribution of photoparticles due to the irradiation of a copper target by bremsstrahlung of 24 MeV maximum energy. Our target thickness is such that protons of energy 3.9 MeV and deuterons of energy 5.2 MeV starting from the back of the target would not quite reach the front. To just reach the position of the nearest plate that was analyzed, a proton from the front of the target must have had an energy of 0.8 MeV. The corresponding energy for deuterons is 0.4 MeV. So few specific particles were identified as deuterons that meaningful and angular or energy distributions for them cannot be found from the data.

4. Discussion

Four investigations of the photodeuteron to photoproton yield ratio for copper have been reported previously. Byerly and Stephens [1]), Forkman [2]) and Medicus *et al.* [3]) have used the grain-density versus range measurements in nuclear emulsion to identify the particles. Byerly and Stephens, with a maximum bremsstrahlung energy of 24 MeV found a ratio of 0.31, and Forkman found the ratio to be 0.16 ± 0.08 at the same beam energy. Medicus *et al.* obtained a ratio of 0.21 ± 0.05 for a 30 MeV beam. At the much higher maximum bremsstrahlung energy of 65 MeV, Smith and Laslett [6]) reported the ratio to be 0.76 for a "thick" target using a magnetic cloud chamber technique. In all the above measurements the particle distributions obtained were calibrated against known protons produced by the knock-on process. In general, the number of particles studied in each case was not very large, ranging from less than 100 to perhaps 300 in the various experiments. The resolution of the proton and deuteron particle distributions in the case of the grain-counting technique is not too clear due to the inherent difficulties in the method, and in addition, the number of grains per unit track length is high enough to cause difficulties in the measurements. The resolution in the case of the magnetic cloud chamber work

was relatively good but the number of particles that could be studied conveniently by this method was small. The ratio we have found at a maximum bremsstrahlung energy of 45 MeV is lower than the four previous measurements by an order of magnitude. The resolution we obtained was rather good and we were able to gather more statistics with the new technique. The method we have used does not require calibration with known particles and, in that sense, is absolute.

High photodeuteron to photoproton yield ratios (0.15 or more) have been found also in experiments on cobalt [2]) sulphur [7, 8]) and gold [5]). A ratio amounting to several per cent has been found for beryllium [9]). Ratios of a few per cent or less have been found for cobalt, indium, cerium, bismuth [4]) and carbon [9]). The high ratios are rather hard to account for by theory. Statistical evaporation theories [11]) result in ratios much less than 0.01 and will not even account for the smaller of the values found. Theories involving production of deuterons by the direct interaction of a photon with a performed deuteron in the nucleus usually result in ratios of the order of a few per cent or less. A two stage pick-up process for deuteron production, in which a nucleon is first excited by direct interaction with the incident photon and then picks up a partner on the way out to form a deuteron, was proposed by Byerly and Stephens [1]) to account for large ratios. An estimate of the ratio for sulphur on this basis by Sawicki and Czyż [12]) gave an answer of about 0.1 for the ratio of deuterons to the protons produced by direct interaction. If many of the photoprotons are produced by an evaporation process the result would be a much lower ratio since only the directly produced particles take part in the pick-up process. In the case of copper, Byerly and Stephens [1]) found that most of the photoprotons are due to evaporation, and it therefore appears that it may be difficult to account for the large ratios even by the pick-up process, at least for elements of intermediate mass. The unique structure of the beryllium nucleus, of course, makes it an exception to any of these arguments. Chizhov and Kul'chitskii [9]) have been able to account for the rather high ratio they obtained experimentally for beryllium and the much lower ratio found for carbon, irradiated by bremsstrahlung of 90 MeV and 80 MeV maximum energy, respectively, by estimates based on the pick-up idea. Their experiment was done with counters and included only particles of 16 MeV energy or more. The results of the other experiments, however, vary in a rather erratic fashion with beam energy and from element to element. It is apparent that much more work must be done both over the range of elements and as a function of beam energy before there will be enough data available to allow clear conclusions to be drawn as to the mechanisms involved.

We wish to express our thanks to Dr. D. J. Zaffarano and the Iowa State University synchrotron group for their continued interest and generous aid in

this work. We also wish to thank Miss Bernice Black for her help in the preliminary parts of the experiment, Mr. Robert Kinsey for his aid in the plate scanning and Mr. Donald Finch for his help with the computer programming. The technique used for this experiment was suggested by Dr. Sven Johansson, Lund University.

References

1) P. R. Byerly, Jr. and W. E. Stephens, Phys. Rev. **81** (1951) 473; **83** (1951) 54
2) B. Forkman, Ark. Fys. **11** (1956) 265
3) H. A. Medicus, J. J. Grant and P. Demers, Bull. Am. Phys. Soc. **3** (1958) 382
4) M. E. Toms and W. E. Stephens, Phys. Rev. **92** (1953) 362; **95** (1954) 1209
5) E. D. Makhnovskii, JETP (Soviet Physics) **36** (1959) 519
6) W. H. Smith and L. J. Laslett, Phys. Rev. **86** (1952) 523
7) L. S. Ring, Jr., Phys. Rev. **99** (1955) 137
8) L. Katz and A. S. Penfold, Phys. Rev. **81** (1951) 815; **83** (1951) 169
9) V. P. Chizhov and L. A. Kul'chitskii, JETP (Soviet Physics) **36** (1959) 239
10) W. H. Barkas and D. M. Young, U. S. Atomic Energy Commission Report UCRL-2579 September 1954
11) V. F. Weisskopf and D. H. Ewing, Phys. Rev. **57** (1940) 472
12) J. Sawicki and W. Czyż, Nuclear Physics **4** (1957) 248, 695

1.C:
1.D.1

Nuclear Physics **27** (1961) 248—269; © *North-Holland Publishing Co., Amsterdam*
Not to be reproduced by photoprint or microfilm without written permission from the publisher

PAIRINGS IN THE SHELL MODEL (III)

M. UMEZAWA

Institut de Recherches Nucléaires, Strasbourg, France

Received 4 April 1961

Abstract: 1) Pairing energies are obtained for a system of both kinds of nucleons forming a spherical nucleus. 2) Methods for obtaining the general expression for the Racah fractional parentage coefficients are developed. To do this each Racah fractional parentage coefficient is decomposed into a multiple of a few coefficients. Each of these coefficients is expressed in a form independent of its specific representation, so that the results can be applied to any of the *j-j*, *L-S* or intermediate pairing schemes. 3) By using these results, the competition between the spin-orbit force and the pairing forces is dealt with for the following cases: a) the spin-orbit force is far stronger than the pairing forces (near the *j-j* limit), b) the singlet pairing force is far stronger than the spin-orbit force and the triplet pairing force is weak (near the *L-S* limit). 4) The Bogoliubov method for carrying out the whole procedure described above is sketched, and the results are compared with those obtained by the Racah method.

1. Introduction

The pairing energy for a system of one kind of fermions has been dealt with in detail by the Racah method and the Bogoliubov treatment. However, the nature of the pairing energy for a system of both kinds of nucleons has not yet been investigated properly.

The pairing energy is important not only in heavy nuclei where the neutrons and the protons may be dealt with separately, but also in medium nuclei and even in light nuclei. In the previous paper the pairing energy for a system of both kinds of nucleons was calculated for some specific cases.

In this paper we first examine what kind of nuclear interaction will pair all or almost all the nucleons and will lower especially the ground states of nuclei. In other words, we examine the kinds of nuclear forces to which the B.C.S. treatment, or equivalently the Bogoliubov treatment is applicable [15]). In terms of Racah's nuclear spectroscopy, for these kinds of nuclear forces it is suitable to start by classifying the eigenstates of nuclei by the seniority quantum number.

In sect. 2, it will be shown that the Bogoliubov method can be applied to any kind of sufficiently long range interaction, when the one-body spin-orbit force is extremely strong. However, it will also be shown in sect. 2 that the Bogoliubov method is not always applicable to even long range interactions, when the spin-orbit force is not strong in comparison with other forces. Since we expect the pairing energy to be predominant in the ground states of nuclei, we choose a case in which the Bogoliubov method is applicable, the case when

the singlet pairing force is predominantly strong in comparison with other forces. In this case the coupling scheme is near the L–S limit of the pairing coupling scheme. This is only a particular case for which the Bogoliubov method is applicable, even though the spin-orbit force is not particularly strong. The most general case for which the Bogoliubov method is applicable will be dealt with in a future paper.

For the purpose of investigating either the general nature of low lying levels of nuclei or those nuclear levels having many nucleons in the outermost shell, it is impossible to use the ordinary spectroscopic method. As is well known the Bogoliubov method is useful to present the result most straight-forwardly in such cases. However, the orbital quantum number is not large enough to allow a precise argument by the present Bogoliubov approximation. Therefore we first treat the pairing energy by the Racah method (sects. 3 to 11) and sketch how we may modify the present Bogoliubov approximation (sect. 12). Further precise treatment according to the Bogoliubov method may be given in a future paper.

In sect. 10, the competition between the strong spin-orbit force and the pairing forces is dealt with by the Racah method. In sect. 11, the competition among the strong singlet pairing force, the spin-orbit force, and the weak triplet pairing force is dealt with, also by the Racah method. The fractional parentage coefficients necessary for the above calculations are obtained as multiples of a few coefficients, which are calculated in sects. 2 to 9.

2. The Bogoliubov Vacuum, the Pairing Scheme and the Nuclear Forces

As is widely known, the ground state of a system of one kind of fermions is particularly lowered because of the pairing energy if the range of the interaction is sufficiently long to give suitable pairing energy to each pair of fermions [15]). One way of expressing this is by saying that the quasi-particles lie in an orbit whose energy is shifted due to the pairing force, and interact with each other through residual interactions [12]). In terms of the Racah fractional parentage coefficient, the above fact can be explained in the following way. For the state with seniority quantum numbers $\mathscr{S}$, the energy matrix elements are distributed over the various spin J states which belongs to the seniority quantum number $\mathscr{S}$. For the special case of $\mathscr{S} = 0$, only one state belongs to the seniority quantum number $\mathscr{S} = 0$ and has zero spin $J = 0$; therefore the energy matrix elements concentrate on this particular state. Because of this the $\mathscr{S} = 0$ state is particularly lowered in comparison to other states. [In other words, we have $(WJ\{W_1 = W,\ J_1 = J,\ W_2 = (00),\ J_2 = 0)^2 = 1$, see eq. (56) sect. 7]. This fact has been already stated by Racah, in terms of the statistical factor, as early as 1950 [3]).

The above result is independent of the spin dependence of the interactions among one kind of fermions. This is most clearly expressed by Racah in his articles R III and R IV, in which it is shown that the pairing forces $2q'(ij)$ and $q(ij) = q'(ij)(\frac{1}{2}+2\sigma_i\sigma_j)$ are equivalent for the system of one kind of fermions. (See also ref. [8]) A similar situation occurs when we treat the pure j–j pairing scheme, even if we are dealing with both kinds of nucleons. In the j–j pairing scheme, $2Q_{jj}$ (ij) and $Q_{ij}(ij)(\frac{3}{2}+2(\tau_i\tau_j))$ are equivalent, where

$$(j^2J|Q_{jj}(ij)|j^2J) = \delta_{J0}(2j+1). \tag{1}$$

Therefore, unless the nuclear interaction is of extremely short range or of specific spin dependency, so that the pairing energy becomes zero or nearly zero, the ideas used in dealing with one kind of fermions (along the line of the Bogoliubov treatment) or the B.C.S. method are still applicable.

However, when the spin-orbit force is weak or absent, the present Bogoliubov method is not always applicable to the general type of interactions, as will be explained later. Also, the pairing coupling scheme is not always a suitable coupling scheme to start with for such cases. This fact can be clearly seen in the following examples. Let us assume the following force:

$$\sum_{i<j} q'(ij)(\tfrac{1}{2}-2(\tau_i\tau_j)) = Q_\tau.$$

Therefore it follows that

$$(l^2LST|Q_\tau|l^2LST) = \delta_{L0}\delta_{T0}2(2l+1). \tag{2}$$

This is entirely analogous to eq. (1) in U II. By exchanging the role of the isobaric spin τ for that of the intrinsic spin σ, we obtain, in analogy to the schemes (1) and (12) in U I, the following coupling scheme and the corresponding quantum numbers:

$$\begin{aligned} &\mathrm{U}^n_{(2l+1)\times 2\times 2} \to \mathrm{U}^n_{\substack{(2l+1)\times 2\\ [\lambda_{l\tau}]}} \times \mathrm{U}_{\substack{2\\ [\lambda_s]}}{}^n, \\ &\mathrm{U}^n_{\substack{(2l+1)\times 2\\ [\lambda_{l\tau}]}} \to \mathrm{Sp}^n_{\substack{(2l+1)\times 2\\ (W_{l\tau})}} \to \mathrm{R}^n_{\substack{2l+1\\ (W_R)}} \times \mathrm{U}^n_T \to \mathrm{R}_3{}^n_L \times \mathrm{U}^n_T. \end{aligned} \tag{3}$$

On the other hand, the present Bogoliubov method gives zero pairing energy from this interaction for the vacuum state in the quasi-particle representation. A similar situation occurs in the case of Wigner forces. As is easy to see, the vacuum in Bogoliubov's quasi-particle representations is far from the ground state in the super-multiplet scheme for a system of both kinds of nucleons.

The author will discuss in a future paper the kinds of forces to which the present Bogoliubov method is applicable when dealing with a system of both kinds of nucleons. In this paper the author assumes three kinds of forces, namely, the spin-orbit force, the singlet pairing force $V^0q(ij)$ introduced in

U II, and the triplet pairing force defined as V^{11} tr (ij), where

$$(l^2LSJT|\ \text{tr}\ (ij)|l^2LSJT) = \delta_{L1}\delta_{S1}\delta_{J0}2(2l+1). \tag{4}$$

At and near the j–j limit a triplet pairing force of some moderate strength will be assumed; the significance of this force will be shown in sect. 10. The author will show the significance of this force for the intermediate pairing scheme in a future paper. In sect. 11 where the scheme at and near the L–S limit is dealt with, only a weak triplet pairing force is assumed, since the triplet pairing force does not preserve the L–S coupling scheme (UI).

3. Method

Racah has developed a method for calculating the fractional parentage coefficient by introducing tensor operators and by diagonalizing them (R III, IV). A further development by Jahn has been to use the Young operator for calculating the fractional parentage coefficients in the Jahn-Young-Yamanouchi representations [9, 10]). However, it is, even now, not certain what the most reasonable nuclear interaction is. Thus, calculating for each nucleus and choosing parameters to fit each case does not always assure the correctness of the explanations.

In this and a future paper, the author would like to attempt to calculate the general expression for the fractional parentage coefficient, in order to see the general trend of the low energy levels of nuclei. It is possible to do this for the ground state and a few low excited states of nuclei, because the pairing force seems to be predominant in the ground state.

To obtain the general expression for the fractional parentage coefficients, it does not seem possible to use the method of diagonalizing tensor operators. However, Racah has also shown that, for the state when $\mathscr{S}$ is 0 or 1, it is possible to obtain the general expression for fractional parentage coefficients by using the equations giving $\sum l_i$, $\sum \sigma_i$ and $\sum \tau_i$ with the related recurrence formulas [4]). This method was directly applied in U II.

Here we deal with pairing schemes which include the j–j and L–S schemes as two limiting cases. Therefore, in order to obtain the general expression for the fractional parentage coefficients, independent of particular representations, such as L–S or j–j, it is necessary to use some other operators which can be introduced independently of particular representations, instead of or apart from $\sum l_i$, $\sum \sigma_i$ and $\sum \tau_i$. We make use of the Casimir operator in each subgroup for this purpose.

When we carry out such procedures, it is desirable to start by decomposing the fractional parentage coefficient into multiples of a few coefficients as follows (See ref. [2])):

$$(l^n \Sigma W \beta\{l^{n-1} \Sigma_1 W_1 \beta_1) = (\Sigma\{\Sigma_1)(\Sigma W\{\Sigma_1 W_1)(W\beta\{W_1\beta_1), \tag{5}$$

where Σ, W and β represent the characters in U_Ω, Sp_Ω and a subgroup of Sp_Ω. Here it should be mentioned that $(W\beta\{W_1\beta_1)$ is independent of Σ and Σ_1. Because the invariant quantities in Sp_Ω are still kept invariant in its subgroup, the representations in $(Sp_\Omega{}^n)$ and $(Sp_\Omega{}^v)$ decompose identically in its subgroup. In the following section we first introduce the Casimir operators and then calculate each coefficient.

4. Casimir Operators in SU_Ω and Sp_Ω

We define the Casimir operators by using the infinitesimal operators which are normalised by the dimension of the group, so that the eigenvalue of the Casimir operator takes on a simple form. Thus the Casimir operators in SU_Ω (the special unitary group of the dimension Ω) and Sp_Ω are brought into the following form in tensorial representation:

$$G(SU_\Omega) = \sum_{r=1}^{\Omega-1} (2r+1)(U^r U^r), \tag{6}$$

$$G(Sp_\Omega) = \sum_{r\ \mathrm{odd}}^{\Omega-1} (2r(+1)(U^{r'} U^{r'}) = 2\sum_{r\ \mathrm{odd}}^{\Omega-1} (2r+1)(U^r U^r), \tag{7}$$

where U^r and $U^{r'}$ are normalised in U_Ω and Sp_Ω spaces respectively.

The eigenfunctions of these operators are given as follows:

$$g[\lambda] = \lambda_1(\lambda_1+\Omega-1)+\lambda_2(\lambda_2+\Omega-3)+\ldots+\lambda_\Omega(\lambda_\Omega-\Omega+1)-\frac{(\Sigma\lambda_i)^2}{\Omega}, \tag{8}$$

$$g(W) = W_1(W_1+\Omega)+W_2(W_2+\Omega-2)+\ldots+W_{\frac{1}{2}\Omega}(W_{\frac{1}{2}\Omega}+2). \tag{9}$$

It is convenient to use the following operator instead of $G(SU_\Omega)$:

$$G'(U_\Omega) = \sum_{r=0}^{\Omega-1} (2r+1)(U^r U^r), \tag{10}$$

whose eigenvalue is simply

$$g'[\lambda] = \lambda_1(\lambda_1+\Omega-1)+\lambda_2(\lambda_2+\Omega-3)+\ldots+\lambda_\Omega(\lambda_\Omega-\Omega+1). \tag{11}$$

(See refs. [1, 10]).

5. Symmetry Character and the Coefficient $(\Sigma\{\Sigma_1)$

The eigenfunction of the nuclear system with conserved isobaric spin T can be written as follows

$$\Psi(n\Sigma\alpha) = \frac{1}{\sqrt{f_\Sigma}} \sum_{\mu=1}^{f_\Sigma} \psi_\mu(\Sigma\alpha)\chi_{\mu^\dagger}(\Sigma^\dagger) \tag{12}$$

where f_Σ is the dimension of the representation Σ, and μ and $\mu^\dagger$ are the suffixes to the bases of the representation Σ and its conjugate representation $\Sigma^\dagger$.

The isobaric wave functions with $\Sigma\tau_i = T$ form automatically the basis of the irreducible representation $\Sigma^\dagger$ of the symmetry groups of an n particle system [6]), where $\Sigma^\dagger = (\frac{1}{2}(n+2T), \frac{1}{2}(n-2T))$.

We represent $\Psi(n\Sigma\alpha)$ as a product of the wave functions $\psi(\Sigma_1\alpha_1)\chi(T_1)$ of $n-1$ particles and the wave function $\psi(1)\ \chi(\frac{1}{2})$ of the remaining particle as follows:

$$\Psi(n\Sigma\alpha) = \frac{1}{\sqrt{f_\Sigma}}\left[\sum_{\Sigma_1} N_{\Sigma_1} \sum_{\mu_1}^{f_{\Sigma_1}} C\psi_{\mu_1}(\Sigma_1\alpha_1)\chi(T_1)\psi(1)\chi(\tfrac{1}{2})\right], \tag{13}$$

where the C are Wigner coefficients which form total isobaric spin T from T_1 and $\frac{1}{2}$. In eq. (13), the isobaric wave functions are designated by their isobaric spins, and N_{Σ_1} is the number of representation Σ_1 which appear in this decomposition. In this case it is clearly one.

By writing eq. (13) in the following form:

$$\Psi(n\Sigma\alpha) = \sum_{\Sigma_1} (\Sigma\{\Sigma_1)C\Psi(n-1\Sigma_1\alpha_1)\Psi(1), \tag{14}$$

we obtain

$$(\Sigma\{\Sigma_1)^2 = f_{\Sigma_1}/f_\Sigma. \tag{15}$$

We also can decompose $\Psi(n\Sigma\alpha)$ into a product of the eigenfunctions, $\Psi(n-2\Sigma^1\alpha_1)$ of $n-2$ particles and the wave functions of the remaining two particles $\Psi(2\Sigma_2\alpha_2)$ as follows:

$$\Psi(n\Sigma\alpha) = \sum_{\Sigma_1\Sigma_2} (\Sigma\{\Sigma_1\Sigma_2)C\Psi(n-2\Sigma_1\alpha_1)\Psi(2\Sigma_2\alpha_2), \tag{16}$$

$$(\Sigma\{\Sigma_1\Sigma_2)^2 = (f_{\Sigma_1}f_{\Sigma_2}/f_\Sigma)N_{\Sigma_1\Sigma_2}. \tag{17}$$

The $N_{\Sigma_1\Sigma_2}$ are 0 or 1 or 2 and can be easily calculated, for example, by using the Young tableau according to the method developed by Jahn [9]).

The f_Σ are given, for example, in ref. [13])

$$f_\Sigma = n!\,\frac{\prod_{i<k}(m_i-m_k)}{m_1!\,m_2!\ldots m_r!}, \tag{18}$$

where $m_i = \lambda_i+r-i$. Inserting the values $\Sigma\lambda_i = n$, $\lambda_i = 2$ for $i \leqq \frac{1}{2}(n-2T)$, $\lambda_i = 1$ for $\frac{1}{2}(n-2T) < i \leqq \frac{1}{2}(n+2T)$ and $\lambda_i = 0$ for $\frac{1}{2}(n+2T) < i$ we obtain the following equations:

$$\begin{aligned} \frac{f_{\Sigma_1}}{f_\Sigma} &= \frac{(n-2T)(T+1)}{n(2T+1)} \quad \text{for} \quad T_1 = T+\tfrac{1}{2}, \\ \frac{f_{\Sigma_1}}{f_\Sigma} &= \frac{(n+2T+2)T}{n(2T+1)} \quad \text{for} \quad T_1 = T-\tfrac{1}{2}. \end{aligned} \tag{19}$$

Also, for the coefficient $(\Sigma\{\Sigma_1\Sigma_2)$ we obtain

$$\frac{f_{\Sigma_1}f_{\Sigma_2}}{f_\Sigma}=\frac{f_{\Sigma_1}}{f_\Sigma}=\begin{cases}\dfrac{(n-2T)(n-2T-2)(2T+3)}{4n(n-1)(2T+1)} & \text{for } T_1=T+1,\ \Sigma_2=(20),\\ \dfrac{(n-2T)(n+2T+2)}{4n(n-1)} & \text{for } T_1=T,\ \Sigma_2=(20) \text{ or } (11),\\ \dfrac{(n+2T)(n+2T+2)(2T-1)}{4n(n-1)(2T+1)} & \text{for } T_1=T-1,\ \Sigma_2=(20).\end{cases} \tag{20}$$

Eqs. (19), (20) can be also obtained by using the equations

$$\begin{aligned}G'(\mathrm{U}_\Omega{}^n)&=\frac{n}{n-2}G'(\mathrm{U}_\Omega{}^{n-1})-\Omega\frac{n}{n-2},\\ G'(\mathrm{U}_\Omega{}^n)&=\frac{n(n-1)}{(n-2)(n-3)}G'(\mathrm{U}_\Omega{}^{n-2})-2\Omega\frac{n}{n-3}.\end{aligned} \tag{21}$$

Because the isobaric functions with T have a good symmetry character, eqs. (19) and (20) can be obtained also by

$$\sum_{i<j}^{n}(\tau_i\tau_j)=\tfrac{1}{2}T(T+1)-\tfrac{3}{8}n. \tag{22}$$

Eqs. (21) and (22) are reduced into the form

$$\sum_{\Sigma_1\Sigma_2}(\Sigma\{\Sigma_1\Sigma_2)(T_1)(T_1+1)=f(n,T). \tag{23}$$

Finally it is worth mentioning that $(\Sigma\{\Sigma_1\Sigma_2)^2$ can be obtained as

$$\sum_{\Sigma'_i}(\Sigma\{\Sigma'_i)^2(\Sigma'_i\{\Sigma_1)^2[\tau]^2, \tag{24}$$

where $[\tau]$ is a recoupling coefficient to form $\Sigma_2{}^\dagger$ as a symmetry character of the isobaric wave function of two particles (U II, also ref. [9]).

6. The Coefficient $(\Sigma W\{\Sigma_1 W_1)$

To obtain these coefficients, we use the equation for $G(\mathrm{Sp}_\Omega)$, in addition to the normalization equation

$$G(\mathrm{Sp}_\Omega{}^n)=\frac{n}{n-2}G(\mathrm{Sp}_\Omega^{n-1})-\frac{n}{n-2}(\Omega+1), \tag{25}$$

$$\sum_{W_1}(\Sigma W\{\Sigma_1 W_1)^2=1. \tag{26}$$

In this paper we limit ourselves to the case where $W=(10)$ or (00). In the case where $W=(00)$, eq. (26) becomes simply

$$(\Sigma(00)(\Sigma_1\{10))^2=1. \tag{27}$$

When $W = 10$), eq. (25) becomes

$$g(10) = \left\{ \frac{n}{n-2} \sum_{\Sigma_1} \sum_{W_1} (\Sigma\{\Sigma_1)^2 (\Sigma W\{\Sigma_1 W_1)^2 g(W_1) \right\} - \frac{n}{n-2}(\Omega+1). \qquad (28)$$

The equation for $(\Sigma W\{\Sigma_1 W_1)$ can be simplified if we use

$$\frac{2n}{n-2} g(10) - G(\mathrm{Sp}_\Omega{}^n) \qquad (29)$$

instead of $G(\mathrm{Sp}^n)$ itself, and we obtain the following equation:

$$(\Omega+1)C(00+)+C(21+)-C(20+)+(\Omega+1)C(00-)+C(21-)-C(20-) = \frac{\Omega+1}{n}, \qquad (30)$$

where

$$C(\mathscr{S}t\pm) = (\Sigma\{\Sigma_1)^2 (\Sigma W\{\Sigma_1 W_1)^2 \quad \text{with} \quad T_1 = T \pm \tfrac{1}{2}. \qquad (30')$$

The coefficient $(\Sigma W\{\Sigma_1 W_1)$ can also be obtained when we diagonalize the antisymmetrical operators (in tensorial representation, odd rank tensors). Because of this, the equations $\Sigma l_{z_i} = L = l$ or $\Sigma \sigma_{z_i} = S_z = \frac{1}{2}$ in L–S representation, and $\Sigma j_{z_i} = J_z = j$ give results equivalent to those obtained from eq. (30) (see U II).

Eq. (30) is further simplified by the following relations:

$$\left.\begin{aligned} (\Sigma(10)\{\Sigma_1(00)) &= 0 \quad \text{for} \quad T_1 = T+\tfrac{1}{2} \\ (\Sigma(10)\{\Sigma_1(20)) &= 0 \quad \text{for} \quad T_1 = T-\tfrac{1}{2} \end{aligned}\right\} \quad \text{if} \quad N_0 > N_e, \qquad (31)$$

$$\left.\begin{aligned} (\Sigma(10)\{\Sigma_1(00)) &= 0 \quad \text{for} \quad T_1 = T-\tfrac{1}{2} \\ (\Sigma(10)\{\Sigma_1(20)) &= 0 \quad \text{for} \quad T_1 = T+\tfrac{1}{2} \end{aligned}\right\} \quad \text{if} \quad N_e > N_0. \qquad (32)$$

We further make use of the following reciprocal relations in order to obtain some coefficient in eq. (30) (see also ref. [10])):

$$(\Sigma W\{\Sigma_1 W_1)^2 = \frac{g_\Sigma g_{W_1}}{g_{\Sigma_1} g_W} (\tilde{\Sigma}_1 W_1\{\tilde{\Sigma} W)^2 \qquad (33)$$

or

$$C(l^n \Sigma W\{l^{n-1}\Sigma_1 W_1) = \left(\frac{f_{\Sigma_1} f_{\tilde{\Sigma}_1}}{f_\Sigma f_{\tilde{\Sigma}}}\right) \frac{g_\Sigma g_{W_1}}{g_{\Sigma_1} g_W} C(l^{2\Omega-n+1} \tilde{\Sigma}_1 W_1\{l^{2\Omega-n} \tilde{\Sigma} W), \qquad (34)$$

where $\tilde{\Sigma} = [\tilde{\lambda}]$ and $\tilde{\Sigma}_1 = [{}_1\tilde{\lambda}]$ designate the symmetry character of $2\Omega-n$, and $2\Omega-n+1$ particles, conjugate to Σ and Σ_1, respectively; that is to say, the sets of $\tilde{\lambda}_i$ and ${}_1\tilde{\lambda}_i$ are equivalent to the sets of $2-\lambda_{\Omega-i+1}$ and $2-{}_1\lambda_{\Omega-i+1}$. Here, $g_\Sigma, g_{\Sigma_1}, g_W$ and g_{W_1} are the degrees of the representations Σ, Σ_1, W and W_1 in U_Ω and Sp_Ω. The quantities g_Σ and g_{Σ_1} are given, for example in ref. [13, 14]).

Their ratio is simply

$$\frac{g_{\Sigma}}{g_{\Sigma_1}} = \begin{cases} \dfrac{(2\Omega-n+2T+4)(2T+1)}{(n-2T)(2T+2)} & \text{for} \quad T_1 = T+\tfrac{1}{2}, \qquad (35) \\ \dfrac{(2\Omega-n-2T+2)}{(n+2T+2)(2T)} & \text{for} \quad T_1 = T-\tfrac{1}{2}. \qquad (36) \end{cases}$$

The quantities f_{Σ} and f_{Σ_1} are already given in sect. 5. The quantities $f_{\tilde{\Sigma}_1}$ and $f_{\tilde{\Sigma}_1}$ can be obtained if we replace n in f_{Σ} and f_{Σ_1}, by $2\Omega-n$. Thus we obtain the following equation:

$$\frac{f_{\Sigma_1} f_{\tilde{\Sigma}_1} g_{\Sigma}}{f_{\Sigma} f_{\tilde{\Sigma}} g_{\Sigma_1}} = \frac{(2\Omega-n+1)(2T_1+1)}{n(2T+1)}. \qquad (37)$$

The g_n are given, for example, in ref. [14]) and

$$g(10) = \Omega, \quad g(11) = (\Omega-1)(2\Omega+1), \quad g(20) = \Omega(2\Omega+1). \qquad (38)$$

Inserting eqs. (21), (35), (36), (37) and (38) into eqs. (33) and (34), we obtain

$$(\Sigma(10)\{\Sigma_1(00))^2 = \begin{cases} \dfrac{(2\Omega-n+2T+4)(2T+1)}{(n-2T)(2T+2)\Omega} & \text{for} \quad T_1 = T+\tfrac{1}{2}, N_e > N_o, \\ \dfrac{(2\Omega-n-2T+2)(2T+1)}{(n+2T+2)(2T)\Omega} & \text{for} \quad T_1 = T-\tfrac{1}{2}, N_o > N_e, \end{cases} \qquad (39)$$

$$C(\Sigma(10)\{\Sigma_1(00)) = \begin{cases} \dfrac{(2\Omega-n+2T+4)}{2n\Omega} & \text{for} \quad T_1 = T+\tfrac{1}{2}, N_e > N_o, \\ \dfrac{(2\Omega-n-2T+2)}{2n\Omega} & \text{for} \quad T_1 = T-\tfrac{1}{2}, N_o > N_e, \end{cases} \qquad (40)$$

where $C(\Sigma W\{\Sigma_1 W_1) = C(\mathscr{S}t\pm)$ in eq. (30′).

Using eqs. (31), (32), (39) and (40) we obtain from eq. (30) the following results:

$$\begin{aligned} (\Sigma(10)\{\Sigma_1(11))^2 &= 1-(\Sigma(10)\{\Sigma_1(00))^2 \quad \text{for} \quad T_1 = T+\tfrac{1}{2}, N_e > N_o, \\ &\text{and} \quad \text{for} \quad T_1 = T-\tfrac{1}{2}, N_o > N_e, \end{aligned} \qquad (40')$$

$$\left.\begin{aligned} (\Sigma(10)\{\Sigma_1(11))^2 &= \frac{2T+3}{4(T+1)} \\ (\Sigma(10)\{\Sigma_1(20))^2 &= \frac{2T+1}{4(T+1)} \end{aligned}\right\} \quad \text{for} \quad T_1 = T+\tfrac{1}{2} \quad \text{if} \quad N_o < N_e, \qquad (41)$$

$$\left.\begin{aligned} (\Sigma(10)\{\Sigma_1(11))^2 &= \frac{2T-1}{4T} \\ (\Sigma(10)\{\Sigma_1(20))^2 &= \frac{2T+1}{4T} \end{aligned}\right\} \quad \text{for} \quad T_1 = T-\tfrac{1}{2} \quad \text{if} \quad N_e > N_o. \qquad (42)$$

7. The Coefficient $(\Sigma W\{\Sigma_1 W_1, \Sigma_2 W_2)$

This coefficient can be indirectly obtained from $(\Sigma W\{\Sigma'_1 W'_1)$ as follows:

$$(\Sigma W\{\Sigma_1 W_1, \Sigma_2 W_2)^2 = \sum_{\Sigma'_1 W'_1} (\Sigma W\{\Sigma'_1 W'_1)^2 (\Sigma'_1 W'_1\{\Sigma_1 W_1)^2. \tag{43}$$

Because Σ_2 is already determined in the course of the calculation of $(\Sigma\{\Sigma_1\Sigma_2)$ and W_2 is uniquely determined from Σ_2 and W_1. On the other hand it is possible to obtain equations which the coefficients $(\Sigma W\{\Sigma_1 W_1, \Sigma_2 W_2)$ must satisfy. First, there are the normalization equations

$$\sum_{W_1 W_2} (\Sigma W\{\Sigma_1 W_1, \Sigma_2 W_2)^2 = 1. \tag{44}$$

To obtain another equation we can make use of $G(\mathrm{Sp}_\Omega)$ as follows:

$$G(\mathrm{Sp}_\Omega{}^n) = \frac{n(n-1)}{(n-2)(n-3)} G(\mathrm{Sp}_\Omega{}^{n-2}) - \frac{2n(\Omega+1)}{n-3}. \tag{45}$$

This equation is useful when $W > 0$. The case of $W > 0$ will be dealt with in a future paper. When $W = 0$, the coefficients $(\Sigma W\{\Sigma_1 W_1, \Sigma_2 W_2)$ can be obtained from the reciprocal equations and the normalization equations. However, eq. (45) is still useful for checking the results.
For $W = 0$, eq. (45) becomes

$$0 = \frac{-2(\Omega+1)n}{n-3} + \frac{n(n-1)}{(n-2)(n-3)} \Big\{ \sum_{T_1=T-1,\,T,\,T+1} C(\Sigma(00)\{\Sigma_1(11), \Sigma_2 = [11](11))g(11)$$
$$+ C\Big(\sum_{\Sigma_1 \text{ for } T_1=T} (00)\{\Sigma_1(11), \Sigma_2 = [20](20)\Big) g(20). \tag{45'}$$

Using a method similar to that applied in the case of eq. (30) in the previous section, equations equivalent to eq. (45) can also be obtained from the operators $\sum_{i<j}(l_i l_j)$ and $\sum_{i<i}(\sigma_i\sigma_j)$ or $\sum_{i<j}(j_i j_j)$ if we choose the L–S or j–j representations respectively. On the other hand, the following results are obtained from eq. (44):

$$\left.\begin{aligned}(\Sigma(00)\{\Sigma_1(11), \Sigma_2(11))^2 = 1\\ (\Sigma(00)\{\Sigma_1(20), \Sigma_2(20))^2 = 1\end{aligned}\right\} \quad \text{for} \quad T = T_1. \tag{46}$$

From eq. (27), eq. (44) becomes equivalent to eqs. (39) for $W = 0$ and $W_1 = 0$:

$$(\Sigma(00)\{\Sigma_1(00), \Sigma_2(00))^2 = \begin{cases} \dfrac{(2\Omega+6-n+2T)(2T+2)}{(n-2-2T)(2T+3)\Omega} & \text{for} \quad T_1 = T+1, \\ \dfrac{(2\Omega+4-n-2T)(2T)}{(n+2T)(2T-1)\Omega} & \text{for} \quad T_1 = T-1. \end{cases} \tag{47}$$

Inserting eqs. (47) into eq. (44) we obtain the rest of the coefficients

$$(\Sigma(00)\{\Sigma_1(11), \Sigma_2(11))^2 = \begin{cases} 1-\dfrac{(2\Omega+6-n+2T)(2T+2)}{(n-2-2T)(2T+3)\Omega} & \text{for } T_1 = T+1, \\ 1-\dfrac{(2\Omega+4-n-2T)(2T)}{(n+2T)(2T-1)\Omega} & \text{for } T_1 = T-1. \end{cases} \tag{48}$$

The results (46), (47) and (48) are checked by putting them into eq. (45′).

8. The Coefficients $(W\beta\{W_1\beta_1)$ and $(W\beta\{W_1\beta_1, W_2\beta_2)$

We have finally arrived at the quantities which are related to the representations we choose. In this paper we still deal with the two extreme cases, namely, the j–j and L–S limits. Accordingly we choose L, S or L, S, J for β in the L–S representation and $\beta = J$ in the j–j representation. (We may need further quantum numbers when there remain degeneracies. However, we ignore this in this paper since we mainly deal with the case when $\sum_i W_i = \mathscr{S}$ is small.)

For the purpose of obtaining these coefficients, we find that the equations $\sum_i j_i = J$ or $\sum_{i<j} (j_i j_i) = (J(J+1)-nj(j+1))^{\frac{1}{2}}$ or the corresponding equations on the L–S representation, are of only minor importance. In this section, we entirely depend upon the reciprocal relations and the normalisation equations. It is possible to do this because we limit ourselves to the case when W is 0 or 1.

The normalization equations for these coefficients are

$$\sum_{\beta_1} (W\beta\{W_1\beta_1)^2 = 1,$$

or

$$\sum_{J_1} (WJ\{W_1J_1)^2 = 1 \text{ in the } j\text{–}j \text{ representation},$$

or

$$\left.\begin{array}{l} \displaystyle\sum_{L_1S_1J_1} (WLSJ\{W_1L_1S_1J_1)^2 = 1 \\ \text{or} \\ \displaystyle\sum_{L_1S_1} (WLS\{W_1L_1S_1)^2 = 1 \end{array}\right\} \text{in the } L\text{–}S \text{ representation.} \tag{49}$$

The following are some special cases:

$$(W = (00) \quad J = 0\{W_1 = (10) \quad J_1 = j)^2 = 1, \tag{50}$$

$$(W = (00) \quad L = 0 \quad S = 0\{W = (10) \quad L = l \quad S = \tfrac{1}{2})^2 = 1,$$

$$(W = (10) \quad J = j\{W_1 = (00) \quad J_1 = 0)^2 = 1, \tag{51}$$

$$(W = (10) \quad L = l \quad S = \tfrac{1}{2} \quad J = j\{W = (00) \quad L = 0 \quad S = 0 \quad J = 0)^2 = 1,$$

$$\left.\begin{array}{l} (WJ\{W \quad = (10) \quad J = j)^2 = 1 \\ (WLS\{W \quad = (10) \quad L = l \quad S = \frac{1}{2})^2 = 1 \\ \sum_j (WLSJ\{W = (10) \quad L = l \quad S = \frac{1}{2} \quad j)^2 = 1 \end{array}\right\} \text{for } W = (20) \text{ or } (11). \tag{52}$$

The reciprocal equations are as follows:

$$\begin{aligned} (W\beta\{W_1\beta_1)^2 &= \frac{g_W g_{\beta_1}}{g_{W_1} g_\beta} (W_1\beta_1\{W\beta)^2, \\ (WJ\{W_1J_1)^2 &= \frac{g_W(2J_1+1)}{g_{W_1}(2J+1)} (W_1J_1\{WJ)^2, \\ (WLS\{W_1L_1S_1)^2 &= \frac{g_W(2L_1+1)(2S_1+1)}{g_{W_1}(2L+1)(2S+1)} (W_1L_1S_1\{WLS)^2, \\ (WLSJ\{W_1L_1S_1J_1)^2 &= \frac{g_W(2J_1+1)}{g_{W_1}(2J+1)} (W_1L_1S_1J_1\{WLSJ)^2. \end{aligned} \tag{53}$$

By using eq. (52), these equations become

$$\begin{aligned} (W = (10) \quad J = j\{W_1J_1)^2 &= \frac{(2j+1)(2J_1+1)}{g_{W_1}(2j+1)} \\ &= \frac{2J_1+1}{g_{W_1}} \text{ for } W_1 = (20) \text{ or } (11), \\ (W = (10) \quad L = l \quad S = \tfrac{1}{2}\{W_1L_1S_1)^2 &= \frac{2(2l+1)(2L_1+1)(2S_1+1)}{g_{W_1}2(2l+1)} \\ &= \frac{(2L_1+1)(2S_1+1)}{g_{W_1}} \text{ for } W_1 = (20) \text{ or } (11). \end{aligned} \tag{54}$$

The normalization equations for the coefficients $(W\beta\{W_1\beta_1, W_2\beta_2)$ are

$$\begin{aligned} &\sum_{\beta_1\beta_2} (W\beta\{W_1\beta_1, W_2\beta_2)^2 = 1, \\ &\sum_{J_1J_2} (WJ\{W_1J_1, W_2J_2)^2 = 1, \\ &\sum_{L_1S_1L_2S_2} (WLS\{W_1L_1S_1, W_2L_2S_2)^2 = 1. \\ &\sum_{J_1J_2} (WLSJ\{W_1L_1S_1J_1, W_2L_2S_2J_2)^2 = 1, \end{aligned} \tag{55}$$

The following are some special cases:

$$
\begin{aligned}
&(WJ\{W_1 = (00)\quad J_1 = 0, W_2 = W\quad J_2 = J)^2 \\
&\qquad = (WJ\{W_1 = W\quad J_1 = J, W_2 = (00)\quad J_2 = 0)^2 = 1, \\
&(WLS\{W_1 = (00)\quad L_1 = 0\quad S_1 = 0, W_2 = W\quad L_2 = L\quad S_2 = S)^2 \\
&\qquad = (WLS\{W_1 = W\quad L_1 = L\quad S_1 = S, W_2 = (00)\quad L_2 = 0\quad S_2 = 0)^2 = 1, \\
&(WLSJ\{W_1 = (00)\quad L_1 = 0\quad S_1 = 0\quad J_1 = 0, W_2 = W\quad L_2 = L\quad S_2 = S\quad J_2 = J)^2 \\
&\quad = (WLSJ\{W_1 = W\quad L_1 = L\quad S_1 = S\quad J_1 = J, W_2 = (00)\quad L_2 = 0\quad S_2 = 0\quad J_2 = 0)^2 = 1.
\end{aligned}
\tag{56}
$$

The reciprocal equations are

$$
\begin{aligned}
&(W\beta\{W_1\beta_1, W_2\beta_2)^2 = \frac{g_W g_{\beta_1}}{g_{W_1} g_\beta}\,(W_1L_1\{WL, W_2L_2)^2, \\
&(WJ\{W_1J_1, W_2J_2)^2 = \frac{g_W(2J_1+1)}{g_{W_1}(2J+1)}\,(W_1J_1\{WJ, W_2J_2)^2, \\
&(WLS\{W_1L_1S_1, W_2L_2S_2)^2 = \frac{g_W(2L_1+1)(2S_1+1)}{g_{W_1}(2L+1)(2S+1)}\,(W_1L_1S_1\{WLS, W_2L_2S_2)^2, \\
&(WLSJ\{W_1L_1S_1J_1, W_2L_2S_2J_2)^2 = \frac{g_W(2J_1+1)}{g_{W_1}(2J+1)}\,(W_1L_1S_1J_1\{WLSJ, W_2L_2S_2J_2)^2.
\end{aligned}
\tag{57}
$$

By using eqs. (56) and (57) for $W = 0$ we get

$$
\begin{aligned}
&(W = (00)\quad J = 0\{W_1J_1,\quad W_2 = W_1\quad J_2 = J_1)^2 = \frac{2J_1+1}{g_{W_1}}, \\
&(W = (00)\quad L = 0\quad S = 0\{W_1L_1S_1,\quad W_2 = W_1\quad L_2 = L_1\quad S_2 = S_1)^2 = \frac{(2L_1+1)(2S_1+1)}{g_{W_1}}, \\
&(W = (00)\quad L = 0\quad S = 0\quad J = 0\{W_1L_1S_1J_1, \\
&\qquad W_2 = W_1\quad L_2 = L_1\quad S_2 = S_1\quad J_2 = J_1)^2 = \frac{(2J_1+1)}{g_{W_1}}.
\end{aligned}
\tag{58}
$$

Finally it should be mentioned that these coefficients $(W\beta\{W_1\beta_1, W_2\beta_2)$ can be derived from the coefficients $(W\beta\{W'_1\beta'_1)$ as follows:

$$
(W\beta\{W_1\beta_1, W_2\beta_2)^2 = \sum_{\beta'_1} (W\beta\{W'_1\beta'_1)^2 (W'_1\beta'_1\{W_1\beta_1)^2[\beta]^2, \tag{59}
$$

where $[\beta]$ represents the recoupling coefficient for reconstructing the two particle wave function with quantum number β_2. The agreement between these two methods gives a check of the results obtained.

9. Pairing energy, the Racah Operator and the Casimir Operator

In the pairing coupling scheme, the Casimir operators $G(\mathrm{SU}_\Omega)$ and $G(\mathrm{Sp}_\Omega)$ are diagonal, therefore $G'(\mathrm{U}_\Omega)$ is too. Thus the operator $R(\mathrm{Sp}_\Omega)$, where

$$R(\mathrm{Sp}_\Omega) = G'(\mathrm{U}_\Omega) - G(\mathrm{Sp}_\Omega) \tag{60}$$

is also diagonal. Let us consider the following operators:

$$\begin{aligned}
\bar{G}'(\mathrm{U}_\Omega) &= \sum_{i\neq j}\sum_{r=0}^{\Omega-1}(2r+1)(u_i^r u_j^r) = \tfrac{1}{2}(G'(\mathrm{U}_\Omega{}^n) - n\Omega), \\
\bar{G}(\mathrm{Sp}_\Omega) &= 2\sum_{i\neq j}\sum_{r_{\mathrm{odd}}}^{\Omega-1}(2r+1)(u_i^r u_j^r) = \tfrac{1}{2}(G(\mathrm{Sp}_\Omega) - n(\Omega+1)), \\
\bar{R}(\mathrm{Sp}_\Omega) &= \bar{G}'(\mathrm{U}_\Omega{}^n) - \bar{G}(\mathrm{Sp}_\Omega{}^n).
\end{aligned} \tag{61}$$

The eigenvalue of the operator $\bar{R}(\mathrm{Sp}_\Omega)$ can be obtained from eqs. (8) and (9).

We consider the following case, in which the characters are

$$\begin{aligned}
[\lambda] \text{ with } \lambda_i &= \begin{cases} 2 & \text{for } i \leqq n_\mathrm{p} = \tfrac{1}{2}(n-2T), \\ 1 & \text{for } \tfrac{1}{2}(n-2T) < i \leqq \tfrac{1}{2}(n+2T) = n_\mathrm{n}, \\ 0 & \text{for } \tfrac{1}{2}(n+2T) < i, \end{cases} \\
(W) \text{ with } W_i &= \begin{cases} 2 & \text{for } i \leqq \mathscr{S}_\mathrm{p}, \\ 1 & \text{for } \mathscr{S}_\mathrm{p} < i \leqq \mathscr{S}_\mathrm{n}, \\ 0 & \text{for } \mathscr{S}_\mathrm{n} < i. \end{cases}
\end{aligned} \tag{62}$$

The eigenvalue q (Sp_Ω) of $\bar{R}(\mathrm{Sp}_\Omega)$ for this case is as follows:

$$\begin{aligned}
q(\mathrm{Sp}_\Omega{}^n) = \tfrac{1}{2}\{&(n_\mathrm{p}-\mathscr{S}_\mathrm{p})(n'_\mathrm{p}-\mathscr{S}_\mathrm{p}) + (n_\mathrm{n}-\mathscr{S}_\mathrm{n})(n'_\mathrm{n}-\mathscr{S}_\mathrm{n}) \\
&+ (n_\mathrm{p}-\mathscr{S}_\mathrm{p}) - (n_\mathrm{n}-\mathscr{S}_\mathrm{n}) + (n-\mathscr{S})\},
\end{aligned} \tag{63}$$

where

$$n'_\mathrm{p} = \Omega - n_\mathrm{p} + 2, \qquad n'_\mathrm{n} = \Omega - n_\mathrm{n} + 2.$$

It follows from eq. (62) that

$$q(\mathrm{Sp}_\Omega{}^n) = \Omega\delta_{\mathscr{S}0} \quad \text{if} \quad n = 2. \tag{64}$$

We see from the above equation that $\bar{R}(\mathrm{Sp}_\Omega)$ is equivalent to the Racah operator Q defined in U I and U II. (In the following paragraph we will use the notation Q for the operator $\bar{R}(\mathrm{Sp}_\Omega)$).

Thus eq. (63) gives the general expression for the pairing energy of the eigenstates designated by n, T and W or $\mathscr{S}$ and t, where

$$T = \tfrac{1}{2}(n_\mathrm{n} - n_\mathrm{p}), \qquad t = \tfrac{1}{2}(\mathscr{S}_\mathrm{n} - \mathscr{S}_\mathrm{p})$$

Eq. (63) satisfies

$$q(\mathrm{Sp}_\Omega{}^{2\Omega-n}) = q(\mathrm{Sp}_\Omega{}^n) + 3(\Omega - n), \tag{65}$$

which corresponds to eq. (41) in R III and also to eq. (38) in U II. Eq. (63) agrees also with eqs. (18), (39) and (40) in U II. This fact verifies the correctness of the fractional parentage coefficient calculated in U II. Also, throughout this paper, the results of the calculation of fractional parentage coefficients are always checked, as far as possible, by calculating the pairing energies independently.

10. Competition Between the Strong Spin-Orbit Force, the Singlet Pairing Force and the Triplet Pairing Force near the *j-j* Limit

10.1 WITHOUT TRIPLET PAIRING FORCE

This has been already treated in U II. In this paper we add only a few remarks. In II it was shown that deviation from the pure j–j limit may occur strongly near closure of the j–j subshell, and this has been demonstrated for nuclei with $n = 2j_+$ and $T = \frac{1}{2}$. The same situation can also be seen in nuclei whose proton shell or neutron shell is almost filled, but whose shells of both protons and neutrons are not necessarily simultaneously almost filled. This can be easily seen from eq. (63). The pairing energy consists of the energy among protons, the energy among neutrons and the energy between pairs, each of which consists of a proton and a neutron. However, the last of these is far smaller than the first and second energies. Therefore, when either the proton shell or the neutron shell is nearly closed, the pairing energy becomes comparatively small and the mixing of the j_- pair into the j_+ pair can increase the resultant energy. This fact was first pointed out in ref. [8]), in which only the neutron shell is taken into account. This paper confirms the result in ref. [8]).

10.2. WITH TRIPLET PAIRING FORCE

First we need to calculate the matrix elements of the triplet pairing force in the j–j representation. We define the triplet pairing force as

$$V^{11}\mathrm{Tr}, \tag{66}$$

where

$$\mathrm{Tr} = \sum_{i<j} \mathrm{tr}\ (ij), \tag{66'}$$

$$(l^2LSJ|\ \mathrm{tr}\ (ij)|l^2LSJ) = \delta_{J0}\delta_{L1}\delta_{S1}\,2(2l+1). \tag{67}$$

The eigenfunctions with $J = 0$ of two particles in the j–j representation can be decomposed into the L–S coupling functions as follows:

$$\begin{aligned}
\sqrt{2(2l+1)}\psi(j_+^2 \quad \mathscr{S}=0) &= \sqrt{2j_++1}\psi(l^2 \quad \mathscr{S}=0, \quad \mathscr{S}_R=0) \\
&\quad +\sqrt{2j_-+1}\psi(l^2 \quad \mathscr{S}=2, \quad \mathscr{S}_R=2); \\
\sqrt{2(2l+1)}\psi(j_-^2 \quad \mathscr{S}=0) &= \sqrt{2j_-+1}\psi(l^2 \quad \mathscr{S}=0, \quad \mathscr{S}_R=0) \\
&\quad -\sqrt{2j_++1}\psi(l^2 \quad \mathscr{S}=2, \quad \mathscr{S}_R=2).
\end{aligned} \tag{68}$$

From this it follows that

$$\begin{aligned}
&(j_+^2 \quad \mathscr{S}=0|\mathrm{Tr}|j_+^2 \quad \mathscr{S}=0) = (2j_-+1),\\
&(j_-^2 \quad \mathscr{S}=0|\mathrm{Tr}|j_-^2 \quad \mathscr{S}=0) = (2j_++1),\\
&(j_+^2 \quad \mathscr{S}=0|\mathrm{Tr}|j_-^2 \quad \mathscr{S}=0) = -\sqrt{(2j_++1)(2j_-+1)}.
\end{aligned} \tag{69}$$

Here it should be specially noticed that the last equation (69) has opposite sign from the last equation in (2A) of ref. [8]).

Thus the competition between spin-orbit force and pairing forces can be resolved by using the results in the sects. 3 and 4 of U II, if we make the following alterations:

$$\begin{aligned}
&V^0 \to V^0+\frac{2j_-+1}{2j_++1}V^{11} \quad \text{in} \quad q(\mathrm{Sp}^n_{2j_++1}) = Q(j_+^n),\\
&V^0 \to V^0+\frac{2j_++1}{2j_-+1}V^{11} \quad \text{in} \quad q(\mathrm{Sp}^n_{2j_-+1}) = Q(j_-^n),\\
&V^0 \to V^0-V^{11} \text{ in the non-diagonal elements of matrix (48) in U II.}
\end{aligned} \tag{70}$$

Thus the final eigenfunctions can be obtained by diagonalizing the following matrix, which corresponds to matrix 48 in U II:

$$\begin{pmatrix}
\left(V^0+\frac{2j_-+1}{2j_++1}\right)(n-1)(n'+3)\frac{1}{4} & (V^0-V^{11})\sqrt{\frac{1}{2}n(n-1)(2j_++1)(2j_-+1)} & (V^0-V^{11})\sqrt{\frac{1}{2}n(n-1)(2j_++1)(2j_-+1)}\\
& \times[j_+^n(1\tfrac{1}{2})\tfrac{1}{2}\{j_+^{n-2}(1\tfrac{1}{2})\tfrac{1}{2}, j_+^2(00)1] & \times[j_+^n(1\tfrac{1}{2})\tfrac{1}{2}\{j_+^{n-2}(1\tfrac{1}{2})\tfrac{3}{2}, j_+^2(00)1]\\
(V^0-V^{11})\sqrt{\frac{1}{2}n(n-1)(2j_++1)(2j_-+1)} & \left(V^0+\frac{2j_-+1}{2j_++1}V^{11}\right)q(j_+^{n-2}(1\tfrac{1}{2})T=\tfrac{1}{2}) & 0\\
\times[j_+^n(1\tfrac{1}{2})\tfrac{1}{2}\{j_+^{n-2}(1\tfrac{1}{2})\tfrac{1}{2}, j_+^2(00)1] & +\left(V^0+\frac{2j_++1}{2j_-+1}V^{11}\right)q(j_-^2(00))-(2l+1)V_{\sigma l} & \\
(V^0-V^{11})\sqrt{\frac{1}{2}n(n-1)(2j_++1)(2j_-+1)} & 0 & \left(V^0+\frac{2j_-+1}{2j_++1}V^{11}\right)q(j_+^{n-2}(1\tfrac{1}{2})T=\tfrac{1}{2})\\
\times[j_+^n(1\tfrac{1}{2})\tfrac{1}{2}\{j_+^{n-2}(1\tfrac{1}{2})\tfrac{3}{2}, j_+^2(00)1] & & +\left(V^0+\frac{2j_++1}{2j_-+1}V^{11}\right)q(j_-^2(00))-(2l+1)V_{\sigma l}
\end{pmatrix} \tag{71}$$

Therefore the weak triplet pairing force does not essentially change the results obtained in U II. If we apply the above results to the Al^{21} and B^{11}, we obtain curves which are bent in lesser degree. Also the values of the ratio $V^0/V_{\sigma l}$ required to explain the magnetic moments of these nuclei will be altered a little (see figs. 1 and 2 of U II).

10.3. WITH A TRIPLET PAIRING FORCE OF MODERATE STRENGTH

In this section we assume V^{11} to be comparable in order of magnitude to V^0. However, when V^0—V^{11} is still of the same order of magnitude as V^0 itself the situation is still similar to that in subsect 10.2. Therefore the coupling scheme gradually deviates from the pure j–j limit as the number of nucleons

increases and approaches $2j_+$. When V^{11} further increases and becomes almost equal to V^0, so that $V^0-V^{11} \approx 0$, we see that the transition from the pure j–j scheme to the intermediate scheme occurs quite suddenly. This transition occurs when the number of nucleons increases so that the following equation is satisfied:

$$\left(V^0+\frac{2j_-+1}{2j_++1}V^{11}\right)(n-1)(n'+3)\tfrac{1}{4} \approx \left(V^0+\frac{2j_-+1}{2j_++1}V^{11}\right) q(j_+{}^{n-2}(1\tfrac{1}{2})\ T=\tfrac{3}{2}) + \left(V^0+\frac{2j_++1}{2j_-+1}V^{11}\right) q(j_-{}^2(00))-(2l+1)V_{\sigma l}. \quad (72)$$

11. Competition Between the Strong Singlet Pairing Force, the Spin Orbit Force, and a Weak Triplet Force

As already mentioned in sects. 1 and 2, we deal only with the case where the triplet pairing force is very weak. We first calculate the perturbation energy due to the weak triplet pairing force.

11.1. THE TRIPLET PAIRING ENERGY NEAR THE *L-S* LIMIT

By using the method developed in sects. 5, 6, 7 and 8, we calculate the triplet pairing energy for the state with $\mathscr{S}=0$. We shall demonstrate this calculation for even nuclei. The triplet energy for even nuclei is

$$\begin{aligned}&\mathrm{tr}\ (l^n\ W=(00)\ T)\\ &=(l^n\ W=(00)\ L=0\ S=0\ J=0\ T|\mathrm{Tr}|l^n\ W=(00)\ L=0\ S=0\ J=0\ T)\\ &=\tfrac{1}{2}n(n-1)\sum_{T_1}[l^n\ W=(00)\ T\{l^{n-2}\ W_1=(11)\ L=1\ S=1\ J=0\ T_1,\\ &\qquad l^2\ W_2=(11)\ L=1\ S=1\ J=0\ T_2=1]^2\ \Omega, \quad (73)\end{aligned}$$

where $\Omega=2(2l+1)$.

From eq. (5) it follows that

$$\begin{aligned}&[l^n\ W=(00)\ T\{l^{n-2}\ W_1=(11)\ L=1\ S=1\ J=0\ T_1,\ l^2\ W_2=(11)\ L=1\ S=1\ J=0\ T_2=1]^2\\ &=(\Sigma\{\Sigma_1\ \Sigma_2)^2(\Sigma\ W=(00)\ \{\Sigma_1\ W_1=(11),\ \Sigma_2\ W_2=(11))^2\ (W=(00)\ L=1\ S=1\\ &J=0\ \{W_1=(11)\ L_1=1\ S_1=1\ J_1=0,\ W_2=(11)\ L_2=1\ S_2=1 J_2=0)^2. \quad (74)\end{aligned}$$

Using the results in sects. 6, 7 and 8, we obtain

$$\begin{aligned}&[l^n\ W=(00)\ T\{l^{n-2}\ W_1=(11)\ L=1\ S=1\ J=0\ T_1,\ l^2\ W_2=(11)\ L=1\ S=1\ J=0]^2\\ &=\frac{(n-2T)(T+1)}{n(2T+1)}\left(\frac{(n-2T-2)(T+\frac{3}{2})}{(n-1)(2T+2)}-\frac{2\Omega+6-n+2T}{2(n-1)\Omega}\right)\frac{1}{(\frac{1}{2}\Omega-1)(\Omega+1)} \quad \text{for } T_1=T+1\\ &=\frac{(n-2T)}{n}\ \frac{(n+2T+2)}{4(n-1)}\ \frac{1}{(\frac{1}{2}\Omega-1)(\Omega+1)} \quad \text{for } T_1=T \quad (75)\\ &=\frac{(n+2T+2)T}{n(2T+1)}\left(\frac{(n+2T)(T-\frac{1}{2})}{(n-1)(2T)}-\frac{(2\Omega+4-n-2T)}{2(n-1)\Omega}\right)\frac{1}{(\frac{1}{2}\Omega-1)(\Omega+1)} \quad \text{for } T_1=T-1.\end{aligned}$$

From the above equations, we obtain

$$\sum_{T_1=T+1,\,T,\,T-1} [l^n\ W=(00)\ T\{l^{n-2}\ W_1=(11)\ L_1=1\ S_1=1\ J_1=0\ T_1,\ l^2\ W_2=(00)\ L_2=1\ S_2=1\ J_2=0]^2$$
$$=\left(1-\frac{(n-2T)}{n}\,\frac{(n+2T+2)}{4(n-1)}-\frac{q(l^n W=(00)T)}{\frac{1}{2}n(n-1)\Omega}\right)\frac{1}{(\frac{1}{2}\Omega-1)(\Omega+1)}. \tag{76}$$

or, more simply,

$$\frac{4n(\Omega+1)(n-2)-(n-2T)(n+2T+2)(\Omega+2)}{4n(n-1)\Omega}\,\frac{1}{\frac{1}{2}(\Omega-2)(\Omega+1)}. \tag{77}$$

We finally obtain the pairing energy from the above equations:

$$\mathrm{tr}\ (l^n\ W=(00)\ T)=\frac{4n(\Omega+1)(n-2)-(n-2T)(n+2T+2)(\Omega+2)}{4(\Omega-2)(\Omega+1)} \tag{78}$$

Eq. (78) is checked by the following requirements.

$$\mathrm{tr}\ (l^2\ W=(00)\ T=1)=0,\quad \mathrm{tr}\ (l^\Omega\ W=(00)\ T=\tfrac{1}{2}\Omega)=\Omega,$$
$$\mathrm{tr}\ (l^{2\Omega}\ W=(00)\ T=0)=3\Omega. \tag{79}$$

It will be proved in a future paper that $\mathrm{tr}(l^nWT)$ has to satisfy eqs. (79).

From eq. (78), we see that weak triplet energy increases as

$$\sim\frac{n^2}{\Omega}V^{11}. \tag{80}$$

The weak triplet energy has its maximum value for the closed shell and

$$V^{11}\mathrm{tr}=3\Omega V^{11}. \tag{81}$$

From this we see that if $V^{11}\ll V^0$ the triplet energy is always negligible.

11.2. PERTURBATION DUE TO THE SPIN-ORBIT FORCE

The spin-orbit force always tends to replace $\psi(l^2,\ L=0\ S=0)$ with $\psi(j^2\ J=0)$. This can happen only when the loss in the singlet pairing energy can be compensated by the increase of the spin-orbit energy. However, the loss in the singlet energy in the component wave function with $\mathscr{S}=2$ is

$$\Delta q=q(l^n\mathscr{S}=0)-q(l^n\mathscr{S}=2)=\Omega, \tag{82}$$

and is independent of n. As we assume $\Omega V^0>(2l+1)V_{\sigma l}$, the spin-orbit force is never big enough to upset the predominance of the pure L–S component in the ground states of nuclei.

12. The Relation Between Our Method and the Bogoliubov Method.

In this section, we deal with the spin-orbit force and the pairing forces in the j–j representation by the Bogoliubov method. The procedure for applying the Bogoliubov method to the calculations of the energies in the L–S representations will be easily understood from the procedure in the j–j representations, without further explanations.

Throughout this section, we calculate the energies with accuracy up to the order of $1/\Omega$. This is because such operators as $C_m{}^* C_m$ or $C_{-m}{}^* C_m C_m{}^* C_{-m}$ need to be dealt with most carefully. In order to obtain correct results it is necessary to define the procedure for dealing with those operators. We intend to deal with this in a future paper.

12.1 THE BOGOLIUBOV TREATMENT OF THE SYSTEM OF ONE KIND OF NUCLEONS

We choose $\psi_m{}^{j+}$ and $\psi_m{}^{j-}$ as the bases of the representation, where

$$J^2 \psi_m{}^{j\pm} = j_\pm(j_\pm+1)\psi_m{}^{j\pm}. \tag{83}$$

We introduce operators $C_m{}^{\pm *}$ and $C_m{}^{\pm}$, which are the creation and annihilation operators of the functions $\psi_m{}^{j\pm}$. The spin-orbit force and the pairing forces are expressed in terms of these operators as follows:

$$V_{\sigma l}[\tfrac{1}{2}l \sum_m C_m{}^{+*} C_m{}^{+} - \tfrac{1}{2}(l+1) \sum_m C_m{}^{-*} C_m{}^{-}], \tag{84}$$

$$\left(V^0 + \frac{2j_-+1}{2j_++1} V^{11}\right) \Big(\sum_{mm'} \varepsilon_m \varepsilon_{m'} C_{-m'}^{+*} C_m^{+} C_{m'}^{+*} C_{-m}^{+} \Big),$$
$$\left(V^0 + \frac{2j_++1}{2j_-+1} V^{11}\right) \Big(\sum_{mm'} \varepsilon_m \varepsilon_{m'} C_{-m'}^{-*} C_m^{-} C_{m'}^{-*} C_{-m}^{-} \Big), \tag{85}$$

$$(V^0 - V^{11}) \Big(\sum_{mm'} \varepsilon_m \varepsilon_{m'} C_{-m'}^{-*} C_m^{+} C_{m'}^{-*} C_{-m}^{+} + \sum_{mm'} \varepsilon_m \varepsilon_{m'} C_{-m'}^{+*} C_m^{-} C_{m'}^{+*} C_{-m}^{-} \Big). \tag{86}$$

By transforming operators $C_m{}^{\pm *}$ and $C_m{}^{\pm}$ by the well-known Bogoliubov-Valatin transformation [11, 12] (eq. (51). U II),

$$C_m{}^{\pm} = U_\pm a_m{}^{\pm} + S_m V_\pm a_{-m}^{\pm *} \text{ and its conjugate,} \tag{87}$$

with $U_\pm$ and $V_\pm$ which satisfy

$$\sum_m C_m{}^{+*} C_m{}^{+} = \Omega_+ V_+{}^2 = n, \qquad U_\pm{}^2 = 1 - V_\pm{}^2,$$
$$\sum_m C_m{}^{-*} C_m{}^{-} = \Omega_- V_-{}^2 = 0, \qquad \Omega_\pm = 2j_\pm + 1, \tag{88}$$

we obtain

$$n \frac{l}{2} V_{ol} \qquad \text{for the spin-orbit energy,} \tag{89}$$

$$\tfrac{1}{2}n(\Omega_+-n)\left(V^0+\frac{2j_-+1}{2j_++1}V^{11}\right) \qquad \text{for the pairing energy.} \tag{90}$$

If we perform the transformation which satisfies

$$\sum_m C_m^{+*}C_m^{+}=\Omega_+V_+^{\,2}=n-2, \qquad \sum_m C_m^{-*}C_m^{-}=\Omega_-V_-^{\,2}=2, \tag{91}$$

we obtain

$$\left\{(n-2)\frac{l}{2}+(-l-1)\right\}V_{sl} \text{ for the spin-orbit energy,} \tag{92}$$

$$\left(\tfrac{1}{2}(n-2)(\Omega_+-n+2)\right)\left(V^0+\frac{2j_-+1}{2j_++1}V^{11}\right)+(\Omega_--2)\left(V^0+\frac{2j_++1}{2j_-+1}V^{11}\right)$$

for the pairing energies. (93)

The cross term between the $(j_+^{\,n})$ and $(j_+^{\,n-2})$ $(j_-^{\,2})$ configurations due to (86) can be obtained by the following transformations:

$$\begin{aligned}
C_m^{+} &= U_+a_m^{+}+S_mV_+a_{-m}^{+*} && \text{with} && \Omega_+V_+^{\,2}=n,\\
C_m^{-} &= U_-a_m^{-}+S_mV_-a_{-m}^{-*} && \text{with} && \Omega_-V_-^{\,2}=0,\\
C_m^{+*} &= U'_+a_m^{+*}+S_mV'_+a_{-m}^{+} && \text{with} && \Omega_+V_+'^{2}=n-2,\\
C_m^{-*} &= U'_-a_m^{-*}+S_mV'_-a_{-m}^{-} && \text{with} && \Omega_-V_-'^{2}=2.
\end{aligned} \tag{94}$$

Inserting eq. (94) into the matrix element (86), we obtain the following non-diagonal energy:

$$2(V^0-V^{11})(\tfrac{1}{2}\sqrt{n(\Omega_+-n)2(\Omega_--2)}. \tag{95}$$

If we compare these results with the exact ones obtained by the Racah method in ref. [8]), we see that results agree if we replace $\Omega-n$ by $\Omega-n+2$ in the results obtained in this section. This small difference, which is of the order of $1/\Omega$, results from improper treatment of the constant operators $c_m^{*}c_m$ and $C_{-m}^{*}C_m$ $C_m^{*}C_{-m}$.

As we have seen in eqs. (4) and (5) in ref. [8]), the pairing energy consists not only of the interaction between particles and holes, which is properly taken into account in the Bogoliubov method, but also of the interaction among the particles themselves. This later energy is due to the constant operators and gives the energy nV^0 for the pairing energy.

12.2 BOGOLIUBOV TREATMENT OF THE SYSTEM OF BOTH KINDS OF NUCLEONS

As we see from eq. (63), the interaction energy between the proton shell and the neutron shell is n_pV^0. This energy comes from the constant operators. As the energy nV^0 was neglected in subsect. 12.2, the energy n_pV^0 is neglected in the present Bogoliubov treatment.

We introduce the operators ${}_{\mathrm{p}}C_m^{\pm}$, ${}_{\mathrm{n}}C_m^{\pm}$, ${}_{\mathrm{p}}C_m^{\pm *}$ and ${}_{\mathrm{n}}C_m^{\pm *}$ which are the annihilation and creation operators for the protons and neutrons. Performing the Bogoliubov-Valatin transformations which satisfy

$$\begin{aligned} \sum_m {}_{\mathrm{p}}C_m^{+*}\,{}_{\mathrm{p}}C_m^{+} &= \Omega_{+\,\mathrm{p}}V_+^{\,2} = \tfrac{1}{2}(n-2T), \\ \sum_m {}_{\mathrm{n}}C_m^{+*}\,{}_{\mathrm{n}}C_m^{+} &= \Omega_{+\,\mathrm{n}}V_+^{\,2} = \tfrac{1}{2}(n+2T), \end{aligned} \tag{96}$$

we obtain the pairing energies of the nuclei:

$$\tfrac{1}{2}\{\tfrac{1}{2}(n-2T)(\Omega_+ - \tfrac{1}{2}(n-2T)) + \tfrac{1}{2}(n+2T)(\Omega_+ - \tfrac{1}{2}(n+2T))\}. \tag{97}$$

As in subsect. 12.1, if we replace $\Omega_+ - \frac{1}{2}(n-2T)$ and $\Omega_+ - \frac{1}{2}(n+2T)$ by $\Omega_+ - \frac{1}{2}(n-2T)+2$ and $\Omega_+ - \frac{1}{2}(n+2T)+2$ and add further the term $n_{\mathrm{p}}V^0$, we obtain the correct result (83).

Thus the Bogoliubov method produces the results in a surprisingly simple way. We may examine further the strict procedure for obtaining exact results in a future paper.

13. Conclusion

The pairing energies are directly derived for the system of both kinds of nucleons by using Casimir operators in Sp_Ω and SU_Ω.

To treat the competition between the spin-orbit force and the pairing forces, the fractional parentage coefficients are calculated and general expressions are obtained for the case where the seniority quantum number is 0 or 1. In the course of the calculation of the fractional parentage coefficients, these are decomposed into the products of the elementary coefficients. Some algebraic equations for these coefficients are derived.

As a result, we found that the deviation from the j–j limit may be greatest near closure of the j–j subshell and may occur suddenly if $V^0 \approx V^{11}$. However, for L–S coupling with a weak triplet force, we do not find especially great deviations from the L–S limit for any particular nucleus.

Finally some correspondences between the present work and the Bogoliubov treatment were discussed. We found that the Bogoliubov method gives results most simply. However, the Racah method always gives the most reliable and accurate results. The fundamental identity between these two methods will be discussed in a future paper.

It is a great pleasure to express my sincere thanks to Prof. Gorodetzky who made it possible for me to carry out this work at Strasbourg. The author also wishes to express his sincere gratitude to Dr. Knipper, who has been constantly helpful and has let me use his personal facilities. Also deep thanks are due to Dr. and Mrs. Ullman who have encouraged me in carrying out this work and

also read this paper and made it presentable. Finally the author is very grateful to Dr. Cohn, Dep. Math. Manchester Univ. for the discussions on the application of Lie algebra to nuclear spectroscopy, which gave me confidence in carrying out this work.

References

1) G. Racah, Phys. Rev. **63** (1943) 367, **76** (1949) 1352 referred to as RIII and RIV
2) G. Racah, Group Theory and Spectroscopy, Princeton 1951 (Mimeographed notes)
3) G. Racah, Phys. Rev. **78** (1950) 622
4) G. Pacah, Birmingham Conference of 1953;
P. Teitelbaum, Bulletin Research Council Israel **3** (1954) 299
5) G. Racah, Bulletin Research Council Israel, Farkas Memorial Volume **1** (1952) 294, Rend. Lincei **8** (1950) 108
6) M. Umezawa, Prog. Theor. Physics **8** (1952) 509
7) M. Umezawa, Proc. Roy. Soc. **232** (1955) 88; Nuclear Physics **25** (1961) 669; referred to as UI and UII
8) M. Umezawa, Nuclear Physics **23** (1961) 296
9) H. A. Jahn, Proc. Roy. Soc. **201** (1950) 516, **205** (1951) 192
10) B. H. Flowers and A. R. Edmonds, Proc. Roy. Soc. **214** (1952) 515
11) J. G. Valatin, Nuovo Cim. **7** (1958) 843
12) M. Baranger, Phys. Rev. **120** (1960) 957;
L. S. Kisslinger and R. A. Sorensen, Mat. Fys. Medd. Dan. Vid. Selsk **32** no. 9 (1960);
S. T. Belyaeb, Mat. Fys. Medd. Dan. Vid. Selsk. **31** no. 11, (1959)
13) H. Weyl, The classical groups (Princeton University Press, 1946)
14) O. E. Littlewood, Theory of group characters (Oxford University Press, 1950)
15) J. Bardeen, L. N. Cooper and J. R. Schrieffer, Phys. Rev. **108** (1957) 1175

2.F:2.L:
3.A

Nuclear Physics **27** (1961) 270—283; © *North-Holland Publishing Co., Amsterdam*
Not to be reproduced by photoprint or microfilm without written permission from the publisher

COLLECTIVE EFFECTS IN INELASTIC SCATTERING FROM NUCLEI

W. T. PINKSTON
Vanderbilt University, Nashville, Tennessee
and
G. R. SATCHLER
Oak Ridge National Laboratory, Oak Ridge, Tennessee

Received 10 April 1961

Abstract: It is shown how inelastic scattering is closely analogous to an electric multipole radiative transition, and will show similar collective enhancement. This enhancement will vary with scattering angle. In general, spin-flip transitions are little effected, the enhancement being found in the spin-independent amplitudes; the consequences of this are discussed. The deformed nucleus model for C^{12} is used to illustrate these effects. Finally, the interaction form factors to be used for inelastic scattering are discussed.

1. Introduction

It has been suggested [1]) that inelastic scattering from nuclei preferentially excites nuclear states having a collective nature. In particular it was found that there is a significant correlation between the cross sections for inelastic scattering by Coulomb excitation and by nuclear excitation [1]). This correlation is readily understood when it is realized the matrix elements for nuclear excitation on a direct interaction model, are closely analogous to those for electric, multipole radiation between the same two states [2]). We conclude from this that, if an electric transition between two states is enhanced by collective effects, the inelastic scattering will be also. Thus, even though the initial and final states may be well classified in terms of the shell model, the transition *strengths* will be strongly affected by any collective correlations present. These collective correlations in the nuclear wave functions reflect the long range effects of the internucleon forces [3]), and in this respect inelastic scattering is to be contrasted with stripping (or pick-up) reactions. The latter determine how much the residual nuclear state resembles the initial, plus (or minus) a nucleon in a definite state. They depend upon a more detailed description of the nuclear wave functions and are thus also sensitive to the short range correlations induced by the pairing properties of the internucleon force [4]).

Although there is an overall similarity between inelastic scattering and electromagnetic transitions, the differences between them are also of interest. The two main sources of difference are, firstly, the short de Broglie wave-

lengths of the colliding systems compared to the corresponding photon wavelength. We shall see this leads to the collective enhancement in inelastic scattering varying with the scattering angle. Secondly, the spin and isospin dependence of the nuclear interaction can be important, but the spin dependent transitions are found not to be enhanced even if the spin independent transitions are, unless the collective states themselves have a "spin-wave" character [5]). In addition, the isospin dependence of the inter-nucleon force (and exchange due to antisymmetrization) allows charge-exchange scattering [6]), for example (p, n). This leads to the interesting possibility of enhanced (p, n) or (n, p) reactions leading to the giant dipole resonance in the residual nucleus.

In the present paper, the amplitudes for excitation by direct interaction inelastic scattering are examined and compared to gamma-ray transition amplitudes. The similarity between them and its consequences are discussed. The spin-independent and spin-flip amplitudes are shown to be affected differently by collective correlations, and the importance of this for the interpretation of polarization and gamma-correlation experiments is stressed. Estimates are made of the collective enhancement of the inelastic scattering of protons by C^{12}, both for spin-independent and spin-flip transitions using the deformed-nucleus model.

2. Similarity of Electromagnetic and Inelastic Operators

The transition amplitude, on a direct interaction model, for excitation from ground state $|A\rangle$ to an excited state $|B\rangle$ by inelastic scattering (neglecting exchange) is given by

$$T_{BA} = \langle B| \int \mathrm{d}\mathbf{r}_0 \phi^{(-)*}(\mathbf{k}_f, \mathbf{r}_0) \sum_i v_{i0} \phi^{(+)}(\mathbf{k}_i \mathbf{r}_0) |A\rangle. \tag{1}$$

The ϕ are distorted waves corresponding to asymptotic initial and final momenta $\mathbf{k}_i$ and $\mathbf{k}_f$, respectively. The potential v_{i0} between projectile and the ith nucleon of the target is in general spin dependent. It may represent an effective or pseudo-potential; for example, in the impulse approximation for the scattering of high energy nucleons one uses for v_{i0} the free two-body scattering amplitude [8]). (This is non-local; however at high energies it seems reasonable to use the local approximation $v_{i0} \approx -(\hbar^2/2\pi^2 m) M(q) \delta(\mathbf{r}_i - \mathbf{r}_0)$, where $\mathbf{q} = \mathbf{k}_f - \mathbf{k}_i$ is the overall momentum transfer [8]). If the properly symmetrized two-body amplitude $M(q)$ is used, this includes exchange between projectile and struck nucleon. Exchange with other target nucleons should be negligible at high energies). The nuclear transition is then effected by an operator

$$N = \int \mathrm{d}\mathbf{r}_0 \phi^{(-)*}(\mathbf{k}_f, \mathbf{r}_0) \sum_i v_{i0} \phi^{(+)}(\mathbf{k}_i, \mathbf{r}_0). \tag{2}$$

Now we need to show that the major part of N has a form similar to the electro-

magnetic interaction operator [9]). If $\phi^{(-)*}\phi^{(+)}$ and v_{i0} are expanded in spherical harmonics

$$\phi^{(-)*}(\mathbf{k}_f, \mathbf{r}_0)\phi^{(+)}(\mathbf{k}_1, \mathbf{r}_0) = \sum_{\lambda\mu} \Phi_{\lambda\mu}(\mathbf{k}_1, \mathbf{k}_f, r_0)Y_{\lambda\mu}(\Omega_0), \tag{3}$$

$$v_{i0} = \sum_{lm} V_l(r_i, r_0)Y^*_{lm}(\Omega_0)Y_{lm}(\Omega_i), \tag{4}$$

then N is given by

$$N = \sum_i \sum_{lm} g_{lm}(r_i)Y_{lm}(\Omega_i), \tag{5}$$

in which

$$g_{lm}(r_i) = \int_0^\infty r^2{}_0 \mathrm{d}r_0 V_l(r_i, r_0)\Phi_{lm}(\mathbf{k}_1, \mathbf{k}_f, r_0). \tag{6}$$

For orientation, we may approximate v_{i0} by a delta function, so that

$$V_l(r_i, r_0) = G\delta(r_i - r_0)/r_0{}^2. \tag{7}$$

If Born approximation, rather than the distorted wave theory, is used so that $\phi(\mathbf{k}, \mathbf{r}) \to \exp i\mathbf{k}\cdot\mathbf{r}$, then

$$g_{lm}(r_i) \propto j_l(Qr_i), \tag{8}$$

in which Q is the recoil momentum, $\mathbf{Q} = \mathbf{k}_1 - \mathbf{k}_f$, and the z-axis has been taken along $\mathbf{Q}$. Thus for the l-th term in expansion (5), we have

$$N_l \propto \sum_i j_l(Qr_i)Y_{l0}(\Omega_i). \tag{9}$$

This has exactly the form of the spin-independent (SI) electric multipole operator of order l, except that the sum here is over all nucleons whereas in the electric multipole moment the sum is over protons only [9]). Of course, angular momentum considerations ensure both operators have the same angular dependence, and we are therefore mainly concerned with their radial dependence. For gamma transitions the Q in (9) is replaced by the photon wavenumber, and for low energy transitions the Bessel function can always be replaced by its leading term, $j_l \propto r_i{}^l$. Because of the heavy masses of the colliding systems in inelastic scattering, the wavelength corresponding to Q can be much smaller than the photon wavelength. Then N_l is proportional to $r_i{}^l$ only at small scattering angles were Q is small. However, this is overrestrictive. All we need is for the radial function to feel out any long range spatial correlations present in the nuclear wave functions. This it will do if it contains no oscillations within the nuclear volume which could produce cancellations between the contributions from different regions of the nucleus. There will be no such oscillations provided QR (where R is the nuclear radius) is less than the value of x at which $j_l(x)$ has its first zero; then $j_l(Qr)$ has the same sign throughout the nucleus. But the angular distribution of the inelastic scattering is given by

$$|T_{BA}|^2 \propto |\langle j_l(Qr)\rangle|^2;$$

therefore this condition will be satisfied by all particles scattered into the first, main peak of the differential cross section. Scattering through angles much larger than this may show inhibition rather than enhancement, compared to an electromagnetic transition. These points will be seen in more detail when the specific example of scattering from C^{12} is discussed in the next section.

The more correct use of distorted waves rather than plane waves leads to qualitatively similar results [7, 10])†. The radial dependence of $g_{lm}(r_i)$ is modified, but is still a monotonically increasing function of r for small Q. The increase in (local) momentum of the projectile when inside the nucleus (due to the attractive potential) increases the possibility of destructive oscillations in N, but this is counter-balanced by the reflection at the nuclear surface and absorption within the interior which damps out these contributions and emphasises the surface region.

As a result of the similarity of the inelastic scattering and gamma ray transition operators we conclude that if the EL transition between two states is enhanced by collective effects, the inelastic scattering is also, that is, σ_L (inelastic) $\propto B(EL)$, as found by Cohen and Rubin [1]). On the other hand, inelastic scattering differs from gamma emission in one very important way. The matrix element of the spin-dependent (SD) electric multipole operator of order L is smaller than the matrix element of the SI electric multipole operator by the ratio of the gamma ray energy to the nucleon rest energy and is, therefore, negligible. In the case of inelastic scattering of nucleons, however, the spin dependence arises from the spin dependence of the nucleon-nucleon interaction and from Pauli Principle exchanges, and is not, in general, negligible. The polarization of the scattered nucleons and the (x', γ) angular correlation depend sensitively on the ratio of the SD matrix element to the matrix element of the SI operator. In the light nuclei this ratio has been used [8, 11, 12]) to determine the shell model angular momentum coupling scheme. These determinations may be in error, especially for $l = 2$ transitions, if the collective enhancements are neglected. Because the SD matrix elements are not enhanced, previous shell theory estimates of the ratio SD/SI are too large.

The fact that the SD matrix element is not enhanced for $\Delta I = 2(3)$ transitions can be understood in terms of a picture of the enhancement as due to the entire nucleus being deformed into a quadrupole (octupole) shape so that all the nucleons coherently contribute. But this coherent motion or deformation does not involve any strong spin coupling; thus there is no enhancement of the SD matrix element, since there are roughly as many spins "up" as there are "down" tending to cancel the effect of the coherent sum.

For a more detailed comparison of inelastic scattering and gamma ray

† See especially ref. [7]) and other refs. cited there.

amplitudes, the transition operators are

$$H_m(El) \propto \sum_i r_i^l Y_{lm}(\Omega_i)\tfrac{1}{2}[1+\tau_3(i)]$$
$$= \tfrac{1}{2}\sum_i r_i^l Y_{lm}(\Omega_i)+\tfrac{1}{2}\sum_i \tau_3(i) r_i^l Y_{lm}(\Omega_i), \qquad (10)$$
$$= h_0+h_\tau,$$

for electromagnetic for electromagnetic processes, and

$$N_{lm\mu\rho} \propto \sum_i g_{lm}(r_i) Y_{lm}(\Omega_i)\{M_0+M_\mu\sigma_\mu(i)+M_\rho\tau_\rho(i)+M_{\mu\rho}\sigma_\mu(i)\tau_\rho(i)\}$$
$$= n_0+n_\sigma+n_\tau+n_{\sigma\tau} \qquad (11)$$

for inelastic scattering of nucleons. In impulse approximation the M become momentum dependent [8]). For small momentum transfers n_0+n_τ are the analogs of h_0+h_τ (except that only τ_3 occurs in h_τ, while n_τ containing $\tau_\pm$ allows charge exchange also). The difference between the electromagnetic and the inelastic operators is in the terms $n_\sigma+n_{\sigma\tau} \propto \sigma_\mu(i)\{M_\mu+M_{\mu\rho}\tau_\rho(i)\}$. For a self-conjugate nucleus such as C^{12} the isospin terms contribute only to the $\Delta T = 1$ transitions; thus the C^{12} $(0 \to 2)$ excitation is effected by n_0+n_σ. The isospin, dependent terms contribute to $\Delta T = 1$ transitions in such nuclei, and to $\Delta T = 0$, $T = 0$ and $\Delta T = 1$ transitions in nuclei for which $T_3 \neq 0$. It is not expected, however, that either n_τ or $n_{\sigma\tau}$ will be enhanced in light nuclei since for these nuclei, $Z \approx N$, that is there are roughly as many isospins up as down. These conclusions are in agreement with phenomonological calculations [13, 14]) in the lp-shell region, where the neutrons and protons are given large effective charges for $\Delta T = 0$ transitions but not for $\Delta T = 1$ transitions.

The above arguments are, of course, based on the assumption of a spatial coherence or cooperative motion. It is expected [15]) that other collective modes, namely spin waves, isospin waves and coupled spin-isospin waves exist at higher energies. Isospin waves correspond to the giant dipole photo-resonance; therefore the $l = 1$, τ-type term should yield a large cross section for either type process. The coupled spinisospin wave has $T = 1, \pi = +$, so that there should be a very fast M1 transition between it and a $T = 0$, $\pi = +$ ground state. The $l = 0$ and $l = 2$, $\sigma\tau$-type terms in the inelastic scattering operator should lead to strong excitation of this level. The spin wave is expected to have a weaker ground state transition since the $\Delta T = 0$, M1 transition operator is much smaller than the $\Delta T = 1$ operator [14, 15]).

In addition to the inelastic scattering, the $\tau_\pm$ operators in n_τ, $n_{\tau\sigma}$ allow charge exchange, namely (n, p) and (p, n) reactions. They will couple strongly to the isospin waves and spin-isospin waves, respectively. In particular, we should see strongly enhanced charge exchange reactions leading to the state in the residual nucleus which corresponds to the giant dipole state of the target. The giant dipole state is roughly described as a coherent mixture of particle-

hole pairs [16]), so evidently has the right structure for strong excitation in this way. Because this process selects the τ-dependent part of the transition operator, its experimental study is of some importance. Analogously enhanced collective transition would be observed in β-decay if parent nuclei of sufficient excitation ($\approx$ 20 MeV) to feed the dipole state could be found.

3. Enhancement in the P-Shell

3.1. APPLICATION TO C^{13}

It is well known [17]) that E2 transition rates in the 1p-shell region are too fast to be accounted for by the independent particle model. Elliott and Flowers[17]) found that the theoretical transition rates for both E2 and E3 transitions in the oxygen isotopes could be brought into agreement with the experimental data by including the effect of quadrupole and octupole vibrations weakly coupled to the low excited nuclear states. This weak coupling model leads to the assignment of effective charges to the proton and the neutron which enhance the transitions. These effective charges are different for different multipole orders. Warburton and Pinkston [13]) found that the same values of effective charge could be used to explain the strength of E2 and E3 transitions in C^{14} and N^{14}. Kurath [18]) has recently given a different account of the E2 enhancements in terms of the procedure whereby shell model wave functions are generated from the states of independent particles moving in a spheroidal potential well. It had been shown in an earlier paper [19]) that the intermediate coupling wave functions for the 1p-shell nuclei could be obtained by this generator method from antisymmetrized states of nucleons in a deformed potential well. These calculations were based on the deformed nucleus orbitals of Nilsson [20]), which consist of linear combinations of states from the same major harmonic oscillator shell. For any value of the intermediate coupling parameter, a/K, a value of Nilsson's deformation parameter η, could be found such that generated states were almost identical to the intermediate coupling states. Similar conclusions have been arrived at for certain (1d, 2s)-shell nuclei [21]). Since the generator procedure was so successful in duplicating the effects of the internucleon potentials for wave function admixtures with the degenerate states of a single major shell, Kurath [18]) made the very reasonable assumption that the admixtures of higher configurations, especially the admixture of 2p and 1f into 1p and of 1d into 1s, could be estimated by the same procedure. Hence by refining the single particle orbitals the amount and character of the states, $(1s)^4(1p)^{n-1}$ 2p, $(1s)^4(1p)^{n-1}$ 1f and $(1s)^3(1p)^n$1d in the wave function of the predominately $(1s)^4(1p)^n$ configuration could be estimated. Kurath also found that the matrix elements of the quadrupole operator r^2Y_{20} between 1p and 1f states and between 1s and 1d states are sufficiently

large to enhance the transitions strongly even though the amounts of the excited configurations are small. For the transition 4.43-MeV to ground in C^{12} the intensity was enhanced by a factor of about two for such admixtures, bringing the theoretical calculations into line with experiment. It is clear, of course, that such admixtures must enhance E2 transitions since the perturbation which introduces the excited states is proportional to r^2Y_{20}, the quadrupole operator. The degree of enhancement is also in line with the results of similar calculations of quadrupole moments for heavier nuclei [22]).

An important difference between the effective charge method and the generator method is that the effective charge method treats the nuclear states as shell model states with small admixtures of highly excited collective vibrational states, whereas the generator method exploits the equivalence of the shell model and the collective model. The collective enhancement is just a configuration mixing effect which it was impossible to calculate by conventional shell model techniques. In the language of current theory [3]) one of the main effects of the internucleon potential is the modification of the self consistent field, a "collective effect" which tends to admix 2p and 1f states into the low excited states. The other effect is the pairing effect, which mainly tends to admix $(1p)^{n-2}\ (2s)^2$ and $(1p)^{n-2}(1d)^2$ into the $(1p)^n$ states. These admixtures, even if they are comparable to the one-particle excitation admixtures, do not contribute appreciably to the gamma transitions or to inelastic scattering events; hence they only effect the wave function normalization in the present considerations.

In this section numerical estimates will be made of the collective enhancement of the inelastic scattering of protons on C^{12} leading to the excitation of the 4.43-MeV, $I = 2^+$ level. If we restrict ourselves to forward angles we may replace the Bessel function of the Born approximation or the impulse approximation by $\approx r^2$. The calculation of Kurath may thus be used for the enhancement of the SI term. Unfortunately no calculations have been made of the matrix elements of the SD operator. Calculation of SD matrix elements by the generator method is quite tedious. even more so than for SI matrix elements. Rather than carry out such calculations we have estimated the matrix elements by using Bohr-Mottelson strong coupling wave functions [23]), These functions assume a perfect overlap between the orientation of the nucleus before and after the excitation. However, the more correct generator wave functions include an averaging over the relative orientation and the consequent mismatch between initial and final intrinsic states leads to a smaller amplitude; that is, using Bohr-Mottelson wave functions we shall need a smaller deformation to obtain the same degree of enhancement. The initial and final states, then, are represented by

$$\Psi_{IM0} = \left[\frac{2I+1}{8\pi^2}\right]^{\frac{1}{2}} D^{I*}_{M0}(\theta)\chi_0(\mathbf{x}'_i), \tag{12}$$

the notation being that of ref. [23]). For the transition 0^+ to 2^+ effected by a tensor operator of the form

$$F_{2M} = \sum_i f_{2M}(\mathbf{x}_i),$$

one has

$$\begin{aligned}(2||F_2||0) &= \int \mathrm{d}\mathbf{x}_1 \ldots \mathrm{d}\mathbf{x}_n |\chi_0|^2 F_{20} \\ &= \sum_{\omega\nu} \int |\phi_{\omega\nu}|^2 f_{20}\,\mathrm{d}\mathbf{x},\end{aligned} \tag{13}$$

summed over occupied orbitals. The reduced matrix element is that of Racah. Here the integrations also imply appropriate spin sums, $\phi_{\omega\nu}$ is an independent particle orbital for the deformed nuclear field with angular momentum projection ω along the nuclear symmetry axis and ν is its "Nilsson number" [20]).

The nucleus C^{12} has a configuration, $(\nu = 1)^4(\nu = 2)^4(\nu = 3)^4$. The $\nu = 1$ orbital is, in Nilsson's approximation, pure 1s. Orbit 2 is a pure $1p_{\frac{1}{2}}$ with projection $\pm\frac{3}{2}$. Orbit 3 has a wave function

$$\phi^{(0)}_{\pm\frac{1}{2},3} = \alpha_0 u(1\mathrm{p};\, 0,\, \pm\tfrac{1}{2}) + \alpha_1 u(1\mathrm{p};\, \pm 1,\, \mp\tfrac{1}{2}).$$

The states $u(Nl;\, \Lambda,\, \Sigma)$ are in the uncoupled ($\Lambda = l_z$, $\Sigma = S_z$) representation. The $\Delta N = 2$ admixtures are calculated according to second order perturbation theory [18]),

$$\phi_{\omega\nu} = \phi^{(0)}_{\omega\nu} + \frac{\delta m\omega_0}{3\hbar}\left(\frac{4\pi}{5}\right)^{\frac{1}{2}} \sum_{l\Lambda\Sigma} \langle N-2\omega\nu|r^2 Y_{20}|Nl\Lambda\Sigma\rangle u(Nl,\, \Lambda\Sigma),$$

in which δ is a measure of the nuclear deformation [20]). To first order in δ we have

$$\begin{aligned}|\phi_{\omega\nu}|^2 \approx |\phi^{(0)}_{\omega\nu}|^2 + \frac{\delta m\omega_0}{3\hbar}\left(\frac{4\pi}{5}\right)^{\frac{1}{2}} \sum_{l\Lambda\Sigma} &\langle N-2\omega\nu|r^2 Y_{20}|Nl\Lambda\Sigma\rangle \\ &\times [u(Nl;\, \Lambda\Sigma)^* \phi^{(0)}_{\omega\nu} + \text{c.c.}].\end{aligned} \tag{14}$$

The operators with which we are concerned are

$$f_{2m}(\mathrm{SI}) = r^2 Y_{2m}, \qquad f'_{2m}(\mathrm{SD}) = r^2\{Y_2\sigma_1\}_{2m},$$

in which the bracket means a tensor product of Y_2 and $\boldsymbol{\sigma}$. For these operators we have for the C^{12} configuration,

$$\begin{aligned}Z(\mathrm{SI}) &\equiv (2||F_2||0) = \tfrac{12}{13}\langle r^2\rangle[-1+2\alpha_0{}^2-\alpha_1{}^2+\delta(\tfrac{7}{3}+\tfrac{4}{3}\alpha_1{}^2+\tfrac{7}{3}\alpha_0{}^2)], \\ Z(\mathrm{SD}) &\equiv (2||F'_2||0) = \tfrac{12}{13}\langle r^2\rangle\alpha_1\alpha_0(\tfrac{3}{4})^{\frac{1}{2}}(1-\tfrac{1}{2}\delta).\end{aligned}$$

For values of α_0 and α_1 corresponding to $\eta = -6.0$, which Kurath and Picman [19]) consider equivalent to an intermediate coupling parameter of $a/K \approx 5$, a value of $\delta \approx -0.2$ is needed to double the value of $|Z(\mathrm{SI})|^2$ (which is required to give the observed E2 transition rate). This causes an increase of only 10 %

in $Z(\mathrm{SD})$ and of 20 % in its square; thus a small admixture of $\Delta N = 2$ states causes a large enhancement of $|Z(\mathrm{SI})|^2$ but very little enhancement of $|Z(\mathrm{SD})|^2$.

This enhancement will clearly increase the magnitude of the inelastic scattering cross section. Levinson and Banerjee [11]) found in their numerical studies of (p, p′) on C^{12} in the distorted-wave approximation that the interaction potential between projectile and target nucleons needed to predict a sufficiently large cross section was about twice the magnitude expected from low-energy scattering data. The collective enhancement will considerably reduce this discrepancy, and what remains is probably within the uncertainties associated with the distorted waves used in their calculations. A more detailed study of this point is under way. A recent distorted-wave calculation for the scattering of protons by Mg^{24}, which includes the enhancement, shows good agreement with experiment [24]).

The above argument is clearly correct at small scattering angles and in fact holds to fairly large scattering angles, but if the momentum transfer gets so large that the Bessel function goes through a minimum inside the nucleus the "enhancement" tends to cancel out the lowest order contribution. Consider eq. (14). The radial dependence of $|\phi^{(0)}_{\omega\nu}|^2$ is

$$|\phi^{(0)}_{\omega\nu}|^2 \propto r^2 \exp(-r^2/a^2)$$

for harmonic oscillator radial functions and for orbits 2 and 3. The introduction of 2p and 1f orbits results in r^2 and r^4 terms in the second term of eq. (14). Then if the angular integrations are carried out in eq. (13) we are left with a radial integral of the form

$$\int_0^\infty r^4 \mathrm{d}r j_2(Qr) \exp(-r^2/a^2)[1+(yr^2/a^2)].$$

For Q so small that $j^2(Qr) \propto r^2$ is a good approximation inside the nucleus there will clearly be an enhancement for positive y. On the other hand for large Q, such that a complete oscillation of the Bessel function occurs inside the nucleus, the extra r^2 in the second term of the integrand tends to reinforce the first minimum of the Bessel function more than the first maximum resulting in a partial cancellation. The differential cross section goes as the square of this intregal, which is proportional to

$$(Qa)^4[1+\tfrac{7}{2}y-\tfrac{1}{4}y(Qa)^2]^2\exp(-\tfrac{1}{2}Q^2a^2).$$

A value of $y \approx \frac{1}{7}$ is given by $\eta = -6$, $\delta = -0.3$ and produces an enhancement of 2.7 at forward angles. Then fig. 1 shows the differential cross sections with and without enhancement, and their ratio as a function of Qa. We see also the importance of including the contributions from the four s-particles. Fig. 1 should be taken as a qualitative illustration only, however, since the Gaussian fall-off of the radial wave functions used causes an unphysically large attenua-

tion of the inelastic scattering amplitude at large angles; thus the use of the oscillator wave functions is suspect. The use of a Bessel function is a very bad approximation in many cases also, although the distorted-wave factor $g_{lm}(r)$ shows analogous oscillations with variation of scattering angle.

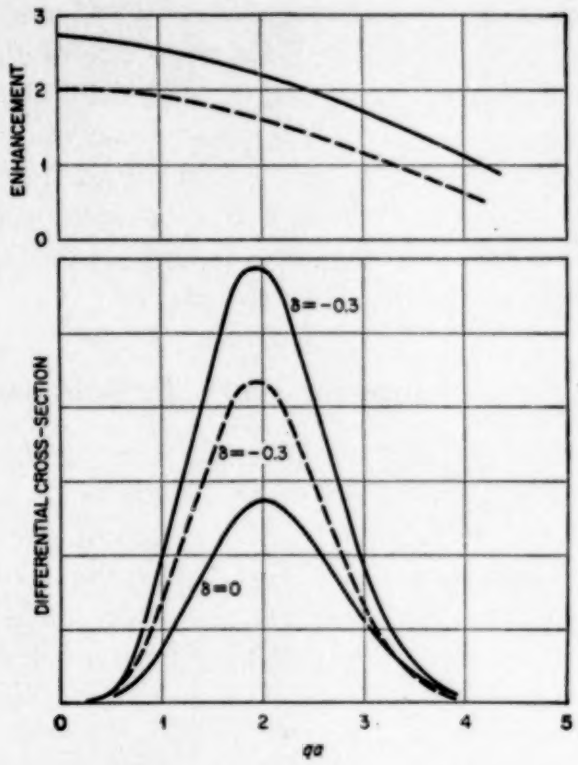

Fig. 1. Differential cross-section for inelastic scattering from C^{12}, as a function of momentum transfer Q, and using plane planes. The dashed curve for deformation $\delta = -0.3$ omits the contributions from the four s-nucleons. Above is shown the ratio of the $\delta = -0.3$ curves to the unenhanced, $\delta = 0$, cross section.

Perhaps the most drastic effect of the collective enhancement on the analysis of inelastic scattering data results from the increase of Z(SI) relatively to Z(SD). The polarization of the protons emmitted in a (p, p') reaction and the (p', γ) angular correlations depend sensitively on this ratio. Banerjee and Levinson [11]) found, for example, that the (p', γ) correlation function for the excitation of the first excited state of C^{12} is to a good approximation

$$A + B \sin^2 2(\theta - \theta_0),$$

for gammas emitted at an angle θ relative to the beam direction and a fixed angle for the outgoing proton. The ratio A/B, which determines the ratio of the "background" to the anisotropy, is a sensitive function of Z(SD) and Z(SI) and increases with increasing Z(SD)/Z(SI). Calculated with intermediate coupling wave functions, A/B was found to be an extremely sensitive function of the

intermediate coupling parameter a/K. It was smaller than the A/B measured with 17 MeV protons for almost any value of a/K short of pure jj-coupling [11]). This is in disagreement with the trend of the data in this mass region where nuclear properties are best explained with a value of $a/K \approx 5$, which implies only about 50 % jj-coupling in the C^{12} ground state. The addition of the collective enhancement seems to make matters worse since it reduces Z(SD) relative to Z(SI) and thus reduces A/B for any value of a/K; thus there is no value of a/K for which A/B is correctly predicted by the usual shell model coupling schemes. The effect of spin dependence in the internucleon interaction potential was investigated but any spin dependence of the kind indicated by low energy scattering seemed to reduce A/B. However, another source of spin-dependence which has not yet been investigated is the spin-orbit coupling which should be included in the distorted waves.

4. Form Factors for Inelastic Scattering

The expression (2) is the effective interaction experienced by the nucleus during the scattering process. In distorted wave calculations it is more convenient to group the factors in the transition amplitude (7) in a different way, to emphasize the effective interaction experienced by the *projectile* when the nuclear transition A to B takes place. The transition operator P, which takes the projectile from the initial state $\phi^{(+)}(\mathbf{k}_1, \mathbf{r}_0)$ the final state $\phi^{(-)}(\mathbf{k}_1, \mathbf{r}_0)$ is given by

$$P = \langle B| \sum_i v_{i0}|A\rangle. \tag{15}$$

Using eq. (4) we can write P as

$$P = \sum_{lm} Y^*_{lm}(\Omega_0) F_l(r_0);$$

$F_l(r_0)$ is referred to as the "form factor," for which simple parametric forms may be adopted in numerical calculations. It is, of course, given by

$$F_l(r_0) = \langle B| \sum_i V_l(r_0, r_i) Y_{lm}(\Omega_i)|A\rangle.$$

In this form, exchange scattering is neglected. Exchange gives rise to a non-local form factor $F_l(r_0, r'_0)$. A local form factor may include exchange with the struck nucleon if a zero range approximation is made for v_{i0}. At high energies this is reasonable provided one uses the impulse approximation with the properly symmetrised two-body scattering matrices [8]). If we use the Bohr-Mottelson strong coupling wave functions as before, and the delta function interaction, we have

$$F_2(r_0) \propto \sum_{\omega\nu} \left\langle \int |\phi_{\omega\nu}|^2 Y_{20}(\Omega) \mathrm{d}\Omega \right\rangle_{\text{spin}}.$$

Using the oscillator radial functions again, and performing the indicated integration and spin summation, results in a form factor,

$$F_2 \propto (r^2+yr^4)\exp(-r^2/a^2),$$

if we consider only the 1p part of $\phi^{(0)}_{\omega\nu}$. There will be a contribution of the form

$$(1+y'r^2)\exp(-r^2/a^2)$$

from the 1s orbitals. For C^{12} we have calculated F_2 as a function of Nilsson's δ for the value $\eta = -6.0$. The results appear in fig. 2 Values of δ of 0, -0.3

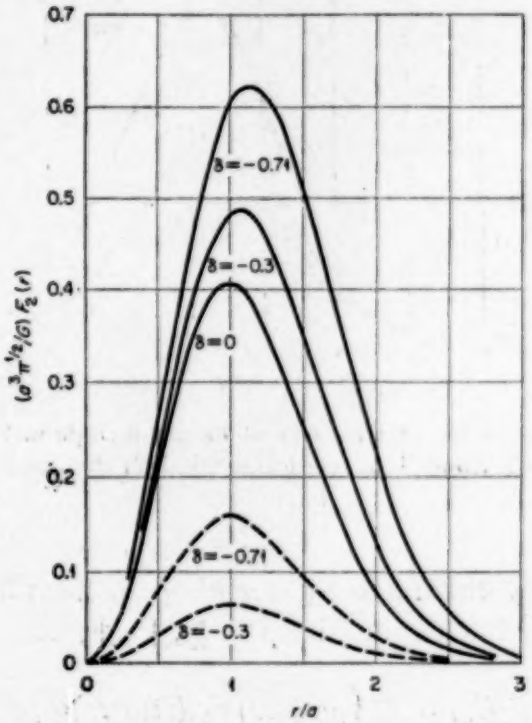

Fig. 2. Interaction form factor $F_2(r)$ for inelastic scattering from C^{12}, for various deformations δ. The dashed curves are the contributions from the four s-nucleons (which vanish for $\delta = 0$).

and -0.7 were chosen. It is seen that the form factor increases in magnitude with increasing δ. This increase, of course, enhances the cross sections. The enhancement is larger for larger radii, and this tends to emphasize the surface region of the nucleus. To further emphasize this surface effect we have plotted in fig. 3 the quantity $r_0^4 F_2(r_0)$, which is the integrand for small Q-values of the matrix element (1) when plane waves are used. It is seen that this quantity peaks out in the nuclear surface region and that the collective enhancement emphasizes this effect. With distorted waves this effect is implemented by the reflections and absorption of the projectile waves which tend to reduce the role of the interior region. This surface effect of the collective enhancement will tend to permit the use of more reasonable nuclear radii in direct interaction calculations. Levinson and Banerjee, for example, found they needed a r.m.s.

nuclear density radius 15 % larger than the value suggested by high energy electron scattering; this increase is of about the magnitude expected from the shift to larger radii of the form factor illustrated in figs. 2 and 3.

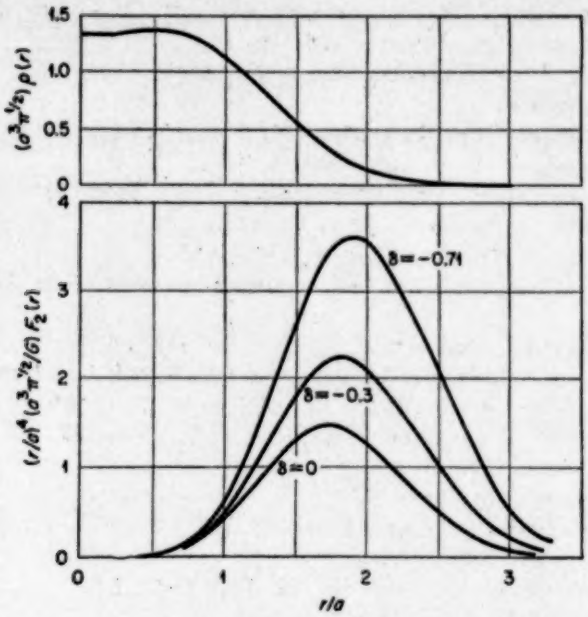

Fig. 3. Radial distribution of the matrix element for small-angle inelastic scattering from C^{13}, when plane waves are used. Above is shown for comparison the density distribution $\rho(r)$ of C^{13} for $\delta = 0$.

The surface effect is illustrated by rewriting the form factor for zero-ranges forces in terms of the nuclear density $\rho = \sum_{\nu\omega}|\phi_{\omega\nu}|^2$, as

$$F_2(r_0) \propto \left\langle \int \rho(r_0, \Omega) Y_{20}(\Omega) \mathrm{d}\Omega \right\rangle_{\mathrm{spin}}.$$

If $\rho(\mathbf{r}_0)$ for a deformed system can be written

$$\begin{aligned} \rho(\mathbf{r}_0) &\approx \rho(r_0[1+\beta Y_{20}(\Omega)]), \\ &\approx \rho(r_0)+\beta r_0(\mathrm{d}\rho/\mathrm{d}r_0)Y_{20}(\Omega), \end{aligned}$$

it follows that $F_2 \propto r\mathrm{d}\rho/\mathrm{d}r$, which peaks at the nuclear surface. This should be a reasonable approximation for heavy nuclei, although poor for light nuclei.

A further point should be made concerning these form factors. Figs. 2 and 3 show that the collective effects not only enhance the magnitude but significantly change the shape of the form factor. This only occurs in the form factor for SI transitions, and thus we now have the possibility of needing different form factors for SI and SD transitions. This could lead to the ratio of SD to SI intensity varying with scattering angle, an effect hitherto neglected; unpublished calculations show that this variation is enhanced by the use of distorted waves[10]).

References

1) B. L. Cohen and A. G. Rubin, Phys. Rev. **111** (1958) 1568
2) W. T. Pinkston and G. R. Satchler, Proc. Int. Conf. Nuclear Structure, eds. D. A. Bromley and E. Vogt (University of Toronto Press, Toronto, 1961) p. 394
3) B. R. Mottelson, Proc. Int. Conf. Nuclear Structure, eds. D. A. Bromley and E. Vogt (University of Toronto Press, Toronto, 1961) p. 525
4) B. L. Cohen and R. E. Price, Phys Rev. **121** (1961) 1441;
   S. Yoshida, to be published
5) S. Hatano, Progr. Theoret. Phys. **24** (1960) 418;
   Glassgold, Heckrotte and Watson, Ann. Phys. **6** (1959) 1
6) Bloom, Glendenning and Moszkowski, Phys. Rev. Lett. **3** (1959) 98
7) E. Rost and N. Austern, Phys. Rev. **120** (1960) 1375
8) Kerman, McManus and Thaler, Ann Phys. **8** (1959) 551
9) J. M. Blatt and V. F. Weiskopf, Theoretical nuclear physics (John Wiley and Sons, New York, 1952)
10) Drisko, Bassel and Satchler, Bull. Am. Phys. Soc. **6** (1961) 56
11) M. K. Banerjee and C. A. Levinson, Ann. Phys. **2** (1958), 499 Ann Phys **3** (1958) 67
12) Clegg, Foley, Salmon and Segel, Bull. Am. Phys. Soc. **4** (1959) 444
13) E. K. Warburton and W. T. Pinkston, Phys. Rev. **118** (1960) 733
14) E. K. Warburton, Phys. Rev. Lett. **1** (1958) 68
15) G. Morpurgo, Phys. Rev. **110** (1958) 721
16) Brown, Castillejo and Evans, Nuclear Physics **22** (1961) 1
17) D. Kurath, Phys. Rev. **106** (1957) 975;
   J. P. Elliott and B. H. Flowers, Proc. Roy. Soc. **242** (1957) 57
18) D. Kurath, Nuclear Physics **14** (1960) 398
19) D. Kurath and L. Picman, Nuclear Physics **10** (1959) 313
20) S. G. Nilsson, Mat. Fys. Medd. Dan. Vid. Selsk. **29** no. 16 (1955)
21) M. G. Redlich, Phys. Rev. **110** (1959) 468;
   J. P. Elliott, Proc. Roy. Soc. **245** (1958) 128
22) N. K. Glendenning and J. A. Sawicki, Nuclear Physics **18** (1960) 596
23) A. Bohr and B. R. Mottelson, Mat. Fys. Medd. Dan. Vid. Selsk. **27** no. 16 (1953)
24) E. Rost and N. Austern, private communication

1.D.3:
2.B

Nuclear Physics **27** (1961) 284—293; © *North-Holland Publishing Co., Amsterdam*
Not to be reproduced by photoprint or microfilm without written permission from the publisher

THE γ-RADIATION OF THE Li^7 (p, γ) RESONANCE AT 441.3 keV

V. MEYER, H. MÜLLER, H. H. STAUB and R. ZURMÜHLE †

Institute of Physics, University of Zurich

Received 10 April 1961

Abstract: Measurements were made of the intensity ratio, the angular distribution and the $\alpha-\gamma$-angular correlation of the resonant γ-radiation of the reaction Li^7(p, γ)Be^8. The results, which are in fair agreement with recent values published elsewhere, permit the determination of the channel spin ratio and the three partial γ-ray widths of the 17.6 MeV M1 radiation and the M1 and E2 components of the 14.8 MeV transition. While the value for the 17.6 MeV component agrees well with calculations using the independent particle model, it is shown that the partial widths of the 14.8 MeV components disagree strongly with the predictions of such a model. It is proposed to explain this discrepancy by the strong collective motion required by the α-particle model for the first excited state of Be^8.

1. Introduction

The γ-radiation of the reaction Li^7(p, γ)Be^8 has been the subject of a large number of investigations [1, 2]). It is well known to consist of two components of energies 17.62 and 14.82 MeV at resonance in the centre-of-mass system. The question whether other γ-rays are present is not yet settled with certainty. Both components are also excited outside the resonance at 441.3 keV proton energy due to formation of broad, perhaps even non-resonant states or direct interaction [2, 3]). Their radiation interferes markedly with the radiation from the relatively sharp resonant level ($\Gamma = 12.5$ keV) and thereby complicates the assignment of spin and parity and the interpretation of the nature of the radiation. The character of the final levels of the two components is well established; they are α-unstable, even spin, even parity levels, 0^+ and 2^+ for the 17.6 and 14.8 MeV radiation, respectively [6]). The initial resonant state, which might have either even spin, odd parity or odd spin, even or odd parity, is known from elastic proton scattering [4, 5]) to be a 1^+ level. Higher lying γ-emitting levels [7]) are known at $E_p = 1.03$, ($\Gamma = 147$ keV), 2.21 ($\Gamma = 400$ keV) and 6.10 MeV ($\Gamma = 350$ keV), for which the assignments 1^+, 3^- $?^+$ have been tentatively made.

In the neighbourhood of the 441 keV resonance the higher interfering states manifest themselves in the occurrence of a pronounced term proportional to $\cos\theta$ in the angular distribution of the γ-rays [3]), indicating that the interfering level is of opposite, i.e. negative, parity to the resonant level 1^+. Close to

† Now at the University of Pennsylvania, Philadelphia

resonance the interference term vanishes because the phase of the resonant radiation passes through $\frac{1}{2}\pi$. At this energy the radiation consists mainly of transitions from the 1^+ (17.62 MeV) to the 0^+ and 2^+ levels and is almost isotropic.

The purpose of the present investigation was to determine the intensity ratio of the E2 to M1 radiation of the 14.82 MeV transition ($1^+ \rightarrow 2^+$) at the resonance value of 441 keV from the angular *correlation* between the γ and the α-particles from the subsequent decay of Be^8. This ratio is of considerable interest, since it can give rather detailed information on the nuclear wave functions of initial and final states. For a given model, it enables one to determine quantitative features of the nuclear forces, e.g. the spin-orbit interaction strength. Therefore it represents one of the most severe tests for the various models proposed for the Be^8 nucleus with ist rather unique features. The angular correlation function depends not only on this ratio but also slightly on the population of the initial 1^+ state which in turn determines the angular *distribution* function of the 17.6 and 14.8 MeV transition relative to the incoming proton. Therefore this angular distribution function had also to be determined with considerable accuracy.

2. Apparatus

For the *angular-correlation* measurements targets of 0.1 mg/cm^2 metallic Li^7 (less than 0.1 % Li^6) were evaporated on supporting aluminium foils of less than 0.05 μm thickness and irradiated with protons from a 2 MeV Van de Graaff operated at the appropriate energy to give maximum yield of γ-rays. The extremely thin and low-Z support kept the number of protons scattered into the α-detector at a tolerable level. The γ-rays were recorded by a 7 cm $\times$ 7 cm NaI(Tl) crystal, with its front face located at a distance of 8 cm from the target at right angle to the proton beam. It could be rotated freely about the beam axis. The pulses of the γ-detector were clipped to 0.04 μsec and fed to the α-γ-coincidence circuit and also through a single channel-analyzer which selected pulses of the proper size. These pulses were fed to the monitor and to one of the two gates of the α-pulse amplifiers. The second gate was operated by the α-γ coincidence pulses. In this manner any difference in absorption of the γ-rays in different positions of the γ-detector was compensated. Data were taken at correlation angles in the centre-of-mass system: $\phi = 90°$, 135° and 180°.

The α-detector was a CsI(Tl) disc of 2.2 cm diameter and 0.5 mm thickness at a distance of 3.5 cm from the target. The pulses were differentiated and had a rise time of 0.2 μ sec and a decay time of 0.6 μ sec. The energy resolution for α-particles of 1.5 MeV was 16 %. The α-detector was positioned at 90° to the proton beam in the centre-of-mass system. In the laboratory system this angle depends also on the correlation angle ϕ. But since the difference for the three

correlation angles is less than 0.5°, the α-detector was set at a fixed angle of 82.5° relative to the proton beam, corresponding to an angle of 90° in the centre-of-mass system for α-particles which originate from the center of the broad 2.8 MeV level. The α-pulses fed to the α-γ-coincidence circuit were further differentiated to 0.04 μ sec while the original pulse passed via the two gated amplifiers to the 100-channel pulse-analyzer. Fig. 1 shows a block diagram of the apparatus. The recording of the spectral distribution of the α-particles is necessary, since for the various correlation angles the α-particles receive different amounts of γ-recoil momentum. As the energy distribution of the α-particles is very broad ($\Gamma \approx 2$ MeV) the finite spectral region measured at the various correlation angles had to be adjusted to the same energy limits in the centre-of-mass system.

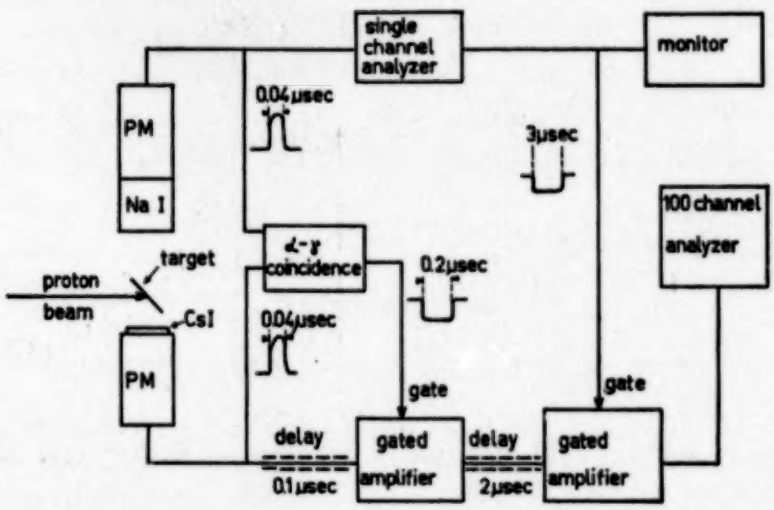

Fig. 1. Block diagram of experimental arrangement for α−γ-correlation measurement.

The *angular distribution* of the γ-rays was also measured with a 7 cm × 7 cm NaI(Tl) scintillator located at a distance of 20 cm from the target. The target consisted of a 20 keV layer of evaporated lithium converted to hydroxide on a thin copper backing. It was housed in a thin-walled aluminium target tube to avoid excessive scattering and angle dependent absorption. The horizontal magnetically analyzed H_2^+-beam from a 5.5 MeV Van de Graaff was collimated to a spot less than 2 mm in diameter. A lead collimator with an entrance channel of 10 mm diameter and 10 cm length was placed in front of the detector The back half of the collimator had an enlarged bore filled with paraffin to absorb electrons emitted by the wall of the front part. The detector assembly could be turned about a vertical axis through the target spot. Data were taken for symmetric angles with respect to the proton beam. A 7 cm × 7 cm NaI(Tl) crystal in a fixed position served as a monitor. The pulse-height distributions were measured by a 100 channel analyzer from maximum pulse size to about $\frac{1}{3}$ of it.

3. Measurements and Results

3.1. THE α—γ ANGULAR CORRELATION

The number of α-γ coincidences per γ-count versus energy E_α of the α-particle in the centre-of-mass system is shown in fig. 2 for the correlation angles $\phi = 90°$ and $\phi = 180°$. The data shown are transformed to the centre-of-mass system by the relation

$$E'_\alpha = E_\alpha + \frac{m_p}{4m_\alpha} E_0 \left(1 + \frac{Q_\gamma^2}{2m_p c^2 E_0}\right) - Q_\gamma \sqrt{\frac{E_\alpha}{2m_\alpha c^2}} \cos\phi,$$

where E'_α is the energy of the alpha particles measured in the laboratory system, E_0 is the proton resonance energy of 441 keV and Q_γ the energy release of the radiative transition preceding the α-decay. We have

$$2E_\alpha + Q_\gamma = 17.65 \text{ MeV}.$$

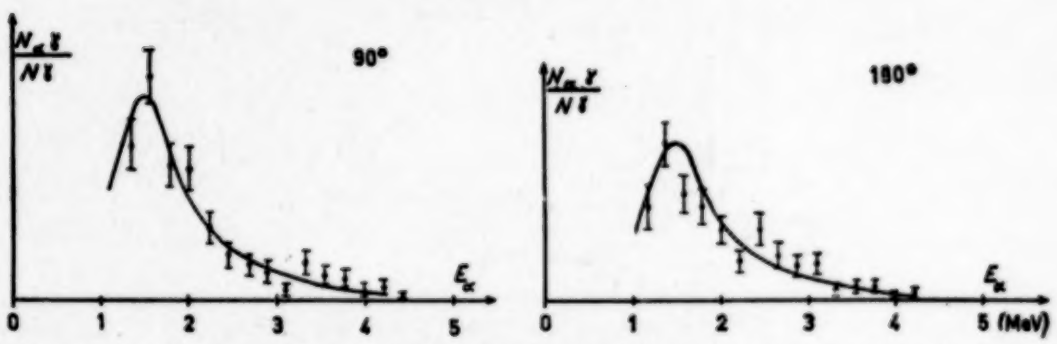

Fig. 2. α—γ-coincidences versus centre-of-mass energy of the α-particles for the correlation angles $\phi = 90°$ and $\phi = 180°$. The solid line is taken from ref. [8]) multiplied by an appropriate scale factor.

The very small Doppler effect and aberration of the γ-quantum are neglected. The spectrum of the α-particles from the decay of the 2.8 MeV state of Be^8 is known to follow very closely a Breit-Wigner single level relation [8]) modified by the effects of γ-transition probability and barrier penetrability. In applying this modification the radiation is assumed to be of pure dipole character, an assumption which is justified by the results of the present work. Fig. 2 shows that a fit could be made in a satisfactory manner with the data by Meyer and Staub [8]) yielding two curves whose only scale factor is the ratio of the angular correlation function as measured in the laboratory system. These ratios were converted to the centre-of-mass system by applying an energy dependent correction for the variation of the solid angle subtended by the counters in the centre-of-mass system. Another correction accounts for the finite solid angle which averages over a certain range of the correlation function. The final ratios of the centre-of mass correlation function are

$$\frac{W(90°)}{W(180°)} = 1.33 \pm 0.15, \quad \frac{W(90°)}{W(135°)} = 1.12 \pm 0.21.$$

3.2. ANGULAR DISTRIBUTION OF THE γ-RAYS

The angular distribution of the γ-rays had to be separated into its two components of 14.8 and 17.6 MeV. The pulse-height distribution is shown in fig. 3 for the angle $\vartheta = 0°$. In order to obtain the response of the γ-detector to

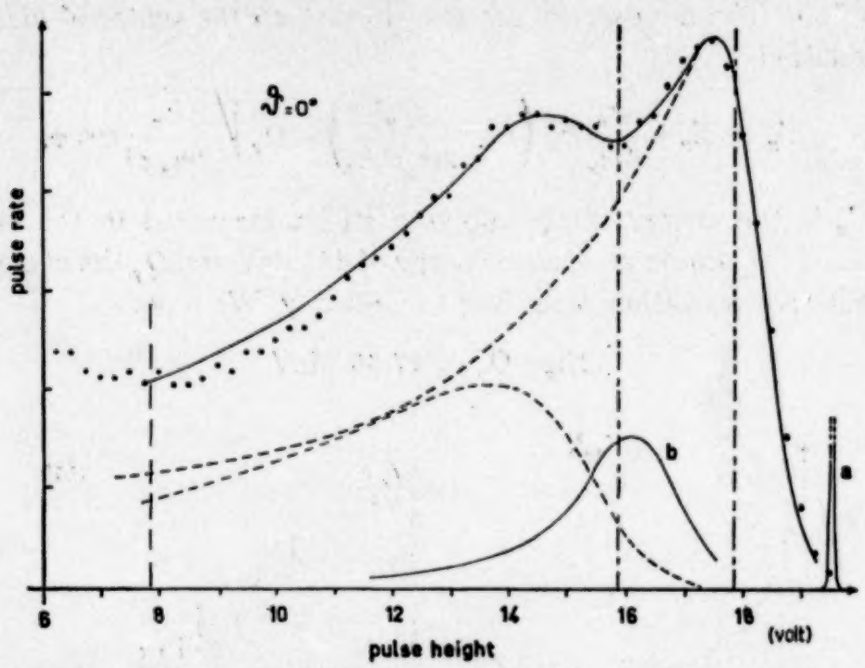

Fig. 3. Pulse-height distribution of the $Li^7(p, \gamma)$-reaction. The solid lines a and b represent the assumed γ-ray spectra for the 17.6 MeV and 14.8 MeV γ-ray, respectively, the dotted lines are the pulse-height distributions of these two lines (see text).

monochromatic γ-rays of approximately the same energy the pulse-height distribution of the 20.5 MeV γ-rays of the reaction $T(p, \gamma)He^4$ at 1.0 MeV proton energy at $\vartheta = 90°$ was measured and is shown in fig. 4. The tritium

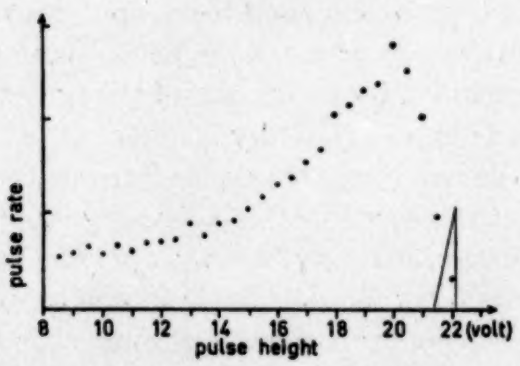

Fig. 4. Pulse-height distribution of the T(p, γ) reaction. The solid line shows the spectral distribution of the γ-rays.

reaction is non-resonant, the γ-ray yield rising approximately linearly with the proton energy. Consequently the γ-rays from a thick target are not strictly

monochromatic but show a narrow distribution as indicated in fig. 4. With the shape function of the distribution established in this way the decomposition of the Li γ-pulse distribution can be performed if the shape of the γ-spectrum is known. It was assumed that the 17.6 MeV line is sharp and that the 14.8 MeV line has an energy distribution which, as in the case of the α-particles, is a modified Breit-Wigner distribution as shown by the solid lines a and b in fig. 3. The pulse size distributions of the components are shown by dotted lines. The sum of the two components given by the solid line fits the observed points remarkably well. For the small pulse sizes the observed distribution is somewhat below the calculated curve, indicating that due to the lower energy of the Li γ-ray the escape of bremsstrahlung and electrons is somewhat smaller than in the case of the tritium γ-rays. A small correction for the dependence of counter efficiency on the γ-ray energy was applied. It amounted to a 3 % difference for quantum energies of 10 and 20 MeV, respectively. Finally the results had to be transformed to the centre-of-mass system. Measurements were taken at the angles 0°, 30°, 45°, 90°, 135°, and 150°. A least square computation yielded for pulses larger than 8 V, which consist of 71 % 17.6 MeV and 29 % 14.8 MeV γ-rays at $\vartheta = 0°$ (see fig. 5):

$$I_1(\theta) = 1+(0.001\pm0.008)\cos\theta+(0.043\pm0.016)\cos^2\theta,$$

and for pulses larger than 16 but smaller than 18 V (91 % 17.6 MeV γ-rays):

$$I_2(\theta) = 1-(0.001\pm0.011)\cos\theta+(0.063\pm0.024)\cos^2\theta.$$

From this we compute the angular distribution functions of the individual lines:

$$I_{17.6}(\theta) = 1+(0.067\pm0.025)\cos^2\theta = 1+a_2(17.6)\cos^2\theta, \quad (1)$$

$$I_{14.8}(\theta) = 1-(0.012\pm0.050)\cos^2\theta = 1+a_2(14.8)\cos^2\theta. \quad (2)$$

The interference terms, proportional to $\cos\theta$, are zero within the accuracy and since the contributions to the $\cos^2\theta$-term of any interfering levels must be extremely small at resonance, the results represent the true distribution of the 441 keV resonant γ-radiation only. The ratio of the intensities of the 17.6 to the 14.8 MeV line at $\theta = 0°$ is 2.1. With the measured angular distribution one obtains for the ratio of the total intensities

$$\frac{I_{17.6}}{I_{14.8}} = 2.0$$

in accordance with previously published results [9]).

4. Discussion

4.1. DETERMINATION OF PARAMETERS

The angular distribution of the two γ-rays at resonance where the interference term vanishes is given by

$$I(\theta) = 1+\frac{1-y}{1+y}\cos^2\theta \quad \text{for } E_\gamma = 17.6 \text{ MeV, transition } 1^+ \to 0^+, \text{ pure M1,} \quad (3)$$

$$I(\theta) = 1+\frac{(1-y)(0.3+1.5c^2-9c/\sqrt{5})}{3.9+2.1y+(3.5+2.5y)c^2+(1-y)3c/\sqrt{5}}\cos^2\theta$$

$$\text{for } E_\gamma = 14.8 \text{ MeV, transition } 1^+ \to 2^+, \text{ mixed M1 and E2,} \quad (4)$$

where y is the ratio of the population of the $m = 0$ substate to that of the $m = \pm 1$ substates of the initial $I = 1^+$ level in a system with the proton momentum as z-axis, and c, a real (positive or negative) number, is the amplitude ratio of E2 to M1 radiation. Let r be the probability ratio of forming the initial state with channel spin $s = 2$ to that with $s = 1$. Then y and r are related by

$$p_2/p_1 \equiv r = 5y/(4-3y).$$

From the anisotropy of the 17.6 MeV γ-ray one obtains from eqs. (1) and (3)

$$y = 0.88\pm 0.04, \text{ and } r = 3.2\pm 0.5. \quad (5)$$

In principle the ratio c could now be determined from eqs. (2) and (4). However the accuracy would be quite poor. On the other hand the α-γ correlation function for the mixed E2-M1-transition is given by

$$\begin{aligned} W(\phi) &= 1+c^2-2c/\sqrt{5}+\cos^2\phi[\tfrac{3}{5}(3y'-4)+(y'-4)c^2+6cy'/\sqrt{5}] \\ &\quad +\cos^4\phi[\tfrac{9}{5}(1-y')+(5-y')c^2+6c(1-y')/\sqrt{5}], \\ &= 1+c^2-2c/\sqrt{5}+\frac{\cos^2\phi}{5+7r}[6(1-r)-2(5+11r)c^2+12c(5+3r)/\sqrt{5}] \\ &\quad +\frac{\cos^4\phi}{5+7r}[\tfrac{9}{5}(r-5)+(15+29r)c^2+6c(r-5)/\sqrt{5}], \end{aligned}$$

where y' is the ratio of the initial state population with the z-axis in the direction of the γ-ray. The ratio y' is related to y and r by

$$y' = 2/(2+y) = (10+6r)/(5+7r).$$

The rather accurately measured ratio W (90°)/W (180°) is independent of r and furnishes a quadratic equation for c with the two roots

$$c_1 = 0.133\pm 0.027, \qquad c_2 = -2.0\pm 0.2.$$

The rough measurement of $W(90°)/W(135°)$ furnishes the two values

$$c_1 = 0.14 \pm 0.15, \qquad c_2 = 3.2 \pm 0.3.$$

This clearly establishes c_1 as the value of c. With this value of c and the value of r from eq. (5), the anisotropy factor a_2 (14.8) can be computed with better accuracy than given in eq. (2). In agreement with this direct experimental value one finds

$$a_2(14.8) = -0.004 \pm 0.008,$$

which signifies isotropy, in contrast to the 17.6 MeV radiation for which we have measured (eq. (1))

$$a_2(17.6) = 0.067 \pm 0.025.$$

The correlation function is

$$W(\phi) = 1 - (0.18 \pm 0.06)\cos^2\phi - (0.07 \pm 0.06)\cos^4\phi.$$

Independent of the value of r we now find for the intensity ratio of the two components of the 14.8 MeV radiation

$$\frac{\text{E2}}{\text{M1}} \equiv c^2 = 0.018 \pm 0.009.$$

The total centre-of-mass γ-ray width of the initial state is known to be

$$\Gamma_\gamma = \Gamma_{17.6} + \Gamma_{14.8} = 25 \text{ eV or}$$
$$\Gamma_{17.6} = 16.7 \text{ eV}, \Gamma_{14.8} = 8.3 \text{ eV}.$$

The widths of the M1 and E2 components are

$$\Gamma_{\text{M1}} = 8.15 \pm 0.07 \text{ eV}, \qquad \Gamma_{\text{E2}} = 0.15 \pm 0.07 \text{ eV}.$$

Previous measurements of Neuert and Retz-Schmidt [10]) gave the following values for the coefficients a_2 of the angular distribution at resonance:

$$a_2(17.6) = +0.028 \pm 0.003,$$
$$a_2(14.8) = +0.043 \pm 0.020.$$

This indicates a much smaller anisotropy for the 17.6 MeV component and a larger one for the 14.8 MeV transition. However, from eq. (4), their value of a_2 (14.8) would yield a negative value of c in strong disagreement with the present result.

4.2. COMPARISON WITH THEORY

The present measurements permit a fairly detailed comparison with the calculations of transition strengths in Be^8 by Kurath [11]) and with the work of

French and Fujii [12]). Kurath uses a usual central two body interaction mixture with a variable spin orbit parameter a/K for computing the independent particle wave function. From the total γ-ray width of 25 eV of the 1^+ initial state a reasonable value of $a/K = 3$ is obtained by Kurath. French and Fujii using a somewhat different central force mixture computed for values of $a/K = 0, 1, 2$, channel spin ratios r of 5, 100, 14 respectively, from where we extrapolate for our measured value of 3.2 to $a/K \approx 3$. Kurath has also calculated the radiative transition probabilities for Be^8 for intermediate coupling with various values of a/K. With $a/K = 3$ he finds for the transitions:

$$1^+ \rightarrow 0^+, \text{M1}; \quad \Gamma_{\text{M1}}(17.6) = 18.8 \text{ eV},$$
$$1^+ \rightarrow 2^+, \text{M1}; \quad \Gamma_{\text{M1}}(14.8) = 3.5 \text{ eV},$$
$$1^+ \rightarrow 2^+, \text{E2}; \quad \Gamma_{\text{E2}}(14.8) = 2.1 \text{ eV}.$$

The width of the ground-state transition is in excellent agreement with the observed value. For the transition to the excited state, however, the calculated value for the M1 component is less than $\frac{1}{2}$ and the E2 contribution 15 times larger than the observed values. The ratio of the total intensity of the 17.6 MeV to that of the 14.8 MeV transition for $a/K = 3$ is, according to Kurath's calculation, equal to 3.4 and therefore already $1\frac{1}{2}$ times larger than the observed value of 2.

It seems significant that a shell model calculation can give agreement for the ground state transition but fails by an order of magnitude in explaining the extremely small E2 contribution in the 14.8 MeV transition and underestimates the strength of the M1 component. The explanation seems to lie in the fact that while the initial $(J^\pi, T) = (1^+, 1)$ state can very well be described by the intermediate coupling shell model, it would be rather surprising if the model were adequate for the description of the low lying states of Be^8 which represent almost pure rotational states of a two α-particle system as evidenced for instance by their level energies 0, 2.9 and 11.4 MeV for the $(0^+, 0)$; $(2^+, 0)$; $(4^+, 0)$ states, and whose behaviour is therefore predominantly governed by a strong collective motion of the α-clusters. The strong collective motion however is missing in the case of the ground state $(0^+, 0)$ and consequently the radiative width of the ground state transition is very well explained by the shell model.

Just after completion of the present work the results of two investigations bearing on this problem were published. Mainsbridge [3]) measured the angular distribution of the separated 17.6 and 14.8 MeV transitions for proton bombarding energies between 0.2 and 1.1 MeV. His results show clearly that near the 441 keV resonance the interference term a_1 disappears for both components. This indicates that interference in the neighbourhood of the 441 keV resonance is due to radiation from a level with opposite parity. This radiation could for instance be E1. The value of the coefficient a_2 of both

components is very small but the accuracy of the data of Mainsbridge certainly does not exclude the values of the present work $a_2\ (17.6) = 0.067 \pm 0.025$ and $a_2(14.8) = -0.004 \pm 0.008$.

Grant [13]) measured the α—γ-angular correlation function for the transition to the excited state 2^+. Having assumed a channel spin ratio $r = 5$, he deduces from his results an amplitude ratio $E2/M1 \equiv c = 0.21 \pm 0.07$ in agreement with the present result. The correlation function of the present work is also consistent with his data.

Grant compares his results with various calculations using different central interaction mixtures and spin-orbit coupling parameters a/K. However, none of them explains the measured radiation widths of the three transitions with one and the same value of a/K satisfactorily. In particular the exchange mixture used recently by Soper requires for the measured values of Γ that

$$17.6 \text{ MeV } M1 \text{ transition: } a/K = 1.2,$$

$$14.8 \text{ MeV } M1 \text{ transition: } a/K = 2.9,$$

$$14.8 \text{ MeV } E2 \text{ transition: } a/K = 0.5.$$

Finally the value $a_2 = +0.067$ of the 17.6 MeV radiation would lead to $a/K = 7$. This in turn shows clearly the impossibility of explaining the radiation width of the 14.8 MeV component by any of the mixtures currently used with the independent particle model.

The authors wish to thank Dr. Kurath for kindly commenting on the results. We gratefully acknowledge the financial support from the Atomic Science Commission of the Swiss National Science Foundation.

References

1) T. W. Bonner and J. E. Evans, Phys. Rev. **73** (1948) 666;
R. L. Walker and B. D. McDaniel, Phys. Rev. **74** (1948) 315;
S. Devons and M. G. N. Hine, Proc. Roy. Soc. **199** (1949) 56;
S. Devons and G. R. Lindsey, Proc. Phys. Soc. **63** (1950) 1202;
M. B. Stearns and B. D. McDaniel, Phys. Rev. **82** (1951) 450;
S. Devons and G. Goldring, Proc. Phys. Soc. **67** (1954) 413
2) A. A. Kraus, Phys. Rev. **93** (1954) 1308
3) B. Mainsbridge, Nuclear Physics **21** (1960) 1
4) W. D. Warters, W. A. Fowler and C. C. Lauritsen, Phys. Rev. **91** (1953) 917
5) D. A. Liberman and R. F. Christy, Phys. Rev. **92** (1953) 1085
6) A. J. F. Boyle, Nuclear Physics **1** (1956) 581
7) F. Ajzenberg-Selove and T. Lauritsen, preprint (1960)
8) V. Meyer and H. H. Staub, Helv. Phys. Acta **31** (1958) 205
9) F. Ajzenberg-Selove and T. Lauritsen, Nuclear Physics **11** (1959) 1
10) H. Neuert and T. R. Retz-Schmidt, Z. f. Natur. **13** (1958) 829
11) D. Kurath, Phys. Rev. **106** (1957) 975
12) J. B. French and A. Fujii, Phys. Rev. **105** (1957) 652
13) I. S. Grant, Proc. Phys. Soc. **76** (1960) 737

1.C

Nuclear Physics **27** (1961) 294—322; © *North-Holland Publishing Co., Amsterdam*

Not to be reproduced by photoprint or microfilm without written permission from the publisher

FORMULATION DE LA MÉCANIQUE STATISTIQUE EN TERMES DE NOMBRES D'OCCUPATION (II)

ROGER BALIAN, CLAUDE BLOCH et CYRANO DE DOMINICIS

Centre d'Études Nucléaires de Saclay, Gif-sur-Yvette (S. et O.), France

Reçu le 4 avril 1961

Abstract: A physical interpretation of the generalized free energy $\hat{F}$, introduced in part I of this work in connection with the variational principle, is obtained by relating it to the statistical distribution of the occupation numbers. The values of the occupation numbers derived from the variational principle are then interpreted as the most probable values in a grand canonical ensemble of identical systems. As a particular consequence of the theory, it is shown that in the case of an infinite system without Bose condensation, the probability distribution of any occupation number has the same form as in the absence of interactions. The classical limit of the theory is then considered. First, the great similarity of our results with the classical expansions expressed in terms of the local density is exhibited by rederiving the well known classical expressions with the methods of part I. Finally the classical limit of the Gibbs potential is shown to be identical, term by term, with the classical virial expansion.

Introduction

Dans la première partie de ce travail[1]), nous avons établi un formalisme dans lequel les fonctions apparaissant en mécanique statistique s'expriment comme des développements en puissances de l'interaction qui font intervenir, à la place des facteurs statistiques f_m^-, les nombres d'occupation $\bar{n}_m$ des états de particule indépendante. Nous avons été ainsi amenés à introduire une fonction $\hat{F}\{\mathscr{F}^-; \beta\}$ dont le minimum, pour des variations des variables $\mathscr{F}_m^-$ telles que $\sum_m \mathscr{F}_m^- = \bar{N}$, est l'énergie libre $F(\bar{N}, \beta)$; les valeurs des variables $\mathscr{F}_m^-$ correspondant à ce minimum sont les nombres d'occupation moyens $\bar{n}_m$.

Ces propriétés variationnelles, établies au § 4 sur le développement de $\hat{F}$ en puissances de l'interaction, présentent des analogies remarquables avec les résultats de la thermodynamique. Afin de comprendre pourquoi l'énergie libre d'un système à l'équilibre thermodynamique est le minimum de $\hat{F}$, nous chercherons une interprétation de cette fonction $\hat{F}\{\mathscr{F}^-; \beta\}$ pour des valeurs quelconques des variables $\mathscr{F}^-$. C'est l'objet du paragraphe 5, où nous montrons comment la fonction $\hat{F}$ est liée à la statistique des nombres d'occupation n_m des états de particule indépendante.

Nous commençons par étudier (§ 5.1) la fonction caractéristique de cette répartition statistique. Le logarithme de cette fonction caractéristique est une fonction $\mathscr{A}$, des variables ν_m associées à chaque état m, qui peut être considérée comme une généralisation du potentiel de Gibbs (§ 5.1.1). On peut donc

établir des développements de $\mathscr{A}$ en puissances de l'interaction analogues à ceux du potentiel de Gibbs (§ 5.1.2.). On aboutit ainsi, par la même méthode qu'aux § 2 et 3, à une formulation de $\mathscr{A}$ en termes de facteurs statistiques modifiés $\mathscr{F}_m^-$ (dépendant maintenant des variables ν_m). Cette expression a la même forme que celle établie au § 3 pour le potentiel de Gibbs, mais les facteurs $\mathscr{F}_m^-$ qui y figurent peuvent maintenant prendre des valeurs arbitraires, puisque chacun d'eux est la dérivée partielle de $-\beta\mathscr{A}$ par rapport à la variable ν_m.

Au § 5.2, on montre que la fonction $\hat{F}\{\mathscr{F}^-; \beta\}$ précédemment introduite résulte, pour des valeurs arbitraires des variables $\mathscr{F}_m^-$, de l'élimination des variables ν_m entre $\mathscr{A}$ et ses dérivées partielles, de la même façon que l'énergie libre $F(\bar{N}, \beta)$ résulte de l'élimination de α entre le potentiel de Gibbs A et la dérivée $\bar{N}$ de $-\beta A$ par rapport à α. Cette interprétation donnée à la fonction $\hat{F}$ explique qu'elle contienne, au même titre que la fonction caractéristique, toute l'information sur la statistique des nombres d'occupation. On retrouve ainsi directement les divers résultats du § 4.3 et de l'appendice C.

L'application des résultats précédents au cas d'un système de volume infini (§ 5.3) conduit à quelques résultats remarquables. On retrouve en effet, qu'à la limite d'un volume infini, les corrélations entre les nombres d'occupation de deux états de particule indépendante disparaissent. Mais de plus, la loi de probabilité pour le nombre d'occupation d'un état donné est une loi exponentielle, comme pour un système de particules sans interaction. Ces résultats sont en défaut pour un système de bosons lorsqu'il y a condensation de Bose-Einstein.

Au § 5.4, nous donnerons une interprétation directe de la fonction $\hat{F}\{\mathscr{F}^-; \beta\}$. On peut en effet donner un sens physique à l'élimination des variables ν_m entre le logarithme $-\beta\mathscr{A}$ de la fonction caractéristique et ses dérivées, de même qu'en thermodynamique à l'élimination de α ou β. Dans le cas d'un système fini (§ 5.4.2), $\hat{F}\{\mathscr{F}^-; \beta\}$ se rattache alors directement à la densité de probabilité pour les variables aléatoires $\mathscr{F}_m^-$ dont chacune est définie comme la moyenne sur un ensemble de Gibbs de systèmes identiques du nombre d'occupation de l'état m. Dans le cas d'un système infini (§ 5.4.3), cet te moyenne peut être remplacée par la moyenne sur les états infiniment voisins, qui joue le même rôle.

Le paragraphe 6 est consacré à l'étude de la limite classique. Nous avons déjà souligné l'analogie entre le remplacement des facteurs statistiques f_m^- par les vrais nombres d'occupation et l'établissement du développement du viriel [2, 3]), pour lequel on remplace la densité du système non perturbé par la densité vraie du système, en mécanique statistique classique.

Pour montrer clairement cette analogie, nous rappelons au § 6.1 comment on peut établir le développement du viriel par la méthode de sommation partielle de diagrammes exposée au § 3. Pour plus de généralité, nous raisonnons ici sur un système inhomogène [3]). On retrouve ici encore un principe variationnel comme conséquence de la structure des diagrammes.

Nous montrons ensuite (§ 6.2) dans le cas d'un système homogène de quelle manière le développement du potentiel de Gibbs en termes de nombres d'occupation tend, diagramme par diagramme, vers le développement du viriel à la limite classique, et comment on retrouve le développement classique du potentiel chimique en puissances de la densité. Une simplification importante se produit pour cette limite, les nombres d'occupation $\bar{n}_m$ devenant alors proportionnels au facteur de Maxwell-Boltzmann, et les fonctionnelles de $\bar{n}_m$ se réduisant à de simples fonctions de la densité. D'autre part, un certain nombre de diagrammes qui ne se réduisent pas à des constellations à la limite classique ont cependant une limite non nulle. On montre (appendice F) que les contributions de ces diagrammes se compensent exactement à un ordre donné de la théorie des perturbations.

5. Répartition Statistique des Nombres d'Occupation †

5.1. LA FONCTION CARACTÉRISTIQUE DE LA LOI DE PROBABILITÉ DES NOMBRES D'OCCUPATION

5.1.1. *Définitions*

Nous allons étudier la répartition statistique des nombres d'occupation n_m dans le système grand canonique à l'équilibre thermodynamique, pour α et β fixés. Comme les opérateurs $n_m = a_m^\dagger a_m$ commutent entre eux, on peut définir sans difficulté une loi de probabilité pour les nombres d'occupation n_m. Sa fonction caractéristique est donnée par

$$\Phi\{\nu; \alpha, \beta\} = \frac{\mathrm{Tr}[e^{\alpha N - \beta H} e^{\sum_m \nu_m a_m^\dagger a_m}]}{\mathrm{Tr}\, e^{\alpha N - \beta H}}, \tag{70}$$

où $\{\nu\}$ désigne l'ensemble des variables ν_m, conjuguées des n_m. Posons

$$\mathscr{A}\{\nu; \alpha, \beta\} = -\frac{1}{\beta} \log \mathrm{Tr}[e^{\alpha N - \beta H} e^{\sum_m \nu_m a_m^\dagger a_m}]. \tag{71}$$

Le potentiel de Gibbs est alors

$$A(\alpha, \beta) = \mathscr{A}\{0; \alpha, \beta\}. \tag{72}$$

La fonction $\mathscr{A}\{\nu; \alpha, \beta\}$ est reliée à la fonction caractéristique Φ par

$$\mathscr{A}\{\nu; \alpha, \beta\} - A(\alpha, \beta) = -\frac{1}{\beta} \log \Phi\{\nu; \alpha, \beta\}. \tag{73}$$

Les moments de la loi de probabilité des n_m se déduisent donc des dérivées de $\mathscr{A}\{\nu; \alpha, \beta\}$ par rapport aux variables ν_m, prises au point où toutes ces

† La numérotation des paragraphes et de équations fait suite à celle de la première partie.

variables $\{\nu\}$ sont nulles. En particulier, pour les deux premiers moments, on a

$$\bar{n}_m = -\beta \frac{\partial \mathscr{A}\{0; \alpha, \beta\}}{\partial \nu_m}, \tag{74}$$

$$\mathscr{C}_{lm} = -\beta \frac{\partial^2 \mathscr{A}\{0; \alpha, \beta\}}{\partial \nu_l \partial \nu_m}. \tag{75}$$

On remarquera enfin que, grâce à la commutativité de N avec H et avec $a_m^\dagger a_m$, $\mathscr{A}\{\nu; \alpha, \beta\}$ ne dépend en fait que des variables $\alpha+\nu_m$ et β.

5.1.2. *Extension à $\mathscr{A}\{\nu; \alpha, \beta\}$ des développements du potentiel de Gibbs*

Le développement de $\mathscr{A}$ en puissances de l'interaction s'établit comme celui du potentiel de Gibbs dans la référence [4]): après avoir développé $e^{\beta H_0} e^{-\beta H}$ dans

$$\mathscr{A} = -\frac{1}{\beta} \log \mathrm{Tr} \left[\prod_m (e^{(\alpha+\nu_m-\beta\varepsilon_m)a_m^\dagger a_m})(e^{\beta H_0} e^{-\beta H})\right],$$

on applique le théorème de Wick généralisé, puis la formule exponentielle, ce qui conduit aux mêmes diagrammes vide-vide connexes que dans l'expression (4) du potentiel de Gibbs A. La seule différence est la valeur des contractions: les règles de calcul de la contribution à $\mathscr{A}$ de chaque diagramme *ne diffèrent de celles énoncées au paragraphe* 2.1. *que par le remplacement de* $\alpha-\beta\varepsilon_m$ *par* $\alpha+\nu_m-\beta\varepsilon_m$ *dans les expressions* (7) *des facteurs statistiques* $f_m^\pm$.

Les raisonnements des paragraphes 2 et 3 (sauf ceux qui concernent le propagateur) s'appliquent à ce développement. Il suffit simplement de remplacer $\alpha-\beta\varepsilon_m$ par $\alpha+\nu_m-\beta\varepsilon_m$ dans tous les facteurs $f_m^\pm$ et leurs dérivées. L'expression (29) (30) des facteurs statistiques modifiés $\mathscr{F}_m^\pm$ (qui sont maintenant des fonctions des ν_m) devient

$$\mathscr{F}_m^+ = 1+\epsilon\mathscr{F}_m^- = \frac{1}{1-\epsilon e^{\alpha+\nu_m-\beta\varepsilon_m-\beta w_m}}, \tag{76}$$

$$w_m = \frac{\partial \mathscr{D}\{\mathscr{F}^-; \beta\}}{\partial \mathscr{F}_m^-}. \tag{77}$$

La fonction $\mathscr{A}\{\nu; \alpha, \beta\}$ est donnée par la même formule (42) que A, soit

$$\mathscr{A} = -\frac{\epsilon}{\beta} \sum_m \log \mathscr{F}_m^+ - \sum_m w_m \mathscr{F}_m^- + \mathscr{D}\{\mathscr{F}^-; \beta\},$$

dans laquelle les $\mathscr{F}_m^\pm$ et w_m sont maintenant solutions des équations (76), (77). Il est remarquable que *la fonction $\mathscr{D}\{\mathscr{F}^-; \beta\}$ qui s'introduit ici est la même que précédemment, mais maintenant les valeurs des $\mathscr{F}_m^-$ qui y figurent peuvent être quelconques* (dans le champ $(0, +\infty)$ pour des bosons, $(0, 1)$ pour des fermions), puisque les valeurs des variables ν_m sont arbitraires.

La formulation variationnelle de ces résultats s'exprime à l'aide de la fonction

$$\hat{\mathscr{A}}\{\mathscr{F}^-; \nu; \alpha, \beta\} = \frac{1}{\beta}\sum_m \mathscr{F}_m^- \log \mathscr{F}_m^- - \frac{\epsilon}{\beta}\sum_m \mathscr{F}_m^+ \log \mathscr{F}_m^+ - \frac{\alpha}{\beta}\sum_m \mathscr{F}_m^- - \sum_m \frac{\nu_m}{\beta}\mathscr{F}_m^- + \sum_m \varepsilon_m \mathscr{F}_m^- + \mathscr{D}\{\mathscr{F}^-; \beta\}, \tag{78}$$

dont la valeur stationnaire (par rapport aux variations des $\mathscr{F}_m^-$, les autres variables étant fixées) est $\mathscr{A}\{\nu; \alpha, \beta\}$. La condition de stationnarité

$$\frac{\partial \hat{\mathscr{A}}\{\mathscr{F}^-; \nu; \alpha, \beta\}}{\partial \mathscr{F}_m^-} = 0 \tag{79}$$

équivaut aux relations (76) (77) entre les $\mathscr{F}_m^-$ et les ν_m. Cette condition (79) entraîne que

$$\frac{\partial \mathscr{A}\{\nu; \alpha, \beta\}}{\partial \nu_m} = \frac{\partial \hat{\mathscr{A}}\{\mathscr{F}^-; \nu; \alpha, \beta\}}{\partial \nu_m} = -\frac{\mathscr{F}_m^-}{\beta},$$

c'est-à-dire

$$\mathscr{F}_m^- = -\beta \frac{\partial \mathscr{A}\{\nu; \alpha, \beta\}}{\partial \nu_m}. \tag{80}$$

Cette nouvelle forme des relations (76) et (77) entre les $\mathscr{F}_m^-$ et les ν généralise l'équation (74) donnant les nombres d'occupation moyens et montre que les facteurs statistiques modifiés $\mathscr{F}_m^-$ se déduisent de $\mathscr{A}$ par dérivation partielle.

5.1.3. *Condensation de Bose-Einstein*

Pour des bosons, $\mathscr{A}\{\nu; \alpha, \beta\}$ n'est pas défini pour toutes les valeurs de α ou des ν_m. Afin que les variables $\mathscr{F}_m^-$ (que nous interpréterons plus loin comme des nombres d'occupation, même pour $\nu_m \neq 0$) soient positives, il faut en effet que, pour toutes les valeurs de m,

$$\alpha + \nu_m < \beta(\varepsilon_m + w_m),$$

où w_m et $\mathscr{F}_m^-$ sont donnés par (76), (77). Le champ de variation des variables α et ν_m est donc borné supérieurement, et la borne supérieure correspond à une condensation de Bose-Einstein, puisque certaines des variables $\mathscr{F}_m^-$ deviennent alors infinies.

5.2. L'ÉNERGIE LIBRE GÉNÉRALISÉE $\hat{F}\{\mathscr{F}^-; \beta\}$

Les résultats du paragraphe précédent montrent que *la fonction* $\hat{F}\{\mathscr{F}^-; \beta\}$, *définie par l'équation* (55) *qui s'écrit*

$$\hat{F}\{\mathscr{F}^-; \beta\} = \frac{1}{\beta}\sum_m \mathscr{F}_m^- \log \mathscr{F}_m^- - \frac{\epsilon}{\beta}\sum_m \mathscr{F}_m^+ \log \mathscr{F}_m^+ + \sum_m \varepsilon_m \mathscr{F}_m^- + \mathscr{D}\{\mathscr{F}^-; \beta\}$$

résulte simplement, pour des valeurs quelconques des variables $\mathscr{F}_m^-$, de l'élimination des variables ν_m entre $\mathscr{A}$ et ses dérivées partielles, c'est-à-dire entre les équations (71), (80) *et*

$$\hat{F}\{\mathscr{F}^-;\beta\} = \mathscr{A}\{\nu;\alpha,\beta\} + \frac{\alpha}{\beta}\sum_m \mathscr{F}_m^- + \sum_m \frac{\nu_m}{\beta}\mathscr{F}_m^-. \tag{81}$$

Le fait que $\mathscr{A}$ ne dépende que des variables $\alpha+\nu_m$ entraîne que α est éliminé du même coup. La méthode décrite dans la première partie permet donc d'effectuer *explicitement* l'élimination des ν_m, et conduit au développement (55) de $\hat{F}$ en puissances de l'interaction.

La fonction $\hat{F}$ apparaît ainsi comme une généralisation de l'énergie libre $F(\bar{N},\beta)$. Celle-ci résulte en effet de l'élimination de α entre l'équation (3) de définition de A, l'équation (53) donnant $\bar{N}$ comme dérivée partielle de $-\beta A$ par rapport à α, et l'équation (54) de définition de F.

Cette interprétation mathématique de $\hat{F}\{\mathscr{F}^-;\beta\}$ permet de retrouver aisément les résultats, établis au paragraphe 4 et dans l'appendice C à l'aide du développement (55). Des équations (71), (80) et (81), on tire d'abord, comme en thermodynamique pour les potentiels A (α,β) et $F(\bar{N},\beta)$,

$$\frac{\partial\hat{F}\{\mathscr{F}^-;\beta\}}{\partial\mathscr{F}_m^-} = \frac{\alpha}{\beta} + \frac{\nu_m}{\beta}, \tag{82}$$

et

$$\frac{\partial[\beta\hat{F}\{\mathscr{F}^-;\beta\}]}{\partial\beta} = \frac{\partial[\beta\mathscr{A}\{\nu;\alpha,\beta\}]}{\partial\beta}. \tag{83}$$

L'équation (82) donne une nouvelle forme, équivalente à (76), (77) ou à (80), de la relation entre les $\mathscr{F}_m^-$ et les ν_m.

La comparaison entre les équations équivalentes (80) et (82) montre que les matrices dont les éléments sont $-\beta\partial^2\mathscr{A}\{\nu;\alpha,\beta\}/\partial\nu_l\partial\nu_m$ et $\beta\partial^2\hat{F}\{\mathscr{F}^-;\beta\}/\partial\mathscr{F}_l^-\partial\mathscr{F}_m^-$ sont inverses l'une de l'autre. Comme

$$-\beta\frac{\partial^2\mathscr{A}\{\nu;\alpha,\beta\}}{\partial\nu_l\partial\nu_m} = \mathrm{Tr}\,[\rho(a_l^\dagger a_l)(a_m^\dagger a_m)] - \mathrm{Tr}\,[\rho(a_l^\dagger a_l)]\,\mathrm{Tr}\,[\rho(a_m^\dagger a_m)],$$

où

$$\rho = \frac{e^{\frac{1}{2}\sum_m \nu_m a_m^\dagger a_m} e^{\alpha N-\beta H} e^{\frac{1}{2}\sum_m \nu_m a_m^\dagger a_m}}{\mathrm{Tr}\, e^{\alpha N-\beta H} e^{\sum_m \nu_m a_m^\dagger a_m}}$$

est un opérateur hermitique, défini positif et de trace unité, $-\beta\partial^2\mathscr{A}/\partial\nu_l\partial\nu_m$ et par suite $\beta\partial^2\hat{F}/\partial\mathscr{F}_l^-\partial\mathscr{F}_m^-$ sont des matrices définies positives, pour toutes les valeurs possibles des ν_m ou des $\mathscr{F}_m^-$. *La fonction $-\hat{F}\{\mathscr{F}^-;\beta\}$ est donc une fonction convexe des variables $\mathscr{F}_m^-$.*

L'interprétation de $\hat{F}\{\mathscr{F}^-;\beta\}$ montre que cette fonction décrit, au même

titre que $\mathscr{A}\{\nu; \alpha, \beta\}$ les propriétés thermodynamiques du système à l'équilibre, et en particulier la loi de probabilité des nombres d'occupation n_m. En effet, l'expression (80) de $\mathscr{F}_m^-$ se réduit au nombre d'occupation moyen $\bar{n}_m$ donné par (74) lorsque toutes les variables ν_m sont nulles. *La condition* $\nu_m = 0$ *(quel que soit* m*) équivaut donc à* $\mathscr{F}_m^- = \bar{n}_m$. Par suite, *écrire que la dérivée* $\partial \hat{F}\{\mathscr{F}^-; \beta\}/\partial \mathscr{F}_m^-$ *(donnée par* (82)*) est indépendante de* m *entraîne que les* $\mathscr{F}_m^-$ *sont égaux aux nombres d'occupation moyens* $\bar{n}_m$, et la valeur de cette dérivée est le potentiel chimique α/β du système. On retrouve ainsi la condition de stationnarité (61) de $\hat{F}$.

Les grandeurs thermodynamiques et les moments de la loi de probabilité des n_m sont directement reliés aux dérivées de $\mathscr{A}$ prises pour $\nu_m = 0$, donc aux dérivées de $\hat{F}$ prises pour $\mathscr{F}_m^- = \bar{n}_m$. En particulier, la relation (81) se réduit pour $\nu_m = 0$ à l'équation (54) et par suite $\hat{F}\{\bar{n}; \beta\}$ *est l'énergie libre* $F(\sum_m \bar{n}_m, \beta)$; l'équation (83) se réduit pour $\mathscr{F}_m^- = \bar{n}_m$ à l'expression (62) de *l'énergie moyenne*; la *fonction de corrélation* (75) est la matrice inverse de la matrice $\beta \partial^2 \hat{F}\{\bar{n}; \beta\}/\partial \mathscr{F}_l^- \partial \mathscr{F}_m^-$.

Enfin la propriété de convexité de $-\hat{F}$ entraîne que *l'énergie libre est le minimum absolu de* $\hat{F}\{\mathscr{F}^-; \beta\}$ pour des variations quelconques des $\mathscr{F}_m^-$ satisfaisant à la restriction (57).

5.3. APPLICATION AU CAS D'UN VOLUME INFINI

Si on s'intéresse à la *répartition statistique non plus de tous les nombres d'occupation* n_m, *mais seulement d'un nombre fini d'entre eux*, la fonction caractéristique est donnée par (70) et (73), où toutes les variables ν_m sont nulles, sauf celles qui correspondent aux états auxquels on s'intéresse. On doit donc étudier la variation de l'expression (42) en fonction de ces variables ν_m en nombre fini. Si dans l'expression (77) ou (30) des w_m, on modifie d'une quantité finie un nombre fini de variables $\mathscr{F}_m^-$, les variations correspondantes des w_m sont infiniment petites comme $1/\Omega$. Par suite, lorsqu'on calcule par la formule (42) $\mathscr{A}\{\nu; \alpha, \beta\}$ d'une part et $A(\alpha, \beta)$ d'autre part, les facteurs statistiques relatifs à un même état différent d'une quantité infiniment petite en $1/\Omega$, sauf ceux relatifs aux états étudiés, qui diffèrent d'une quantité finie, et sont donnés par (76) et (29) respectivement. En se limitant aux termes indépendants de Ω, on trouve alors pour la fonction caractéristique

$$-\frac{1}{\beta}\log \Phi\{\nu; \alpha, \beta\} = \mathscr{A}\{\nu; \alpha, \beta\} - A(\alpha, \beta)$$

$$\xrightarrow[\Omega \to \infty]{} -\frac{\epsilon}{\beta}\sum_m{}' \log \frac{1-\epsilon e^{\alpha-\beta\epsilon_m-\beta w_m}}{1-\epsilon e^{\alpha+\nu_m-\beta\epsilon_m-\beta w_m}}, \qquad (84)$$

où la sommation porte sur le nombre (fini) d'états étudiés.

Il résulte de la forme de (84) qu' *à la limite* $\Omega \to \infty$, *les variables* n_m *deviennent*

indépendantes. Il en est d'ailleurs de même si le nombre de variables n_m étudiées est infini, mais petit par rapport au nombre de particules du système.

On tire également de (84) que *la loi de probabilité pour le nombre d'occupation n_m d'un état m*

$$P(n_m) \underset{\Omega \to \infty}{\propto} e^{[\alpha - \beta(\varepsilon_m + w_m)]n_m}$$

est de la même forme que s'il n'y a pas d'interaction, la seule modification étant le remplacement de ε_m par $\varepsilon_m + w_m$. Ce résultat, évident pour des fermions quel que soit le volume puisque n_m ne peut prendre que les valeurs 0 ou 1, devient vrai pour des bosons à la limite $\Omega \to \infty$.

Il est important de noter que le raisonnement précédent suppose *toutes les variables $\mathcal{F}_m^-$ finies lorsque $\Omega \to \infty$*. Les résultats ci-dessus sont donc en défaut pour un système de bosons lorsque certains nombres d'occupation sont infinis, en particulier lorsqu'il y a condensation de Bose-Einstein ou lorsqu'on s'intéresse à la probabilité pour qu'un nombre d'occupation devienne très grand.

5.4. INTERPRÉTATION PHYSIQUE DE $\hat{F}\{\mathcal{F}^-; \beta\}$

5.4.1. *Introduction*

Les diverses propriétés de la fonction $\hat{F}$ nous incitent à essayer de la rattacher à une densité de probabilité. Mais il ne peut s'agir de la densité de probabilité pour la répartition statistique des nombres d'occupation n_m, qui se déduit de $\Phi\{\nu; \alpha, \beta\}$ par une transformation de Laplace par rapport aux ν_m. En effet, alors que les $\mathcal{F}_m^-$ peuvent varier continuement dans $\hat{F}\{\mathcal{F}^-; \beta\}$ (de 0 à $+\infty$ pour des bosons, de 0 à 1 pour des fermions), les n_m ne peuvent prendre que des valeurs discrètes (0, 1, 2, ...$+\infty$ pour des bosons, 0 ou 1 pour des fermions) et leur loi de probabilité est totalement discontinue.

La situation est la même que lorsqu'on cherche à rattacher l'entropie $S(\bar{E}, \bar{N})$ d'un système à l'équilibre thermodynamique à sa densité de niveaux. Alors que la densité de niveaux se déduit du potentiel de Gibbs par une transformation de Laplace, l'entropie s'en déduit par élimination de α et β entre $A(\alpha, \beta)$ et ses dérivées premières. L'entropie peut se rattacher simplement à la densité de niveaux lorsque cette élimination équivaut au calcul de l'intégrale de Laplace (par la méthode du col), ce qui a lieu dans deux cas asymptotiques: d'une part pour un système infini, d'autre part pour un système fini (avec des niveaux d'énergie discrets) en introduisant non pas la densité de niveaux du système, mais celle d'un ensemble de Gibbs de systèmes identiques. Dans ces deux cas, nous allons de la même façon rattacher $\hat{F}\{\mathcal{F}^-; \beta\}$ à une densité de probabilité.

5.4.2. *Cas général: lien avec la statistique d'un ensemble de Gibbs*

Considérons un ensemble de Gibbs d'un nombre $\mathcal{N}$ (que nous ferons tendre vers l'infini) de systèmes identiques au système étudié. Ces systèmes peuvent

échanger des particules. Ils sont *faiblement couplés entre eux et avec un thermostat* de température $1/k\beta$. L'introduction de ce thermostat extérieur à l'ensemble de Gibbs est inhabituelle, mais elle simplifie l'interprétation de la fonction $\hat{F}$. Le nombre total de particules, fixé, est égal à $\mathcal{N}\bar{N}$, où $\bar{N}$ est le nombre moyen de particules par système. Soit $P_{\mathcal{N}}\{\mathcal{F}^-; \bar{N}, \beta\}$ la densité de probabilité des variables aléatoires définies par

$$\mathcal{F}_m^- = \frac{1}{\mathcal{N}} \sum_{k=1}^{\mathcal{N}} n_{m,k}, \tag{85}$$

où $n_{m,k}$ est le nombre d'occupation, dans le système k, de l'état m. Lorsque $\mathcal{N} \to \infty$, ces variables $\mathcal{F}_m^-$, dont chacune est la moyenne sur l'ensemble de Gibbs du nombre d'occupation de l'état m, ont le même champ de variation que celles qui interviennent dans la fonction $\hat{F}\{\mathcal{F}^-; \beta\}$.

Un calcul dont le détail est donné dans l'appendice D montre qu' *à la limite* $\mathcal{N} \to \infty$, *la densité de probabilité des variables* $\mathcal{F}_m^-$ *tend vers*

$$P_{\mathcal{N}}\{\mathcal{F}^-; \bar{N}, \beta\} \underset{\mathcal{N}\to\infty}{\propto} \delta\Big(\sum_m \mathcal{F}_m^- - \bar{N}\Big) e^{-\mathcal{N}\beta\hat{F}\{\mathcal{F}^-;\beta\}}, \tag{86}$$

pour un nombre total de particules

$$\mathcal{N} \sum_m \mathcal{F}_m^- = \mathcal{N}\bar{N}$$

fixé, et à la constante de normalisation près.

La forme de la loi de probabilité (86) entraîne alors immédiatement que *le nombre d'occupation moyen* $\bar{\mathcal{F}}_m^-$, *qui est aussi égal à* $\bar{n}_m$, *s'obtient en cherchant le maximum de la densité de probabilité, donc le minimum* $F(\bar{N}, \beta)$ *de* $\hat{F}\{\mathcal{F}^-; \beta\}$ *compte tenu de la restriction* $\sum_m \mathcal{F}_m^- = \bar{N}$. Les moments d'ordre supérieur des $\mathcal{F}_m^-$, qui tendent vers zéro quand $\mathcal{N} \to \infty$, se calculent à partir de (86) en fonction des dérivées successives de $\hat{F}\{\mathcal{F}^-; \beta\}$ pour $\mathcal{F}_m^- = \bar{n}_m$ par la méthode du col, et on peut en déduire les moments des n_m.

5.4.3. *Cas particulier d'un volume infini*

Dans le cas d'un système de volume infini, il est connu que l'introduction d'un ensemble de Gibbs est inutile. La moyenne (85) des nombres d'occupation n_m sur l'ensemble de Gibbs peut en effet être remplacée par une moyenne sur les nombres d'occupation des états ayant des impulsions infiniment voisines. La fonctionnelle $\hat{F}\{\mathcal{F}^-; \beta\}$ va donc s'interpréter directement en fonction de la loi de probabilité de ces nombres d'occupation moyens (qui sont d'ailleurs plus accessibles à l'expérience que les nombres d'occupation de chaque état individuel $\mathbf{m}$), à une température $1/k\beta$ donnée, et pour un nombre total de particules N fixé.

Divisons l'espace des impulsions en volumes élémentaires $d\mathbf{m}_i$ (centrés autour d'un ensemble de points $\mathbf{m}_i$), que nous ferons tendre vers 0 *après* avoir

fait tendre le volume Ω vers l'infini. Le nombre d'états compris dans le volume élémentaire $\mathrm{d}\mathbf{m}_i$ est $(\Omega/\hbar^3)\,\mathrm{d}\mathbf{m}_i$, et c'est ce nombre qui joue maintenant le rôle de $\mathcal{N}$. La variable aléatoire $\mathscr{F}^-_{\mathbf{m}_i}$ est la moyenne

$$\mathscr{F}^-_{\mathbf{m}_i} = \frac{1}{\frac{\Omega}{\hbar^3}\mathrm{d}\mathbf{m}_i} \sum_{\mathbf{m}'_i} n_{\mathbf{m}'_i}, \tag{87}$$

où la sommation est étendue à tous les états $\mathbf{m}'_i$ contenus dans le volume $\mathrm{d}\mathbf{m}_i$ de l'espace des impulsions. Comme précédemment, on montre (appendice E), après remplacement dans $\hat{F}\{\mathscr{F}^-;\beta\}$ de toutes les variables $\mathscr{F}^-_{\mathbf{m}_i}$ relatives aux états $\mathbf{m}'_i$ contenus dans chaque élément de volume $\mathrm{d}\mathbf{m}_i$ par la variable $\mathscr{F}^-_{m_i}$ relative au point $\mathbf{m}_i$, que *la loi de probabilité des variables* $\mathscr{F}^-_{\mathbf{m}_i}$ *tend vers*

$$P\{\mathscr{F}^-;N\,\beta\} \underset{\Omega\to\infty}{\propto} \delta\left(\frac{1}{\hbar^3}\int \mathrm{d}\mathbf{m}\,\mathscr{F}^-_{\mathbf{m}} - \frac{N}{\Omega}\right) \mathrm{e}^{-\beta\hat{F}\{\mathscr{F}^-;\beta\}} \tag{88}$$

lorsque le volume tend vers l'infini, à la constante de normalisation près, et pour une densité donnée

$$\frac{N}{\Omega} = \frac{1}{\hbar^3}\int \mathrm{d}\mathbf{m}\,\mathscr{F}^-_m.$$

6. La Limite Classique

6.1. RAPPEL DES DÉVELOPPEMENTS DE LA MÉCANIQUE STATISTIQUE CLASSIQUE EN FONCTION DE LA DENSITÉ LOCALE

Nous allons montrer, dans ce paragraphe, comment on peut retrouver par la méthode de sommation partielle du § 3 le développement du viriel en mécanique statistique classique [2]). Pour plus de généralité, nous traiterons le cas de particules de masse m interagissant deux à deux par le potentiel $v(\mathbf{r}_i-\mathbf{r}_j)$ et soumises à un champ extérieur $u(\mathbf{r}_i)$. La densité peut alors varier d'un point à l'autre, et nous rétablirons les développements en fonction de cette densité locale [3]).

Rappelons d'abord le développement en puissances de l'activité e^{α} du potentiel de Gibbs d'un système grand canonique classique

$$A = -\frac{1}{\beta}\log\sum_{N=0}^{\infty}\frac{\mathrm{e}^{\alpha N}}{\hbar^{3N}N!}\int \mathrm{d}\mathbf{r}_1\ldots\mathrm{d}\mathbf{r}_N\mathrm{d}\mathbf{p}_1\ldots\mathrm{d}\mathbf{p}_N\,\mathrm{e}^{-\beta\sum_{i=1}^{N}\left[\frac{\mathbf{p}_i}{2m}+u(\mathbf{r}_i)\right]-\beta\sum_{i>j}v(\mathbf{r}_i-\mathbf{r}_j)} \tag{89}$$

$$= -\frac{1}{\beta}\log\sum_{N=0}^{\infty}\frac{1}{N!}\int \mathrm{d}\mathbf{r}_1\ldots\mathrm{d}\mathbf{r}_N\prod_{i>j}(1+g_{ij})\prod_i f(\mathbf{r}_i) \tag{90}$$

$$= -\frac{1}{\beta}\left[\sum_{\nu=0}^{\infty}\frac{1}{\nu!}\int \mathrm{d}\mathbf{r}_1\ldots\mathrm{d}\mathbf{r}_\nu\prod_{i>j}(1+g_{ij})\prod_i f(\mathbf{r}_i)\right]_{\mathrm{c}}. \tag{91}$$

On a posé

$$g_{ij} = e^{-\beta v(\mathbf{r}_i - \mathbf{r}_j)} - 1, \tag{92}$$

$$f(\mathbf{r}_i) = e^{\alpha - 3 \log \lambda - \beta u(\mathbf{r}_i)}, \tag{93}$$

$$\frac{1}{\lambda} = \frac{1}{h}\sqrt{\frac{2\pi m}{\beta}}. \tag{94}$$

Dans (91) il ne faut garder que les termes correspondant à des diagrammes connexes (ce qui est rappelé par l'indice C) formés avec un nombre arbitraire ν de points. Pour éviter les difficultés de comptage, ces points sont considérés comme discernables. La contribution d'un diagramme se calcule en associant à chaque point (d'indice i tel que $1 \leqq i \leqq \nu$) le facteur $f(\mathbf{r}_i)$, et à chaque ligne (joignant les points i et j) le facteur g_{ij}, puis en intégrant indépendamment sur les positions $\mathbf{r}_i$ correspondant à chaque point, et enfin en divisant par $-\beta(\nu!)$.

Le facteur $f(\mathbf{r})$ s'interprète immédiatement comme la densité moyenne de particules au point $\mathbf{r}$ pour le système non perturbé. Considérant (89) comme une fonctionnelle du champ $u(\mathbf{r})$ (voir réf. [5]) et (91) comme une fonctionnelle de $f(\mathbf{r})$, la densité au point $\mathbf{r}$ pour le système perturbé est donnée par

$$\begin{aligned} \tilde{n}(\mathbf{r}) = \frac{\delta A}{\delta u(\mathbf{r})} &= -\beta \frac{\delta A}{\delta f(\mathbf{r})} f(\mathbf{r}) \\ &= \left[\sum_{\nu=0}^{\infty} \frac{1}{\nu!} \int d\mathbf{r}_1 \ldots d\mathbf{r}_\nu \Big[\sum_i \delta(\mathbf{r}_i - \mathbf{r})\Big] \prod_{i>j} (1 + g_{ij}) \prod_i f(\mathbf{r}_i)\right]_C . \end{aligned} \tag{95}$$

Elle est représentée par des diagrammes analogues à ceux de $-\beta A$, mais dont l'un des points est *distingué*. Au lieu d'intégrer sur les coordonnées de ce point, on les fixe à $\mathbf{r}$. Il est commode de ne pas considérer comme différents deux diagrammes déduits l'un de l'autre en changeant l'indice du point distingué. Le facteur $1/\nu!$ de (95) doit être alors remplacé par $1/(\nu-1)!$

Enfin la fonction de corrélation

$$\mathscr{C}(\mathbf{r}, \mathbf{r}') = -\frac{1}{\beta} \frac{\delta^2 A}{\delta u(\mathbf{r}) \delta u(\mathbf{r}')} = \tilde{n}(\mathbf{r}) \delta(\mathbf{r} - \mathbf{r}') - \beta \frac{\delta^2 A}{\delta f(\mathbf{r}) \delta f(\mathbf{r}')} f(\mathbf{r}) f(\mathbf{r}') \tag{96}$$

est représentée de même, pour $\mathbf{r} \neq \mathbf{r}'$, par des diagrammes à deux points distingués, fixés à $\mathbf{r}$ et $\mathbf{r}'$ respectivement. Si on n'affecte pas ces points d'indices, on doit remplacer $1/\nu!$ par $1/(\nu-2)!$

Appelons point d'articulation un point d'un diagramme tel que celui-ci cesse d'être connexe si on l'ôte, et constellation un diagramme connexe sans point d'articulation. Chaque diagramme contribuant à A, $\tilde{n}(\mathbf{r})$ ou $\mathscr{C}(\mathbf{r}, \mathbf{r}')$ est alors constitué de *constellations reliées en arbre par l'intermédiaire des points d'articulation*. On ne considérera pas le diagramme formé d'un seul point comme une constellation.

Etudions d'abord (comme au § 3.1.) l'effet de l'insertion d'un diagramme de ν_1 points, contribuant à $\tilde{n}(\mathbf{r}_i)$, en un point $\mathbf{r}_i$ (non distingué) d'un diagramme squelette dont ν_2 points possèdent des indices (le diagramme squelette ayant ν_2, ν_2+1 ou ν_2+2 points selon qu'il contribue à A, $\tilde{n}(\mathbf{r})$ ou $\mathscr{C}(\mathbf{r}, \mathbf{r}')$. On obtient $(\nu_1+\nu_2-1)\,!/\nu_2!\,(\nu_1-1)!$ diagrammes distincts, donnant la même contribution, en permutant de toutes les manières possibles les indices des points de l'insertion par rapport à ceux du squelette. L'insertion dans un diagramme squelette d'un diagramme contribuant à $\tilde{n}(\mathbf{r}_i)$ remplace donc, dans la contribution du squelette, $f(\mathbf{r}_i)$ par la contribution de l'insertion à $\tilde{n}(\mathbf{r}_i)$. Par suite, *effectuer toutes les insertions possibles en un point $\mathbf{r}_i$ d'un squelette remplace le facteur $f(\mathbf{r}_i)$ associé à ce point par $\mathscr{F}(\mathbf{r}_i) = \tilde{n}(\mathbf{r}_i)$.*

Considérons alors la *contribution à* (91) *des diagrammes formés d'une seule constellation* comme une fonctionnelle $\mathscr{D}\{f; \beta\}$ des facteurs $f(\mathbf{r}_i)$ associés à chaque point, et comme une fonction de β par l'intermédiaire des facteurs g_{ij}. La contribution à $\tilde{n}(\mathbf{r})$ des diagrammes n'ayant pas d'autre point d'articulation que $\mathbf{r}$ est

$$f(\mathbf{r})\left[1+\left(-\beta\frac{\delta\mathscr{D}\{f;\beta\}}{\delta f(\mathbf{r})}\right)+\frac{1}{2!}\left(-\beta\frac{\delta\mathscr{D}\{f;\beta\}}{\delta f(\mathbf{r})}\right)^2+\ldots\right]. \tag{97}$$

En effet, la dérivation fonctionnelle de $\mathscr{D}$ supprime, successivement pour chaque point $\mathbf{r}_i$, le facteur $f(\mathbf{r}_i)$ et fixe $\mathbf{r}_i$ en $\mathbf{r}$. La densité $\tilde{n}(\mathbf{r})$ s'obtient en effectuant, dans les diagrammes contribuant à (97), toutes les insertions possibles sur les points autres que $\mathbf{r}$, ce qui remplace (97) par

$$f(\mathbf{r})\left[1+\left(-\beta\frac{\delta\mathscr{D}\{\tilde{n};\beta\}}{\delta\mathscr{F}(\mathbf{r})}\right)+\frac{1}{2!}\left(-\beta\frac{\delta\mathscr{D}\{\tilde{n};\beta\}}{\delta\mathscr{F}(\mathbf{r})}\right)^2+\ldots\right].$$

La densité $\tilde{n}(\mathbf{r})$ est donc déterminée par les équations couplées (équations de l'ordre à grande distance)

$$\tilde{n}(\mathbf{r}) = \mathscr{F}(\mathbf{r}) = f(\mathbf{r})e^{-\beta w(\mathbf{r})} = e^{\alpha-3\log\lambda-\beta u(\mathbf{r})-\beta w(\mathbf{r})}, \tag{98}$$

$$w(\mathbf{r}) = \frac{\delta\mathscr{D}\{\mathscr{F};\beta\}}{\delta\mathscr{F}(\mathbf{r})}, \tag{99}$$

analogues à (29) (30), où $w(\mathbf{r})$ apparaît comme un potentiel self consistant.

La sommation des diagrammes vide-vide se fait (comme au § 3.3) à l'aide de la relation analogue à (37)

$$\mathscr{N}_P-\mathscr{N}_{PS}+\mathscr{N}_S=1, \tag{100}$$

caractéristique de la structure en arbre et valable pour tout diagramme à $\mathscr{N}_P$ points, $\mathscr{N}_S$ constellations; $\mathscr{N}_{PS}$ est le nombre de points des constellations, chacun étant compté avec un poids égal au nombre de constellations auquel il appartient ($\mathscr{N}_P$, $\mathscr{N}_{PS}$ et $\mathscr{N}_S$ jouent respectivement le même rôle que le nombre

de nœuds, de chaines incomplètes et de bulles composées au § 3.3). L'expression $\mathscr{D}\{\bar{n};\beta\}$ est représentée par les mêmes diagrammes que A, mais avec une constellation distinguée, de sorte que chaque diagramme contribue $\mathscr{N}_S$ fois plus à $\mathscr{D}\{\bar{n};\beta\}$ qu'à A. L'expression $-(1/\beta)\int d\mathbf{r}\bar{n}(\mathbf{r})$ est également représentée par les mêmes diagrammes, mais avec un point distingué; elle contribue donc $\mathscr{N}_P$ fois plus qu'à A. Enfin le terme de poids $\mathscr{N}_{PS}$ se calcule en effectuant des insertions à partir d'un point distingué d'une constellation distinguée, ce qui donne d'une part $w(\mathbf{r})$ pour cette constellation (et les insertions effectuées sur tous ses points autres que $\mathbf{r}$) et d'autre part $\bar{n}(\mathbf{r})$ pour l'ensemble des insertions au point $\mathbf{r}$, soit en définitive $\int d\mathbf{r} w(\mathbf{r})\bar{n}(\mathbf{r})$.

Le potentiel de Gibbs s'écrit donc

$$A = -\frac{1}{\beta}\int d\mathbf{r}\,\bar{n}(\mathbf{r}) - \int d\mathbf{r} w(\mathbf{r})\bar{n}(\mathbf{r}) + \mathscr{D}\{\bar{n};\beta\}, \tag{101}$$

soit, en posant

$$\hat{A}\{\mathscr{F};\alpha,\beta\} = \frac{1}{\beta}\int d\mathbf{r}\,\mathscr{F}(\mathbf{r})[\log \mathscr{F}(\mathbf{r}) - 1 + 3\log\lambda + \beta u(\mathbf{r}) - \alpha] + \mathscr{D}\{\mathscr{F};\beta\}, \tag{102}$$

$$A(\alpha,\beta) = \hat{A}\{\bar{n};\alpha,\beta\}, \tag{103}$$

où $\bar{n}(\mathbf{r})$ *est déterminé par la condition*

$$\frac{\delta\hat{A}\{\bar{n};\alpha,\beta\}}{\delta\mathscr{F}(\mathbf{r})} = 0. \tag{104}$$

Comme au § 4.2, *ce principe variationnel trouve son origine dans la structure en arbre des diagrammes.*

Comme dans l'appendice C, on peut effectuer la sommation partielle des diagrammes contribuant à $\mathscr{C}(\mathbf{r},\mathbf{r}')$, et obtenir un développement de cette quantité en puissances de $\bar{n}(\mathbf{r})$ (équation de l'ordre à petite distance). On voit alors que $\mathscr{C}(\mathbf{r},\mathbf{r}')$ est la matrice inverse de

$$\beta\frac{\delta^2\hat{A}\{\bar{n};\alpha,\beta\}}{\delta\mathscr{F}(\mathbf{r})\delta\mathscr{F}(\mathbf{r}')}.$$

L'énergie libre $F(\bar{N},\beta)$ est le minimum de

$$\hat{F}\{\mathscr{F};\beta\} = \frac{1}{\beta}\int d\mathbf{r}\,\mathscr{F}(\mathbf{r})[\log \mathscr{F}(\mathbf{r}) + \beta u(\mathbf{r}) + 3\log\lambda - 1] + \mathscr{D}\{\mathscr{F};\beta\}, \tag{105}$$

pour des variations de $\mathscr{F}(\mathbf{r})$ telles que

$$\int d\mathbf{r}\,\mathscr{F}(\mathbf{r}) = \bar{N}. \tag{106}$$

Le potentiel thermodynamique à champ externe $u(\mathbf{r})$ constant

$$F - \int \mathrm{d}\mathbf{r}\bar{n}(\mathbf{r})u(\mathbf{r})$$

s'exprime uniquement en fonction de la densité $\mathscr{F}(\mathbf{r}) = \bar{n}(\mathbf{r})$, $u(\mathbf{r})$ étant éliminé.

Enfin, de la même façon qu'au § 5, on peut donner de $\hat{F}$ une interprétation en fonction de la *répartition statistique des particules dans l'espace*: on fait jouer à $-\beta u(\mathbf{r})$ le rôle des variables v_m, et la fonctionnelle de $u(\mathbf{r})$ (voir ref. [5])) définie par (89) s'interprète comme le logarithme de la fonction caractéristique pour la répartition des particules dans l'espace. La densité de probabilité correspondante s'exprime alors, de même qu'au § 5.4.3., comme l'exponentielle de $-\beta\hat{F}$.

Dans le cas où $u(\mathbf{r}) = 0$, et en l'absence de phénomènes de condensation, les équations (98) (99) se réduisent à la *relation entre l'activité* e^{α} *et la densité* $\bar{n}$, qui est constante, et le développement (101) se réduit au *développement du viriel* [2]) lorsqu'on remplace w par son développement en puissances de la densité tiré de (99).

6.2. LA LIMITE CLASSIQUE

Dans l'établissement des développements quantiques en fonction des nombres d'occupation, nous nous sommes restreints à des systèmes pour lesquels l'impulsion est conservée par les interactions, c'est-à-dire à des systèmes invariants par translation. Nous établirons ici qu'à la limite classique, le développement (42) du potentiel de Gibbs tend terme à terme (ou plus exactement après regroupement des contributions de certains diagrammes) vers le développement du viriel (101) dans le cas d'un système homogène. Nous considérons un système de particules identiques en interaction dans un volume Ω tendant vers l'infini, et sans potentiel externe $u(\mathbf{r})$ de façon que l'impulsion soit conservée. Nous supposons pour simplifier l'écriture qu'elles n'ont pas de spin. Les éléments de matrice (6), non symétrisés ou antisymétrisés, s'écrivent

$$\langle \mathbf{pq}|v|\mathbf{mn}\rangle = \frac{1}{\Omega^2}\int \mathrm{d}\mathbf{r}\,\mathrm{d}\mathbf{r}' v(\mathbf{r}-\mathbf{r}')\,\mathrm{e}^{-i[\mathbf{p}\cdot\mathbf{r}+\mathbf{q}\cdot\mathbf{r}'-\mathbf{m}\cdot\mathbf{r}-\mathbf{n}\cdot\mathbf{r}']/\hbar}, \qquad (107)$$

où $\mathbf{m}, \mathbf{n}, \mathbf{p}, \mathbf{q}$ désignent les impulsions des états de particule indépendante, et il y a conservation de l'impulsion à la limite d'un volume Ω infini.

Les développements de la mécanique statistique classique s'expriment en fonction de la densité (constante) $\bar{n}(\mathbf{r}) = \bar{N}/\Omega$ dans l'espace des coordonnées et non de la densité dans l'espace des impulsions; nous devons donc, avant de passer à la limite classique, effectuer dans la formulation en termes des nombres d'occupation $\mathscr{F}_m^-$ une transformation de Fourier. Attribuons à chaque point d'un diagramme (fig. 15) contribuant à $\mathscr{D}$ ou à w, une coordonnée $\mathbf{r}$. La contribu-

tion de ce diagramme se calcule en associant à chaque interaction joignant par exemple des points $\mathbf{r}_2$ et $\mathbf{r}'_2$ (situés au même temps) le facteur $\frac{1}{2}v(\mathbf{r}_2-\mathbf{r}'_2)$ provenant de (107), à chaque ligne $\mathbf{m}_1$ allant du point $\mathbf{r}_1$ au point $\mathbf{r}_2$ (situés respectivement aux temps u_1 et u_2) le facteur

$$\frac{1}{\Omega} e^{\frac{i}{\hbar}\mathbf{m}_1\cdot(\mathbf{r}_2-\mathbf{r}_1)-\epsilon_{\mathbf{m}_1}(u_2-u_1)}, \tag{108}$$

à chaque chaîne $\mathbf{m}_i$ un facteur $\mathscr{F}^{\pm}_{\mathbf{m}_i}$, et enfin en sommant sur toutes les valeurs des $\mathbf{m}$ et en intégrant sur toutes les positions des $\mathbf{r}$ et sur tous les temps.

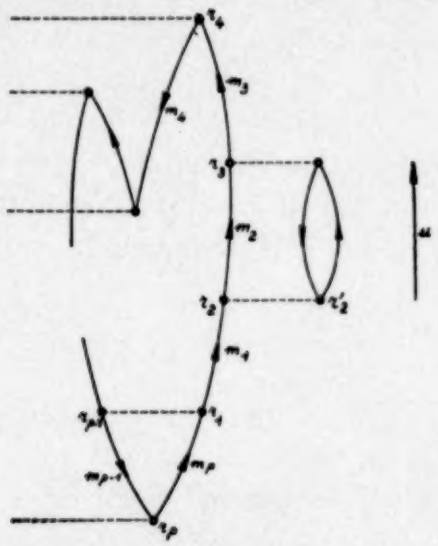

Fig. 15. Une partie d'un diagramme contribuant à $\mathscr{D}$ ou à w. On a tracé ici toutes les lignes en traits pleins, même lorsqu'elles font partie de chaînes, comme $\mathbf{m}_1$ et $\mathbf{m}_3$. A chaque point d'une boucle est associée une coordonnée $\mathbf{r}_1$, $\mathbf{r}_2$, ... et à chaque ligne une impulsion $\mathbf{m}_1$, $\mathbf{m}_2$, ...

6.2.1. *Calcul de la contribution d'une boucle*

Effectuons, à la limite classique, *la sommation sur les impulsions associées à toutes les lignes d'une boucle* (fig. 15). Soient $\mathbf{r}_1$, $\mathbf{r}_2$ ..., $\mathbf{r}_p$ les points de cette boucle, u_1, u_2, ..., u_p les instants correspondants (qui ne sont pas nécessairement tous différents, dans le cas où deux points de la boucle sont reliés par une interaction. Par exemple u_1 et u_{p-1} sur la figure 15 sont égaux), $\mathbf{m}_1$, $\mathbf{m}_2$, ..., $\mathbf{m}_p$ les impulsions correspondant aux lignes. Certaines des lignes de la boucle peuvent constituer des chaînes (par exemple $\mathbf{m}_1$, $\mathbf{m}_3$ sur la figure 15). Mais nous pouvons (tout en associant un seul facteur $\mathscr{F}^{\pm}_{m}$ par chaîne) sommer indépendamment sur toutes les valeurs de $\mathbf{m}_1$ et $\mathbf{m}_3$ sans tenir compte de la condition $\mathbf{m}_1 = \mathbf{m}_3$ imposée par la structure du diagramme. Plus généralement, nous pouvons sommer sur toutes les impulsions d'un diagramme de manière indépendante, sans avoir à tenir compte de la conservation de l'impulsion par chaque interaction. En effet, si l'on prend les éléments de matrice sous la forme

(107), cette condition de conservation apparaît automatiquement lors de l'intégration sur $\mathbf{r}$ et $\mathbf{r}'$ (pour un volume Ω infini). En définitive, en appelant $\varphi(\mathbf{m}_1, \mathbf{m}_2, \ldots \mathbf{m}_p)$ le produit des facteurs statistiques $\mathscr{F}^{\pm}_{\mathbf{m}}$ associés aux chaînes qui constituent la boucle (un par chaîne), nous avons à calculer l'expression

$$\frac{1}{\Omega^p} \sum_{\mathbf{m}_1 \mathbf{m}_2 \cdots \mathbf{m}_p} \varphi(\mathbf{m}_1, \mathbf{m}_2 \ldots \mathbf{m}_p) \, e^{-\epsilon_{\mathbf{m}_1}(u_2-u_1)-\epsilon_{\mathbf{m}_2}(u_3-u_2)\cdots-\epsilon_{\mathbf{m}_p}(u_1-u_p)} \, e^{i[\mathbf{m}_1\cdot(\mathbf{r}_2-\mathbf{r}_1)+\mathbf{m}_2\cdot(\mathbf{r}_3-\mathbf{r}_2)+\ldots\mathbf{m}_p\cdot(\mathbf{r}_1-\mathbf{r}_p)]/\hbar}. \quad (109)$$

Effectuons d'abord les sommations sur $\mathbf{m}_2, \ldots \mathbf{m}_p$ en laissant $\mathbf{m}_1$ fixé à la valeur $\mathbf{m}$. Le résultat nous sera utile pour le cas où la ligne $\mathbf{m}_1$ fait partie de la chaîne d'impulsion $\mathbf{m}$ fixée qui apparaît dans les diagrammes contribuant à $w_{\mathbf{m}}$. L'expression (109) devient à la limite $\Omega \to \infty$, et après changement de variables

$$\frac{1}{h^{3p-3}\Omega} \int d\mathbf{m}_2 \ldots d\mathbf{m}_p \varphi(\mathbf{m}, \mathbf{m}_2 \ldots \mathbf{m}_p) \, e^{-\epsilon_{\mathbf{m}}(u_2-u_1)-\epsilon_{\mathbf{m}_2}(u_3-u_2)\ldots\epsilon_{\mathbf{m}_p}(u_1-u_p)} \times e^{i[\mathbf{m}\cdot(\mathbf{r}_2-\mathbf{r}_1)+\mathbf{m}_2\cdot(\mathbf{r}_3-\mathbf{r}_2)+\ldots\mathbf{m}_p\cdot(\mathbf{r}_1-\mathbf{r}_p)]/\hbar}$$

$$= \frac{1}{(2\pi)^{3p-3}\Omega} \int d\mathbf{k}_2 \ldots d\mathbf{k}_p \varphi(\mathbf{m}, \mathbf{m}+\hbar\mathbf{k}_2, \ldots, \mathbf{m}+\hbar\mathbf{k}_p)$$

$$\times e^{-\epsilon_{\mathbf{m}}(u_2-u_1)-\epsilon_{\mathbf{m}+\hbar\mathbf{k}_2}(u_3-u_2)\cdots-\epsilon_{\mathbf{m}+\hbar\mathbf{k}_p}(u_1-u_p)} \, e^{-i[\mathbf{k}_2\cdot(\mathbf{r}_2-\mathbf{r}_3)+\ldots\mathbf{k}_p\cdot(\mathbf{r}_p-\mathbf{r}_1)]}$$

$$\underset{\hbar\to 0}{\approx} \frac{1}{\Omega} \int \varphi(\mathbf{m}, \mathbf{m}, \ldots \mathbf{m}) \delta(\mathbf{r}_2-\mathbf{r}_3)\delta(\mathbf{r}_3-\mathbf{r}_4)\ldots\delta(\mathbf{r}_p-\mathbf{r}_1). \quad (110)$$

On voit ainsi qu'à la limite classique, les impulsions de toutes les chaînes d'une boucle donnée deviennent égales. Il en résulte que la contribution d'un diagramme ne dépend plus des instants d'interaction, sur lesquels on peut donc intégrer immédiatement. D'autre part, tous les points $\mathbf{r}_1, \mathbf{r}_2, \ldots, \mathbf{r}_p$ d'une même boucle ont les mêmes coordonnées.

La limite classique de l'expression (109), correspondant à une boucle sans chaîne fixée, s'obtient en effectuant dans (110) la sommation sur $\mathbf{m}$, ce qui donne

$$\left[\frac{1}{h^3}\int d\mathbf{m}\varphi(\mathbf{m}, \mathbf{m}, \ldots \mathbf{m})\right] \delta(\mathbf{r}_2-\mathbf{r}_3)\delta(\mathbf{r}_3-\mathbf{r}_4)\ldots\delta(\mathbf{r}_p-\mathbf{r}_1). \quad (111)$$

6.2.2. *Comportement de $\mathscr{F}^-_m$, $\mathscr{D}$ et w_m*

La constante de Planck apparaît non seulement dans les facteurs exponentiels (108) et dans la sommation sur les impulsions $\mathbf{m}$ (puisque $\sum_{\mathbf{m}}$ tend pour $\Omega \to \infty$ vers $(\Omega/h^3)\int d\mathbf{m}$) mais aussi, *de façon implicite, dans les facteurs statistiques* $\mathscr{F}^+_{\mathbf{m}}$. En effet, on a

$$\bar{n} = \frac{\bar{N}}{\Omega} = \frac{1}{\Omega}\sum_{\mathbf{m}} \mathscr{F}^-_{\mathbf{m}} = \frac{1}{h^3}\int d\mathbf{m}\mathscr{F}^-_{\mathbf{m}},$$

d'où il résulte que les facteurs $\mathscr{F}_m^-$ tendent vers zéro comme h^3 lorsque $h \to 0$ à une densité fixée. Par suite α tend vers $-\infty$ comme $3 \log h$ (à condition que w_m reste fini, ce que nous vérifierons par la suite).

Les termes dominants à la limite classique s'obtiennent donc en remplaçant les facteurs $\mathscr{F}_{\mathbf{m}}^+$ par 1 et les facteurs $\mathscr{F}_{\mathbf{m}}^-$ par

$$h^3 e^{\alpha - 3 \log h - \beta \varepsilon_{\mathbf{m}} - \beta w_{\mathbf{m}}}, \tag{112}$$

pour des bosons comme pour des fermions, et on a

$$\bar{n} = \frac{\bar{N}}{\Omega} = \int d\mathbf{m}\, e^{\alpha - 3 \log h - \beta \varepsilon_{\mathbf{m}} - \beta w_{\mathbf{m}}}. \tag{113}$$

Les diagrammes dominants à la limite classique sont donc ceux pour lesquels le nombre de facteurs $\mathscr{F}_{\mathbf{m}}^-$, c'est-à-dire le nombre de chaînes descendantes complètes, est minimum. Ce sont donc *les diagrammes ayant une chaîne descendante par boucle*. Comme la fonction φ se réduit à un seul facteur (112) provenant de la chaîne descendante (toutes les chaînes montantes donnant 1), la contribution d'une boucle s'écrit

$$\left[\int d\mathbf{m}\, e^{\alpha - 3 \log h - \beta \varepsilon_{\mathbf{m}} - \beta w_{\mathbf{m}}}\right] \delta(\mathbf{r}_1 - \mathbf{r}_2)\delta(\mathbf{r}_2 - \mathbf{r}_3) \ldots \delta(\mathbf{r}_{p-1} - \mathbf{r}_p)$$
$$= \bar{n}\delta(\mathbf{r}_1 - \mathbf{r}_2)\delta(\mathbf{r}_2 - \mathbf{r}_3) \ldots \delta(\mathbf{r}_{p-1} - \mathbf{r}_p). \tag{114}$$

Il en résulte que *la fonctionnelle $\mathscr{D}$ tend à la limite classique vers une simple fonction $\mathscr{D}(\bar{n}, \beta)$ de $\bar{n}$ et de β.*

Dans le calcul de $w_{\mathbf{m}}$, et pour la boucle contenant l'impulsion fixée $\mathbf{m}$ (à laquelle on n'associe aucun facteur statistique), le terme dominant s'obtient lorsque la chaîne $\mathbf{m}$ est descendante, et lorsque toutes les autres lignes de la boucle sont montantes. A la limite classique, la fonction φ tend vers 1, et la contribution de cette boucle vers

$$\frac{1}{\Omega}\, \delta(\mathbf{r}_1 - \mathbf{r}_2)\delta(\mathbf{r}_2 - \mathbf{r}_3) \ldots \delta(\mathbf{r}_{p-1} - \mathbf{r}_p). \tag{115}$$

Les termes dominants dans l'expression (30) de $w_{\mathbf{m}}$ sont donc indépendants de $\mathbf{m}$, et $w_{\mathbf{m}}$ *tend vers une simple fonction w de $\bar{n}$ et de β.* On retrouve ainsi le fait que le nombre d'occupation $\mathscr{F}_{\mathbf{m}}^-$ dans l'espace des impulsions tend à la limite classique vers une quantité (112) ne dépendant de $\mathbf{m}$ que par l'intermédiaire du facteur de Maxwell-Boltzmann

$$e^{-\beta \varepsilon_{\mathbf{m}}} = e^{-\beta \frac{\mathbf{m}^2}{2m}}.$$

Le développement de w en diagrammes se déduit immédiatement de celui de $\mathscr{D}(\bar{n}, \beta)$ en remplaçant successivement la contribution (114) de chacune des

p boucles par (115), donc le facteur $\tilde{n}^p$ associé aux boucles par $(p/\Omega)\ \tilde{n}^{p-1}$. Par suite,

$$w = \frac{1}{\Omega}\frac{\partial \mathscr{D}(\tilde{n}, \beta)}{\partial \tilde{n}}. \tag{116}$$

La densité $\tilde{n}$ est liée à w par la relation (113), qui se réduit à

$$\tilde{n} = \int \mathrm{d}\mathbf{m}\, \mathrm{e}^{\alpha - 3\log\lambda - \beta\varepsilon_{\mathbf{m}} - \beta w} = \mathrm{e}^{\alpha - 3\log\lambda - \beta w}, \tag{117}$$

où λ est défini par la relation (94).

6.2.3. *Limite du potentiel de Gibbs*

Le premier terme du développement (42) de A devient alors à la limite classique

$$-\frac{\epsilon}{\beta}\frac{\Omega}{h^3}\int \mathrm{d}\mathbf{m}\log \mathscr{F}^+_{\mathbf{m}}$$

$$= -\frac{\epsilon}{\beta}\frac{\Omega}{h^3}\int \mathrm{d}\mathbf{m}\log\left(1+\epsilon h^3\,\mathrm{e}^{\alpha-3\log\lambda-\beta\varepsilon_{\mathbf{m}}-\beta w_{\mathbf{m}}}\right)$$

$$\underset{\lambda\to 0}{\approx} -\frac{\Omega}{\beta}\int \mathrm{d}\mathbf{m}\,\mathrm{e}^{\alpha-3\log\lambda-\beta\varepsilon_{\mathbf{m}}-\beta w} = -\frac{\Omega}{\beta}\tilde{n},$$

qui est, pour un système homogène, le premier terme de l'expression (101).

Comme w_m tend vers une constante, le second terme de (42) tend vers le second terme de (101) puisque

$$\frac{\Omega}{h^3}\int \mathrm{d}\mathbf{m}\mathscr{F}^-_{\mathbf{m}} w_m \underset{\lambda\to 0}{\approx} \Omega w\tilde{n}.$$

Il nous reste à vérifier que $\mathscr{D}(\tilde{n}, \beta)$ *peut s'exprimer au moyen des mêmes diagrammes que ceux qui s'introduisent en mécanique statistique classique.* Alors l'expression (42) du potentiel de Gibbs tendra vers l'expression (101), qui, pour un système homogène, se réduit au développement du viriel; l'équation (116) sera représentée en diagrammes de la même manière que (99), et l'équation (117) donnera le développement (98) de α en fonction de la densité $\tilde{n}$.

Jusqu'à présent $\mathscr{D}(\tilde{n}, \beta)$ est encore représenté par l'ensemble des diagrammes D comprenant une seule bulle composée, et tels qu'il n'y ait qu'une chaîne descendante par boucle, à laquelle on associe un facteur $\tilde{n}$ provenant de (114). A chaque boucle est associée une seule coordonnée. Il est donc naturel de réduire chacune des boucles de ces diagrammes à des points reliés les uns aux autres par les interactions. Mais, parmi les diagrammes ainsi obtenus, certains ne sont pas des constellations. Ainsi, les deux diagrammes de la figure 16 deviennent le diagramme de la figure 17, la boucle centrale se réduisant à un

point d'articulation. De manière générale, ce phénomène se produira pour *toute boucle telle que le diagramme se réduise à plus d'une partie connexe lorsqu'on ôte cette boucle* (fig. 18). En particulier, tous les diagrammes comprenant des chaînes sont de ce type (fig. 16a); ce ne sont cependant pas les seuls (fig. 16 b).

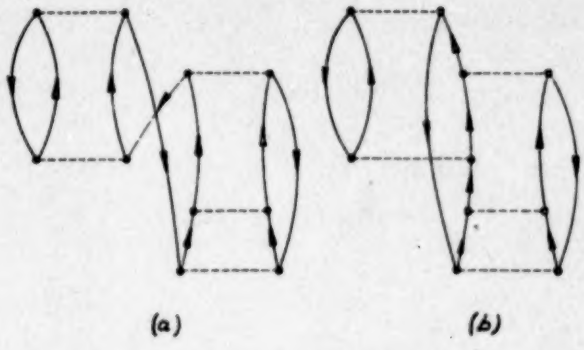

Fig. 16. Deux diagrammes contribuant à $\mathscr{D}$ à la limite classique.

Fig. 17. Le diagramme auquel se réduisent les diagrammes de la figure 16 lorsqu'on réduit leurs boucles à des points: la boucle centrale des diagrammes de la figure 16 devient un point d'articulation.

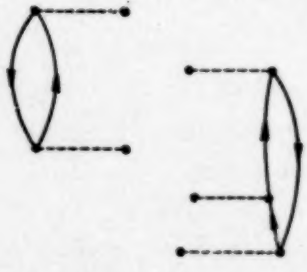

Fig. 18. Les parties connexes qui sont reliées par la boucle centrale des diagrammes de la figure 16.

Etant donnée une boucle reliant entre elles plusieurs parties connexes de diagramme, groupons les contributions de tous les diagrammes (tous distincts) que l'on peut former en reliant entre elles ces parties à l'aide d'une seule boucle; les lignes formant cette boucle devront être placées de manière à satisfaire aux règles de construction des diagrammes D; d'autre part, afin d'obtenir une limite classique non nulle, la boucle ne devra comporter qu'une chaîne descendante. Les diagrammes que nous considérons sont donc ceux pour lesquels l'ensemble des lignes descendantes de la boucle constitue une chaîne. Par exemple, la famille des diagrammes formés à partir des parties connexes de la figure 18 est représentée par la figure 16. Les contributions des diagrammes d'une telle famille ne diffèrent que par le signe, qui ne dépend, pour des fermions comme pour des bosons, que de la parité du nombre h de lignes descendantes de la

boucle considérée. Sur l'exemple de la figure 16, il y a un diagramme pour lequel $h = 2$, et un diagramme pour lequel $h = 1$, et leurs contributions se retranchent donc exactement. Nous montrons dans l'appendice F, dans le cas général, que *le nombre de diagrammes pour lesquels h est pair est égal au nombre de diagrammes pour lesquels h est impair, de sorte que la contribution totale de la famille considérée est nulle.*

Il ne reste donc plus dans $\mathscr{D}(\bar{n}, \beta)$ que les diagrammes qui deviennent des constellations lorsqu'on réduit chaque boucle à un point. Dans ces diagrammes, chaque boucle comprend une seule ligne descendante, constituant à elle seule une chaîne, de sorte que le signe (24) qui leur est associé est toujours positif, pour des bosons comme pour des fermions. A chaque interaction est associé un facteur $\frac{1}{2} v(\mathbf{r}_i - \mathbf{r}_j)$, mais plusieurs interactions peuvent relier deux boucles. Nous montrons dans l'appendice G, par comptage et sommation partielle, que la somme de tous les diagrammes D qui se réduisent à la même constellation redonne la contribution à $\mathscr{D}$ de cette constellation telle qu'est est calculée en mécanique statistique classique.

Appendice D

CALCUL DE LA DENSITÉ DE PROBABILITÉ $P_{\mathscr{N}}\{\mathscr{F}^-; \bar{N}, \beta\}$ POUR UN ENSEMBLE DE GIBBS

Introduisons pour chaque système de l'ensemble de Gibbs une base $|i\rangle$ d'états propres des opérateurs N et H, de valeurs propres N_i et E_i. Groupons ensuite les états de l'ensemble de Gibbs en classes $[\mathscr{N}_i]$, caractérisées par le nombre $\mathscr{N}_i$ de systèmes se trouvant dans l'état $|i\rangle$. Si l'ensemble de Gibbs est dans un de ces états purs, la fonction caractéristique de la loi de probabilité des variables $\mathscr{F}_m^-$ est

$$\prod_i (\langle i | e^{\frac{1}{\mathscr{N}} \sum_m \varphi_m a_m^\dagger a_m} | i \rangle)^{\mathscr{N}_i}, \tag{D.1}$$

où φ_m est la variable conjuguée de $\mathscr{F}_m^-$. La probabilité relative pour que l'ensemble de Gibbs soit dans chacune des classes $[\mathscr{N}_i]$ d'états purs est, à la température $1/k\beta$ et pour un nombre total de particules $\mathscr{N}\bar{N}$ fixé

$$\frac{\mathscr{N}!}{\prod_i (\mathscr{N}_i!)} e^{-\beta \sum_i \mathscr{N}_i E_i}, \tag{D.2}$$

où les $\mathscr{N}_i$ vérifient les conditions

$$\sum_i \mathscr{N}_i = \mathscr{N}, \tag{D.3}$$

$$\sum_i \mathscr{N}_i N_i = \mathscr{N}\bar{N}. \tag{D.4}$$

La fonction caractéristique $\Phi_{\mathcal{N}}\{\varphi; \bar{N}, \beta\}$ de la loi de probabilité des $\mathcal{F}_m^-$ se déduit donc de (D.1) et (D.2) par la relation

$$\Phi\{\varphi; \bar{N}, \beta\} = \frac{\sum_{[\mathcal{N}_i]} \frac{\mathcal{N}!}{\prod_i (\mathcal{N}_i!)} \prod_i (e^{-\beta E_i} \langle i | e^{\frac{1}{\mathcal{N}} \sum_m \varphi_m a_m^\dagger a_m} | i \rangle)^{\mathcal{N}_i}}{\sum_{[\mathcal{N}_i]} \frac{\mathcal{N}!}{\prod_i (\mathcal{N}_i!)} e^{-\beta \sum_i \mathcal{N}_i E_i}} \tag{D.5}$$

où les sommations sont étendues aux $\mathcal{N}_i$ satisfaisant aux conditions (D.3), (D.4). On s'affranchit de la condition (D.4) par une transformation de Laplace, ce qui permet d'effectuer la sommation sur les $\mathcal{N}_i$. On obtient

$$\Phi_{\mathcal{N}}\{\varphi; \bar{N}, \beta\} = \frac{\int_{\alpha_1 - i\pi}^{\alpha_1 + i\pi} d\alpha' \, e^{-\mathcal{N}[\beta \mathscr{A}\{\varphi/\mathcal{N}; \alpha', \beta\} + \alpha' \bar{N}]}}{\int_{\alpha - i\pi}^{\alpha + i\pi} d\alpha' \, e^{-\mathcal{N}[\beta A(\alpha', \beta) + \alpha' \bar{N}]}}, \tag{D.6}$$

où A et $\mathscr{A}$ sont définis par les équations (3) et (71), et où α et α_1 sont des abscisses arbitraires. Les ordonnées $\pm i\pi$ du champ d'intégration pour α' proviennent de la périodicité de A et $\mathscr{A}$ par rapport à α', et du fait que $\mathcal{N}\bar{N}$ est un entier.

La probabilité pour que les variables $\mathcal{F}_m^-$ prennent un ensemble donné de valeurs $\mathcal{F}_m^-$ (multiples entiers de $1/\mathcal{N}$) se déduit de $\Phi_{\mathcal{N}}\{\varphi; \bar{N}, \beta\}$ par la transformation de Laplace

$$\prod_m \left(\frac{1}{2\pi i \mathcal{N}} \int_{\varphi_m - i\pi\mathcal{N}}^{\varphi_m + i\pi\mathcal{N}} d\varphi'_m \, e^{-\varphi'_m \mathcal{F}_m^-} \right) \Phi_{\mathcal{N}}\{\varphi'; \bar{N}, \beta\}, \tag{D.7}$$

où le champ d'intégration est fini pour la même raison que ci-dessus.

Cette densité de probabilité $P_{\mathcal{N}}\{\mathcal{F}^-; \bar{N}, \beta\}$ des variables $\mathcal{F}_m^-$, qui pour $\mathcal{N}$ fini est une somme de fonctions δ, tend asymptotiquement vers une fonction continue, que l'on calcule à partir de (D.6) (D.7) par la méthode du col. On effectue pour cela les changements de variables $\varphi'_m/\mathcal{N} = \nu'_m - \alpha'$ et on utilise le fait que $\mathscr{A}\{\nu; \alpha, \beta\}$ ne dépend que des variables $\nu_m + \alpha$ et β. Alors, $P_{\mathcal{N}}\{\mathcal{F}^-; \bar{N}, \beta\}$ prend la forme du produit des facteurs suivants:

a) Le dénominateur provenant de (D.6), que l'on calcule par la méthode du col

$$\frac{1}{2\pi i} \int_{\alpha - i\pi}^{\alpha + i\pi} d\alpha' \, e^{-\mathcal{N}[\beta A(\alpha', \beta) + \alpha' \bar{N}]} \underset{\mathcal{N} \to \infty}{\approx} \frac{1}{\sqrt{2\pi \mathcal{N} D}} e^{-\mathcal{N}[\beta A(\alpha, \beta) + \alpha \bar{N}]}$$

$$= \frac{1}{\sqrt{2\pi \mathcal{N} D}} e^{-\mathcal{N} \beta F(\bar{N}, \beta)}, \tag{D.8a}$$

dans lequel α est déterminé par l'équation

$$-\beta \frac{\partial A(\alpha, \beta)}{\partial \alpha} = \bar{N}.$$

On a utilisé la définition (53) (54) de F, et posé

$$D = -\beta \frac{\partial^2 A(\alpha, \beta)}{\partial \alpha^2} = \frac{1}{\beta \dfrac{\partial^2 F(\bar{N}, \beta)}{\partial \bar{N}^2}} = \overline{(N - \bar{N})^2}. \tag{D.9}$$

b) Une intégrale sur les variables ν_m, que l'on calcule de la même façon

$$\prod_m \left(\int_{\nu_m - i\pi}^{\nu_m + i\pi} \frac{d\nu'_m}{2\pi i} \right) e^{-\mathcal{N}[\beta \mathcal{A}\{\nu'; 0, \beta\} + \sum_m \nu'_m \mathcal{F}_m^-]} \tag{D.8b}$$

$$\underset{\mathcal{N} \to \infty}{\approx} \frac{1}{\sqrt{\hat{D}}} e^{-\mathcal{N}[\beta \mathcal{A}\{\nu; 0, \beta\} + \sum_m \nu_m \mathcal{F}_m^-]} \prod_m \left(\frac{1}{\sqrt{2\pi \mathcal{N}}} \right) = \frac{1}{\sqrt{\hat{D}}} e^{-\mathcal{N} \beta \hat{F}\{\mathcal{F}^-; \beta\}} \prod_m \left(\frac{1}{\sqrt{2\pi \mathcal{N}}} \right),$$

dans lequel les ν_m sont déterminés par les équations

$$-\beta \frac{\partial \mathcal{A}\{\nu; 0, \beta\}}{\partial \nu_m} = \mathcal{F}_m^-.$$

On a utilisé la définition (80) (81) de $\hat{F}$, et posé

$$\hat{D} = \text{dét} \left(-\beta \frac{\partial^2 \mathcal{A}\{\nu; 0, \beta\}}{\partial \nu_l \partial \nu_m} \right) = \frac{1}{\text{dét} \left(\beta \dfrac{\partial^2 \hat{F}\{\mathcal{F}^-; \beta\}}{\partial \mathcal{F}_l^- \partial \mathcal{F}_m^-} \right)} = \text{dét } \mathcal{C}_{lm}. \tag{D.10}$$

c) Une intégrale portant sur la variable α et provenant du numérateur de (D.6), qui donne

$$\frac{1}{2\pi i} \int_{\alpha_1 - i\pi}^{\alpha_1 + i\pi} d\alpha' \, e^{\mathcal{N}[\sum_m \mathcal{F}_m^- - \bar{N}]\alpha'} = \delta_{\mathcal{N} \sum_m \mathcal{F}_m^-, \, \mathcal{N} \bar{N}}, \tag{D.8c}$$

ce qui impose que $\mathcal{N} \sum_m \mathcal{F}_m^-$ soit égal au nombre total de particules $\mathcal{N} \bar{N}$.

Rassemblant ces résultats et passant aux variables continues $\mathcal{F}_m^-$, on trouve donc la densité de probabilité

$$P_{\mathcal{N}}\{\mathcal{F}^-; \bar{N}, \beta\} \underset{\mathcal{N} \to \infty}{\propto} \delta\left(\sum_m \mathcal{F}_m^- - \bar{N} \right) e^{-\mathcal{N} \beta \hat{F}\{\mathcal{F}^-; \beta\}}, \tag{D.11}$$

avec comme constante de normalisation

$$\sqrt{\frac{2\pi D}{\mathcal{N}}} \frac{1}{\sqrt{\hat{D}}} e^{\mathcal{N} \beta F(\bar{N}, \beta)} \prod_m \left(\sqrt{\frac{\mathcal{N}}{2\pi}} \right). \tag{D.12}$$

Appendice E

CALCUL DE LA DENSITÉ DE PROBABILITÉ $P\{\mathscr{F}^-; N, \beta\}$ POUR UN SYSTÈME DE VOLUME INFINI

La fonction caractéristique de la loi de probabilité des variables $\mathscr{F}^-_{\mathbf{m}_i}$ est, après transformation de Laplace,

$$\Phi\{\varphi; N, \beta\} = \frac{\int_{\alpha_1 - i\pi}^{\alpha_1 + i\pi} \mathrm{d}\alpha' \, \mathrm{e}^{-\beta \mathscr{A}\{\nu; \alpha', \beta\} - \alpha' N}}{\int_{\alpha - i\pi}^{\alpha + i\pi} \mathrm{d}\alpha' \, \mathrm{e}^{-\beta A(\alpha', \beta) - \alpha' N}}, \tag{E.1}$$

où les variables $\nu_{\mathbf{m}}$ qui interviennent dans $\mathscr{A}\{\nu; \alpha, \beta\}$ sont égales à

$$\frac{\varphi_{\mathbf{m}_i}}{\frac{\Omega}{h^3} \mathrm{d}\mathbf{m}_i},$$

pour toutes les valeurs de $\mathbf{m}$ comprises dans le volume $\mathrm{d}\mathbf{m}_i$ entourant le point $\mathbf{m}_i$.

La densité de probabilité des variables $\mathscr{F}^-_{\mathbf{m}_i}$ est donc

$$P\{\mathscr{F}^-; N, \beta\} = \prod_{\mathbf{m}_i} \left(\frac{1}{2\pi i} \int_{\varphi_{\mathbf{m}_i} - i\pi \frac{\Omega}{h^3} \mathrm{d}\mathbf{m}_i}^{\varphi_{\mathbf{m}_i} + i\pi \frac{\Omega}{h^3} \mathrm{d}\mathbf{m}_i} \mathrm{d}\varphi'_{\mathbf{m}_i} \mathrm{e}^{-\varphi' \mathbf{m}_i \mathscr{F}^-_{\mathbf{m}_i}} \right) \Phi\{\varphi'; N, \beta\}. \tag{E.2}$$

Le calcul se poursuit comme dans l'appendice D. La méthode du col est maintenant justifiée par le fait que toutes les grandeurs apparaissant en exponentielle, A, $\mathscr{A}$, N, $(\Omega/h^3)\mathrm{d}\mathbf{m}_i$ sont proportionnelles à Ω lorsque $\Omega \to \infty$. Après passage à la limite $\mathrm{d}\mathbf{m}_i \to 0$, on trouve à la normalisation près

$$P\{\mathscr{F}^-; N, \beta\} \underset{\substack{\Omega \to \infty \\ \text{puis} \\ \mathrm{d}\mathbf{m}_i \to 0}}{\propto} \delta \left(\frac{1}{h^3} \int \mathrm{d}\mathbf{m} \mathscr{F}^-_{\mathbf{m}} - \frac{N}{\Omega} \right) \mathrm{e}^{-\beta \hat{F}\{\mathscr{F}^-; \beta\} + \beta F(N, \beta)}. \tag{E.3}$$

Appendice F

ÉLIMINATION DES DIAGRAMMES D NE SE RÉDUISANT PAS À DES CONSTELLATIONS À LA LIMITE CLASSIQUE

Considérons la famille des diagrammes D constitués de plusieurs parties connexes déterminées, reliées les unes aux autres par l'intermédiaire d'une boucle dont toutes les lignes descendantes (en nombre h) constituent une chaîne relative à l'état m. Il nous suffit de montrer que le nombre de diagrammes pour lesquels le nombre h est pair („diagrammes pairs") est égal au nombre de diagrammes pour lesquels h est impair („diagrammes impairs").

Soit un diagramme d'une telle famille (figure 19). Nous schématisons chacune des parties connexes $\mathscr{C}_1, \mathscr{C}_2, \ldots, \mathscr{C}_p$ reliées par la boucle, par une zone hachurée et par les interactions „libres" (représentées par des lignes pointillées), qui aboutissent aux divers points de la boucle. Celle-ci est constituée par des lignes descendantes (1'2, 2'3, 3'4, 4'1 sur l'exemple de la figure), séparées par des tronçons montants (11', 22', 33', 44'), dont la longueur peut être nulle (par exemple 22'). Comme toutes les lignes descendantes constituent une chaîne, toutes les interactions libres de chaque partie connexe sont reliées au même tronçon montant. Aucune des lignes montantes de la boucle ne peut être identiquement relative au même état m que les lignes descendantes, et l'ensemble des parties connexes reliées entre elles par un tronçon montant constitue une partie propre du diagramme (relativement à l'état m). Il en résulte

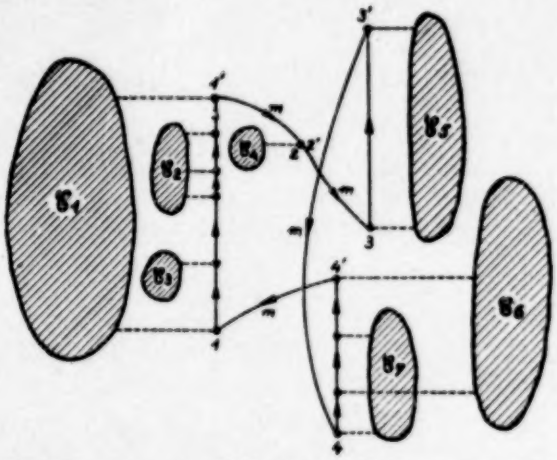

Fig. 19. Structure d'un diagramme ne se réduisant pas à une constellation à la limite classique: une boucle, dont toutes les lignes descendantes constituent une chaîne m, relie les parties connexes $\mathscr{C}_1, \mathscr{C}_2, \ldots$. Nous avons représenté ici toutes les lignes de la boucle par des traits pleins, même lorsqu'elles constituent des chaînes.

que des parties connexes rattachées au même tronçon montant sont nécessairement „enchevêtrées" † au sens suivant: il n'existe pas de temps qui soit à la fois supérieur à tous les instants des interactions libres d'un certain nombre de parties connexes, et inférieur à tous les instants des interactions libres des autres parties connexes.

On peut en définitive caractériser chaque diagramme de la famille formée à partir des parties connexes $\mathscr{C}_1, \mathscr{C}_2, \ldots, \mathscr{C}_p$ de la manière suivante:

1) On classe les parties connexes en sous-ensembles comprenant chacun une ou plusieurs parties connexes. Les parties connexes formant chacun de ces sous-ensembles doivent être enchevêtrées, et on peut alors relier toutes leurs interactions libres au moyen de lignes montantes de manière à constituer une partie propre (dans l'exemple, les parties connexes enchevêtrées $\mathscr{C}_1, \mathscr{C}_2, \mathscr{C}_3$

† Ce mot est employé ici dans un sens un peu différent de celui qu'il avait au paragraphe 2 et dans l'appendice A.

sont reliées pour former la partie propre 11', $\mathscr{C}_4$ constitue la partie propre 22', etc.).

2) On ordonne les parties propres ainsi obtenues de manière à déterminer leur mode de jonction par la chaîne descendante. Cet ordre doit être tel que l'interaction la plus haute d'une partie propre (qui est son point de sortie) soit plus élevée que l'interaction la plus basse (point d'entrée) de la partie propre suivante, afin que la ligne qui les joint soit descendante (par exemple les parties propres de la figure 19 peuvent être jointes dans l'ordre 1 2 3 4 ou dans l'ordre 1 3 2 4).

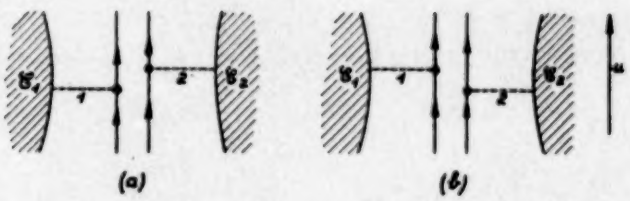

Fig. 20. Une étape du désenchevêtrement: cas où les parties connexes $\mathscr{C}_1$ et $\mathscr{C}_2$ appartiennent à des parties propres différentes. Les lignes ouvertes relient les interactions 1 et 2 au reste du diagramme, qui est le même dans les situations (a) et (b). Certaines de ces lignes pourraient également être descendantes.

Fig. 21. Une étape du désenchevêtrement: cas où les parties connexes $\mathscr{C}_1$ et $\mathscr{C}_2$ appartiennent à la même partie propre.

Dans ces conditions, on voit immédiatement qu'on ne peut former aucun diagramme avec des parties connexes dont l'une est désenchevêtrée des autres (c'est-à-dire si ses interactions libres ont lieu à des instants tous supérieurs aux instants des autres interactions libres). Dans ce cas, il y a donc évidemment autant de diagrammes pairs que de diagrammes impairs. Ce serait par exemple le cas dans l'exemple de la figure 19 si l'interaction 3 de la partie connexe $\mathscr{C}_5$ était à un instant supérieur à celui de l'interaction 1', le reste du diagramme étant inchangé.

Nous allons nous ramener à ce cas particulier en procédant par désenchevêtrement. Pour cela, nous comparerons les diagrammes qu'on peut former à l'aide de parties connexes fixées $\mathscr{C}_1, \mathscr{C}_2, \ldots, \mathscr{C}_p$, aux diagrammes correspondant aux mêmes parties connexes, mais dont les interactions libres sont placées à des instants relatifs différents. Il nous suffira donc de montrer que, étant donné deux interactions libres 1 et 2 appartenant à des parties connexes

différentes $\mathscr{C}_1$ et $\mathscr{C}_2$, et telles que l'instant de 1 soit immédiatement inférieur à celui de 2, *la variation du nombre des diagrammes pairs lorsque l'interaction* 1 *passe au-dessus de l'interaction* 2 *est égale à la variation du nombre des diagrammes impairs.*

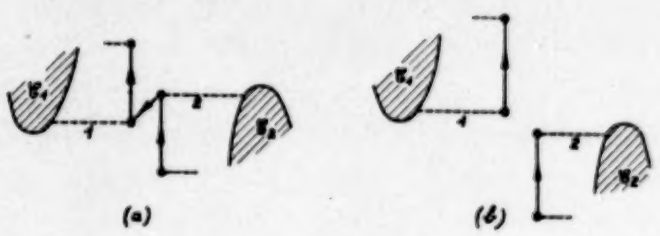

Fig. 22. Une étape du désenchevêtrement: cas où il y a une ligne descendante 21 dans la situation (a). Le diagramme correspondant dans la situation (b) n'existe pas.

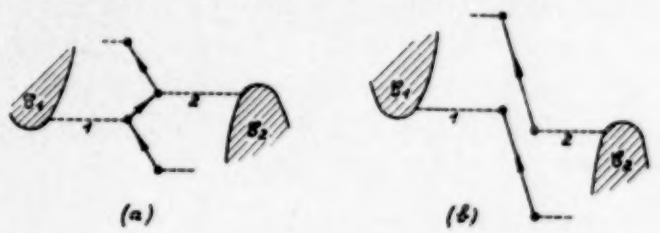

Fig. 23. Une étape du désenchevêtrement: cas où il y a une ligne montante 12 dans la situation (a). Le diagramme correspondant dans la situation (b) n'existe pas. Les diagrammes des types 22 (a) et 23 (a) sont en correspondance biunivoque.

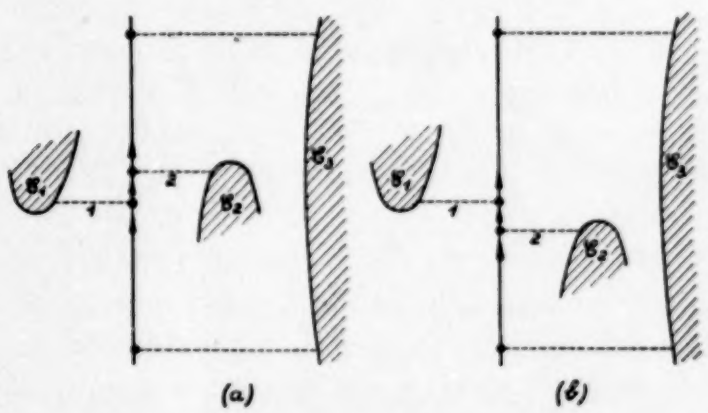

Fig. 24. Une étape du désenchevêtrement: cas où la partie propre contenant $\mathscr{C}_1$ et $\mathscr{C}_2$ contient une partie $\mathscr{C}_3$ recouvrant 1 et 2.

Considérons le cas général (fig. 20, 21), laissant de côté un cas exceptionnel que nous étudierons par la suite. Les règles de formation des diagrammes énoncées plus haut montrent qu'il y a correspondance biunivoque entre les diagrammes de la situation (a) (interaction 1 précédant immédiatement l'interaction 2) et les diagrammes de la situation (b) (interaction 1 suivant immédiatement l'interaction 2), cette correspondance conservant le nombre de lignes descendantes des diagrammes.

La conclusion précédente est en défaut dans le cas exceptionnel où l'interaction 1 est l'interaction libre la plus basse de la partie $\mathscr{C}_1$ et l'interaction 2 l'interaction libre la plus élevée de la partie $\mathscr{C}_2$, et dans le cas inverse. Supposons par exemple que nous soyons dans le premier cas, et comparons les diagrammes qu'on peut former dans les deux situations (a) et (b), avant et après avoir déplacé l'interaction 1 (fig. 22—24).

1° Les diagrammes dans lequels les parties connexes $\mathscr{C}_1$ et $\mathscr{C}_2$ appartiennent à des parties propres différentes, et dans lesquelles les interactions 1 et 2 ne sont pas reliées par une ligne, se correspondent dans la situation (a) et la situation (b), comme dans le cas général (figure 20).

2° Les diagrammes de la situation (a) dans lesquels l'interaction 1 est l'interaction libre la plus basse de la partie propre contenant $\mathscr{C}_1$, et l'interaction 2 la plus haute de la partie propre contenant $\mathscr{C}_2$, et dans lesquels une ligne descendante va de l'interaction 2 à l'interaction 1, n'ont aucun équivalent dans la situation (b), comme on le voit d'après la règle 2 de formation des diagrammes. Tous ces diagrammes disparaissent donc lorsqu'on croise l'interaction 1 avec l'interaction 2 (fig. 22).

3° A chacun des diagrammes du type de la fig. 22 (a) correspond un diagramme (fig. 23a), dans lequel $\mathscr{C}_1$ et $\mathscr{C}_2$ appartiennent à la même partie propre, et qui n'a aucun équivalent dans la situation (b), comme on le voit d'après la règle 1 de formation des diagrammes; en effet, la partie propre contenant $\mathscr{C}_1$ et $\mathscr{C}_2$ dans la situation (a) n'est plus enchevêtrée dans la situation (b). On a donc formé un nouvel ensemble de diagrammes qui disparaissent lorsqu'on croise l'interaction 1 avec l'interaction 2 (fig. 23). Chacun des diagrammes du type de la figure 23a correspond à un diagramme du type de la figure 22a, et possède une ligne descendante de moins. On peut donc associer les diagrammes qui disparaissent par paires, de parité opposée, et *il disparaît donc autant de diagrammes pairs que de diagrammes impairs.*

4° Enfin, il existe encore un dernier type de diagrammes qui se correspondent de la situation (a) à la situation (b) avec le même nombre de lignes descendantes. Ce sont ceux pour lesquels $\mathscr{C}_1$ et $\mathscr{C}_2$ appartiennent à la même partie propre, lorsque celle-ci est constituée d'un ensemble de parties connexes enchevêtrées, dans la situation (a) comme dans la situation (b). Cette partie propre contient (au moins) une partie connexe $\mathscr{C}_3$ qui recouvre les interactions 1 et 2, c'est-à-dire qui possède au moins une interaction libre située plus haut que les instants des interactions 1 et 2, et une interaction libre située plus bas (figure 24).

En définitive, on voit donc que le fait de changer l'ordre relatif de deux interactions appartenant à des parties connexes différentes modifie le nombre de diagrammes pairs de la même quantité que le nombre de diagrammes impairs, ce qui établit la proposition cherchée.

Appendice G

LIMITE CLASSIQUE DES DIAGRAMMES D SE RÉDUISANT À DES CONSTELLATIONS

Nous allons montrer que la contribution de l'ensemble des diagrammes D qui se réduisent à la même constellation lorsqu'on remplace chaque boucle par un point est la même que la contribution, en mécanique statistique classique, de cette constellation.

Nous pouvons d'abord, en ne considérant plus comme distincts deux diagrammes qui ne diffèrent que par un échange droite gauche dans une interaction, supprimer le facteur $\frac{1}{2}$ dans la contribution $\frac{1}{2}v(\mathbf{r}-\mathbf{r}')$ de cette interaction (voir la remarque faite à ce sujet au paragraphe 2.1.) Un cas exceptionnel est celui des diagrammes en échelle, auxquels il faut attribuer un poids 1/2 lorsqu'on effectue cette opération. L'intégration sur les temps d'interaction d'un diagramme d'ordre p donnant un facteur $\beta^p/p!$, la contribution des diagrammes en échelle est à la limite classique

$$-\frac{\bar{n}^2}{2\beta}\int d\mathbf{r}_1\, d\mathbf{r}_2 \sum_{p=1}^{\infty} (-)^p \frac{\beta^p}{p!}[v(\mathbf{r}_1-\mathbf{r}_2)]^p = -\frac{\bar{n}^2}{2\beta}\int d\mathbf{r}_1\, d\,\mathbf{r}_2 g_{12}, \qquad \text{(G.1)}$$

c'est-à-dire la contribution de la constellation constituée de deux points.

Pour les autres diagrammes (qui ont un nombre b de boucles au moins égal à 3), dans lesquels on ne distingue plus la droite de la gauche, on peut, sans rien modifier, affecter des indices aux boucles (qui deviennent à la limite classique b points affectés d'indices) à condition d'introduire en même temps un facteur $1/b!$ pour chaque diagramme. La contribution de chaque diagramme (d'ordre p) sera donc

$$-\frac{1}{\beta}(-)^p \frac{\beta^p}{p!}\frac{1}{b!}\bar{n}^b \int d\mathbf{r}_1 \ldots d\mathbf{r}_b \prod [v(\mathbf{r}_i-\mathbf{r}_j)]^{p_{ij}}, \qquad \text{(G.2)}$$

où p_{ij} est le nombre d'interactions (au moins égal à 1) reliant les boucles i et j, et où le produit porte sur l'ensemble des boucles reliées les unes avec les autres par des interactions.

Le nombre de diagrammes distincts que l'on peut former avec b boucles (affectées d'indices) reliées deux à deux par un nombre total p d'interactions est $p!/\prod(p_{ij}!)$, de sorte que leur contribution totale est

$$-\frac{1}{\beta}\frac{1}{b!}\bar{n}^b \int d\mathbf{r}_1 \ldots d\mathbf{r}_b \prod \frac{[-\beta v(\mathbf{r}_i-\mathbf{r}_j)]^{p_{ij}}}{p_{ij}!}.$$

Si maintenant on groupe les contributions des diagrammes dans lesquels les boucles i et j sont reliées par un nombre quelconque d'interactions, on reconstitue pour deux boucles i et j liées ensemble le facteur g_{ij}.

Références

1) R. Balian, C. Bloch et C. De Dominicis, Nuclear Physics **25** (1961) 529
2) H. D. Ursell, Proc. Camb. Phil. Soc. **23** (1927) 685;
J. E. Mayer, J. Chem. Phys. **5** (1937) 67
3) J. Yvon, Actual. Sc. et Indust. **203** (Paris, 1935)
4) C. Bloch et C. De Dominicis, Nuclear Physics **7** (1958) 459
5) N. N. Bogolioubov, Problèmes de dynamique en physique statistique (Moscou, 1948).

2.1 *Nuclear Physics* **27** (1961) 323—336; © *North-Holland Publishing Co., Amsterdam*
Not to be reproduced by photoprint or microfilm without written permission from the publisher

TWO-BODY FORCES AND THE GIANT RESONANCE IN PHOTO-NUCLEAR REACTIONS

V. V. BALASHOV, V. G. SHEVCHENKO and N. P. YUDIN
Nuclear Research Institute of the Moscow State University, Moscow, USSR

Received 18 January 1961

Abstract: Partial cross sections as well as energy and angular distributions of photodisintegration products of the Ca^{40} nucleus are calculated using the shell model. It is shown that the use of empirical data on the levels of the adjacent nuclei and the account of nucleon-nucleon interactions make it possible to describe satisfactorily the photodisintegration of the giant resonance region.

1. Introduction

According to Wilkinson's single-particle model of photo-nuclear reactions [1]), the giant resonance in the cross-section of the reactions (γ, n) and (γ, p) corresponds to the transition of a nuclear absorbing a γ-quantum to the next, higher shell with the subsequent decay of the resulting quasi-stationary state either through the direct emission of a nucleon or through a compound nucleus. While explaining satisfactorily the magnitude of the cross sections, the width of the giant resonance maximum and the angular distribution of the reaction products, this model involves serious difficulties if used to interpret the energy position of the giant resonance, the relation of the cross-sections (γ, p) and (γ, n), the disintegration of the giant resonance observed in light nuclei, etc. It becomes necessary therefore to resort, in describing photonuclear reactions, to additional assumptions on the nuclear properties characteristic of these reactions alone. Thus, to explain the increase of the observed energy of the giant resonance in heavy nuclei as compared with that calculated according to the single-particle model, the concept of the nucleon effective mass considerably less than its true mass has to be introduced, though the aggregate body of experimental data on other reactions and electromagnetic transitions in this region of nuclei indicates that actually the mass of a nucleon in a nucleus is close to the true one.

The most essential assumption of Wilkinson's single-particle model is the neglect of the residual interaction between nucleons. Elliott and Flowers took account of this interaction in their work concerned with oxygen photodisintegration [2]). The work by Elliott and Flowers gives a self-consistent approach to the description of photo-nuclear reactions in the framework of the shell model. This approach reduces to the following points:

(1) The energies of excited quasi-stationary nuclear levels in zero approximation (without taking account of nucleon interaction) are calculated, with allowance for spin-orbit splitting from the experimental values of the respective levels of the adjacent nuclei. Thus, data on nuclear levels with $A = 15$ and $A = 17$ are used in describing the photodisintegration of O^{16} for determining the energy of the transitions of a nucleon from the p-shell to the 2s, 1d shell.

(2) Account is taken of the interaction between nucleons which leads to the mixture of the different nuclear states formed in the absorption of γ-quanta.

These propositions have made it possible to explain the principal properties of oxygen photodisintegration. Besides, investigating the photodisintegration of the magic nucleus of O^{16} in terms of the shell model is the simplest method technically. Additional assumptions are therefore made in considering the giant resonance in other nuclei in order to avoid difficulties, inevitable in the calculation if the shell model is used consistently.

On the one hand, Neudachin *et al.* [3]) used empirical data for determining the nuclear excitation energy, but neglected the mixture of the configurations (only the diagonal part of the residual interaction leading to a level shift being taken into account). This approach has proved its worth when applied to the calculation of the total cross-sections of γ-quantum absorption in the giant resonance region for nuclei with $A \leqq 70$. Yet the question of the energy dependence of the partial cross sections $\sigma(\gamma, p)$ and $\sigma(\gamma, n)$ and the spectra of neutrons and protons remains open.

On the other hand, the work by Brown and Bolsterli [4]) has become widely known. This work is concerned with a schematic model (as is emphasized by its authors) of the residual interaction between nucleons in the giant resonance. The principal inference from the calculation performed by Brown and Bolsterli — the formation of a high "dipole state" which absorbs nearly all dipole strength — presupposes a number of special assumptions, the principal of them being the neglect of the splitting of the zero approximation level attaining scores of MeV in these nuclei and the rejection of "weak transitions" which actually make a small contribution of the absorption, but are no less essential as "strong transitions" from the viewpoint of the mixing of states.

Against this background it is of interest to extend the scheme of calculation by Elliott and Flowers for O^{16} on to medium and heavy nuclei. In the present paper the role of pairing interactions in the giant resonance is exemplified by Ca^{40}.

2. Photodisintegration of Ca^{40}

2.1. CALCULATING TECHNIQUE

The shells 1s, 1p, 2s and 1d are filled in Ca^{40}. In the dipole absorption of a γ-quantum, a nucleon of the external shell passes into the adjacent free shell

(2p, 1f). This transition corresponds to 8 different excited states of the nucleus with $J^\pi = 1^-$ and $T = 1$. One of the following independent shell configurations corresponds to each such state in zero approximation:

$$\begin{aligned} \varphi_1 &= 1d_{\frac{3}{2}}^{-1}\, 2p_{\frac{3}{2}}, & \varphi_5 &= 2s_{\frac{1}{2}}^{-1}\, 2p_{\frac{3}{2}}, \\ \varphi_2 &= 1d_{\frac{3}{2}}^{-1}\, 2p_{\frac{1}{2}}, & \varphi_6 &= 1d_{\frac{5}{2}}^{-1}\, 1f_{\frac{7}{2}}, \\ \varphi_3 &= 1d_{\frac{3}{2}}^{-1}\, 1f_{\frac{5}{2}}, & \varphi_7 &= 1d_{\frac{5}{2}}^{-1}\, 2p_{\frac{3}{2}}, \\ \varphi_4 &= 2s_{\frac{1}{2}}^{-1}\, 2p_{\frac{1}{2}}, & \varphi_8 &= 1d_{\frac{5}{2}}^{-1}\, 1f_{\frac{5}{2}}. \end{aligned} \tag{1}$$

2.1.1. Zero Approximation

Determining the energy of the excited states of Ca^{40} in zero approximation is based on empirical data on nuclear levels of $A = 39$ and $A = 41$. Fig. 1

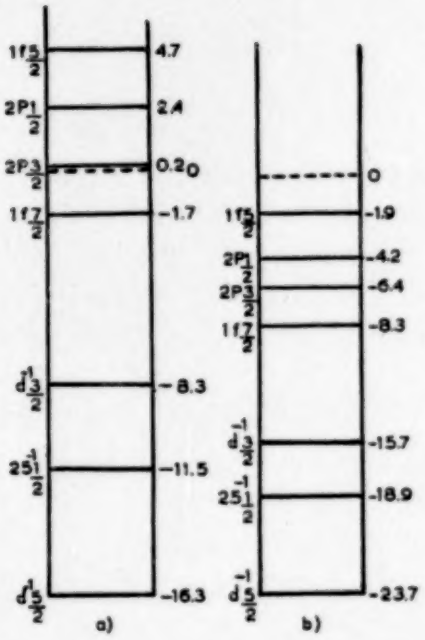

Fig. 1. Single-particle and hole states of Ca^{40}. a) proton states. b) neutron states.

shows the spectra of single-particle states in the shell (2p, 1f) taken from the experimental data [5]) on the nuclear levels of Ca^{41} and Sc^{41}. Fig. 1 also shows the energies of the hole states in Ca^{40} corresponding to the experimental values of the coupling energy of the last neutron and proton in the shells $1d_{\frac{3}{2}}$, $2s_{\frac{1}{2}}$ and $1d_{\frac{5}{2}}$. The spacing of the excited states $\frac{1}{2}$ and $\frac{5}{2}$ in Ca^{39} and K^{39} corresponding to the hole in the shells $2s_{\frac{1}{2}}$ and $1d_{\frac{5}{2}}$ is unknown experimentally. It may be supposed [3]) that the splitting $1d_{\frac{3}{2}} - 1d_{\frac{5}{2}}$ for the holes will be twice or half as much again as large as that for the particles determined by the levels of O^{17} and F^{17}. In the given calculation we vary the energy of the excited levels $2s_{\frac{1}{2}}^{-1}$ and $1d_{\frac{5}{2}}^{-1}$, namely, $E(2s_{\frac{1}{2}}^{-1})$ and $E(1d_{\frac{5}{2}}^{-1})$.

In the zero approximation, the energy of an excited state of configuration $j_1^{-1} j_2$ is determined as a difference of the energies of the states j_2 and j_1^{-1} indicated in fig. 1 (see table 1).

TABLE 1

Energy of the excited states $J^\pi = 1^-$, $T = 1$ in zero approximation for different values $E(s_{\frac{1}{2}}^{-1})$ and $E(d_{\frac{1}{2}}^{-1})$

	$E(s_{\frac{1}{2}}^{-1})=3.2$ $E(d_{\frac{1}{2}}^{-1}=8$	$E(s_{\frac{1}{2}}^{-1})=6.2$ $E(d_{\frac{1}{2}}^{-1})=8$	$E(s_{\frac{1}{2}}^{-1})=3.2$ $E(d_{\frac{1}{2}}^{-1})=6.5$
$d_{\frac{1}{2}}^{-1}\,2p_{\frac{1}{2}}$	9.1	9.1	9.1
$d_{\frac{1}{2}}^{-1}\,2p_{\frac{3}{2}}$	11.3	11.3	11.3
$d_{\frac{1}{2}}^{-1}\,1f_{\frac{5}{2}}$	13.7	13.7	13.7
$2s_{\frac{1}{2}}^{-1}\,2p_{\frac{1}{2}}$	14.5	17.5	14.5
$2s_{\frac{1}{2}}^{-1}\,2p_{\frac{3}{2}}$	12.3	15.3	12.3
$d_{\frac{3}{2}}^{-1}\,1f_{\frac{7}{2}}$	15.2	15.2	13.7
$d_{\frac{3}{2}}^{-1}\,2p_{\frac{1}{2}}$	17.2	17.2	15.7
$d_{\frac{3}{2}}^{-1}\,1f_{\frac{5}{2}}$	12.7	21.7	20.2

Energies in MeV.

The physics of zero approximation implies reducing the interaction of the external 2p or 1f nucleon with the other nucleons of the nucleus to an average single-particle potential. The transfer onto the nucleus with $A = 40$ of the empirical spectrum of the single-particle 2p and 1f states determined for the nucleus with $A = 41$ means the neglect of the change of this potential during the ejection of one nucleon from the closed shell (2s, 1d). In other words, in zero approximation we totally neglect the interaction between a hole and a particle: both its diagonal part leading merely to a level shift and the off-diagonal one responsible for the mixture of configurations. The zero approximation differs from the Wilkinson single-particle model in that the former enables the investigator to evaluate, proceeding from empirical data on nuclear levels, the interaction among the nucleons of the closed shell, leading to a substantial increase in the nucleon coupling energy in the transition from the beginning to the end of the shell. For example, the $1d_{\frac{3}{2}}$ neutron-coupling energy changes from -0.93 MeV in O^{17} to 15.7 MeV in Ca^{40}. The evaluation of this interaction is the principal effect responsible for a shift of the giant resonance maximum as compared with the single-particle model.

2.1.2. Particle-Hole Interaction (Mixture of Configurations)

The particle-hole interaction leads to the mixture of pure shell states. With this interaction taken into account, the wave function of each excited level from $J^\pi = 1^-$ and $T = 1$ is a mixture of all eight configurations of (1),

$$\Psi_i = \sum_k \alpha_{ik}\varphi_k, \qquad i = 1, 2, \ldots 8. \tag{2}$$

The matrix elements of particle-hole interaction are calculated by the conventional formulae of the shell model-through reducing to the matrix elements of two-particle states [6])

$$\langle j_1^{-1} j_2 : 11|v|j_1^{-1'} j_{,2} : 11\rangle = -\tfrac{1}{2} \sum_{L\tilde{L}SS\tilde{T}} (2\tilde{L}+1)(2\tilde{S}+1)$$
$$\times W(l'_2 l'_1 l_1 l_2 : \tilde{L}L) W(\tfrac{1}{2}\tfrac{1}{2}\tfrac{1}{2}\tfrac{1}{2} : \tilde{S}S) \begin{vmatrix} \frac{1}{2} & \frac{1}{2} & S \\ l_1 & l_2 & L \\ j_1 & j_2 & 1 \end{vmatrix} \begin{vmatrix} \frac{1}{2} & \frac{1}{2} & S \\ l'_1 & l'_2 & L \\ j'_1 & j'_2 & 1 \end{vmatrix} \qquad (3)$$
$$\times \langle l_1' l_2 : \tilde{T}\tilde{S}\tilde{L}|V_{12}|l_1 l_1' : \tilde{T}\tilde{S}\tilde{L}\rangle,$$

where $W(abcd : ef)$ is the Racah coefficient,

$$\begin{vmatrix} a & b & c \\ d & f & e \\ j & k & l \end{vmatrix}$$

is the generalized Racah coefficient and $V = \sum_{i<j} V_{ij}$ is the two-body potential among the nucleons in the nucleus. From eq. (3) it is clear that the nucleon-attraction potential corresponds to a particle-hole repulsion. By the "diagonal approximation" we shall understand the approximation in which only the diagonal portion of particle-hole interaction is taken into account and the off-diagonal portion is rejected, i.e., the mixture of configurations is neglected. It is in this approximation that absorption cross sections are calculated in ref. [3]). The potential of nucleon-nucleon interaction in a nucleus was chosen in the form of the Wigner, Serber and Majorana forces. The radial dependence of forces is assumed to be Gaussian $V(r) = V_0 \exp(-r^2/b^2)$. The parameter b was taken equal [7]) to 1.73 fm and the interaction amplitude varied from 0 to 50 MeV. To evaluate the effect of the range of forces the calculation of the δ-interaction among the particles $V(r) = -g\delta(\mathbf{r})$ was performed; and the parameter g was chosen equal 825 MeV/cm^3, which corresponds to $V_0 = 50$ MeV. The level energies of $J^\pi = 1^-$ and $T = 1$ and the corresponding wave functions are obtained by diagonalizing the matrix of the 8th order for the following variants:

(i) $E(s_{\frac{1}{2}}^{-1}) = 3.2$ MeV, $E(d_{\frac{5}{2}}^{-1}) = 8$ MeV, $V = -50 \exp(-r^2/b^2)$ MeV;

(ii) $E(s_{\frac{1}{2}}^{-1}) = 3.2$ MeV, $E(d_{\frac{5}{2}}^{-1}) = 8$ MeV, $V = -50\frac{1}{2}(1+P_x) \exp(-r^2/b^2)$ MeV;

(iii) $E(s_{\frac{1}{2}}^{-1}) = 3.2$ MeV, $E(d_{\frac{5}{2}}^{-1}) = 8$ MeV, $V = -50\, P_x \exp(-r^2/b^2)$MeV;

(iv) $E(s_{\frac{1}{2}}^{-1}) = 6.2$ MeV, $E(d_{\frac{5}{2}}^{-1}) = 8$ MeV, $V = -50\frac{1}{2}(1+P_x) \exp(-r^2/b^2)$ MeV;

(v) $E(s_{\frac{1}{2}}^{-1}) = 3.2$ MeV, $E(d_{\frac{5}{2}}^{-1}) = 6.5$ MeV, $V = -50\frac{1}{2}(1+P_x) \exp(-r^2/b^2)$ MeV;

(vi) $E(s_{\frac{1}{2}}^{-1}) = 3.2$ MeV, $E(d_{\frac{5}{2}}^{-1}) = 8$ MeV, $V = -825\, \delta(\mathbf{r})$MeV/cm^3.

2.1.3. *Calculation of Matrix Elements of Interaction and of Radial Integrals and Particle Widths*

The radial single-particle functions necessary for calculating the matrix elements of eq. (3) as well as the radiative widths were chosen in the form of harmonic oscillator functions with the parameter $r_0 = \sqrt{(\hbar/m\omega)} = 1.96$ fm determined by Talmi and Carlsson by the Coulomb shift of levels [8]). For the forces of finite range (the first five variants of (4)) the two-particle matrix elements are reduced to the radial intervals with the aid of the Talmi coefficients [9]). In the case of δ-interaction, eq. (3) can be simplified even more

$$\langle j_1^{-1} j_2 : 11|V|j_1^{-1'} j'_2 : 11\rangle = -\sqrt{ll'} \sum_S \begin{vmatrix} \frac{1}{2} & \frac{1}{2} & S \\ l_1 & l_2 & 1 \\ j_1 & j_2 & 1 \end{vmatrix} \times \begin{vmatrix} \frac{1}{2} & \frac{1}{2} & S \\ l_1' & l_2' & 1 \\ j_1' & j_2' & 1 \end{vmatrix} \frac{g}{4\pi} \int_0^\infty R_1 R_2 R_1 R_2 r^2 \mathrm{d}r, \quad (5)$$

where $l = \max\{l_1, l_2\}$, g is the amplitude of the forces and R are the radial wave functions. When oscillator functions are used for the calculation of the radiative widths the relation between transition strengths is approximately the same as in the case of the rectangular pit function [1]). In our case, the "strongest" are the transitions $d_{\frac{1}{2}} \to f_{\frac{7}{2}}$ and $d_{\frac{3}{2}} \to f_{\frac{7}{2}}$ (see table 2). The proton

TABLE 2

Relative magnitudes of the squares of the reduced matrix elements of radiative transitions for oscillator functions

$1d_{\frac{3}{2}} \to 2p_{\frac{3}{2}}$	$1d_{\frac{3}{2}} \to 2p_{\frac{1}{2}}$	$1d_{\frac{3}{2}} \to 1f_{\frac{5}{2}}$	$2s_{\frac{1}{2}} \to 2p_{\frac{3}{2}}$	$2s_{\frac{1}{2}} \to 2p_{\frac{1}{2}}$	$1d_{\frac{5}{2}} \to 1f_{\frac{7}{2}}$	$1d_{\frac{5}{2}} \to 2p_{\frac{3}{2}}$	$1d_{\frac{5}{2}} \to 1f_{\frac{5}{2}}$
0.022	0.111	0.700	0.189	0.278	1.00	0.200	0.050

and neutron widths Γ_p and Γ_n of the excited states are calculated by the conventional formula

$$\Gamma = 2kP_e\gamma^2, \quad (6)$$

where k is the momentum of the outgoing nucleon, P_e is the permeability of the barrier and γ^2 is the reduced width. For the transition to the given level of the final nucleus when a nucleon of orbital momentum l is emitted, we have

$$\gamma_i^2 = \frac{3\hbar^2}{2mR} \frac{1}{2} \sum_k |\alpha_{ik}|^2, \quad (7)$$

where the summation is performed over all configurations contributing to the given channel (i.e., actually over the total moment of the outgoing nucleon

$j = l \pm \frac{1}{2}$ with allowance for the conservation of J). The radius R was taken the same for all channels and was assumed, in accordance with the formula $R = 1.3 \times A^{\frac{1}{3}}$ fm $= 4.45$ fm.

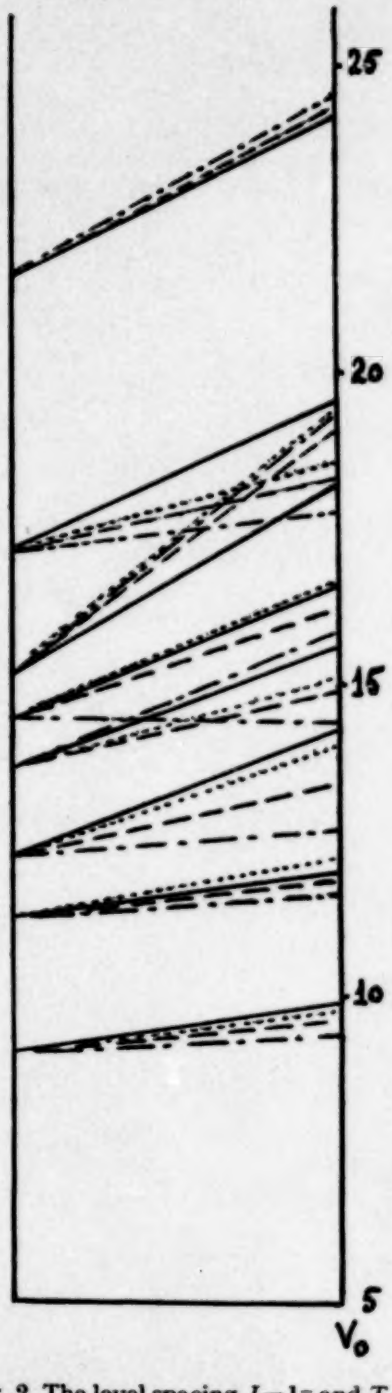

Fig. 2. The level spacing $J = 1^-$ and $T = 1$ depending on the amplitude of forces.
——— First variant.
– – – – Second variant.
– · – · – Third variant.
····· Fourth variant.

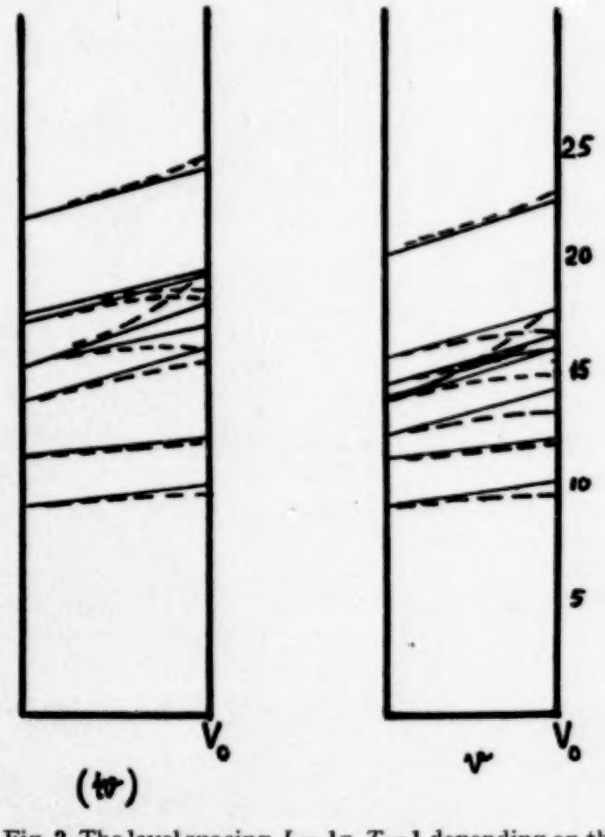

Fig. 3. The level spacing $J = 1^-$, $T = 1$ depending on the amplitude of forces for the fourth and fifth variants.
– – – – Precise calculation.
——— Diagonal approximation.

TABLE 3

Wave functions

Wave funtion no.	E^* (MeV)	$d_{\frac{3}{2}}^{-1} p_{\frac{3}{2}}$	$d_{\frac{3}{2}}^{-1} p_{\frac{1}{2}}$	$d_{\frac{3}{2}}^{-1} f_{\frac{5}{2}}$	$s_{\frac{1}{2}}^{-1} p_{\frac{3}{2}}$	$s_{\frac{1}{2}}^{-1} p_{\frac{1}{2}}$	$d_{\frac{3}{2}}^{-1} f_{\frac{7}{2}}$	$d_{\frac{5}{2}}^{-1} p_{\frac{3}{2}}$	$d_{\frac{5}{2}}^{-1} f_{\frac{5}{2}}$	Γ_γ (keV)
1	9.8	0.966	−0.251	0.0021	−0.014	−0.021	−0.025	0.034	−0.010	8.5 × 10
2	12.0	0.249	0.964	−0.013	−0.008	−0.054	−0.057	−0.030	−0.013	0.220
3	15.6	0.020	0.002	0.933	0.180	−0.029	−0.257	−0.077	0.148	1.1
4	18.7	0.045	0.040	0.65	0.682	0.288	0.615	−0.165	−0.199	4.0
5	16.2	0.017	0.022	−0.076	−0.024	0.912	−0.400	−0.006	−0.007	0.012
6	19.6	0.007	0.063	0.291	−0.511	0.264	0.571	0.495	0.008	28
7	18.4	0.025	0.016	−0.088	0.462	0.091	−0.232	0.845	0.005	0.26
8	24.4	0.025	0.013	−0.169	0.157	0.046	0.111	−0.072	0.964	2.6

3. Results of Calculations

The calculation of the energy levels of Ca^{40} with $J = 1^-$, $T = 1$ and the wave functions corresponding to them was performed on the Strela electronic computor of the Moscow State University. Figs. 2 and 3 show the change in the spacing of these levels depending on the amplitude of the pairing interaction V_0 in the interval from 0 to 50 MeV. The wave functions of the state for one of the variants (IV) are represented in table 3.

TABLE 4

Variants of level energies and cross sections of absorption

Wave funct. No.	(i)		(ii)		(iii)		(iv)		(v)		(vi)	
	E^* (MeV)	σ (mb · MeV)	E^* (MeV)	σ (mb · MeV)	E^* (MeV)	σ (mb · MeV)	E^* (MeV)	σ (mb · MeV)	E^* (MeV)	δ (mb · MeV)	E^* (MeV)	δ (mb · MeV)
1	9.9	0.4	9.7	0.7	9.5	1.5	9.8	1.0	9.7	0.7	9.8	0
2	12.1	6.6	12.0	12.7	11.8	22.0	12.0	17.4	12.0	11.1	12.3	34.6
3	15.7	44.5	15.0	9.6	15.9	46.0	15.6	51.7	15.0	0.7	15.2	12.3
4	16.6	63.2	16.3	67.2	14.5	1.6	18.7	129.0	16.0	1.4	16.6	25.5
5	14.3	41.5	13.5	29.6	12.8	17.6	16.2	0.5	13.4	18.0	14.2	10.6
6	18.3	439	19.2	775.0	19.4	907.0	19.6	815.0	18.0	860.0	19.4	820
7	19.6	384.0	18.4	72.2	17.9	10.7	18.4	8.8	16.9	50.3	18.7	117.0
8	24.3	43.7	24.4	40.7	24.6	40.0	24.4	50.0	22.9	52.0	24.6	34.0

3.1. TOTAL ABSORPTION SECTIONS

The calculated integral cross sections of absorption $\int \sigma_\gamma dE_\gamma$ for each level are listed in table 4 and fig. 4 (a), (b) and (c). The position of the maximum of the absorption cross-section does not change essentially with the change in the exchange character of the forces. The calculations involving the δ-forces (4th variant) lead to a result close to that of the 2nd variant (Serber forces).

for variant (iv)

Γ_p(keV)					Γ_n(keV)							$\Sigma(\Gamma_n+\Gamma_p)$ (keV)
$pd_{\frac{3}{2}}^{-1}$	$fd_{\frac{3}{2}}^{-1}$	$ps_{\frac{1}{2}}^{-1}$	$fd_{\frac{5}{2}}^{-1}$	$pd_{\frac{5}{2}}^{-1}$	total	$pd_{\frac{3}{2}}^{-1}$	$fd_{\frac{3}{2}}^{-1}$	$ps_{\frac{1}{2}}^{-1}$	$fd_{\frac{5}{2}}^{-1}$	$pd_{\frac{5}{2}}^{-1}$	total	
7.1	2.0×10^{-5}				7.1							7.1
3414	0.036				3414							3414
2.6	810	0.025			813							813
40	12	996	4.3	0.8	1050	29	2.4				3.2	1082
5.8	7.7	13			26	1.1	0.011				1.1	27.1
48	420	1080	168	5.4	1720	38	92				130	1850
9.3	21	290	50	0.02	372	6.1	3				9.1	381
140	250	270	411	1010	2040	13	180	170	10	5.4	378	2418

This is natural since in both cases the interaction of the state with odd orbital momentum of the relative motion of two nucleons is excluded. In variant (v), we observed a certain decrease in the absorption energy maximum as compared with other variants, which is caused by the shift of the "hole level" $d_{\frac{3}{2}}^{-1}$. At the same time the change of the position of the level $2s_{\frac{1}{2}}^{-1}$ responsible for the weak transition practically has no effect on the shape of the absorption cross section (variants (ii) and (iv).

In all cases the "main transition" absorbing the bulk of the dipole sum is determined by the transition energy $d_{\frac{3}{2}} \rightarrow f_{\frac{7}{2}}$ and lies in the region from 17 to 19 MeV.

Table 5 compares the absorption cross section calculated in "diagonal approximation" and with allowances for the mixture of configurations (iv) variant). From the data given it is clear that taking account of the off-diagonal

TABLE 5

Comparison of zero and diagonal approximations with the data of the total calculation

Zero approx. energies	Energies and absorption cross sections		Absorption energies and cross sections [a])	
E^*	E^*	σ_γ %	E^*	σ_γ %
9.1	10.2	0.51	9.8	0.09
11.3	12.1	3.1	12.0	1.6
13.7	16.2	26.0	15.6	4.8
17.5	19.5	6.2	18.7	12.0
15.3	17.3	11.0	16.2	0.
15.2	18.2	42.0	19.6	76.1
17.2	19.4	8.9	18.4	0.82
21.7	24.0	2.4	24.4	4.7

[a]) Using the total calculation for variant (iv).
Energies in MeV.

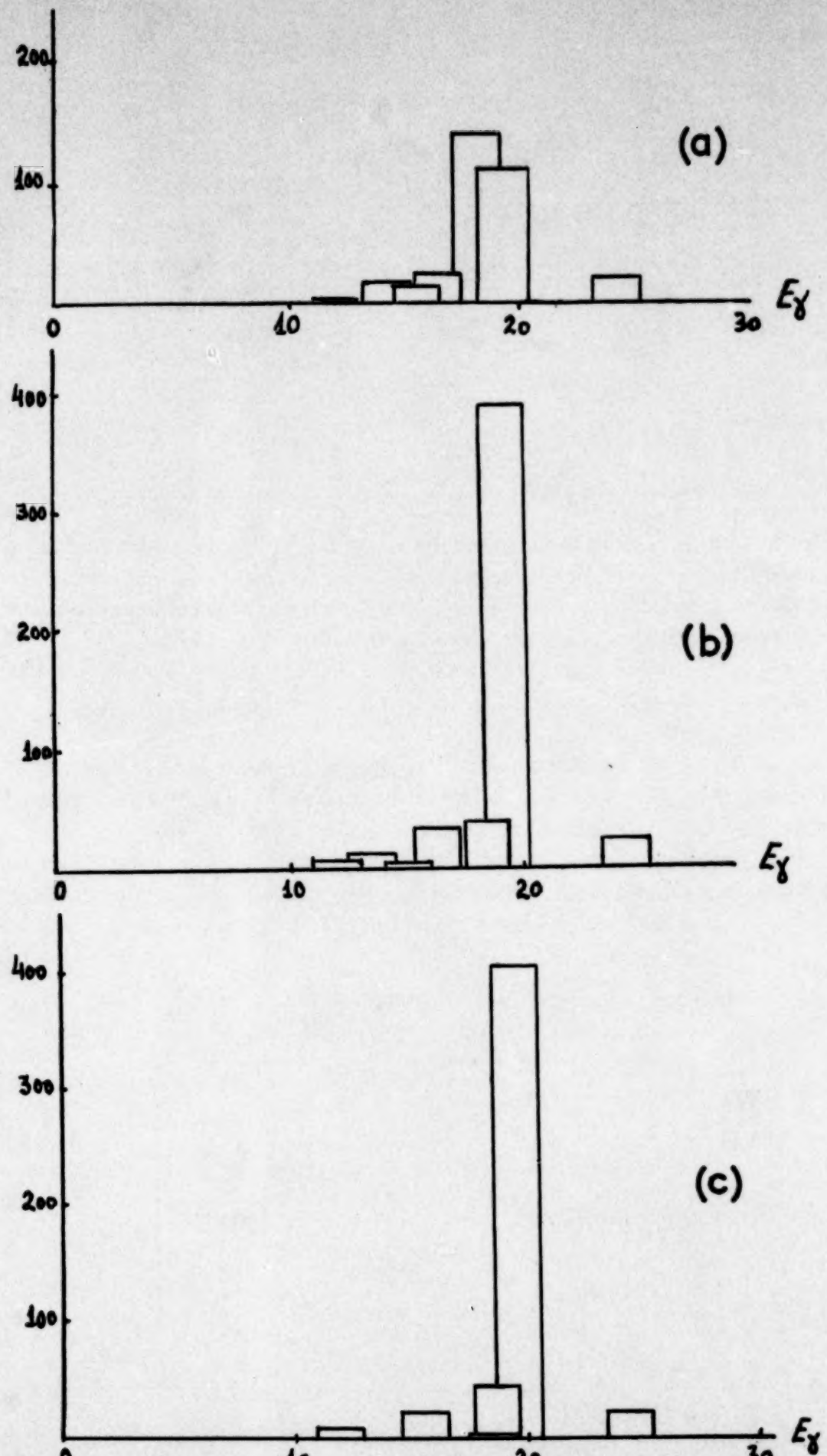

Fig. 4. Absorption cross sections to the levels $J = 1^{-1}$, $T = 1$. (a) Variant (i). (b) Variant (ii). (c) Variant (vi).

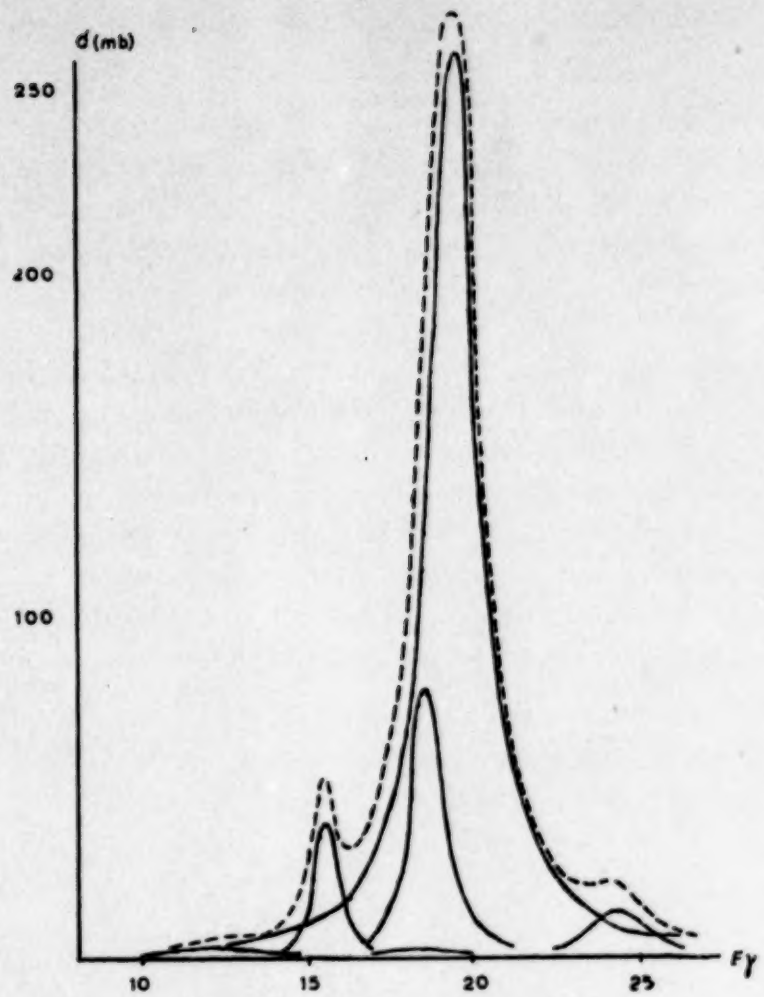

Fig. 5. Cross section of the reaction γ, p. _____ For individual levels. — — — — Total cross section.

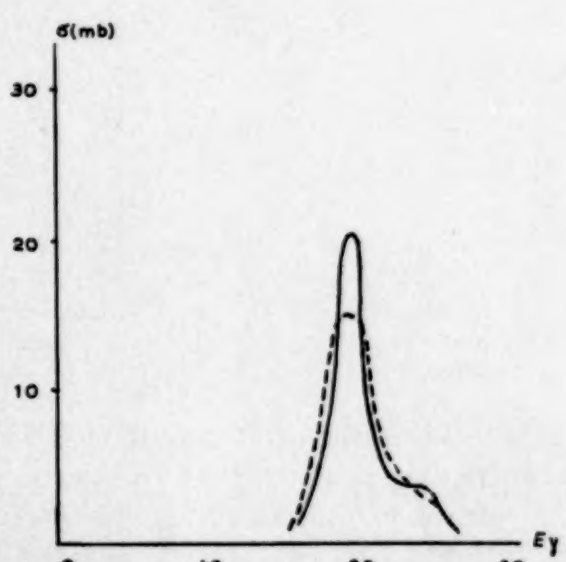

Fig. 6. Comparison of the calculated cross section of the reaction γ, n with experiment [10]).

particle-hole interaction does not change essentially the form of the absorption curve.

3.2. CROSS SECTION OF THE REACTIONS (γ, p) AND (γ, n)

The partial cross sections (γ, p) and (γ, n) were calculated for one, namely variant (iv) (table 3, figs. 5 and 6).

The maximum of the cross sections of the reactions (γ, p) and (γ, n) lies in the neighbourhood of 19 MeV, which corresponds to the main transition of 19.6 MeV.

In calculating the partial cross sections, taking account of the mixture of configurations is of decisive importance. In the zero and diagonal approximations all neutron channels proved to be closed and consequently the reaction (γ, n) does not occur. The cross section of the reaction (γ, p) in the diagonal approximation has a form entirely different from fig. 5. It is clear from table 3 that the main maximum of the cross section of the reaction (γ, p) is caused by the decay of the excited state at 19.6 MeV to the level $2s_{\frac{1}{2}}^{-1}$, which it is impossible to evaluate without taking account of the mixture of configurations.

3.3. ENERGY SPECTRA OF PROTONS AND NEUTRONS

The calculated spectrum of protons is represented in fig. 7. The most intense group of protons with energies from 3 to 5 MeV is due to the transitions from

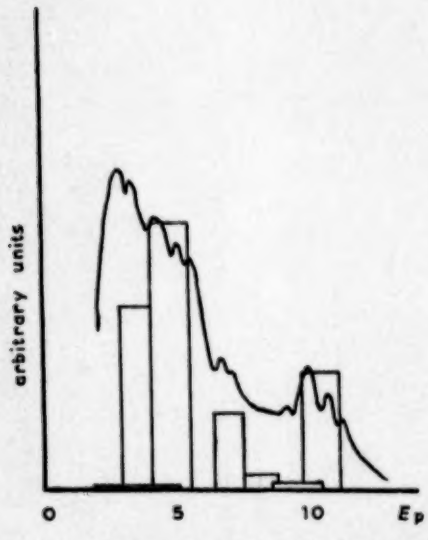

Fig. 7. Comparison of the calculated energy distribution of protons (columns) with experiment taken from ref. [11]).

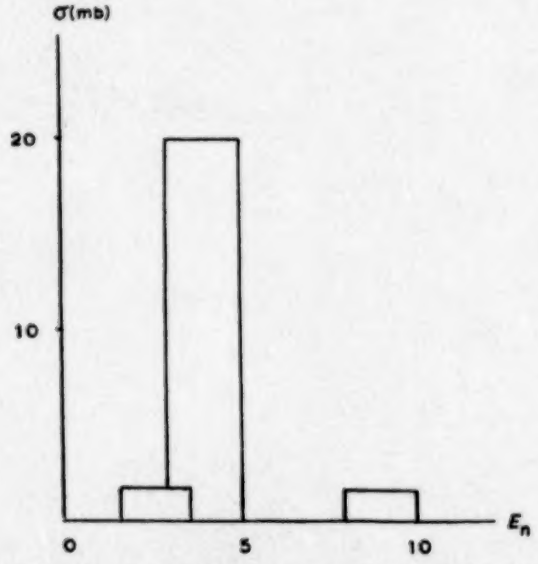

Fig. 8. Calculated energy distribution of neutrons.

18.7 MeV and 19.6 MeV levels to the excited state of K^{39} with $J^\pi = \frac{1}{2}^+$. Thus the energy position of this group is directly determined by the position of the hole level $2s_{\frac{1}{2}}^{-1}$. Protons with energies from 10 to 11 MeV are conditioned by the transition from the 19.6 MeV to the ground state of K^{39}.

The calculated neutron spectrum is given in fig. 8.

4. Comparison with Experiment

At present there are no data either on the total cross section on Ca^{40} or for the cross section of the dominant reaction (γ, p). The comparison of the theory with experiment is possible only for the cross section of the reaction (γ, n) (fig. 6) and the energy distribution of photo-protons (fig. 7).

Good agreement with experiment of the calculated cross section of the reaction (γ, n) giving a small contribution to the total cross section of photo-absorption into Ca^{40} is probably the most striking evidence of the success of the shell model in describing the giant resonance. It has been pointed out above that the energy position of the most intense group of protons with energies from 3 to 5 MeV depends on the choice of the position of the excited level of K^{93} with $J = \frac{1}{2}^+$. As is clear from fig. 7, agreement with experiment can be improved by a small shift of this level, which will practically have no effect on the form of cross sections (see sect. 2). Against this background it seems extremely important to determine the position of the excited levels $\frac{1}{2}^+$ and $\frac{5}{2}^+$ of K^{39} and Ca^{39} experimentally, with the aid of the usual pick-up reactions (p, d), (n, d) and (t, α), (He^3, α), for example. The calculation of the angular distribution of the most intense group of protons with $E_p \approx 4$ MeV yields $W(\theta) \approx 1 + 0.9 \sin^2 \theta$; thus the angular distribution of photo-protons contains with, agreement with experiment[11]), a large isotropic part.

5. Conclusions

1. Taking account of the pairing interactions in the nucleus makes it possible to explain the energy position of the giant resonance maximum without resorting to the concept of the nucleon effective mass. The zero approximation, relying on the empirical data on nuclear levels, already leads to a shift of the giant resonance maximum by a factor of 1.5 or 2 as compared with the single-particle model. Taking account of the diagonal part of the particle-hole interaction increases the excitation energy by 2 or 3 MeV. The off-diagonal part of interaction responsible for the mixture of configurations does not lead to an essential shift of excited states and pushes the absorption maximum by 1 to 1.5 MeV. Thus, it may be claimed that the Brown-Bolsterli effect plays no essential rôle in light nuclei.

2. The mixing of states due to two-body interactions opens up additional canals of the decay of quasi-stationary states, arising in the absorption of γ-quanta. Due to the great number of the resulting transitions the character of the nucleon spectra becomes close to the statistical one. Taking account of the nucleon-nucleon interactions reveals thereby the microscopic nature of the decay through a compound nucleus. Determining the coupling of the canals through a detailed shell calculation can justify the application of the complex potential for describing photo-nuclear reactions in the giant resonance region.

The photodisintegration of Ca^{40} considered in this paper shows that the shell model can be successfully used, taking account of two-body interactions, for an exhaustive description of the giant resonance in photo-nuclear reactions. The role of pairing interactions in forming photonucleur reaction spectra will prove especially essential in heavy nuclei in which the proton excitation levels should, due to the channel binding, disintegrate largely through the emission of neutrons. The corresponding calculations for Pb^{208} are being performed at present.

The authors are grateful to V. G. Neudachin and Yu. M. Shirokov for stimulating discussions and L. L. Suzdaltseva for help in the calculations.

References

1) D. H. Wilkinson, Physica **22** (1956) 1039
2) J. P. Elliott and B. H. Flowers, Proc. Roy. Soc. **242** (1957) 57
3) V. G. Neudachi, V. G. Shevchenko and N. P. Yudin, JETP **39** (1960) 109
4) J. E. Brown and M. Bolsterli, Phys. Rev. Lett. **3** (1959) 472
5) C. M. Class, R. H. Davis and J. H. Johnson, Phys. Rev. Lett. **3** (1959) 41
6) D. Brink and G. Satchler, Nuovo Cim. **4** (1956) 549;
V. V. Balashov, K. A. Tumanov and Yu. M. Shirokov, Nuclear reactions at small and mean energies (Moscow, 1957)
7) W. M. Vischer and R. A. Ferrell, Phys. Rev. **107** (1957) 781
8) B. C. Carlson and J. Talmi, Phys. Rev. **96** (1954) 436
9) V. V. Balashov and V. A. Eltekov, Nuclear Physics **16** (1960) 423
10) R. Summers, R. Maslam and L. Katz, Can. J. Phys. **31** (1953) 70
11) A. P. Komar and T. N. Drachnev, DAN SSSR **126** (1959) 1234

2.I

Nuclear Physics **27** (1961) 337—343; © *North-Holland Publishing Co., Amsterdam*

Not to be reproduced by photoprint or microfilm without written permission from the publisher

RÔLE OF NUCLEON CLUSTERS IN DEEP PHOTO-DISINTEGRATION OF LIGHT NUCLEI

V. V. BALASHOV and V. N. FETISOV

Nuclear Research Institute of the Moscow State University, Moscow, USSR

Received 18 January 1961

Abstract: The paper elucidates the general properties of the manifestation of nucleon clusters in photo-nuclear reactions and gives a theoretical interpretation, in good agreement with experiment, of the reaction C^{12} (γ, pt) 2α. The paper discusses the use of deep photodisintegration for investigating the internal nuclear shells.

Under deep photodisintegration is understood the decay of a nucleus due to a γ-quantum, with the emission of compound particles, tritons, α-particles, etc. as well as the ejection of strongly bound nucleons from the internal shells of the nucleus, leading to the production of highly excited states of the residual nucleus. These effects have received very little experimental attention so far. Yet they are extremely interesting in particular, there is abundant qualitative evidence [1]) pointing to the existence of clusters of nucleons in nuclei leading to a number of singularities in the cross sections, angular distributions and spectra of photo-nuclear reaction products.

It was shown in ref. [2]) (concerned with the calculation of the reduced widths of light nuclei for nucleon clusters) that the most essential features of nucleon association in a nucleus are described satisfactorily by the shell model.

The present paper is concerned with the application of the methods proposed in ref. [2]) for studying deep photodisintegration of light nuclei.

The analysis is based on the experimental work of Maikov [3]) in which the author gave the most systematic treatment (though not very rich in statistics) to the reaction

$$C^{12}+\gamma \rightarrow p+H^3+He^4+He^4. \qquad (1)$$

According to ref. [3]), the main maximum of the cross section of reaction (1) lies at the γ-quantum energy $E \approx 43$ MeV and the second maximum is in evidence in the region $E = 60$ to 65 MeV (see fig. 1).

In analyzing his experimental data, the author [3]) concludes that the reaction (1) has two stages. The absorption of the γ-quantum by the C^{12} nucleus leads to the ejection of a proton which carries away most of the quantum energy (direct photoeffect). The resulting highly excited state of the B^{11} nucleus

disintegrates, with the emission of a triton, into the lower levels of the Be^8 nucleus (the ground state 0+ and the first excited state 2^+ at $E^* \approx 2.9$ MeV).

The direct photoeffect on C^{12}, during which the γ-quantum transfers nearly all its energy to the emitted particle may in principle occur with the ejection of a nucleon from 1p as well as from the 1s shell. Yet the ejection of a proton from the 1p shell of C^{12} leads to a weak excitation of the B^{11} nucleus when no further decay with triton emission is energetically possible. Now, the ejection of the s proton corresponds to a far higher excitation of the B^{11} nucleus. It is rather difficult to calculate the excitation energy of this state. Rough theoretical estimates given for the O^{16} nucleus [4]) show that in our case we should expect the value of the excitation energy of the B^{11} nucleus to be in the neighbourhood of 20 MeV. In the present paper the calculation is performed for different energy values of the excitation of B^{11} taken from the experiment [3]) in which they are determined under the assumption of the following decay-scheme:

$$\begin{array}{l} C^{12}+\gamma \rightarrow p+B^{11*} \\ \qquad\qquad\quad \downarrow \\ \qquad\qquad\quad Be^8+He^3. \end{array} \tag{2}$$

In the calculation of the first stage of eq. (1) $-C^{12}$ (γ, p) B^{11*}, we take the wave function of the s state of the harmonic oscillator with $\hbar\omega = 16$ MeV as a function of the initial state. The function of the final state is selected in the form of a plane wave. In doing this we take no account of the interaction of the proton with the B^{11} nucleus in the final state. It is known [5]) that taking account of this interaction can essentially change the magnitude of the cross section in the giant resonance region. Yet in our energy region, far removed from the giant resonance, this influence is probably not large. The use of the oscillator function of the initial state is also a rough assumption. Calculations show that the use of a rectangular well function instead of an oscillator function changes the cross section appreciably. This, however, little affects the position of the cross section maximum and consequently cannot alter the qualitative conclusions.

The Hamiltonian of radiation-nucleus interaction is taken in the form

$$H_\gamma = \frac{i\hbar}{c}\sqrt{\frac{2\pi\hbar c}{k}}\sum_{i=1}^{2} e^{i\mathbf{k}\cdot\mathbf{r}_i}\frac{e_i}{\mu_i}(\mathbf{s}\nabla_i), \tag{3}$$

where $\mathbf{k}$ is the photon momentum and $\mathbf{s}$ is the polarization vector. The calculated curve of the cross section of the reaction C^{12} (γ, p) B^{11*} with the ejection of an s proton is represented in fig. 1. It is clear from fig. 1 that it is possible to obtain good agreement with experiment for the position of the first maximum by varying $E^*_{B^{11}}$ within the limits indicated in ref. [3]) for the given reaction

scheme. The assumption on the ejection of an s proton is confirmed by comparing the calculated and measured angular proton distributions (see fig. 2).

The second stage of (1) presupposes the decay of B^{11} into H^3 and Be^8. The calculation of the widths is given in the framework of the theory evolved in ref. [2]).

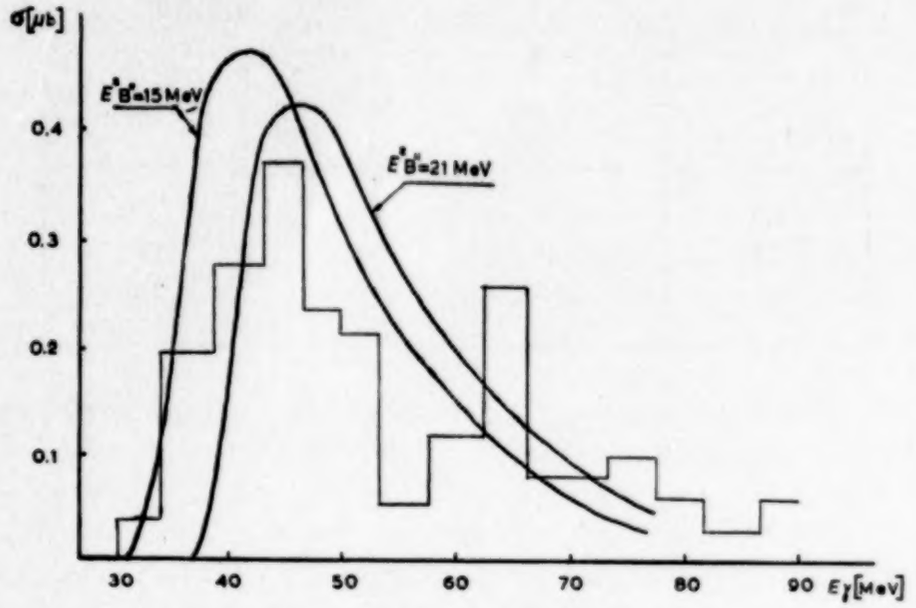

Fig. 1. Comparison of theoretical cross sections C^{13} (γ, p) B^{11*} with experiment [3]) for different values of E^*_{B11}.

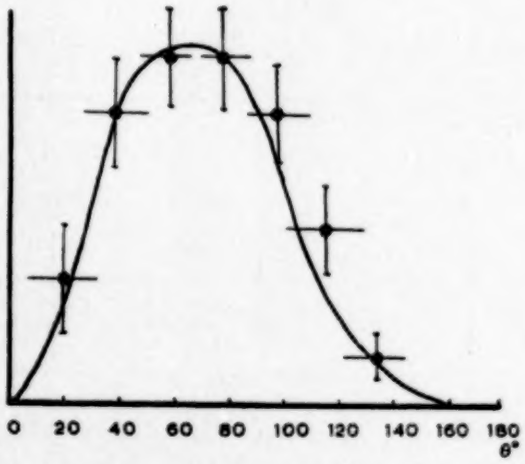

Fig. 2. Proton angular distribution. Dots designate the experimental values [3]).

The excited state of B^{11} may disintegrate not only with the emission of a triton, but also according to the scheme which would correspond to the reaction

$$C^{12}+\gamma \rightarrow p+He^4+Li^7. \qquad (4)$$

Table 1 represents the calculated ratio of the probabilities of the decay of the excited state of B^{11} through the channels Be^8+He^3 and Li^7+He^4 for

different excitation energies and channel radii, from which it is clear that the decay probability for the channel Be^8+He^3 is on the average 20 times as large as for the channel Li^7+He^4 (as for (4), this reaction probably materializes through a mechanism different from the decay of B^{11*} into $\alpha+Li^7$).

TABLE 1

Ratio of the decay probabilities of excited state for the canals Be^8+H^3 and Li^7+He^4

R(fm) \ $E^*_{B^{11}}$	15 MeV	19 MeV	21 MeV
4.0	12.9	21.6	22.4
4.5	15.0	25.0	29.2
5.0	22.3	38.8	39.0

Speaking formally, the one-nucleon decay of B^{11} described by the configuration $|s^3p^8\rangle$ is allowed for the configuration only with the production of the state $|s^3p^7\rangle$, but this process is impossible from energy considerations. Actually, the shell state $|s^3p^8\rangle$ contains about 10 % of "spurious" states corresponding to the excited motion of the nuclear centre of gravity as a whole. Taking account of these effects can give a small nucleon width of the decay of the B^{11} state of the order of a triton width.

TABLE 2

Ratio of the probabilities of the decay of B^{11*} for the canal Be^8+H^3 into different levels of the Be^8 nucleus

R(fm) \ $E^*_{B^{11}}$	15 MeV	19 MeV	21 MeV
4.0	140.0	2.4	1.9
4.5	78.0	2.3	1.9
5.0	53.0	2.2	1.9

Table 2 represents the ratio of the decay probabilities of B^{11*} through the channel Be^8+H^3 into different levels of the Be^8 nucleus. The ratio $\Gamma(0^+)/\Gamma(2^+)$ decreases with the growth of the excitation energy of B^{11}. This ratio is in satisfactory agreement for $E^*_{B^{11}} = 19$ MeV.

Fig. 3 represents the curve of the cross section of reaction (1) calculated at $E^*_{B^{11}} = 19$ MeV. It is clear from fig. 3 that the position of the first maximum agrees well with the calculation.

The present calculation does not aim at obtaining the absolute cross section value. On the other hand, fig. 3 compares the experimental cross section of

the reaction C^{12} (γ, pt) 2α with the calculated cross section of the formation of the B^{11} nucleus, including other than triton decays. On the other hand, in the calculation of the formation we neglected, as has been pointed out above, the interaction in the final state and confined ourselves to the use of the oscillator function. The above mechanism for the consecutive emission of a proton and a triton in reaction (1) does not explain the presence of the second maximum in the cross section. The reaction (γ, np) at high energies is known to materialize through the two-nucleon absorption of a γ-quantum. While considering the reaction (γ, pt) it is natural to assume the presence of a similar mechanism of "quasi-alpha particle" absorption, in which the γ-quantum

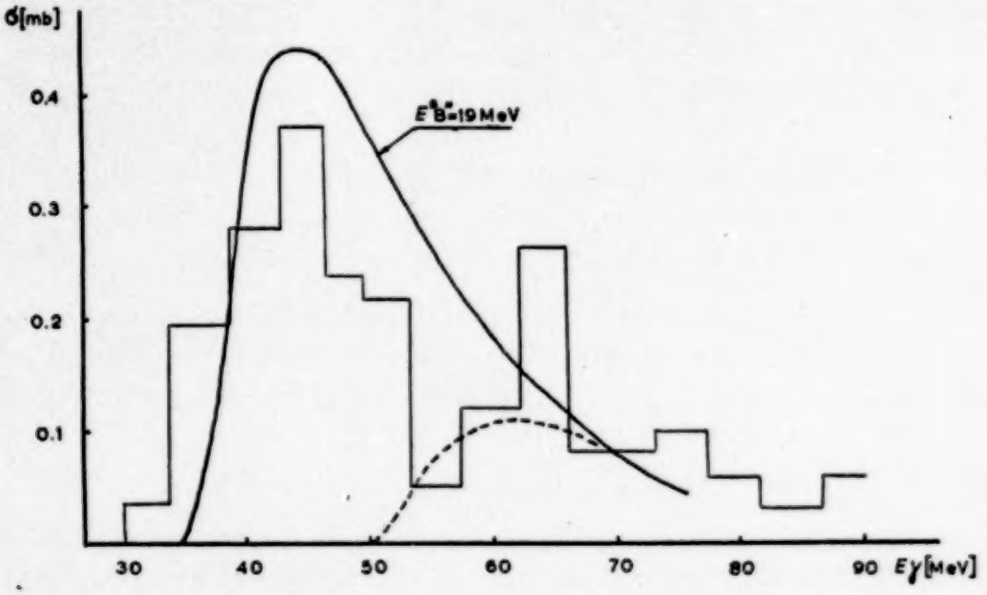

Fig. 3. Relation between the mechanism of the consecutive emission of a proton and a triton in the reaction C^{12} (γ, pT) Be^8 and the "quasi-alpha-particle" absorption mechanism.

breaks up the alpha-cluster as it penetrates the nucleus. The technique evolved in ref. [2]) makes it possible to obtain what is known as the "effective number of alpha particles" in C^{12} corresponding to different states of Be^8. For 0^+, 2^+ and 4^+ levels of Be^8, these numbers are 0.67, 0.84 and 0.86 respectively.

Having identified the photodisintegration cross section of the α-cluster and the experimental photodisintegration cross section [6]) and performed a rough calculation of the kinematics of the discharge of the three particles with this absorption of the γ-quantum, we obtain an additional contribution to the cross section of reaction (1) in the range from 60 to 70 MeV (see fig. 3).

The above analysis of the reaction C^{12} (γ, pt) Be^8 shows that the method proposed in ref. [2]) for evaluating nucleon association in the framework of the shell model can be successfully applied for explaining the peculiarities of the cross section, angular distribution and energy spectra of deep photodisintegration products of light nuclei.

Bearing in mind the approximate character of our investigation as well as the low accuracy of the experimental data used, we do not seek to obtain full agreement with experiment in the present paper. Rather our purpose is to establish a general pattern of nucleon clusters in photonuclear reactions and give a point of reference for further investigation of the effects involved.

The above analysis of the reaction C^{12} (γ, pt) 2α leads us to the following conclusions.

There are two possibilities of the manifestation of the clusters in the deep photodisintegration reactions of light nuclei:

1) Compound particles (α-particles, tritons etc.) originate in the decay of the nuclear excited states arising in the absorption of a γ-quantum. These decays can be observed in the region of the giant resonance region (wherever this is possible energetically and is not prohibited by the conventional rules) as well as at energies above the giant resonance, which usually corresponds to the ejection of a nucleon out of the inner shells of the nucleus. The decay probabilities of these states in transitions to different states of the residual nucleus can be calculated by the shell model.

2) At a γ-quantum energy of the order of 60 to 70 MeV there may be a peculiar "quasi-alpha particle" mechanism of absorption of γ-quanta, leading to the simultaneous emission of a proton and a triton from the nucleus — a mechanism similar to the well-known "quasi-deuteron" mechanism of absorption at high γ-quantum energies.

In conclusion we shall emphasize the important role of photo-nuclear reactions for investigating the internal shells of the nucleus. It is common knowledge that the hole excitations are investigated mainly in the "pick-up reactions" (p, d), (d, t), etc. Yet the ejection of nucleons from the internal closed shells is effective only for nuclei containing a very small number of external nucleons. As soon as the number of the nucleons over the closed shells increases there arises a peculiar screening of the internal nucleons, which strongly suppresses the "pick-up cross section". This screening makes the investigator go far beyond the limits of the energies usually used in nuclear physics while investigating these hole excitations in particle reactions. The respective investigations undertaken by Tyrén *et al.* [7]) in irradiating light nuclei by 450 MeV protons are well known.

The deep photodisintegration reactions suggest another possibility for investigating the above states. A γ-quantum penetrates the nucleus freely and ejects a nucleon from the internal closed shells. In this process, it is probably difficult to isolate experimentally the respective group of particles from the total spectrum of the reactions (γ, n) and (γ, p). The fact is that in the most interesting cases, when the number of nucleons in the closed shells is large, the nucleons ejected from the external non-closed shells account for an over-

whelming portion of the (γ, n) and (γ, p) spectrum. The transitions with ejection of nucleons out of the closed shells can be isolated through the analysis of secondary processes (of a type considered above in the reaction C^{12} (γ, pt) 2α of the decay of B^{11} with the emission of a triton).

In this connection it should be noted that the excitation energy of the B^{11} nucleus formed during the ejection of an s nucleon from C^{12} is equal, according to the above analysis, to $\approx$ 19 MeV and corresponds to the coupling energy of the s nucleon in C^{12} E $\approx$ 35 MeV. This agrees with the respective value given by Tyrén *et al.* [7]).

The authors express their gratitude to Prof. Komar as well to as I. N. Gorbunov and V. N. Maikov for stimulating discussions.

References

1) N. V. Chuvilo and V. G. Shevchenko, Nuclear reactions at low and medium energies (Moscow, 1958)
2) V. V. Balashov *et al.*, JETP **37** (1959) 1385
3) V. N. Maikov, Nuclear reactions at low and medium energies, Thesis, P. N. Lebedev Physical Institute, Moscow, 1959
4) G. E. Tauber and T. Y. Wu, Phys. Rev. **105** (1957) 1772
5) D. H. Wilkinson, Physica **22** (1956) 1039
6) A. N. Gorbunov and V. M. Spiridonov, Nuclear reactions at low and medium energies (Moscow, 1958)
7) Tyrén, report Second All-Union Conf. nuclear reactions at low and medium energies, Moscow, 1960

1.D.1:
3.A

Nuclear Physics **27** (1961) 344—347; © *North-Holland Publishing Co., Amsterdam*
Not to be reproduced by photoprint or microfilm without written permission from the publisher

ISOMERIC LEVEL IN Y^{90}

J. M. FERGUSON

U.S. Naval Radiological Defense Laboratory, San Francisco 24, California

Received 4 April 1961

Abstract: A 3.5 h activity was produced by fast neutron bombardment of yttrium and zirconium. The evidence indicates this activity is Y^{90m}. Two gamma rays in cascade were found with energies of 200 keV and 493 keV. It is felt that the isomer consists of a 7+ level at 693 keV decaying to the 3− level in Y^{90} at 200 keV.

1. Introduction

The jj-coupling shell model predicts [1]) an isomeric level in Y^{90}. If we regard $_{38}Sr^{88}_{50}$ as a closed-shell nucleus, then $_{39}Y^{90}_{51}$ has one proton and one neutron outside closed shells. The two lowest states available for the 39th proton are the $p_{\frac{1}{2}}$ and $g_{\frac{9}{2}}$ states. The 51st neutron is expected to be in a $d_{\frac{5}{2}}$ state. Thus there should be the following two sets of levels in Y^{90}: the two levels of the $p_{\frac{1}{2}}$, $d_{\frac{5}{2}}$ configuration and the six levels of the $g_{\frac{9}{2}}$, $d_{\frac{5}{2}}$ configuration. Since the energy difference between the $\frac{9}{2}$+ and $\frac{1}{2}$−levels in $_{39}Y^{89}_{50}$ is 915 keV, the "centre of gravity" of the $g_{\frac{9}{2}}$, $d_{\frac{5}{2}}$ levels in Y^{90} should be about 915 keV above that of the $p_{\frac{1}{2}}$, $d_{\frac{5}{2}}$ levels. Also, the 2+ and 7+ states should be the lowest of the $g_{\frac{9}{2}}$, $d_{\frac{5}{2}}$ configuration [1]).

G. A. Bartholomew *et al.* have studied the Y^{90} level structure using the Y^{89} (n, γ) reaction [2]). They found the two lowest levels of Y^{90} to have characters of 2− and 3−; these are presumably the states of the $p_{\frac{1}{2}}$, $d_{\frac{5}{2}}$ configuration. Also they found a level at 776.7 keV which probably has a 2+ character. This would be a level of the $g_{\frac{9}{2}}$, $d_{\frac{5}{2}}$ configuration. The other states of this configuration would not be excited in the Y^{89} (n, γ) reaction using thermal neutrons.

If the 7+ level lies below the other levels of the $g_{\frac{9}{2}}$, $d_{\frac{5}{2}}$ configuration, as predicted, its decay would be strongly hindered by its high angular momentum. In this work we have obtained evidence for such an isomeric level.

2. Experimental Results

The Zr^{90} (n, p) and Y^{89} (n, γ) reactions were used to search for the isomer. To form a 7+ level with these reactions it is necessary to supply at least 3 or 4 units of angular momentum to the nucleus. Thus there is a rather large centrifugal barrier for the formation of Y^{90m}. At high energies, however, the penetra-

tion of high angular momentum neutrons into the nucleus should be comparable to that of low angular momentum neutrons [3]). Hence we used the highest energy neutrons available. In the original runs samples of $Zr(OH)_4$ and Y_2O_3 were irradiated with 14.5 MeV neutrons.

The gamma-ray spectra from these samples were studied with 10 cm high, 10 cm diam NaI(Tl) crystals and a 100-channel pulse-height analyzer. The samples were placed directly on top of the crystal housing to obtain maximum counting rates. The pulse-height spectrum from a yttrium sample is shown in fig. 1. The background and the contribution from long-lived Y^{88} has been

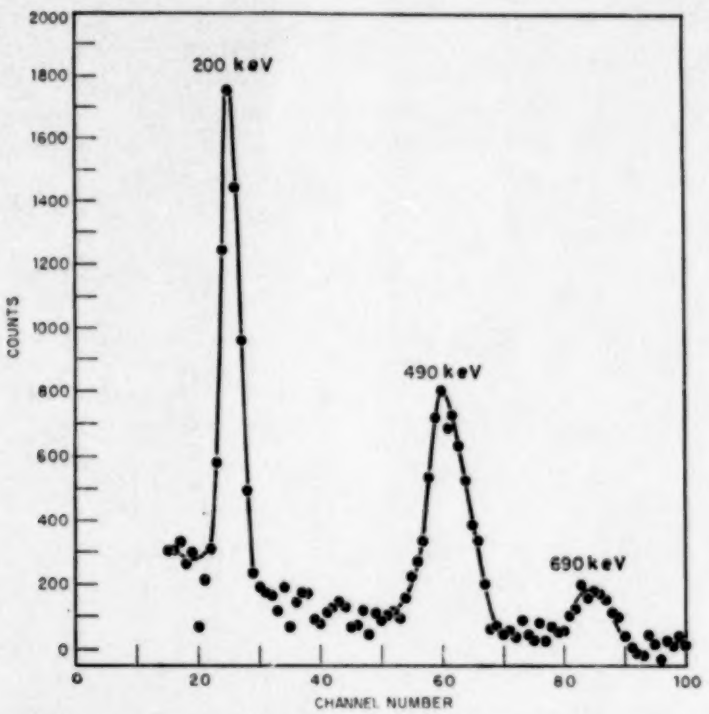

Fig. 1. Gamma-ray pulse-height spectrum from a yttrium sample bombarded with 14.5 MeV neutrons. The sample was placed directly on top of the crystal housing for counting. The pulse height spectrum due to long-lived Y^{88} and the background has been subtracted. The peak at channel 85 is a sum peak due to simultaneous detection of both gamma rays.

subtracted from this spectrum. The two larger peaks correspond to gamma energies of 200 ± 5 keV and 493 ± 5 keV. The peak at channel 85 corresponds to 693 MeV and is a sum peak (see below), indicating the two gammas are in cascade. The 200 keV and 493 keV peaks correspond to gammas of about equal intensity, after correcting for the crystal efficiency. The half period of the activity is 3.5 ± 0.5 h.

The following seven neutron reactions are energetically allowed: $Y^{89}(n,\gamma)Y^{90}$, $Y^{89}(n, 2n)Y^{88}$, $Y^{89}(n, p)Sr^{89}$, $Y^{89}(n, n')Y^{89m}$, $Y^{89}(n, \alpha)Rb^{86}$, $Y^{89}(n, d)Sr^{88}$ and $Y^{89}(n, t)Sr^{86}$. In a chemical analysis the activity stayed with the yttrium, hence it is either Y^{88m}, Y^{89m} or Y^{90m}.

The same activity was produced by 14.5-MeV neutron bombardment of

zirconium. The cross section for the production of the activity was found to be larger by a factor of 4 for zirconium than for yttrium. An elimination process makes Y^{90m} appear to be the most likely assignment. If the activity were Y^{88m} it would be produced by the Y (n, 2n) (11.8 MeV threshold) and Zr(n, t) (13 MeV threshold) reactions. The Zr(n, t) cross section would be expected to be much smaller than the Y(n, 2n) cross section. If the activity were Y^{89m} it would be produced by the Y(n, n′) reaction (0.5 MeV threshold) and the Zr(n, d) reaction (7 MeV threshold). Again, the Zr(n, d) reaction

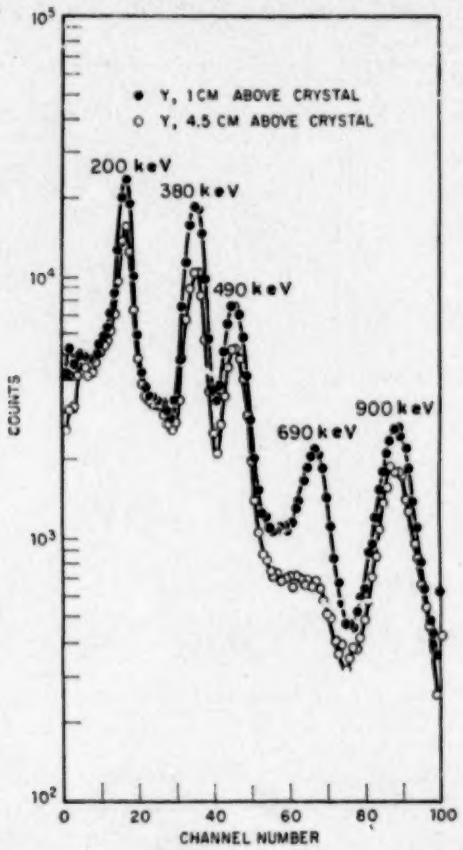

Fig. 2. Gamma-ray pulse height spectrum from a yttrium sample bombarded by fast neutrons. The peaks at channels 17, 46 and 67 are from the same activity as shown in fig. 1. The peak at channel 35 is from Y^{87m} and the peak at channel 88 is due to Y^{88}. In the upper curve the sample was 1 cm from the crystal face and in the lower curve the sample was 4.3 cm from the crystal face. The large reduction of the 693 keV peak indicates it is a sum peak.

would be expected to be smaller than the (n, n′) reaction. For Y^{90m} the reactions are Y^{89} (n, γ) (exoergic) and Zr(n, p) (2 MeV threshold). While it is harder to compare these two reactions, since one is radiative decay of the compound nucleus and the other is particle emission, it is not unreasonable to have the (n, p) cross section larger than the (n, γ) cross section at 14 MeV.

The 200 ± 5 keV energy of the lower gamma ray also indicates that the activity is Y^{90m}. Bartholomew [2]) found the first level of Y^{90} to be at 202.4 ± 0.3 keV.

Intense sources containing the 3 h activity were produced by bombarding yttrium with cyclotron produced neutrons. Because of the higher energy of the neutrons additional contaminating activities were produced, notably Y^{87} and Y^{87m} from the (n, 3n) reaction. However, the more intense source was useful for verifying that the 200 keV and 493 keV gamma rays are in cascade.

Fig. 2 shows the pulse-height spectrum from the sample. The upper spectrum was taken with the samples placed 1 cm above the crystal face, while the lower curve was taken with the sample 4.3 cm above the crystal face. In the upper curve, the peak at 693 keV could be the sum peak of the 200 keV and 493 keV peaks, or a cross-over gamma transition. It is seen that the 693 keV peak disappears in the lower curve. This verifies that it is a sum peak and not another gamma ray, for if it were another gamma ray it would have about the same height relative to the other peaks in both runs. Because of the differences in the efficiencies of the two positions the sum peak should be reduced by a factor of 8 in the second run, and that is what is indicated by the data.

To summarize, the data indicate an isomeric level in Y^{90m} at 693 keV which decays through a 493 keV or 200 keV level. It is very likely that the intermediate level is the 200 keV level found by Bartholomew.

3. Discussion

The reduced lifetime [4]) of the 493 keV transition indicates it is an M4 transition. Since Bartholomew found that the 200 keV level has a character of 3−, the 693 keV level would be 7+. The 693 keV level is presumably the 7+ level of the $g_{\frac{9}{2}}$, $d_{\frac{5}{2}}$ configuration. According to the shell model the ratio of lifetimes of this transition to the lifetime of the $\frac{9}{2}+$ level in Y^{89m} should be just proportional to the 9th power of the energy ratios. On this basis the predicted lifetime of the Y^{90m} level should be 1.2 h. The discrepancy of a factor of 3 between this predicted value and the observed 3.5 h half period is not unreasonable in the comparison of gamma lifetimes.

The author would like to express his gratitude to Dr. A. de-Shalit for pointing out the possibility of a Y^{90} isomer and for some very enlightening discussions. Also, the author wishes to thank Dr. D. L. Love for making the chemical separations.

References

1) A. de-Shalit, private communication
2) G. A. Bartholomew, P. J. Campion, J. W. Knowles and G. Manning, Nuclear Physics **10** (1959) 590
3) H. Feshbach, Nuclear spectroscopy (Academic Press, Inc., New York 1960) part B, capt. V.A.
4) M. Goldhaber and A. W. Sunyar, Beta and gamma-ray spectroscopy (Interscience Publishers, Inc., New York (1955) p. 453

2.J

Nuclear Physics **27** (1961) 348—351; © *North-Holland Publishing Co., Amsterdam*

Not to be reproduced by photoprint or microfilm without written permission from the publisher

DEPENDENCE OF THE ANGULAR DISTRIBUTION OF FISSION FRAGMENTS ON THE TARGET NUCLEAR SPIN

V. M. STRUTINSKI

I. V. Kurchatov Atomic Energy Institute, Academy of Sciences, Moscow, USSR

Received 20 February 1961

Abstract: Angular distribution of fission fragments is calculated for small anisotropy. The analytical expression obtained takes into account the dependence of the fission and neutron widths on nuclear angular momentum. The theoretical data are compared with experiment.

In ref. [1]) a method of calculating the angular distribution of fission fragments was set down and analytical expressions were obtained for the angular distribution when the target nucleus spin is finite. In case of a Gaussian-type probability distribution in K (the projection of the angular momentum of the compound nucleus J on the direction of the fission) given by

$$\alpha(K) \propto \exp(-K^2/2K_0^2), \tag{1}$$

the angular distribution of the fragments weakly depends on the initial spin: the spin-dependent terms in the angular distribution are of the order $l^2s^2/(2K_0^2)^2$, where s is the initial spin and l the neutron orbital momentum, while the principal angle-dependent term is of the order $l^2/2K_0^2$. The dependence of the total decay probability of the compound nucleus $\Gamma_t(J)$ on the nuclear angular momentum also leads to second order corrections in the angular distribution. This effect also leads to an additional weak dependence of anisotropy on the initial spin. When the anisotropy of the angular distribution is small and dependence of Γ_t on J is weak, one can obtain an analytical expression for the angular distribution taking account of the J dependence of Γ_t.

The total width of a compound-nucleus state is the sum of radiative, neutron and fission widths. The first of the three is usually negligibly small while the dependence of Γ_f and Γ_n on the momentum can be determined by the statistical theory as

$$\Gamma_n(J) \approx \Gamma_n(0) \exp[-(\alpha_f-\alpha_1)J(J+1)], \tag{2}$$

$$\Gamma_f(J) \approx (2J+1)^{-1}\Gamma_f(0) \exp[(\alpha_1-\alpha_\perp^*)J(J+1)] \sum_{K=-J}^{J} \exp[-K^2/2K_0^2]. \tag{3}$$

In (2) and (3) we use $\alpha = \hbar^2/2\mathcal{I}T$, where $\mathcal{I}$ is the nuclear moment of inertia and T is the temperature of the nucleus. The subscript i designates the quantities

for the initial compound nucleus, the subscript f those for the compound nucleus state after emission of a neutron and the asterisks the quantities for the deformed "transitional" nucleus. The constant $\alpha_\perp{}^* = \hbar^2/2\mathscr{I}_\perp{}^* T^*$, where $\mathscr{I}_\perp$ is the moment of inertia of the transitional nucleus with respect to the axis normal to the symmetry axis. In the other cases the moment of inertia is equal to that of a spherical nucleus $\mathscr{I}_0 = \frac{2}{5} AmR^2$. Expanding $\Gamma_n(J)$ and $\Gamma_f(J)$ into a series we have

$$\gamma_f(J) = \Gamma_f(J)/\Gamma_i(J) = \gamma_f{}^{(0)}[1+qJ(J+1)+\ldots], \tag{4}$$

where

$$q = \gamma_n{}^{(0)}(\alpha_f - \alpha_\perp{}^*) + \gamma_f{}^{(0)}/2K_0{}^2,$$

$$\gamma_n{}^{(0)} = \Gamma_n(0)/\Gamma_f(0), \qquad \gamma_f{}^{(0)} = \Gamma_f(0)/\Gamma_i(0).$$

This expression for $\gamma_f(J)$ should be substituted into the general expression for the angular distribution of the fragments, which, with the fixed values of l, the channel spin $S = J_0 \pm \frac{1}{2}$ and J, is the form [1])

$$W_{lSJ}(\vartheta) = \frac{2J+1}{2(2J_0+1)} \sum_{m\mu K} (C^{JK}_{S\mu\, lm})^2 a_J(K) |Y_{lm}(\vartheta)|^2, \tag{5}$$

where

$$a_J(K) = \gamma_f(J)\alpha(K).$$

The total angular distribution of the fragments is given by the expression

$$\overline{W}(\vartheta) = \sum_{lSJ} \xi_l W_{lSJ}(\vartheta) / \sum_{lSJ} (2l+1)\xi_l, \tag{6}$$

where ξ_l is the neutron absorption coefficient assumed to be independent of J and S. Let us substitute eqs. (5) and (4) into (6) and perform the summation, for which we shall use the following formulas of summation of Clebsch-Gordan coefficients:

$$\sum_{J=|l-S|}^{l+S} (C^{JK}_{S\mu\, lm})^2 = \begin{cases} 1 & \text{for} \quad |K-m| \leqq S, \\ 0 & \text{for} \quad |K-m| > S, \end{cases}$$

$$\sum_{J=|l-S|}^{l+S} J(J+1)(C^{JK}_{S\mu\, lm})^2 = \begin{cases} l(l+1)+S(S+1)+2m\mu & \text{for} \quad |\mu| \leqq S,\ |m| \leqq l, \\ 0 & \text{for} \quad |\mu| > S,\ |m| > l. \end{cases}$$

The last equation is taken from ref. [1])†.

† Let us also note the following useful relations [1]):

$$\Sigma'_J (C^{J0}_{S\mu\, lm})^2 = \tfrac{1}{2}(1+(-1)^{J+l+S}\delta_{m0}) \equiv \omega_m(J+l+S),$$

$$\Sigma'_J (C^{J0}_{S\mu\, lm})^2 J(J+1) = \omega_m(J+l+S)[l(l+1)+S(S+1)]-m^2,$$

where the summation is restricted to the even or the odd values of J.

After the summation over J, we obtain

$$W_{lS}(\nu) = \sum_J W_{lSJ}(\nu) = C \sum_{m=-l}^{l} |Y_{lm}(\nu)|^2 \times \sum_{K=m-S}^{m+S} \{1+q[l(l+1)+S(S+1)+2m(k-m)]\}\alpha(K), \quad (7)$$

where the constant C does not depend on l and S. Let us express $\alpha(K)$ as

$$\alpha(K) \approx 1-K^2/2K_0^2+\tfrac{1}{2}\eta K^4/(2K_0^2)^2+\ldots. \quad (8)$$

The arbitrary coefficient η was introduced in eq. (8) in order to take account of a possible deviation of the K-distribution from the Gaussian distribution for large values of K. The term with K^4 leads to the corrections of second order. The correction of the angular distribution due to the J dependence of γ_f is as small as $q/2K_0^2$, i.e., is also a small magnitude of second order (q and $\frac{1}{2}K_0^2$ being of the same order). Taking this into consideration we obtain from (6), (7) and (8) after a simple evaluation

$$\begin{aligned} A(\nu) &= [\sigma_f(\nu)-\sigma_f(90^\circ)]J/\sigma_f(90^\circ) \\ &= (\overline{l^2}/4K_0^2)\{1+\overline{S^2}/6K_0^2+q[(\overline{l^4}/\overline{l^2}-\overline{l^2}+\tfrac{4}{3}\overline{S^2})\cos^2\nu \\ &+ (\eta/2K_0^2)[\tfrac{3}{8}[\overline{l^{4'}}(1-\sin^4\nu)+\overline{l^2}/\overline{S^2}+\tfrac{1}{2})\cos^2\nu]\}, \end{aligned} \quad (9)$$

where

$$\overline{l^2} = \sum_l (2l+1)\xi_l\, l(l+1)/\sum_l (2l+1)\xi_l$$

is the average square of the momentum transferred to the nucleus by the neutron, $\overline{l^4}$ and $\overline{l^{4'}}$ are similar averages of $l^2(l+1)^2$ and $l(l^2-1)(l+2)$, while $\overline{S^2} = (J_0+\frac{1}{2})^2+\frac{1}{2}$. In (9) the terms of third order are discarded. To the first order with respect to $l^2/2K_0^2$, the angular distribution does not depend on the target nucleus spin. The change is the angular distribution anisotropy as $\overline{S^2}$ changes by $\Delta\overline{S^2}$ equals

$$\Delta_S A(0^\circ) = \frac{\overline{l^2}}{4K_0^2}\{(1-3\eta)/6K_0^2+\tfrac{4}{3}q\}\Delta\overline{S^2}. \quad (10)$$

According to the experimental data of ref. [2]) there is a small systematic difference in the magnitude of anisotropy for the nuclei U^{235}, U^{233} and Pu^{239}; one has $A(0^\circ)$ $(U^{235})-A(0^\circ)$ $(U^{233}) \approx A(0^\circ)(U^{233})-A(0^\circ)(Pu^{239}) \approx 0.02-0.03$. It is natural to interpret this as the initial spin effect. For the three above-mentioned nuclei the values of $\Delta\overline{S^2}$ equal 7 and 8 units, respectively. For a theoretical estimate of $\Delta_S A(0^\circ)$, we shall put $T_f = T^* = T$ in (4). The magnitude of $\mathscr{I}_f^{-1}-\mathscr{I}_\perp^{-1} = \mathscr{I}_0\,(1.2z+5.6z^2)$, where $\mathscr{I}_0$ is the moment of inertia for a spherical nucleus and $z = 1-(Z^2/A)/(Z^2/A)_{crit}$ (ref. [3])). At $T = 0.3$ MeV, $\gamma_n^{(0)} \approx \gamma_f^{(0)} \approx 0.5$ and the solid-body value of $\mathscr{I}_0$, we obtain $q \approx 0.01$. The

parameter $\bar{l}^2/4K_0^2$ is determined directly by the experimental value of the anisotropy, since this parameter simply coincidences with the latter to a first approximation. For neutrons of energy from 3 to 5 MeV $(\bar{l}^2/4K_0^2) \approx 0.12$, $K_0^2 = 12$—15 (refs. [2,4]). From (10) we find that at $\eta = 1$ (i.e., at the Gaussian $\alpha(K)$) q four or five times exceeding the thermodynamic value would correspond to the experimental value of the difference $A(0°)$, which appears improbable. Another possible effect consists in cutting off the distribution $\alpha(K)$ as compared with the Gaussian at large K, which can well be expected since the dimensions of the nucleus are finite (see also ref. [1]). The coefficient η in this case must be less than unity of even negative. The value $\eta \approx 0$ would correspond to the experimental values of $\Delta A(0°)$ if the above-mentioned thermodynamic value of q was used.

A rough estimate of the maximum value K_{max} of K can be obtained from the conditions of equality of the nuclear rotation energy

$$E_{rot} \approx \frac{\hbar^2 K^2}{2\mathcal{J}_{eff}} = \frac{K^2}{2K_0^2} T^*,$$

and the excitation energy of the "transitional" nucleus E^*. Thus we obtain

$$K_{max} \approx \sqrt{(E^*/T^*)2K_0^2}.$$

At $E^* \approx 2$—3 MeV, $K_{max} \approx nK_0$, where the factor n is equal to several units. This value K_{max} agrees with $\eta \approx 0$ since the distribution $\alpha(K)$ goes to zero at $K \approx \sqrt{2K_0^2}$, $\eta = 0$.

The author expresses his gratitude to Dr. J. Griffin for valuable discussions.

References

1) V. M. Strutinski, JETP **39** (1960) 781
2) L. Blumberg and R. B. Leachman, Phys. Rev. **116** (1959) 102
3) G. A. Pik-Pichak, JETP **36** (1959) 962
4) E. Simmons and R. L. Henkel, Phys. Rev. **120** (1960) 198

10.E *Nuclear Physics* **27** (1961) 352 © *North-Holland Publishing Co., Amsterdam*
Not to be reproduced by photoprint or microfilm without written permission from the publisher

ERRATUM

E. Arbman, S. Bjørnholm and O. B. Nielsen, Levels in Th^{228} in the electron capture decay of Pa^{228}, Nuclear Physics **21** (1960) 406—437.

On page 432, the following table should be inserted:

TABLE 7

Rotational bands

$E_{rot} = A\,I(I+1)+B[I(I+1)]^2$

Band head		A	$-B$	$4\sqrt{A^3/B}$
keV	K, I, π	$\hbar^2/2\mathscr{I}$ (keV)	$2\left(\frac{1}{E_{vib}}\right)^2\left(\frac{\hbar^2}{\mathscr{I}}\right)^3$ (keV)	E'_{vib} (keV)
0	0,0+	9.70±0.03	0.020±0.002	860±40
327.5	0,1−	6.96±0.03	0.009±0.001	780±60
969	2,2+	9.43±0.07	0.027±0.003	710±40
1123	2,2−	7.93±0.08	0.021±0.004	640±60
(1620)	(2,2+)	(5.0±0.5)		
Rigid Rotor:		3.9 [14])		

NORTH-HOLLAND BOOKS

Just out

Elements of Hamiltonian Mechanics

by D. TER HAAR
University Reader in Theoretical Physics and Fellow of Magdalen College, Oxford

CONTENTS:

1. Newtonian mechanics
2. The Lagrangian equations of motion
3. Small vibrations
4. Dynamics of rigid bodies
5. The canonical equations of motion
6. Hamilton-Jacobi theory
7. Perturbation theory
8. Continuous systems

Bibliography - Problems

This book is based upon a course of lectures given to final year undergraduates and first year graduate students at Oxford University. The emphasis and the selection of subject matter differs in a number of points from those in existing modern text-books. The main differences are in the way constraints are introduced by freezing in of degrees of freedom, and in the discussion of classical perturbation theory.

6 x 9" 196 pp. Gld. 20.— (40s.)

NORTH-HOLLAND PUBLISHING COMPANY
P. O. BOX 103 - AMSTERDAM

Distributor for U.S.A.: Interscience Publishers, Inc. — New York

NORTH-HOLLAND BOOKS

QUANTUM MECHANICS

Just out

VOL. I

by ALBERT MESSIAH (Centre d'Etudes Nucléaires de Saclay)

translated from the French by G. M. Temmer (Florida State University, Tallahassee)

6×9" 520 pp. Gld. 50.- (100s.)

CONTENTS VOL. I. *The formalism and its interpretation.* Origins of the Quantum Theory. Matter waves and the Schrödinger equation. One dimensional quantum systems. Statistical interpretation of the wave-corpuscle duality and uncertainty relations. The development of the formalism of Wave Mechanics and its interpretation. Classical approximation and WKB method The general formalism of Quantum Theory: A) Mathematical framework. B) Description of physical phenomena. — *Simple systems.* Solution of the Schrödinger equation by separation of variables. Central force field. Scattering problems. Central force field and the method of phase shifts. Coulomb interaction. Harmonic oscillator. — *Appendices:* «δ function» and distributions. Special functions and related formulae.

"*. . . . the reviewer would like to recommend the book to students taking a beginner's course in quantum mechanics, to teachers for broadening the scope of such courses, and also to research workers in understanding the principles and methods of quantum mechanics and for acquiring the necessary knowledge for an understanding of the advanced parts of the field.*"

(PHYSICS TODAY on the original French Edition)

VOLUME II
in preparation

Ask your bookseller or

NORTH-HOLLAND PUBLISHING COMPANY

P.O. BOX 103—AMSTERDAM

Distributor for U.S.A.: Interscience Publishers, Inc. — New York